



შოთა რუსთაველის საქართველოს ეროვნული სამეცნიერო ფონდი
SHOTA RUSTAVELI NATIONAL SCIENCE FOUNDATION OF GEORGIA



ფერდინანდ თავაძის მეტალურგიისა და მასალათმცოდნეობის ინსტიტუტი
FERDINAND LAVADZE INSTITUTE OF METALLURGY AND MATERIALS SCIENCE

IMS 2021

4th International Conference

MODERN TECHNOLOGIES AND METHODS OF INORGANIC
MATERIALS SCIENCE

Proceedings

SEPTEMBER 20-21, 2021
TBILISI, GEORGIA



შოთა რუსთაველის საქართველოს ეროვნული სამეცნიერო ფონდი
SHOTA RUSTAVELI NATIONAL SCIENCE FOUNDATION OF GEORGIA



ფერდინანდ თავაძის მეტალურგიისა და მასალათმცოდნეობის ინსტიტუტი
FERDINAND TAVADZE INSTITUTE OF METALLURGY AND MATERIALS SCIENCE

IMS 2021

4th International Conference

**MODERN TECHNOLOGIES AND METHODS
OF INORGANIC MATERIALS SCIENCE
Proceedings**

**SEPTEMBER 20-21, 2021
TBILISI, GEORGIA**

Dedicated to the 75th anniversary of foundation of Ferdinand
Tavadze Institute of metallurgy and materials science

ISBN 978-9941-8-3594-0

ORGANIZING COMMITTEE

Gachechiladze Archil – Chairman (Georgia)

Badzoshvili Tamar – Secretary (Georgia)

Abashidze Nino (Georgia), **Alymov Mikheil** (Russia), **Antashvili Levan** (Georgia), **Berner Alex** (Israel), **Ivasishin Orest** (Ukraine), **Khantadze Jumber** (Georgia), **Khvadagiani Avtandil** (Georgia), **Mukasyan Alexander** (USA), **Namicheishvili Teimuraz** (Georgia), **Onuralp Yucel** (Turkey), **Peikrishvili Akaki** (Georgia), **Rusishvili Zurab** (Georgia), **Solonini Yuriy** (Ukraine), **Todadze Aleksandre** (Georgia), **Tsagareishvili Otar** (Georgia), **Tsitsishvili Vladimer** (Georgia).

Contents

R.Abdulkarimova, K.Kamunur, A.Batkal, N.Assanbek SH-SYNTHESIS OF COMPOSITION MATERIALS ON THE BASIS OF TiB ₂ -TiC- MgO	8
M.Alymov, B.Seplyarskii NEW DIRECTIONS OF APPLICATION OF MACROKINETIC APPROACHES IN ISMAN	12
K.Amirkhanashvili, A.Sobolev, V.Tsitsishvili, N.Zhorzholiani MOLECULAR STRUCTURE OF BIS (LIDOCAINE) TETRATHIOCYANOCOBALTATE(II) MONOHYDRATE.....	14
K. Barbakadze, G.Bokuchava, Z.Isakadze, A.Kutsia, I.Tabatadze, M.Barbakadze, M. Rekhviashvili SiGe ALLOYS SYNTHESIZED BY HOT PRESSING AND A THERMOELECTRIC GENERATOR CREATED ON THEIR BASE.....	18
O. Berdnikova, V. Sydorets, A. Bernatskyi, T. Alekseitenko, O. Bushma, I. Alekseitenko LASER AND HYBRID WELDED JOINTS OF LOW-ALLOY HIGH-STRENGTH STEELS: THE RELATIONSHIP OF STRUCTURE AND OPERATION PROPERTIES.	22
A.I. Berner STUDY OF CRYSTALLOGRAPHIC STRUCTURE WITH THE HELP OF ELECTRON DIFFRACTION IN SCANNING ELECTRON MICROSCOPY	26
B. Bendeliani, G. Dgebuadze, Z. Azmaiparashvili, G. Bokuchava, N. Ebralidze, I.Metskhvarishvili CONTROL OF THE SYNTHESIS PROCESS OF SUPERCONDUCTING MATERIALS	30
M. Busurina, A. Sytshev, I. Kovalev, A. Karpov, A. Shchukin THERMAL EXPLOSION IN Ti-Al-Me SYSTEMS (Me=Co, Cu, Fe): COMBUSTION, PHASE FORMATION AND PROPERTIES	33
L. Chkhartishvili, L. Antashvili, L. Dalakishvili, R. Chedia, O. Tsagareishvili ON MATHEMATICAL MODELING CHEMICAL SYNTHESIZING PROCESS OF BORON CARBIDE / TITANIUM DIBORIDE COMPOSITE IN NANOPOWDERED FORM FROM LIQUID CHARGE.....	37
G.Gordeziani, I.Tsintsadze, S.Gvazava, R.Tabidze, N.Khidasheli, G.Tavadze INFLUENCE OF HOT PLASTIC DEFORMATION ON AUSTENITIZATION PROCESS DURING AUSTEMPERING OF DUCTILE IRON.....	45
V. Garibashvili, Z. Mirijanashvili, A. Kandelaki, V. Tsiklauri, Z. Tsikaridze OBTAINING HEAT AND WEAR-RESISTANT COATING BY ELECTROSPARK ALLOYING	50
D. Ikornikov, V. Sanin, D. Andreev, N.Sahkova, V. Yukhvid REPROCESSING OF MILL SCALE WASTES BY SHS –METALLURGY FOR PRODUCTION OF CAST FERROSILICON, FERROSILICO ALUMINUM AND FERROBORON	54
G.Inanishvili, T.Badzoshvili ANCIENT IRON PRODUCTION MONUMENTS OF GEORGIA (XII-I CC B.C.).....	57

N.Jalagonia, T.Kuchukhidze, T.Archuadze, L.Kalatozishvili, N.Darakhvelidze, M. Mumladze, G.Bokuchava GRAPHENE DERIVATIVES INFLUENCE ON MECHANICAL PROPERTIES AND MICROSTRUCTURE OF ALUMINA BASED CERAMIC MATERIALS.....	61
L.Jibuti, A.Bibilashvili, Z.Kushitashvili FABRICATION OF MEMRISTOR ON THE BASES OF ZrO ₂ AND HfO ₂ DIOXIDES AND RESEARCH OF ITS PHYSICAL CHARACTERISTICS	65
Z.Jibuti, A.Bibilashvili, L.Jibuti, Z.Kushitashvili SYSTEMS OF PULSED PHOTON IRRADIATION (PPI) OF MATERIALS AND STRUCTURES IN ELECTRONICS	69
E.Khutsishvili, T.Qamushadze, N.Kobulashvili, Z.Chubinishvili, R.Razmadze ALLOY DISORDERS IN InP _x As _{1-x} SOLID SOLUTIONS	73
S. Kvinikadze, N. Chikhradze, A. Vanishvili, G. Abashidze, R. Katsarava BIODEGRADABLE POLYMER COMPOSITE MATERIALS MADE FROM INORGANIC FILLERS AND FIBERS	77
L. Kirtadze, G. Jibuti DETERMINING AMOUNT OF NITROGEN DIOXIDE (NO ₂) IN THE ATMOSPHERE BY USING OF THE COST-EFFECTIVE SENSORS AND ANALYSIS OF THE COLLECTED DATA.....	82
G. Kevkhashvili, T. Namichishvili, [L.Jordania], J. Loria, V. Ramishvili, J. Gamsakhurdia DETERMINATION OF TECHNOLOGICAL PARAMETERS FOR THE PRODUCTION OF ALUMINUM ALLOYS (8-22 MM) BY THE METHOD OF "WITHOUT INGOT ROLLING"	86
I.Kurashvili, T.Kimeridze, G.Chubinidze, D.Mkheidze, M.Kadaria, T.Melashvili, N.Gogolashvili, V.Kirtskhalia, G.Darsavelidze INFLUENCE OF γ -RAYS IRRADIATION ON THE PHYSICAL-MECHANICAL PROPERTIES OF MONOCRYSTALLINE p-Si	90
E.Levashov, S.Vorotilo, V.Kurbatkina, Yu. Pogozhev ADVANCED SHS COMPOSITES AND COATINGS FOR THE HIGH-TEMPERATURE FIELDS OF APPLICATIONS	94
Z. Mansurov, Zh. Supiyeva, G. Smagulova, V. Pavlenko ELECTROCHEMICAL BEHAVIOUR OF GOLD IONS ON CARBON ELECTRODES PRODUCED FROM RICE HUSK	96
Z. Mansurov, N. Mofa, A. Zhapekova SYNTHESIS OF NANOCOMPOSITION CERAMICS BASED ON A SYSTEM WITH MODIFIED WOLLASTONITE	100
Z.Melashvili, T.Namicheishvili, [G.Tavadze], [A.Tutberidze], G.Parunashvili, Z.Aslamazashvili, J.Gamsakhurdia RESEARCHING OF SHS ELECTRICAL-ROLLING PROCESS OF METAL-CERAMIC MATERIALS ON BASE OF Ti-B SYSTEM.....	105
Z. Mirijanashvili, V. Gharibashvili, A. Kandelaki, V. Tsiklauri, K. Ukleba OBTAINING COMPOSITE POWDERS STRENGTHENED WITH HIGH-MELTING COMPOUNDS.....	111

S. Mebonia, J. Sharashenidze, A. Shermazanashvili RADIAL FORGING MACHINE FOR PROCESSING POROUS SINTERED WORKPIECES	117
A. Mikeladze, R. Chedia, L. Chkhartishvili, O.Tsagareishvili, N. Barbakadze, K. Sarajishvili, T. Korkia, M. Darchiashvili, V. Ugrekheldidze LIQUID CHARGE PRECURSORS FOR PRODUCTION OF B ₄ C–MeB ₂ FINE COMPOSITE POWDERS	121
M.Mikaberidze, D.Ramazashvili, S. Gvazava, V.Tediashvili, <u>G.Tavadze</u> , V.Tsintsadze, R.Bagratioti, A.Chkhikvadze, O.Gurushidze CORROSION RESISTANCE OF STEEL MIILUX -500 IN SALT SPRAY CHAMBER AND SUBTROPICAL CLIMATE OF THE ATMOSPHERE	127
M. Mikaberidze, Z.Melashvili, V. Tediashvili, S. Gvazava, D. Ramazashvili, N.Kvataia ELECTROCHEMICAL INVESTIGATIONS OF TiB _{0.6} ALLOYS OBTAINED BY SHS-ELECTRIC ROLLING METHOD.....	131
A. Mukasyan COMBUSTION SYNTHESIS OF CERAMICS: FUTURE DIRECTIONS	135
A.Peikrishvili, <u>G.Tavadze</u> , B.Godibadze, E.Chagelishvili, G.Mamniashvili, A.Shengelaya EXPLOSIVE CONSOLIDATION AND SYNTHESSES OF SUPERCONDUCTIVE COMPOSITES BASED ON MgB ₂	138
T.Qamushadze, E.Khutsishvili, Z. Davitaja, N.Kobulashvili, Z.Chubinishvili, R. Razmadze RADIATION-RESISTANT MATERIAL FOR THERMOELECTRIC PERFORMANCE	143
V. Sanin, D. Ikornikov, D. Andreev, S. Zherebtsov, V. Yukhvid CENTRIFUGAL METALLOTHERMIC SHS OF CAST CoCrFeNiMn BASED HIGH ENTROPY ALLOYS AND COATINGS OF THEM.....	147
A. Sytshev, S. Vadchenko, A. Shchukin, O. Boyarchenko INTERACTION OF CARBON WITH A Ti-Al MELT DURING SELF-PROPAGATING HIGH-TEMPERATURE SYNTHESIS	150
T.Sakharova, M.Heuken, Z.Jibuti, L.Sanikidze, M.Ksaverieva THE IMPROVEMENT OF Ti/Al/Ni/Au OHMIC CONTACTS TO UNDOPPED AlGa _N /Ga _N HEMT HETEROSTRUCTURES BY PULSE-PHOTON TREATMENT	154
R. Sakhvadze, G. Abashidze, D. Tsverava, L. Kirtadze DESIGN OF VACUUM FURNACE WITH PRESSING CAPACITY FOR POLYMER COMPOSITE MATERIALS	158
J.Sharashenidze, D.Gventsadze, S.Mebonia, G.Dadianidze, K.Papava INVESTIGATION OF TRIBOLOGICAL PROPERTIES OF WEAR-RESISTANT SURFACES WELDED BY POWDERY WIRE.....	161
V. Shapovalov, O. Berdnikova, Yu. Nikitenko, V. Yakusha, O. Gnizdylo PRODUCTION OF SUPER LARGE TUNGSTEN SINGLE CRYSTALS.....	165
V. Shapovalov, C.Shapovalov, R. Kachan, T. Skuba, O. Berdnikova THE APPLICATION OF ADDITIVE TECHNOLOGIES TO CONTROL THE PROCESS OF SEGREGATION IN THE PRODUCTION OF INGOTS AND CASTING.....	170

G.Tavadze, G.Zakharov, A.Khvadagiani, Z.Aslamazashvili, T.Batsikadze, A.Peikrishvili, G.Urushadze INTERMEDIATE RESULTS OF A STUDY OF THE SYNTHESIS OF GRAPHENE OXIDE	174
G. Tavadze, G. Oniashvili, Z. Melashvili, Z. Aslamazashvili, G. Zakharov OBTAINING AND STRUCTURAL ANALYSIS OF TiB _{0.6} METAL-CERAMIC TILES WITH SHS ELECTRIC-ROLLING PROCESS	179
V.Tsitsishvili SECONDARY POROUSITY OF MICROPOROUS ZEOLITES.....	184
V.Tsitsishvili, N. Dolaberidze, M.Nijaradze, N.Mirdzveli, Z.Amiridze NATURAL ANALCIME AS A RAW MATERIAL FOR ION EXCHANGERS	188
J. Khantadze, L. Chkhartishvili, G.Mikaberidze DYNAMIC MODELLING OF METAL MELTING PROCESS	192
N.Khuchua, R.Melkadze, A.Tutunjyan, N.Dolidze, T.Sakharova, L.Sanikidze, M.Ksaverieva, R.Gulyaev CHARACTERISTICS OF INFRARED P-I-N PHOTODIODES BASED ON VARIOUS In _{0.53} Ga _{0.47} As/InP HETEROSTRUCTURES	197
V.Yukhvid, D.Andreev, Yu.Vdovin SHS-METALLURGY OF MOLIBDENUM-BASED COMPOSITE MATERIALS	201
G.Zakharov, Z. Aslamazashvili, D.Kvaskhvadze, G.Tavadze, G.Oniashvili, G.Mikaberidze, G.Urushadze OBTAINING OF LOW CARBON LIGATURE IN THE Fe-B SYSTEM FROM STEEL ROLLING WASTE BY THE TECHNOLOGY SHS METALLURGY	205
G. Mikaberidze, K. Ukleba, J. Khantadze THE IDEAL REACTION AREA AND THE THRESHOLD OF SHS.....	209

SH-SYNTHESIS OF COMPOSITION MATERIALS ON THE BASIS OF TiB₂-TiC- MgO

R.Abdulkarimova*, K.Kamunur, A.Batkal, N.Assanbek

al-Farabi Kazakh National University, 71, al-Farabi str., Almaty, Kazakhstan

abdulkarimovaroza@mail.ru

ABSTRACT

In the present study TiB₂, TiC containing composite materials were obtained by SHS from a mixture of TiO₂, B₂O₃ (ore), C - carbonated rice husk (CRH) and Mg. The products SH-synthesis were characterized using X-ray diffraction analysis and scanning electron microscopy.

INTRODUCTION

Boron, borides and related compounds have unique bonding characteristics, structural, peculiarities and superior intrinsic properties. These materials, especially transition metal borides show high hardness, high melting point and electrical conductivity. Hence borides are strong candidates for wear resistant applications metals lead to low plasticity and low strength that considerably limits the field of their application [1]. However, strong covalent bonds inherent to the phases of pure diborides of transition. In this regard, at present great attention is paid to the technology of producing multi-component metals in combination with more plastic materials playing the role of binding. They are, for example, aluminium or magnesium oxide which play the role of a high-temperature binder and filler decreasing the content of expensive diboride, when obtaining composition materials.

One of the promising methods for obtaining composition materials is the method of self-propagating high temperature synthesis. Self-propagating high-temperature synthesis (SHS) is a method for producing inorganic compounds by exothermic reactions, usually involving salts. Since the process occurs at high temperatures, the method is ideally suited for the production of refractory materials with unusual properties, for example: powders, metallic alloys, or ceramics with high purity, corrosion-resistance at high-temperature or super-hardnessity [2].

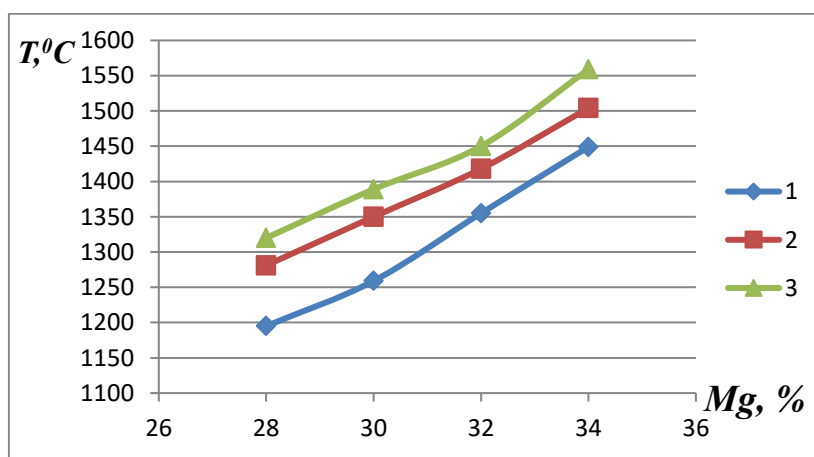
One of the main sources of boron ores in Kazakhstan are borates from the Inder deposit [3]. These wide available raw materials can be used to obtain boron-containing refractory composition materials [4].

METHODOLOGY OF EXPERIMENT

The mixtures were prepared with the different ratio of components: magnesium powder, borate ore, titanium oxide, carbonated rice husk (CRH). Preliminary mechanical activation of the samples was performed in the «Pulverizette-5» of a high-energy planetary centrifuge mill. Cylinders with the diameter of 20 mm and height 20÷30 mm were obtained with the help of a hydraulic press of the brand CARVER for production of pressed samples. The dried samples were burned at room temperature initiating ignition by magnesium. The temperature of SHS was measured using optical pyrometer. After combustion, the samples were structurally characterized by X-ray diffraction (XRD) using Dron – 4 diffractometers (operating with a Cu- Ka radiation source). The microstructure of the ceramic composite was studied by scanning electron microscopy (QUANTA 3D 200i, FEI, USA) electron.

RESULTS AND DISCUSSION

The study on the effect of preliminary mechanical activation (MA) of the charge on macrokinetic characteristics of SHS, phase composition and structure of the obtained composites in the system B_2O_3 –Mg–TiO₂–C with the use of borate ore is of both theoretical and practical application. The preliminary series of experiments showed that for initiating synthesis by burning local heating up to short duration with the help of initiation of the system by magnesium is quite enough, then the process occurs in the mode of a self-propagating combustion. The system under study is so active that does not require an additional heating up of the reaction medium.



1- non-activated; 2- activated for 5 min; 3- activated for 10 min

Fig. 1- Dependence of the combustion temperature of activated and non-activated systems in the atmosphere on the time of MA and the content of magnesium in the system Mg–TiO₂– B₂O₃(ore)-C

The use of preliminary MA of the charge in a high-power planetary mill significantly decreases the temperature of beginning of exothermal interaction of the mixture components, reduces the synthesis time of the final product, and results in a more complete procedure of chemical reactions [5].

Therefore, the powder of the prepared charge was activated for 3-10 minutes before SH-synthesis. As is seen in Figure 1, maximum temperature of combustion increases with both the increase in the content of magnesium and increase in the time of preliminary mechanical activation of the charge.

Acceleration of the chemical reaction after mechanical reaction is conditioned by «pumping » of additional (excessive) energy into the reacting substances, the energy accumulating in the formed structural defects. Excessive energy reduces the activation barrier of the chemical reaction. The effect of excessive energy on the reaction rate is a kinetic factor of acceleration of a chemical reaction [5,6].

A qualitative and semi-qualitative X-ray phase analysis of the composition of SHS products for the system Mg–TiO₂ – B₂O₃(ore) -C was carried out. The presence of high temperature phases – titanium diboride, titanium carbide, magnesium oxide and their spinels in the SHS products are determined by the method of X-ray analysis.

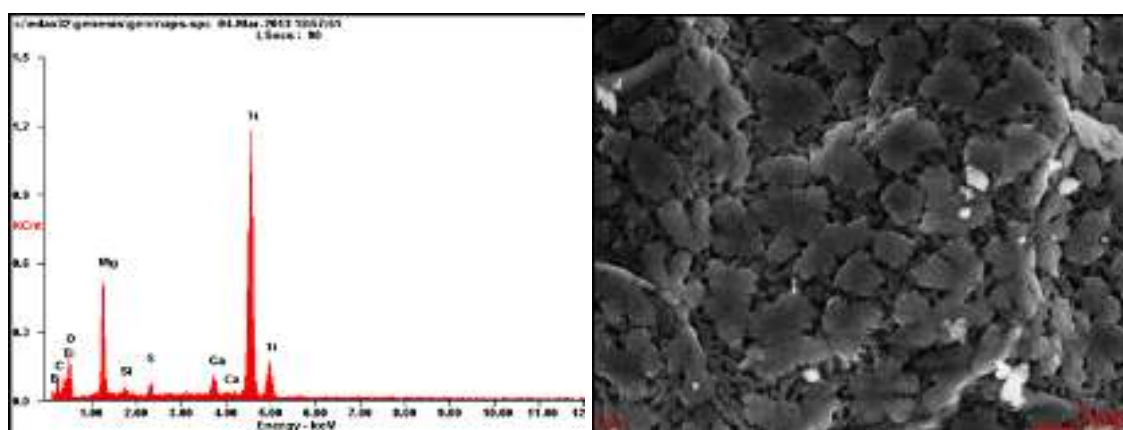


Fig. 2 – Microstructure of the composition material on the basis of TiB₂-TiC- MgO

Fig. 2 shows the microstructure of the resulting composite.

CONCLUSIONS

The possibility of using borate ore of Inder deposit of the Republic of Kazakhstan and model compounds of boron for production of boron containing composition materials in the system Mg-TiO₂-B₂O₃-C is shown. The effect of preliminary mechanical activation of the charge on macrokinetic characteristics of SHS, the phase composition and structure of the obtained composites in the system Mg-TiO₂-B₂O₃-C using borate ore is stated. The regularities of combustion depending on the charge composition and conditions of SH-synthesis have been studied.

REFERENCES

1. W.Weimin, F.Zhengyi, W.Hao, Y.Runzhang. Chemistry reactions processes during combustion synthesis of B₂O₃-TiO₂ - Mg system // J. Mater. Proc.Technol. - 2002. – P. 162-168.
2. Promising materials and technologies of self-propagating high-temperature synthesis / E.A. Levashov, A.S. Rogachev, V.V. Kurbatkina, Yu.M. Maximov, V.I.Yukhvid - MISIS, Moscow, 2011. - 377p.
3. Inder's natural wealth and use / M.D. Diyarov, D.A. Kalicheva, S.V. Meshcheryakov – Almaty. Science,1981. - 102p.
4. A.A. Aytkaliyeva, A. Zh. Seydualieva, R.G. Abdulkarimova Obtaining composite materials based on ZrB₂-Al₂O₃ by the method of self-propagating high-temperature synthesis // Chemical Journal of Kazakhstan. 2016. – №2. – p.10-15.
5. Fundamental bases of mechanical activation, mechano-synthesis and mechano-chemical technologies / under ed. of E.G. Avakumov. – Novosibirsk: Nauka, 2009. – 342 p.
6. M.A.Kopchagin, D.V. Dudin The use of self-propagating high temperature synthesis and mechanical activation for production of nanocomposites // Physics of combustion and explosion. – 2007. – Vol.43, №2. – P. 58-71.

NEW DIRECTIONS OF APPLICATION OF MACROKINETIC APPROACHES IN ISMAN

M.Alymov^{*}, B.Seplyarskii

Merzhanov Institute of Structural Macrokinetics and Materials Science, Russian Academy of Sciences, Russia, Chernogolovka

* director@ism.ac.ru

Merzhanov Institute of Structural Macrokinetics and Materials Science, Russian Academy of Sciences is a developing research institution. In the mid fifties, A.G. Merzhanov and co-workers began to study thermal explosion and wave propagation in condensed systems. These researches became a direct continuation and development of the ideas and methods of N.N. Semenov and his school. In a short period, the theory of thermal explosion in condensed systems was developed, and appropriate experimental techniques for determining the parameters of thermal explosion were designed and manufactured.

In 1967, A.G. Merzhanov, I.P. Borovinskaya, and V.M. Shkiro came to a scientific discovery officially termed the "solid flame phenomenon". Solid flame is a process in which starting reactants, intermediate products, and final products are present in their solid state throughout the entire process. Solid flame combustion turned out to yield valuable refractory compounds. The problem of the "solid flame" relates to many scientific disciplines, as a result the directions of researches related to thermodynamics, physicochemical kinetics, structural and phase transformations, nonlinear effects in highly nonequilibrium systems, and heat and mass transfer processes appeared. This circumstance has led to creating a novel, highly efficient production method – Self-propagating High-temperature Synthesis (SHS) – which is based on ideas of N.N. Semenov, Ya.B. Zel'dovich, and D.A. Frank-Kamenetskii.

Combination of ideas and development of novel experimental and theoretical methods have led to foundation of a new research direction – structural macrokinetics – studying physicochemical and structure transformations of substance in the nonequilibrium systems.

Combination of the macrokinetic and materials studies has become a distinctive feature of the Institute, which was founded in 1987.

The purpose and scope of Institute activities are to carry out fundamental, research, and applied scientific studies in the field of physics and chemistry of combustion and explosion processes, including self-propagating high-temperature synthesis, physicochemical transformations of substances under high temperatures and pressures, and materials science.

The works of Institute have interdisciplinary character. Scientific and production organizations implementing new technologies and manufacturing new materials were established. SHS-produced materials allow finding new solutions to a wide variety of problems (from ecology to the description of natural phenomena).

Particular attention in the presentation is drawn to the application of methods of the theory of ignition and combustion to ensure the safety of operations with non-passivated nanopowders and related compact products. Metal nanopowders are pyrophoric, i.e. capable of self-igniting upon contact with air due to high chemical activity and large specific surface. In order to make the safe process of further processing of nanopowders into products, they are passivated. Within the framework of the RSF project (no. 16-13-00013P), various macrokinetic modes (self-ignition or combustion mode) of interaction between the compact samples of pyrophoric iron nanopowders and the air were detected and investigated. The effect of porosity of compact samples on the dynamics of their heating was studied.

It was found that the maximum temperature of self-heating decreases with increasing relative density of samples, which indicates that the oxidation process is limited by the diffusion supply of the oxidizing agent. It was shown that the process of interaction between the samples and the air is superficial. A qualitative agreement between the results of theoretical analysis and experimental data was obtained. The dependence of mode of sample-air interaction on the duration of the presence of boxes in air was found. The possibility of passivation of samples made of iron nanopowders was experimentally established.

The work was supported by the Russian Science Foundation (project no. 16-13-00013P).

MOLECULAR STRUCTURE OF BIS (LIDOCAINE) TETRATHIOCYANOCOBALTATE(II) MONOHYDRATE

K.Amirkhanashvili*¹, A.Sobolev², V.Tsitsishvili¹, N.Zhorzholiani¹

¹ Petre Melikishvili Institute of Physical and Organic Chemistry at Tbilisi State University, 31 A.Politkovskaia str., Tbilisi 0186, Georgia

²University of Western Australia, 35 Stirling Highway, Perth 6009 WA, Australia.

* amirhan@hotmail.com

A new cationic-anionic complex was obtained in water-methanol solution with 1:2:4 molar ratio of the cobalt chloride, lidocaine, and potassium thiocyanate; the composition of the complex is described by an empirical formula $C_{32}H_{48}CoN_8O_3S_4$. The crystal and molecular structure of the complex was determined using single crystal (blue plate with sizes $0.33 \times 0.30 \times 0.10$ mm³) X-ray diffraction method. X-ray diffraction measurements were carried out with an Oxford Diffraction XCALIBUR E CCD diffractometer equipped with graphite-monochromated MoK α radiation ($\mu = 0.709$ mm⁻¹, $F_{000} = 822$, $\lambda = 0.71073$ Å, $T = 100(2)$ K). The data collection, cell refinement and data reduction were carried out with the CrysAlis^{PRO} package of Rigaku Oxford Diffraction [1]; theta range for data collection was up to $2\theta_{max} = 64.0^\circ$, 40364 reflections collected, 12544 unique ($R_{int} = 0.0338$). The structure was solved by direct methods and refined against F^2 with full-matrix least-squares using the programs complex SHELXL-2014 [2]; final $GOF = 1.001$, $R_I = 0.0361$, $wR_2 = 0.0882$, R indices based on 10495 reflections with $I > 2\sigma(I)$ (refinement on F^2), $|\Delta\rho|_{max} = 0.54(7)$ e Å⁻³, 465 parameters, 5 restraints.

The compound crystallizes in the triclinic centrosymmetric space group $P-1$ (No. 2), with the following unit cell parameters: $a = 8.7209(2)$, $b = 11.8438(3)$, $c = 19.9384(5)$ Å, $\alpha = 80.581(2)$, $\beta = 78.485(2)$, $\gamma = 72.783(2)^\circ$, $V = 1915.47(8)$ Å³, $Z = 2$, $D_c = 1.352$ g/cm³.

According to the X-ray crystallography, the investigated compound has a molecular crystal structure of bis(lidocaine) tetrathiocyanatocobaltate(II) monohydrate, in which coordination of the Co²⁺ ion with four thiocyanate (rhodanide) anions generates distorted tetrahedral anion $Ni[(NCS_4)]^{2-}$ with N -bonded thiocyanates, while two protonated cations LidH⁺ and one water molecule remain in an outer coordination field (Fig. 1).

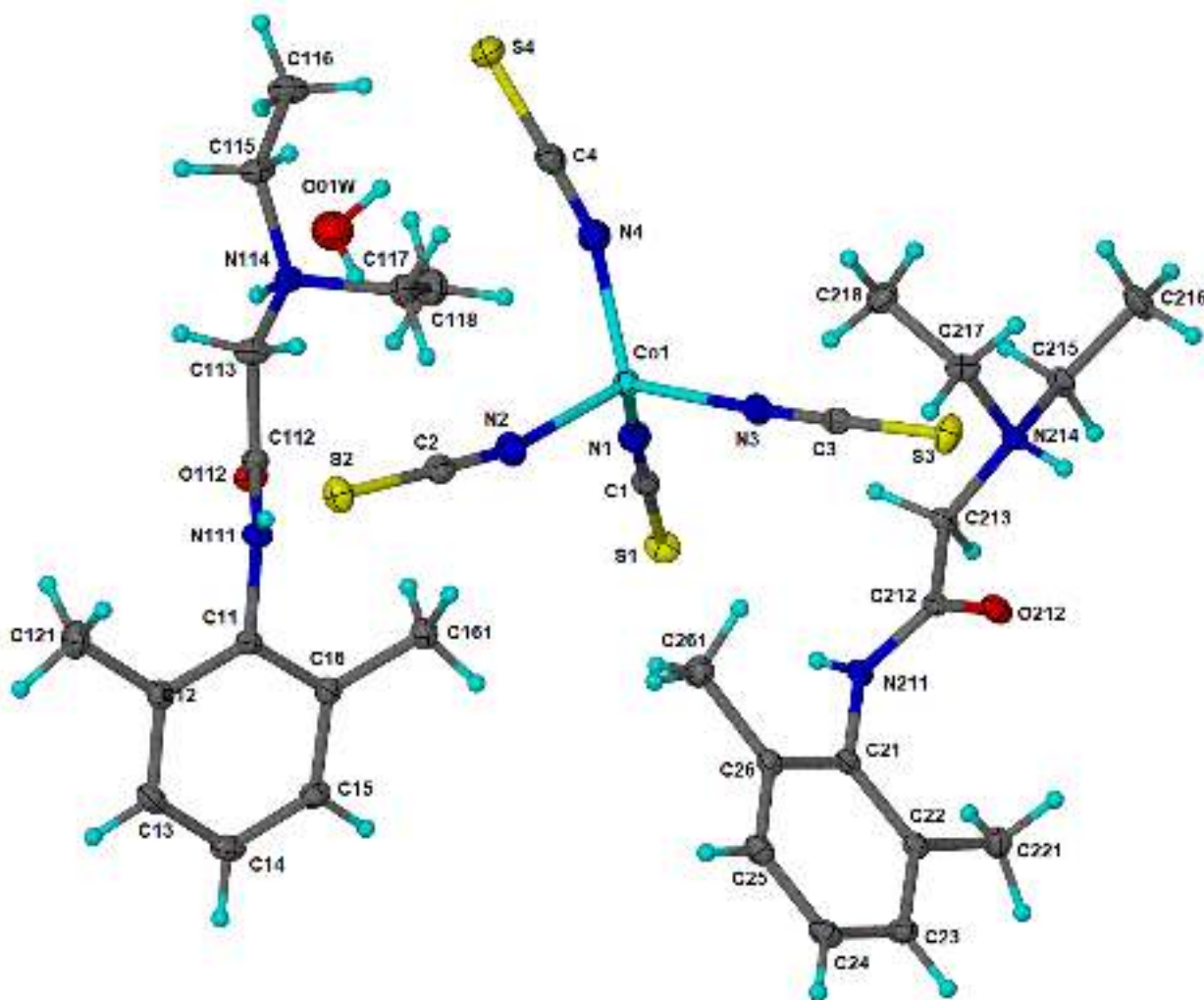


Fig. 1. Molecular structure of the $(\text{LidH})_2[\text{Co}(\text{NCS})_4]\cdot\text{H}_2\text{O}$ complex with atom labelling.

Nitrogen atoms in the CoN_4 tetrahedron are located at approximately equal distances from the central cobalt atom (the lowest value is $1.9531(13)$ Å for the Co-N1 bond, the largest $1.9694(12)$ Å for the Co-N2 bond), but the angles between the N-Co-N bonds deviate from tetrahedral with a minimum of $104.95(5)^\circ$ for angle N2-Co-N4 and a maximum value of $111.22(4)^\circ$ for angles N1-Co-N4 and N2-Co-N3 . The cobalt atom and the atoms of nitrogen, carbon and sulfur of the thiocyanate groups do not lie on the straight line, deviations relate to the greatest extent to the angles Co-N-C , having values from $160.61(12)^\circ$ for Co-N4-C4 to $177.28(11)^\circ$ for Co-N3-C3 ; -N-C-S angles are close to 180 degrees (from $178.56(12)^\circ$ for angle N3-C3-S3 to $179.36(14)^\circ$ for angle N1-C1-S1). Apparently, the tetrahedral coordination distortions are caused by hydrogen bonds in which the sulfur atoms of three thiocyanate groups participate (see Table 1).

Table 1. Hydrogen-bond geometry.

D–H···A	D–H (Å)	H···A (Å)	D···A (Å)	D–H···A (°)
N211—H211···S1	0.83 (1)	2.87 (2)	3.6550(12)	157(2)
N111—H111···S2	0.83 (1)	2.52 (2)	3.3295(12)	164(2)
O01 <i>W</i> —H01 <i>B</i> ···S2	0.86 (1)	2.84 (2)	3.4870(14)	134(3)
O01 <i>W</i> —H01 <i>A</i> ···S4	0.86 (1)	2.52 (1)	3.3479(15)	162(3)
N114—H114···O112 ^{II}	0.88 (1)	1.95 (2)	2.8036(14)	166(2)
N214—H214···O212 ^{IV}	0.88 (1)	2.16 (2)	2.9158 (14)	143(2)

Symmetry codes: (ii) $-x+2, -y+1, -z$; (iii) $x+1, y, z$.

So, sulfur atom S1 enters into a hydrogen bond with the nitrogen atom N211 of the “right” cation of lidocaine, sulfur atom S2 forms a bifurcated hydrogen bond with the nitrogen atom N111 of the “left” cation and a water molecule, while sulfur atom S4 forms a hydrogen bond through the second hydrogen atom of the water molecule. The distance between the donor and the acceptor exceeds 3.3 Å, and these hydrogen bonds are relatively weak.

Generally, the aromatic rings in the LidH⁺ cations are asymmetric, but the deviations of the C–C bond lengths and angles from the standard ones are insignificant, the torsion angles are small, and the aromatic rings can conditionally be considered flat.

The C11–N111, N111–C112, C112–O112 and C112–C113, as well as the C21–N211, N211–C212, C212–O212 and C212–C213 bond lengths are typical for crystalline carboxamides [3]. According to the values of the corresponding torsion angles (see Table 2), in the “left” cation the amide group is twisted out from the plane of the aromatic ring by $\approx 68^\circ$, in the “right” cation – by $\approx 104^\circ$. For both cations the aromatic ring and the oxygen atom adopt a *synperiplanar* (cis) conformation with respect to the N111–C112 and N211–C212 bonds, while the aromatic ring and diethylamino chain adopt the *antiperiplanar* (trans) conformation.

Table 2. Torsion angles in LidH⁺ cations from aromatic rings to diethylamino chain.

Atoms	(°)	Atoms	(°)
C16–C11–N111–C112	67.49(17)	C26–C21–N211–C212	103.84(14)
C11–N111–C112–O112	–4.0(2)	C21–N211–C212–O212	–3.2(2)
C11–N111–C112–C113	173.06(12)	C21–N211–C212–C213	173.29(11)
N111–C112–C113–N114	158.65(11)	N211–C212–C213–N214	167.90(11)
O112–C112–C113–N114	–24.20(18)	O212–C212–C213–N214	–15.45(17)

In general, the flexible parts of lidocaine cations have the same conformations, but differ in structural details. In both cations the amido and amino nitrogen atoms adopt an *antiperiplanar* conformation. Such staggered conformation excludes the formation of an intramolecular hydrogen bond N–H···N noted in the lidocaine free base [4] and its molecular complex, when

the nitrogen atoms adopt a *synperiplanar* conformation [5]. On the contrary, if the carbonyl oxygen atom and the nitrogen atom of the amino group adopt the *synperiplanar* conformation, it leads to the formation of a relatively strong intramolecular hydrogen bond N–H···O in the LidH⁺ cations [6]. However, in the studied compound, the interatomic distance between the donor and the acceptor exceeds 3.1 Å, while the distance between the amino nitrogen atom and the carbonyl oxygen atom in the neighboring cell is 2.8-2.9 Å (see Table 1), as generated by the SHELXL program. According to this data, the picture of intermolecular hydrogen bonding in bis(lidocaine) tetrathiocyanatocobaltate(II) monohydrate is rather complicated, and consideration of the crystal packing, as well as participation in its formation of “non-classical” C–H···O and C–H···S hydrogen bonds, is the next step in our work.

This research was carried out with the financial support of the Shota Rustaveli National Science Foundation of Georgia, project FR 18-3889.

REFERENCES

1. CrysAlis PRO, version 1.171.38.46, Rigaku Oxford Diffraction, 2015.
2. G.M. Sheldrick, Acta Crystallographica, C71(1), 2015, pp. 3-8.
3. The chemistry of amides, ed. by J. Zabitsky, Interscience, London, New York, 1970, pp. 2.
4. M. Bambagiotti-Alberti, B. Bruni, M. Di Vaira, V. Giannellini, A. Guerri, Acta Crystallographica, E63, 2007, pp. 768-770.
5. N.E. Magaña-Vergara, P. de la Cruz-Cruz, A.L. Peraza-Campos, F.J. Martinez-Martinez, J.S. Gonzalez-Gonzalez, Crystals, 8, 2018, pp. 130-138.
6. K. Amirkhanashvili, A. Sobolev, N. Zhorzholiani, V. Tsitsishvili, T. Vardosanidze, XXI Mendeleev Congress on General and Applied Chemistry, Saint-Petersburg, Russia, Book of abstracts, 5, 2019, p. 300.

SiGe ALLOYS SYNTHESIZED BY HOT PRESSING AND A THERMOELECTRIC GENERATOR CREATED ON THEIR BASE

K. Barbakadze*, G.Bokuchava, Z.Isakadze, A.Kutsia, I.Tabatadze, M.Barakadze, M. Rekhviashvili

Ilia Vekua Sukhumi Institute of Physics and Technology, Tbilisi, Mindeli street, 7, Georgia

* barbaqa@gmail.com

A thermoelectric generator (TEG) converts heat energy (temperature differences) directly into electrical energy. Its operation does not depend on weather and/or time. TEGs are widely used in distant regions of the Earth for autonomous servicing special objects located under water and in space. Their use is urgent for electric supply of information and monitoring systems operating in hardly accessible localities.

The wide use of microelectronic devices necessitated the creation of low-power (1-5 W), durable (1 year and more), continuous sources of power. Many such TEGs have been created, wherein radioactive isotope or natural gas is used as a source of heat. They are built on the base of low-temperature (Bi-Te-Se-Sb) and medium-temperature (Pb-Te-Ge) alloys. The building of a similar TEG on the base of high-temperature SiGe alloy seems to be more promising.

The main working node of a TEG presents branched made of n- and p-type thermoelectric materials. They convert the heat energy into electric power. The efficiency (η) of branch is proportional to the temperature differences between its hot and cold ends $T_h - T_c$ and to the efficiency of the thermoelectric material used in it $Z = \alpha^2 \sigma / \lambda$ (where α is the Seebeck coefficient $V \cdot K^{-1}$, σ – electrical conductivity $Ohm^{-1} cm^{-1}$, and λ – thermal conductivity $W \cdot cm^{-1} K^{-1}$). Hence, the building of high-temperature TEG on the base of highly efficient thermoelectric materials is energetically justified.

To build a high-temperature TEG from the known thermoelectric material, the n- and p-type alloys have been used [1,2]. An intensive research work at Sukhumi Institute of Physics and Technology in the direction of their development and practical use has been conducted since 1954. In particular, the n- and p-type $Si_{0.93}Ge_{0.07}$ and $Si_{0.68}Ge_{0.32}$ thermoelectric alloys have been developed. In 1984, a reactor TEG ROMASHKA was built on the base of the first of them; in 1989, a reactor TEG BUK of space designation was built on the base of the second alloy. The both of them were successfully tested in practice. The SiGe alloys combine well high working temperature (up to 1100 °C) and comparatively high efficiency ($Z=0.6-0.8 \cdot 10^{-4}$).

³.K⁻¹). By these features the potential η of these alloys exceeds 10%. Additionally, the SiGe alloys are capable of stable operation in the air at up to 1000 °C and generate the greatest electrical power (up to 2 W) from the effective area unit [3].

Polycrystalline Si and Ge were used as main components of the SiGe alloys, amorphous B as doping components for p-type alloys, as well as amorphous phosphorus for n-type alloys [4-6]. Si and Ge mass fragments were preliminarily ground by in a metal mortar and the produced powder was sieved in a 0.16 mm screen. Thereafter the SiGe alloy charge was placed in a chamber of RETSCH planetary ball mill PM-100 CM to be ground into 0.1 μ m grain-containing powder for 20 hours. The mass samples produced from the powder were compacted in an induction press, in vacuum, at the temperature of 1250-1370 °C, by 480 kg pressing, for 20-30 minutes. The matrix and punches were made from solid graphite. The isothermal homogenizing annealing of the samples in the air and vacuum took place at the temperature of 1200–1300 °C. Table 1 presents the study results of the thermoelectric features of the produced SiGe alloy. The described SiGe alloys synthesis method is easily performed, the thermoelectric characteristics being similar to those obtained by another method.

Thermoelectric characteristics of n- and p-type Si_{1-x}Ge_x alloys at 25 °C

x	0	1	2	3	4	5	10	20	32*
$\alpha_n \cdot 10^{-6} \cdot \text{v} \cdot \text{K}^{-1}$	98	94	90	88	88	92	97	105	142
$\alpha_p \cdot 10^{-6} \cdot \text{v} \cdot \text{K}^{-1}$	145	130	101	96	95	85	92	93	105
$\sigma_n \cdot \text{Om}^{-1} \cdot \text{cm}^{-1}$	2381	2000	1923	1887	1887	1666	1613	1587	769
$\sigma_p \cdot \text{Om}^{-1} \cdot \text{cm}^{-1}$	2222	2128	2000	2000	1960	1923	1754	1587	1042
$\lambda_n \cdot 10^{-2} \cdot \text{W} \cdot \text{K}^{-1} \cdot \text{cm}^{-1}$	47	24	14	11	8.2	7.0	6.4	5.6	5.0
$\lambda_p \cdot 10^{-2} \cdot \text{W} \cdot \text{K}^{-1} \cdot \text{cm}^{-1}$	51	29	14	11	9,6	7.6	6.8	6.2	5.7
(n) $\alpha^2 \sigma \cdot 10^{-6} \cdot \text{W} \cdot \text{K}^{-2} \cdot \text{cm}^{-1}$	22.8	17.7	15.6	14.6	14.6	14.1	15.2	17.5	15.5
(p) $\alpha^2 \sigma \cdot 10^{-6} \cdot \text{W} \cdot \text{K}^{-2} \cdot \text{cm}^{-1}$	46.7	35.9	20.4	18.4	1.7	13.9	14.8	13.73	11.5
$Z_n \cdot 10^{-3} \cdot \text{K}^{-1}$	0.05	0.07	0.10	0.13	0.18	0.20	0.24	0.31	0.31
$Z_p \cdot 10^{-3} \cdot \text{K}^{-1}$	0.09	0.12	0.15	0.17	0.18	0.18	0.20	0.22	0.22

32*- Characteristics of SiGe alloys used in space power engineering [6].

Given the electrophysical characteristics of the SiGe alloys, it was decided to build a monolithic mini TEG containing 16 branches (8 of n-type and 8 of p-type), the cross-section area of which will be 1.3x1.3 cm², height - 2 cm. The cross-section area of each its branch will be 0.3x0.3 cm², the height – 1.5 cm. The branches will be interconnected in succession. A natural gas burner will be used as heater, whereas an air radiator operating on the principle of

a heat pipe – as cooler. Under conditions of operation, the temperature of the converter's hot ends will make 700 °C, and 70 °C – of the cold ends.

Pre-estimates show that the TEG's potential energetic characteristics in case the n- and p-type $\text{Si}_{0.68}\text{Ge}_{0.32}$ alloys are used [7] will be: $E=1.85$ V; $R= 0.56$ Ohm; $W=1.5$ W; $Q=31.2$ W; $\eta=6,5\%$. In the future, for raising the electrodriving force, 2-3-times higher α -possessing n- and p-type SiGe alloys will be developed.

Figure 1 shows a photograph of a mini TEG of the mentioned design built on the base of n- and p-type $\text{Si}_{0.90}\text{Ge}_{0.10}$ alloys. Its branches are separated from one another by electrically insulating layers.



Fig. 1. Mini TEG based on n- and p-type $\text{Si}_{0.90}\text{Ge}_{0.10}$ alloys

The B-doped Si is used as an interconnect material of the hot side, electrode graphite being used as an interconnect material of the cold side. Soldering of interconnect plates with the SiGe alloy was carried out by the Fe-Ni alloy. The converter is mechanically stable and heat-resistant. Its electric resistance is 0.284 Ohm, which exceeds by 6% the value calculated from the electric resistance of the used thermoelectric material.

REFERENCES

1. Braun J.F. In: proc. of XIX International Conference of the Energy Conversion. S.-Petersburg, 1995, pp. 394-400
2. G. V. Bokuchava. ВАНТИ, Серия: ФПП и РМ. 2005, №3 (86), с. 68-72. 82.
3. K. Barbakadze, G. Bokuchava, Z. Isakadze, A. Kutsia, I. Tabatadze, M. Barbakadze, M. Rekhviashvili. Electrical insulating assembly on base aluminum nitride for thermoelectric batteries. ENERGY. №3(91), Tbilisi, 2019, pp 18-23
4. K. Barbakadze, M. BiliseiSvili, Z. Isakadze, I. Tabatadze, V. Gabunia, A. Kutsia, M. Barbakadze, M. Rekhviashvili. Development of thermoelectric n- and p-tipe $\text{Si}_{0.95}\text{Ge}_{0.05}$ alloys and creation on their base thermoelectric batteries, working in till temperature 1000°C . Proceedings of International Conference “Advanced Materials and Technologies”. 2015, Tbilisi, Georgia, pp.110-114 (in Russia).
5. K. G. Barbakadze, Z. N. Isakadze, A. A. Kutsia, M. G. Barbakadze, M. G. Rekhviashvili and I. M. Tabatadze. Manufacturing and investigation of the thermoelectric alloys $\text{Si}_{0.95}\text{Ge}_{0.05}$ n- and p - type conductivity. 3rd International Conference “Inorganic Materials Science Modern Technologies and Methods”. 2018, Tbilisi, Georgia. pp.16-18.
6. G. V. Bokuchava, F. Marquis, B. M. Shirokov, K.G. Barbakadze, G.Sh. Darsavelidze. The Main Stages of Development of Thermoelectricity in Ilia Vekua Sukhumi Institute of Physics and Technology. SIPS 2017 Vol. 5. Marquis Intl. Symp. / New and Advanced Materials and Technologies. ISSN: 2291-1227
7. А.М.Глазова, В.ФЖуков, П.Н. Инглизян, С.П.Лалыкин, И.М.Шевченко. Термоэлектрические свойства сплавов Si-Ge при высоких температурах. ИБ ППТЭЭ и ТЭ, 6 (80), 1977, с. 101-105.

LASER AND HYBRID WELDED JOINTS OF LOW-ALLOY HIGH-STRENGTH STEELS: THE RELATIONSHIP OF STRUCTURE AND OPERATION PROPERTIES.

O. Berdnikova*, V. Sydorets, A. Bernatskyi, T. Alekseienko, O. Bushma, I. Alekseienko

E. O. Paton Electric Welding Institute of the NAS of Ukraine, Kazimir Malevich Str., 03650, Kyiv, Ukraine

* omberdnikova@gmail.com

Low-alloyed high-strength steels are widely used in various branches of modern industry, including construction, agricultural, transport, engineering and defense, for the manufacture of welded metal structures. Machinery and constructions of critical purpose require the use of steels of a wide class of strength in a fairly wide range of mechanical properties and, accordingly, of different structural and phase composition. Many structures of high-strength steels are structures of long-term use under external loading conditions. Therefore, the study of the influence of structural factors on the mechanical properties and crack resistance of welded joints of these steels becomes important. Nowadays in the manufacture of these metal structures, mechanized or automatic welding in shielding gases is used. Often they are replaced such progressive technologies as laser and hybrid laser-arc welding, which allow to obtain welded joints at increased speed with much smaller dimensions of welds and heat-affected zones (HAZ), as well as to improve the quality of joints of high-strength steel and the to raise productivity of their manufacture.

OBJECTIVES OF THE RESEARCH

Our main idea is to obtain welded joints with high operational properties, using both traditional and advanced welding technologies by selecting the requisite modes for each process. The aim of the work was to determine the regularities of influence of the structural-phase composition of the metal of welded joints of low-alloyed high-strength steel on the mechanical properties of these joints; revealing ways to optimize the welding process parameters (heating and cooling rates, heat input) for each method (laser and hybrid laser-arc) fusion welding.

TECHNIQUES AND EQUIPMENT

A comprehensive approach is needed to solve this problem. We adhere to it and recommend everyone to do it. Its essence consists in carrying out materials science research at all structural levels from grain to dislocation. This is done using three types of microscopy: Optical microscopy, Analytical scanning electron microscopy, and Transmission electron

microscopy. Optical microscopy allows determining: size and microhardness of grains and volume fraction of the phases of the structure. Analytical scanning electron microscopy allows determining: chemical composition size and distribution of phase particles and make fractographic analysis. Transmission electron microscopy allows determining: density and distribution of dislocation, substructures, segregations.

RESULTS AND DISCUSSION

Studies were carried out on samples of welded joints of high-strength steel (0.14% C) with an 8 mm thick bainite-ferrite structure produced by an laser (modes #1-#3) and a hybrid laser-arc (modes #4-#6) welding. In the case of hybrid laser-arc welding, filler wire was used. Nd:YAG-laser DY 044 was used as a source of laser radiation. Table 1 presents the parameters of the welds: the weld width, the total width of the HAZ and the width of the overheating zone – I HAZ as the most important zone. The small dimensions of welds and HAZ should help reduce the level of local internal stresses in the metal of welded joints and increase their crack resistance.

Table 1. Welds and HAZ parameters and their mechanical and structural properties.

No.	Weld			HAZ			I HAZ		
	Width (mm)	Micro-hardness (MPa)	Grain sizes (μm)	Dislocation density (cm^{-2})	Width (mm)	Width (mm)	Micro-hardness (MPa)	Grain size (μm)	Dislocation density (cm^{-2})
#1	5.0	2850...3510	50...90×150...410	(2...4)·10 ¹⁰	2.0	0.4	3830...4170	50...90	(4...6)·10 ¹⁰
#2	4.0	3450...4010	30...100×120...400	–	1.9	0.3	4010...4420	30...80	–
#3	3.3	3870...4330	20...40×100...400	(4...6)·10 ¹⁰	0.8	0.25	4010...4250	30...60	(8...10)·10 ¹⁰
#4	4.0	3800...4010	30...120×170...350	(4...6)·10 ¹⁰	1.9	0.3	3540...3900	30...60	(6...8)·10 ¹⁰
#5	4.3	4050...4420	30...80×150...300	–	1.6	0.35	3830...4010	25...50	–
#6	4.2	3360...3940	20...80×150...250	(6...8)·10 ¹⁰	1.4	0.23	3360...4010	20...40	(8...10)·10 ¹⁰

In laser welding, studies have shown that at 880 J/mm (#1) a bainite-ferrite structure is formed in the weld metal and HAZ, mainly the B_U (correspondingly 55% and 35%), Fig. 1a. When the heat input decreases to 316 J/mm (#3), the phase composition of the weld metal and HAZ changes from bainite-ferrite to bainite-martensite, Fig. 1b, c. Also crushing of the grain and subgrain structure in 1.3...1.4 times occurs with a certain increase in microhardness. Fine-grained grain structure of lower bainite (B_L) is mostly (45...50%) formed under conditions of uniform redistribution of the volume dislocation density in the weld metal $\rho = (6...8) \times 10^{10} \text{ cm}^{-2}$, and in the metal of HAZ $\rho = (8...9) \times 10^{10} \text{ cm}^{-2}$.

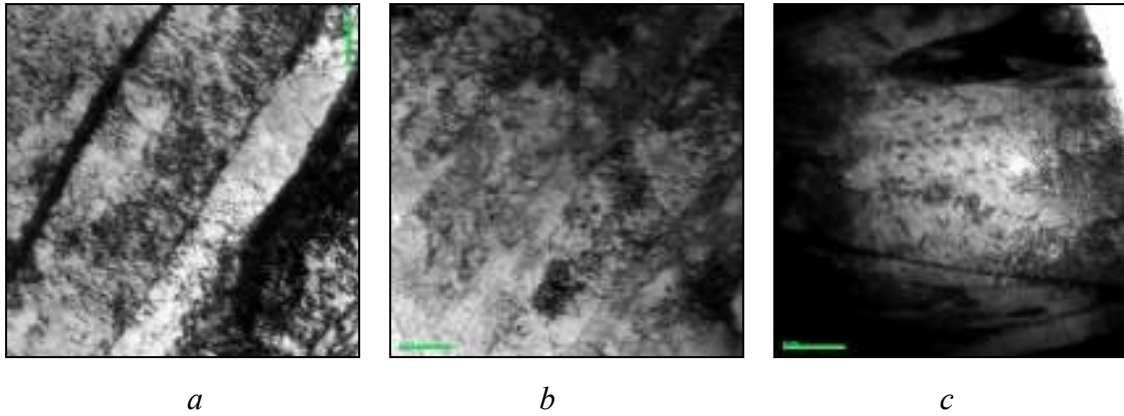


Fig. 1. The microstructure of welded joints produced by laser welding at 880 J/mm (a); 316 J/mm (b, c).

Studies of the structure and phase composition of welded joints in hybrid laser-arc welding have shown that when going from 363 J/mm (#4) to 314 J/mm (#6), the phase composition of metal of the weld and the overheated HAZ remains the same (bainite-martensite). However, the volume fraction of B_L decreases noticeably (up to 10...20%). Herewith, in the case of 314 J/mm, the integral value of the dislocation density increases to $\rho = 1.5 \times 10^{11} \text{ cm}^{-2}$ and the mostly structure of the B_U is formed, Fig. 2c. And the most uniform distribution of dislocation density $\rho = (4...6) \times 10^{10} \text{ cm}^{-2}$ is characteristic for the B_L structures at 363 J/mm, Fig. 2a, b.

It should be noted that in this case an increase in the density of dislocations is observed while a decrease in heat input from 363 J/mm to 314 J/mm. Perhaps this is due to a change in the ratio of the contribution of the arc and laser components of the hybrid process in the resulting value of heat input, namely, with a relative increase in the contribution of the arc component from 39% to 54%.

As a result of mechanical testing of welded joints, it was found that the most stable values of strength and ductility are characteristic of laser welding conditions. However, welded joints produced by hybrid laser-arc welding are characterized by the highest ultimate strength. Herewith, the optimal structure, from the point of view of phase composition (mainly B_L , more than 50%) and a gradient-free dislocation density distribution, is formed at 363 J/mm with a maximum contribution to the heat input of the laser component.

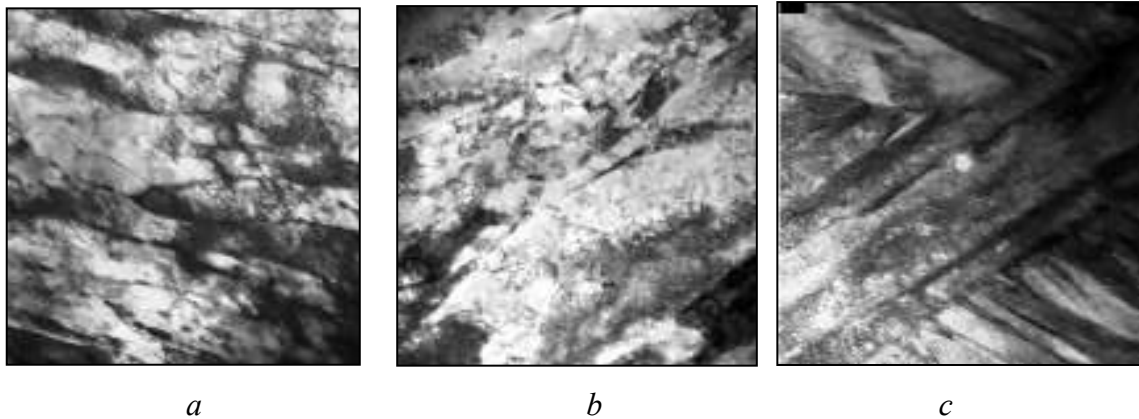


Fig. 2. The microstructure of welded joints produced by hybrid welding at 363 J/mm (a,b); 314 J/mm (c).

CONCLUSIONS

The structure and properties of welded joints of low-alloyed high-strength steel depend on the welding methods and the modes used.

Under various welding conditions, the following structure transformations are observed: the ratio of the phase components forming in the welding zones (lower bainite, upper bainite, martensite), as well as their parameters and volume fraction, changes.

Hybrid laser-arc and laser welding is characterized by the formation of lower bainite structures with significant refinement of the grain and subgrain structure with a uniform distribution of the dislocation density.

A significant increase in strength, ductility and crack resistance of welded joints of low-alloyed high-strength steel at a decrease in heat input and a transition to laser and hybrid laser-arc welding evidences the validity of the relationship “welding method (modes) → structure → properties”.

REFERENCES

1. R. Oyyaravelu, P. Kuppan and N. Arivazhagan. Metallurgical and mechanical properties of laser welded high strength low alloy steel. *Journal of Advanced Research*, 3, 2016, pp. 463-472.
2. V. Poznyakov, O. Berdnikova and O. Bushma. Laser and hybrid laser-arc welding of high strength steel N-A-XTRA-70. *Mater. Sci. Forum*, 870, 2016, pp. 630–635.

STUDY OF CRYSTALLOGRAPHIC STRUCTURE WITH THE HELP OF ELECTRON DIFFRACTION IN SCANNING ELECTRON MICROSCOPY

A.I. Berner*

Technion – Israel Institute of Technology, Technion city, Haifa 32000, Israel.

[*alik.berner@gmail.com](mailto:alik.berner@gmail.com)

Scanning electron microscopy (SEM) is one of most important techniques for materials characterization. The easy of SEM application to imaging surface morphology of different specimens in their natural state makes this technique a necessary instrument for research study in such fields as metallurgy, semiconductors, ceramics, composite materials, mineralogy, etc. Recently the development of a new generation of high resolution (HR) and environmental SEM expanded its applicability to the investigation of new nanostructured and bio-materials. Chemical characterization of materials at micrometer scale is performed as a rule by a combination of SEM and Energy Dispersive Spectroscopy (EDS) techniques. EDS in SEM faces frequently essential problems connected, first, to small sizes (micron and sub-micron) of structural constituents, which can be smaller than the characteristic size of X-ray excited volume. This leads to considerable inaccuracy in results of EDS. An additional problem decreasing accuracy of chemical analysis is a presence of light elements (B, C, N and O). Currently, determination of light elements by EDS is not specified well even for cases when the analyst has not restrictions in sizes of analyzed particles. One more difficulty is a possible overlap of characteristic X-ray peaks of metals with peaks of light elements (for example, strong overlap of Ti $L\alpha$ and N $K\alpha$ characteristic peaks). Taking into account that carbon is most frequently contained in surface contaminations and presence of oxygen can be often explained by partial surface oxidation one can conclude that EDS analysis of such specimens is extremely difficult and ambiguous. One way to override the indicated difficulties is to combine a local chemical data with a local crystallographic data. However, obtaining a local crystallographic information about structure, orientation relationship, preferred orientation, etc. in SEM presented a real challenge until recently. In the present paper, principles and possibilities of two techniques for determination and analysis of local crystallographic structure in SEM: Electron Back Scatter Diffraction (EBSD) and Transmission Kikuchi Diffraction (TKD) [1, 2] will be considered.

EBSD patterns are formed in SEM when a stationary probe is focused on a steeply inclined specimen. Initially, the incident beam is scattered quasi-elastically through large angles within the specimen, so that the electrons diverge from a point source just below the specimen surface and impinge upon crystal planes in all possible directions (Fig.1, at the left). Subsequent elastic scattering of the divergent electrons by crystal planes forms an array of Kikuchi cones whenever the Bragg condition

$$2d \sin\theta = n\lambda$$

is satisfied (Fig.1, at the right).

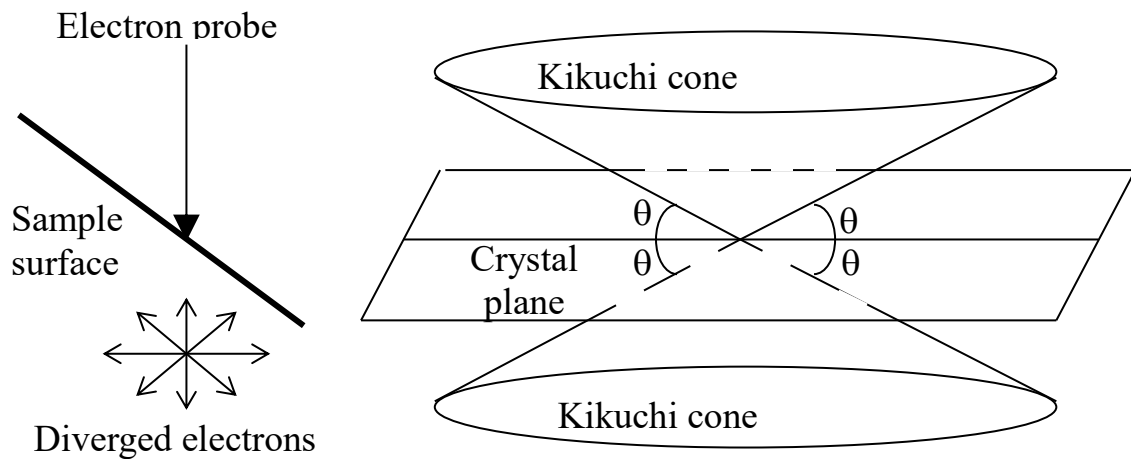


Fig.1: Schematic of EBSD patterns formation.

Two Kikuchi cones are associated with each crystal plane. The diffracted electrons emerge from the specimen on the surface of these cones whose axes are normal to the diffracting plane. The distribution of diffracted intensities is recorded by the intersection of the Kikuchi cones with a CCD, where the resulting EBSD pattern can be viewed (Fig.2). An example of a real EBSD pattern measured from Ni is shown in Fig.3. Analysis of EBSD patterns provides the crystal symmetry of the analyzed phase, and crystallographic information from highly localized regions on the sample surface. The analyzed region in EBSD technique has lateral dimensions about $0.1 \mu\text{m}$ and the depth less than $0.05 \mu\text{m}$.

TKD utilizes the same principles as EBSD but is applied to thin specimens transparent for primary electrons with 20–30 KeV energy. TKD allows improving dramatically the lateral resolution. Twins of 5 nm size in gold membrane can be easily seen in TKD map (Fig.4).

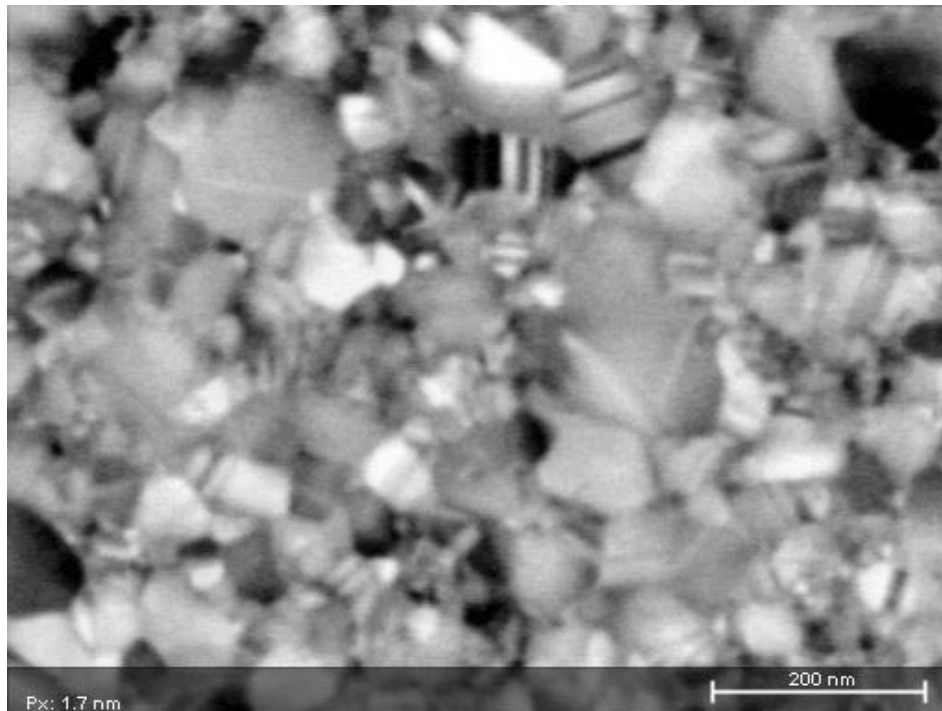


Fig.4: TKD map measured from unsupported gold membrane of 50 nm thick.

Use EBSD & TKD in SEM provides the researcher with valuable structural information. Typical applications are as follows: phase identification, point group determination, EBSD & TKD mapping making it possible grain boundary determination, grain size analysis, misorientation and preferred orientation analysis, phase distribution analysis, etc. In addition, a combination of EBSD & TKD results with those obtained by EDS allows overriding the fore mentioned difficulties in interpretation of EDS results and doing these results unambiguous.

REFERENCES

1. V. Randle, *Microstructure determination and its application*, Maney publishing, London, 2008, 138 p.
2. D.J. Dingley, K.Z. Baba-Kishi, V. Randle, *Atlas of Backscattering Kikuchi Diffraction Patterns*, Institute of Physics Publishing, Bristol and Philadelphia, 1995, 135 p.

CONTROL OF THE SYNTHESIS PROCESS OF SUPERCONDUCTING MATERIALS

B. Bendeliani^{1,2}, G. Dgebuadze¹, Z. Azmaiparashvili², G. Bokuchava¹, N. Ebralidze³, I. Metskhvarishvili^{1,2}

¹Laboratory of Cryogenic Technique and Technologies, Ilia Vekua Sukhumi Institute of Physics and Technology, Mindeli St.7, Tbilisi, 0186, Georgia

²Department of microprocessor and measurement systems, Georgian Technical University, Kostava St. 77, 0160, Tbilisi, Georgia

* bezhan2003@yahoo.com

Synthesis and oxygenation of high-temperature superconducting specimens is a complex process [1,2], which in order to obtain an optimal result requires the settling of such problems as: achieving in the oven an exactly fixed temperature in the definite time; temperature rate control; the given temperature stability in a desired time interval; visual control of the going process parameters, etc.

On the basis of these requirements a device MEISSA has been developed to control and record data in a system for oxygenating high-temperature superconducting specimens (Fig. 1).



Fig.1. Unit MEISSA

The oxygenation process of specimens is going in a high-temperature compact continuous cylindrical oven. It accommodates a quartz pipe (Fig. 2), containing, in turn, test specimens. A K-type thermocouple is mounted in the same quartz pipe as a temperature transmitter; the control scheme is built on the OMEGA-made SN7200 temperature controller.



Fig.2. Quartz tube with thermocouple

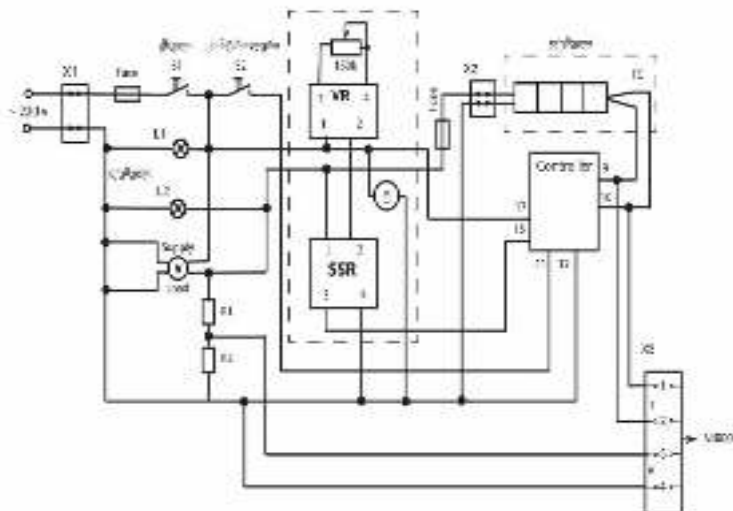


Fig.3. Schematic circuit of the MEISSA unit

The schematic circuit of the MEISSA unit is given in Fig. 3.

For more comfortable control over the technological process, visualization and memorization of the current physical parameters, the National Instrument NI USB-6009 multifunctional I/O device has been added to the system. Information about the current temperature and oven voltage is supplied from the MEISSA unit at its input, the output being connected to a personal computer. LabView - a software using graphical diagrams to create virtual instruments, enables making a virtual device on a PC monitor [3-5] for demonstrating the technological process.

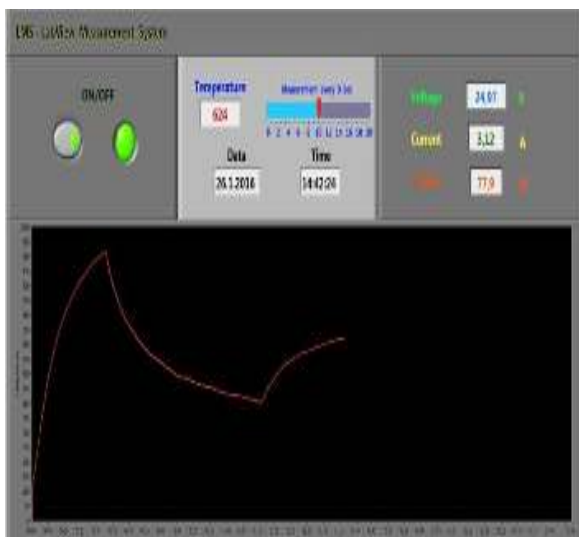


Fig.4. Front panel of the virtual instrument

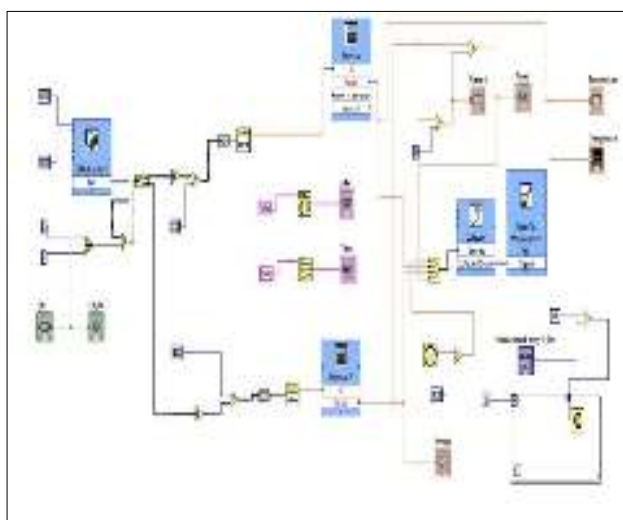


Fig.5. Block diagram of the virtual instrument

The front view of the created virtual device is depicted in Fig. 4, while the flowchart in Fig. 5.

Thus, MEISSA – a device for controlling and data recording the system of high-temperature superconducting specimens' synthesis in the oxygen environment has been designed and manufactured. It allows for oxygenating superconducting specimens placed into a compact continuous cylindrical oven under different algorithms of temperature conditions, its temperature stability within $20 \div 1000^{\circ}\text{C}$ not exceeding $\pm 1^{\circ}\text{C}$. The process control is exercised by the OMEGA-made SN7200 temperature controller; as for data organization and communication, it is ensured by the National Instrument NI USB-6009 multifunctional I/O device. The current technological process parameters can be controlled both on the front panel of the physical device, as well as on the front panel of the virtual device created in a PC environment by the graphical diagrams of the LabView software. Similarly, the automatic recording of data in a PC takes place in the form of Excel files. The device has been functioning for several years now and has proved itself as a simple and reliable operational tool for controlling ovens of different type.

ACKNOWLEDGMENTS

This work was supported by Shota Rustaveli National Science Foundation (SRNSF), grant number: CARYS-19-1832, Project title: Innovative Cryostat for Studying High-temperature Superconductors.

REFERENCES

1. Metskhvarishvili, T. Lobzhanidze, G. Dgebuadze, M. Metskhvarishvili, B. Bendeliani, V. Gabunia, "HgBa₂Ca₂Cu₃O_y Superconductor Prepared by As Vapour Diffusion Process" Nova Science Publishers, Book, 2016.
2. I.Metskhvarishvili, G.Dgebuadze, B.Bendeliani, M.Metskhvarishvili, T. Lobzhanidze, L.Gugulashvili, "Low-Field High-Harmonic Studies in Hg-1223 High-Temperature Polycrystalline Superconductor", Journal of Superconductivity and Novel Magnetism, 28 (2015) 1491
3. Jianghua Bai, Andres La Rosa Essentials of Building Virtual Instruments with LabVIEW and Arduino for Lab Automation Applications, International Journal of Science and Research (IJSR) ISSN (Online): 2319-7064 Volume 6 Issue 5, May 2017 pp. 640-644
4. LabVIEW for Everyone: Graphical Programming Made Easy and Fun, 3rd Edition Prentice Hall; New Jersey, USA, August 6, 2006, pp.1040

THERMAL EXPLOSION IN Ti-Al-Me SYSTEMS (Me=Co, Cu, Fe): COMBUSTION, PHASE FORMATION AND PROPERTIES

M. Busurina^{*}, A. Sytshev, I. Kovalev, A. Karpov, A. Shchukin

Merzhanov Institute of Structural Macrokinetics and Materials Science Russian Academy of Sciences (ISMAN), 142432, Osipyan str., 8, Chernogolovka, Moscow Region, Russia.

* busurina@ism.ac.ru

Ternary intermetallic systems based on Ti-Al-Me are actively studied for the alloys production with a unique set of properties (low density, strength, heat resistance, oxidation resistance, as well as biological compatibility with human tissues) due to which they are widely used in the aerospace industry, medicine, electronics etc. [1,2]. Among these ternary intermetallic the Heusler alloys (compounds of the general formula X_2YZ , where X, Y are transition metals, Z are elements of III-IV groups) are of special interest. Heusler alloys exhibit shape memory properties, superelasticity, magneto-optical and magnetocaloric properties, and possibility for control of these properties by magnetic field [3].

Basically, the Heusler alloys are produced by spark plasma sintering (SPS), selective laser sintering (SLS), but in most cases in industry these alloys are produced by arc-melting (AM) in argon atmosphere. In this work the method of self-propagating high-temperature synthesis (SHS) was used as an alternative process for Co_2TiAl , Fe_2TiAl and Cu_2TiAl Heusler alloys production.

Metal powders of Co ($d \sim 20 \mu m$), Fe ($d \sim 20 \mu m$), Ti (PTM, $d \sim 11 \mu m$), Al (ASD-4, $d \sim 6 \mu m$) and Cu ($d \sim 20 \mu m$) were used. Initial powders were thoroughly mixed for 10 min in a molar ratio of $(2Co+Ti+Al)$, $(2Cu+Ti+Al)$ and $(2Fe+Ti+Al)$ in a porcelain mortar until a homogeneous mixture. The powder mixture was pressed into cylindrical samples with a diameter of 12 mm and height of 15 mm, which then were placed in a reaction furnace 80 mm high and 20 mm in diameter. Samples were heated preliminary up to the initiation of the SHS reaction. After the initiation of the SHS reaction, the heating of the reaction furnace was turned off. The synthesis was carried out in vacuum at a pressure of $1.33 \cdot 10^{-3}$ Pa or in an argon atmosphere of $\sim 10^5$ Pa.

2Co-Ti-Al system: The synthesis of samples in the 2Co-Ti-Al system occurred in the thermal explosion mode. The reaction proceeded simultaneously throughout the entire volume of the sample, while the maximum rate of temperature rise reached 3500 °C/sec. The temperature of the ignition temperature in vacuum (Fig. 1(a)) is 565 °C, which is almost 100 °C lower than

the Al melting point and indicates the beginning of the solid-phase reaction. The maximum combustion temperature of thermal explosion in vacuum is 1470 °C.

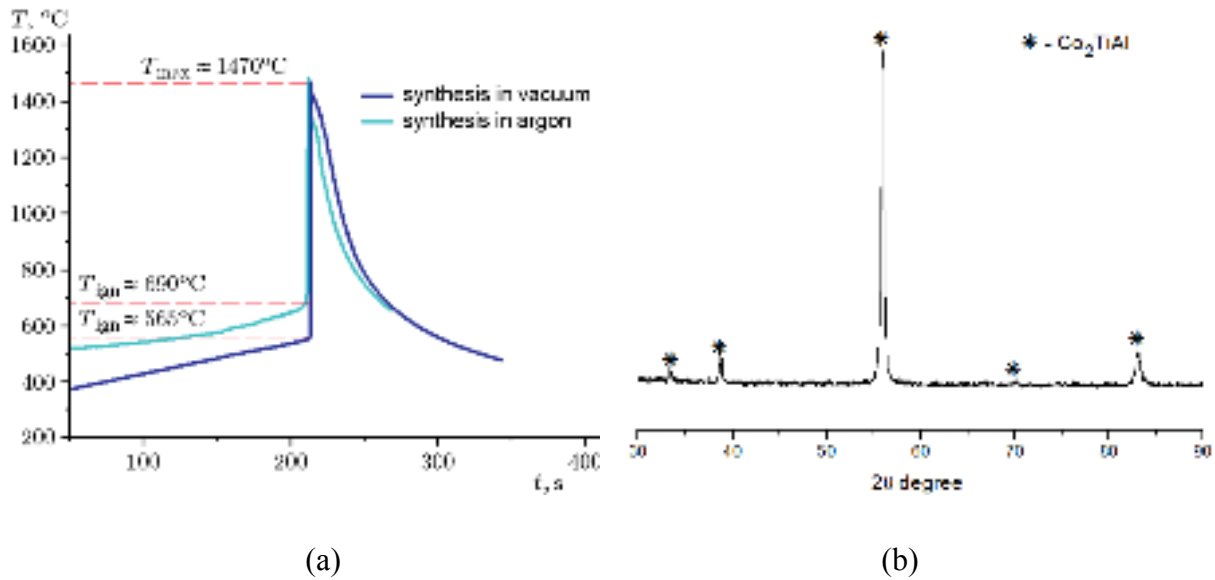


Fig.1 Temperature profile of the combustion of (2Co+Ti+Al) mixture in vacuum and argon (a) and XRD of combustion products of 2Co-Ti-Al system (b).

The XRD analysis (Fig.1, a) of synthesized materials in vacuum showed the presence of the Co_2TiAl phase (Heusler phase), the content of which was 99 wt. %. The unit cell parameter of Co_2TiAl was $a=5,8433\pm 0,0002 \text{ \AA}$. The synthesized product has a homogeneous microstructure (Fig.2, a) and consists of Co_2TiAl grains with an average size of 20 μm . The results of energy-dispersive analysis (EDA) confirmed the chemical composition of the main phase Co_2TiAl (points 5.6 in Fig. 2, b).

2Fe-Ti-Al system: Phase formation in the 2Fe-Ti-Al system during SHS largely depends on the experimental conditions (particle size of the initial mixture, initial temperature, heating conditions, heat transfer, etc.). SHS in the 2Fe-Ti-Al system took place in the thermal explosion mode. The maximum combustion temperature of the SHS reaction reached 1136 °C, the ignition temperature was 590 °C. X-ray phase analysis (XRD) of products synthesized in vacuum showed that the main phase is Fe_2TiAl (Heusler phase) (Fig. 3, a,b) with content no less than 82,8 wt. %.

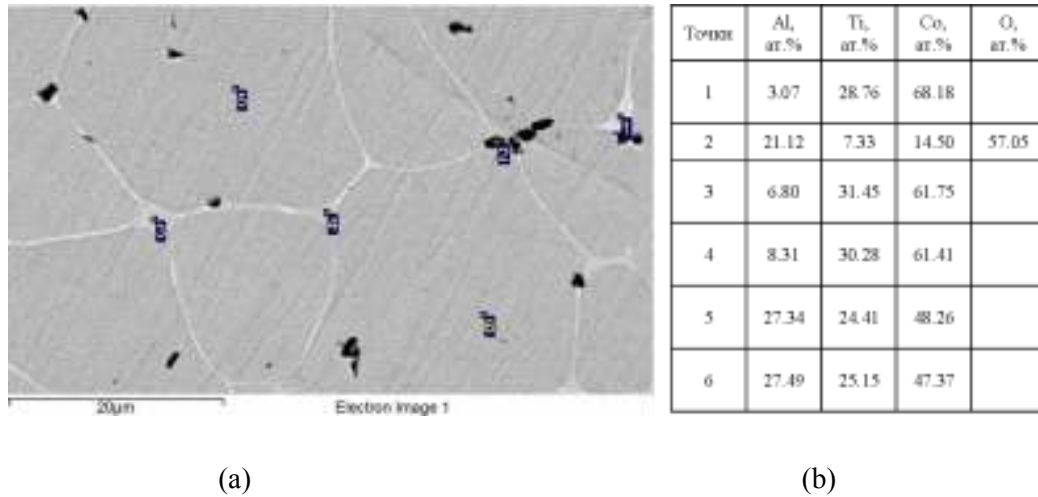


Fig.2 Microstructure of cross-section and EDA in points of combustion product of 2Co-Ti-Al system.

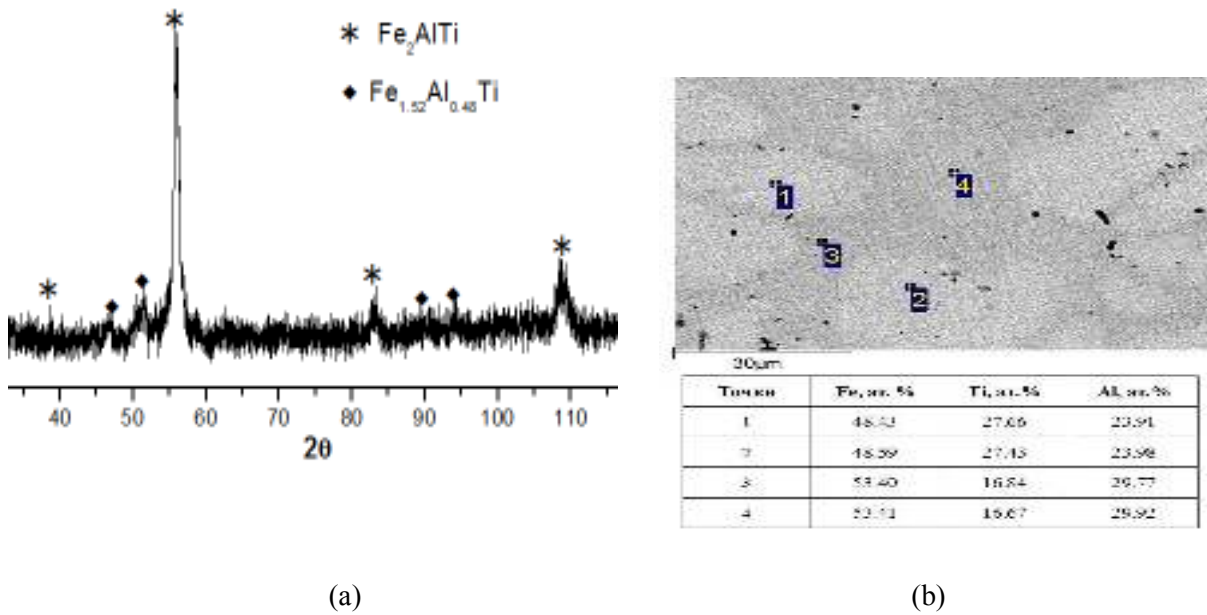


Fig. 3. XRD and EDA of the combustion products of the 2Fe-Ti-Al system.

2Cu-Ti-Al system: Combustion in the 2Cu-Ti-Al system in the SHS process took place in the frontal mode with a combustion velocity ~ 10 -15 mm/s. The maximum combustion temperature reached 982 °C. X-ray phase analysis of combustion products (Fig.4, a) showed that the main phase is Cu_2TiAl (Heusler phase) with a content about 96.4 wt. %. Secondary aluminides phases (Cu_9Al_4 and Ti_3Al_2) were also formed in the synthesized product. In the

microstructure (Fig. 4, b), grains of the Cu_2TiAl ternary phase is surrounded by an interlayer with inclusions of titanium and copper aluminides.

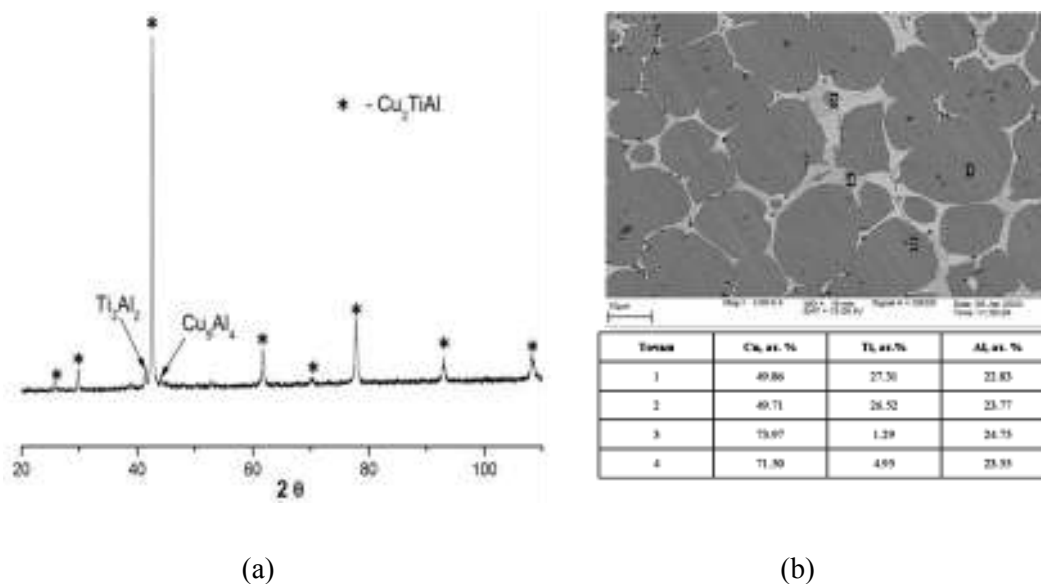


Fig.4. XRD (a) and (b) of of the combustion products of the 2Cu-Ti-Al.

For all systems, the properties of the synthesized products were investigated. Porosity and microhardness were measured. Magnetic and electrophysical measurements were carried out in a wide temperature range.

REFERENCES

1. Leyens C., Peters M. Titanium and Titanium Alloys: Fundamentals and Applications. WILEY-VCH Verlag GmbH & Co. KGaA, Weinheim, 2003. First Edition.
2. Irkhin V., Katsnelson M. Physics-Uspekhi. 1994. V.37. № 7. P. 659.
3. Graf T., Felser C., Parkin S. Simple rules for understanding of Heusler compounds. Progress in Solid State Chemistry. 2011. V. 39. P. 1-50.

ON MATHEMATICAL MODELING CHEMICAL SYNTHESIZING PROCESS OF BORON CARBIDE / TITANIUM DIBORIDE COMPOSITE IN NANOPOWDERED FORM FROM LIQUID CHARGE

L. Chkhartishvili^{1,2}, L. Antashvili^{1*}, L. Dalakishvili², R. Chedia³, O. Tsagareishvili¹

¹Ferdinand Tavadze Metallurgy and Materials Science Institute, 8b E. Mindeli Str., Tbilisi, 0186, Georgia

²Georgian Technical University, 77 M. Kostava Ave., Tbilisi, 0175, Georgia

³Peter Melikishvili Institute of Physical and Organic Chemistry, 31 A. Politkovskaya Str., Tbilisi, 0186, Georgia

levaniantashvili@yahoo.com.

ABSTRACT

A system of differential equations is derived that simulates the process of chemical synthesis of boron carbide / titanium diboride composites in nanopowdered form from a liquid charge is suggested and analyzed in view possible routes of its solution. Such a mathematical modeling should lead to optimized parameters of the technology of production boron carbide based nanocomposites, the important class of hard materials with diversity of industrial applications.

Because of complex of properties useful for diversity of industrial applications, boron carbide based nanocomposites serve for the important class of advanced hard materials. In previous works [1 – 9], authors have developed an effective method of their chemical synthesizing in nanopowdered form from corresponding liquid charge. As is known, e.g. see [10], optimization of parameters of chemical technologies is possible through their mathematical modeling. Here, we develop a system of differential equations describing time-evolution of concentrations of reactants, intermediate substances, and products of chemical reactions leading to the formation of boron carbide / titanium diboride B_4C-TiB_2 nanocomposites.

In this case, the precursors must contain sources of boron B, carbon C, and titanium Ti. In the original technology developed, the sources of boron are powders of elemental boron in the amorphous structure a-B, boron oxide B_2O_3 or boric acid H_3BO_3 . A carbon source is some liquid organic compound $C_xH_yO_z$, and titanium source is a powder of titanium dioxide TiO_2 . From these precursors, a liquid mixture is prepared in the form of a suspension aqueous solution, which is subjected to a multi-stage heat treatment in order to obtain reactants.

As a result, the boron-containing reactant is always obtained in the form of amorphous boron a-B powder. By pyrolysis of the organic solvent, carbon is reduced in the form of graphite carbon black in turbostratic structure t-C. Carbon is also contained in the emitted carbon dioxide CO_2 . At the high temperature ($> 700^\circ C$) heat treatment stage, these two components

interact with the formation of carbon monoxide CO: $\text{CO}_2 + \text{C} \rightarrow 2 \text{CO}$. The production of a carbide-based composite product requires an excess of free carbon over its dioxide. Under relevant conditions, the carbon-containing reactants are C and CO (not CO_2 and CO). The titanium-containing reactant is TiO_2 powder, which practically does not undergo any change during the preliminary heat treatment.

In the physical chemistry standard approach [11], mathematical modeling of a technological process is carried out based on its representation by a combination of homogeneous, irreversible, and formally simple chemical reactions that are isothermally occurring in a closed system. As the reactants are B, C, CO, and TiO_2 , and B_4C and TiB_2 must be contained in the products, it is needed to write down a system of formally simple chemical reactions leading to the corresponding transformation.

A qualitative analysis of the problem leads to the conclusion that this transformation is feasible through the following chemical reactions:



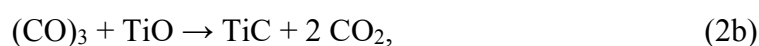
Hence, in addition to boron carbide with the approximate chemical formula B_4C and titanium diboride TiB_2 the product is carbon dioxide CO_2 as well. Free carbon C being a reactant in reactions (1) and (4) in reaction (3) is an intermediate substance. Similarly, carbon monoxide CO being a reactant in reaction (2) in reaction (1) is an intermediate substance. And finally, according to reactions (1) and (2) titanium oxide TiO and according to reactions (2) and (3) titanium carbide TiC serve for intermediate substances.

By standard definition, the order of a chemical reaction is the total number of particles – “molecules” interacting in an elementary act of collision. Therefore, for reactions (1 – 4), the orders are 2, 4, 3, and 5, respectively. As practice shows, the order of a simple chemical reaction cannot exceed 3 and, therefore, reactions (2) and (4) seem to be complex. The establishment of real, i.e. effective, orders for these reactions requires more detailed consideration of their chemical mechanisms.

First, note that the icosahedral cluster B_{12} is the main structural motif for any condensed phase of elemental boron (as well as boron-rich compounds), including amorphous boron [12]. It remains stable only in the powder particle bulk and upon (in our case, high-temperature) ablation from the particle surface the B_{12} cluster takes a quasiplanar form with broken bonds

and, accordingly, greatly increased chemical activity [13]. For this reason, it is natural to think that not 4 individual B atoms enter into the reaction, but a B₁₂ quasiplanar cluster. Clusters formation is also characteristic of carbon ablation. One of the highest mass spectrometric peaks corresponds just to C₃ clusters [14]. Therefore, the mechanism of reaction (4) can be represented as the interaction of only two particles – clusters B₁₂ and C₃. Similarly, mechanism of the reaction (3), in which elemental boron also acts as a reactant, seems to be the interaction of B₁₂ cluster with (TiC)₆ fragment of the titanium carbide structure. At high temperatures, in a medium containing both carbon and oxygen various oxycarbon structures are formed. Among small oxycarbon clusters [15] only (CO)₃ is metastable and, for this reason, hyperactive chemically. Therefore, mechanism of the reaction (2) is represented as the interaction of a metastable cluster (CO)₃ with a fragment of the titanium oxide structure in the form of a diatomic TiO molecule. Already in its original form, order of the reaction (1), is 2. However, most likely, it is carried out not by the interaction between C atom and TiO₂ molecule [16], but some small carbon cluster, for example, C₃ and the corresponding fragment (TiO₂)₃ of the titanium dioxide structure.

Finally, the process for producing boron carbide / titanium diboride composite is represented by a combination of simple reactions,



which are second-order chemical reactions, since the reactants are formally representable by pairs of interacting clusters. As all components of the process – reactants, intermediates, and products – are in finely dispersed phases (nanopowders, clusters, and gases), it can be assumed that components mixing achievable is reasonably good to consider system to be homogeneous. In this case, the reaction space is the volume and the components are quantitatively characterized by the concentration, the number of “molecules” of a substance per unit volume.

Now we discuss the applicability of another important assumption of the mathematical model, which is the closeness of the system, i.e. lack of exchange of matter between the reaction chamber and the environment. The final – most high-temperature stage of heat treatment of the precursors mixture is carried out in the same chamber in which the main process of composite synthesis in an inert gas – argon flow. The gaseous products of the precursor

pyrolysis, which do not turn into reactants of the main process, are carried away by this flow. Three of the four reagents, namely B, C, and TiO₂ are in the solid phase. The fourth reagent CO most likely is not a diatomic molecular gas, but exists in the form of oxycarbon clusters (CO)₃ and others. So, it is clear that the reactant is not supplied to the system.

Target products B₄C and TiB₂ are obtained in the solid phase. As for the non-target product CO₂, it is formed in the gas phase and, therefore, is carried out by argon flow from the chamber. Despite the presence of such exchange of CO₂ gas with environment, the reaction chamber can still be considered to be effectively closed. The fact is that with an adequate choice of the composition of the charge the system has not any excess of free carbon, with which carbon dioxide could react. In other words, CO₂ even left in the system would behave like an inert gas, would not affect the composition and quantity of the target product.

According to the acting masses law, the power-law dependence of a simple chemical reaction rate on the concentrations of reagents determines its order. Therefore, the rates of reactions (1 – 4) should be the square functions of the concentrations of corresponding reactants. This significantly simplifies the system of kinetic equations. It is convenient to operate with concentrations of “molecules”, compositions of which correspond to the formula units of substances, and not clusters actually participating in the reactions. In this case, for the rates V_1 , V_2 , V_3 , and V_4 of these reactions we have:

$$V_1 = k_1[C][TiO_2], \quad (1c)$$

$$V_2 = k_2[CO][TiO], \quad (2c)$$

$$V_3 = k_3[B][TiC], \quad (3c)$$

$$V_4 = k_4[B][C]. \quad (4c)$$

The reaction constants k_1 , k_2 , k_3 , and k_4 included here by definition are positive and do not depend on the reactants concentrations. They noticeably (according to the Arrhenius law) depend on temperature and, to a lesser extent, on other process conditions – pressure of the flowing gas, reactants phase states and dispersion, etc. If the process is not isothermal, i.e. temperature in the chamber changes these parameters become complex functions of time, which significantly complicates the solution of the equations of chemical kinetics.

In the considered technological process, during the heating period the basic chemical reactions described above proceed too slowly. As for the cooling stage effect, it begins after the almost complete consumption of all reactants and, therefore, the practical completion of

the formation of products. Therefore, the assumption that the process in question is isothermal, and the reaction parameters are time constants is quite acceptable.

Chemical reactions reduce the concentration of reactants. Therefore, the rates of their change in sign are opposite to the reaction rate sign, i.e. are negative. As the concentrations of products increase, the rate of change, on the contrary, turns out to be positive. In any case, the magnitude of the reaction rate is multiplied by the stoichiometric coefficient of this component in the reaction. Based on these comments, the desired system of kinetic equations is written in the following form:

$$\frac{d[B]}{dt} = -4k_4[B][C] - 2k_1[C][TiO_2], \quad (5)$$

$$\frac{d[C]}{dt} = -k_4[B][C], \quad (6)$$

$$\frac{d[TiO_2]}{dt} = -k_1[C][TiO_2], \quad (7)$$

$$\frac{d[CO]}{dt} = -2k_1[CO][TiO_2], \quad (8)$$

$$\frac{d[B_4C]}{dt} = +k_4[B][C], \quad (9)$$

$$\frac{d[TiB_2]}{dt} = +k_1[C][TiO_2], \quad (10)$$

$$\frac{d[CO_2]}{dt} = +2k_1[C][TiO_2]. \quad (11)$$

These equations, which determine the rates of change in the concentrations of reactants and products, were obtained by excluding the concentrations of intermediates TiO and TiC. The condition that the rates of change in their concentrations equal zero leads to the relations:

$$k_2[CO][TiO] = k_3[B][TiC] = k_1[C][TiO_2].$$

Since mathematical modeling of chemical process kinetics involves solving system of first-order differential equations describing the reactant and product concentrations evolution with time t , it is necessary to provide the initial conditions in the form of concentrations at the initial ($t = 0$) and final ($t = \infty$) time points, respectively, for reactants and products: $[B]_0$, $[C]_0$, $[TiO_2]_0$, $[CO]_0$, $[B_4C]_\infty$, $[TiB_2]_\infty$, and $[CO_2]_\infty$. Some of these values can be related with each other. In order to find a relation for the process under consideration, we introduce the stoichiometric coefficients $1 - x$ and x of the product component $(B_4C)_{1-x}(TiB_2)_x$, where $x < 1$. Since we deal with a composite based on boron carbide, not titanium diboride, the inequality $1 - x > x$ or $x < 1/2$ must be held, and $[B_4C]_\infty/[TiB_2]_\infty = 1/x - 1$. The concentrations of reactants and products at the final and initial time points, respectively, should be zero.

Subsystem of 3 equations (5 – 7) contains just 3 unknown functions – concentrations of solid-phase reactants $[B]$, $[C]$, and $[TiO_2]$. We have converted it into the form, where each equation contains only one unknown function and parameter $p = 4k_4/k_1$. In particular, equation for $[TiO_2]$ contains term proportional to $[TiO_2]^p$. In general, p ratio is not a rational number and, consequently, such equation cannot be integrated in elemental functions. But, if p is a rational number a simple transformation of unknown function converts equation into form with integer instead of p . The choice of $p = 1$ is impossible because divergent coefficients in the equation. So, simplest choice for analytical solvability is: $p = 2$. For this test case we have find non-explicit, but analytical solution:

$$\left(1 - \frac{a_1}{[TiO_2]}\right)^{\frac{1}{a_2-1}} \left(1 - \frac{a_2}{[TiO_2]}\right)^{\frac{1}{a_2-1}} = a_3 \exp(-a_1 a_2 k_1 t) ,$$

where a_1 , a_2 , and a_3 are the integration constants to be determined via initial concentrations of these reactants: $[B]_0$, $[C]_0$, and $[TiO_2]_0$.

Our further efforts will be directed on obtaining analytical solutions in special functions and / or numerical solutions.

This work was supported by Shota Rustaveli National Science Foundation of Georgia (SRNSFG) – Grant # AR–18–1045: “Obtaining of boron carbide-based nanostructured heterophase ceramic materials and products with improved performance characteristics”.

REFERENCES

1. A. Mikeladze, O. Tsagareishvili, L. Chkhartishvili, R. Chedia. Obtaining B_4C – TiB_2 ceramic nanostructured alloys. Proc. Georg. Natl. Acad. Sci. (Ser. Multi-Disciplinary Studies), 2017, 2, 37-44. – in Georgian
2. L. Chkhartishvili, A. Mikeladze, O. Tsagareishvili, A. Gachechiladze, A. Oakley, B. Margiev. Ch. 2: Boron-containing nanocrystalline ceramic and metal–ceramic materials. In: Handbook of Nanomaterials for Industrial Applications (Ed. Ch. M. Hussain), 2018, Amsterdam, Elsevier, 13-35.
3. O. Tsagareishvili, A. Mikeladze, R. Chedia, L. Chkhartishvili. Method of obtaining boron carbide based hard nanocomposite materials. National Center for Intellectual Property of Georgia “Geo Patent” – Patent # GE P 2018 6709 B, 2018 October 11. – in Georgian
4. A. Mikeladze, L. Chkhartishvili, O. Tsagareishvili, R. Chedia, M. Darchiashvili. Ceramic composites B_4C – TiB_2 in nanocrystalline state: Production, structure, and

- mechanical properties. In: Book of Abstracts of 3rd International Conference “Inorganic Materials Science Modern Technologies and Methods”, 2018, Tbilisi, Georg. Natl. Acad. Sci. Press, 62-65.
5. A. Mikeladze, O. Tsagareishvili, L. Chkhartishvili, R. Chedia, M. Darchiashvili. Production of titanium-containing metal-ceramic composites based on boron carbide in the nanocrystalline state. *Adv. Appl. Ceram.*, 2019, 118, 4, 196-208.
 6. A. Mikeladze, O. Tsagareishvili, L. Chkhartishvili, R. Chedia. Obtaining of some boron-containing and related nanocrystalline systems from solutions and suspensions. In: *Proceedings Book of International Symposium on Boron*, 2019, Nevsehir, Boren, 181-191.
 7. A. Mikeladze, O. Tsagareishvili, L. Chkhartishvili, R. Chedia, R. Tsiskarishvili. Method for manufacturing nanocrystalline systems from liquid charge. *Nano Studies*, 2019, 19, 15-36. – in Russian
 8. L. Chkhartishvili. On obtaining boron carbide based nanocomposites. In: *Proceedings of International Conference on Materials Science, Mechanical and Automotive Engineerings and Technology in Cappadocia* (Eds. B. Kurt, C. Carboga, Z. Bayer Ozturk, N. Kuckdeveci), 2019, Nevsehir, Bektas Veli Univ., 17-21.
 9. N. Barbakadze, K. Sarajishvili, R. Chedia, L. Chkhartishvili, O. Tsagareishvili, A. Mikeladze, M. Darchiashvili, V. Ugrekhelidze. Obtaining of ultrafine powder composites of tungsten, molybdenum, titanium and boron carbides using liquid precursors. In: *Book of Abstracts of 11th Japanese–Mediterranean Workshop on Applied Electromagnetic Engineering for Magnetic, Superconducting, Multifunctional & Nanomaterials*, 2019, Batumi State Univ., 114-115.
 10. N. V. Bogomazova. *Modeling and Optimization of Chemical-Technological Processes in Industry*, 2018, Minsk, Belarus State Technol. Univ., 83 pages. – in Russian
 11. A. G. Stromber, D. P. Semchenko. *Physical Chemistry*. 1988, Moscow, Vysshaya Shkola, 496 pages. – in Russian
 12. G. V. Tsagareishvili, M. E. Antadze, F. N. Tavadze. *Obtaining and Structure of Boron*. 1991, Tbilisi, Metsniereba, 144 pages. – in Russian
 13. L. Chkhartishvili. Relative stability of planar clusters B₁₁, B₁₂, and B₁₃ in neutral- and charged-states. *Char. Appl. Nanomater.*, 2019, 2, 2, 761, 1-7.

14. Ch. Lifshitz. Carbon clusters. *Int. J. Mass Spectrometry*, 2000, 200, 423-442.
15. D. Schröder, H. Schwarz, S. Dua, S. J. Blanksby, J. H. Bowie. Mass spectrometric studies of the oxocarbons C_nO_n ($n = 3 - 6$). *Int. J. Mass Spectrometry*, 1999, 188, 1/2, 17-25.
16. M. V. Ramana, D. H. Phillips. A computational study of the TiO_2 molecule. *J. Chem. Phys.*, 1988, 88, 4, 2637-2640.

INFLUENCE OF HOT PLASTIC DEFORMATION ON AUSTENITIZATION PROCESS DURING AUSTEMPERING OF DUCTILE IRON

G.Gordeziani*¹, I.Tsintsadze, S.Gvazava, R.Tabidze, N.Khidasheli, G.Tavadze

Ferdinand Tavadze Metallurgy and Materials Science Institute, 8b E. Mindeli Str., Tbilisi, 0186, Georgia

*ggordeziani@yahoo.com

INTRODUCTION

Last years, more and more attention is paid to the development of a new class of structural materials - deformable high-strength cast irons. It is explained by the fact that the use of hot plastic deformation methods for the manufacture of cast-iron products make it possible to intensify technological processes, reduce metal losses and increase the level of its mechanical and exploitation characteristics. Besides this, the combination of hot plastic deformation with austempering and isothermal quenching processes have a multifactorial effect on the structure and properties of high strength cast iron. At the same time, the influence of the degree of preliminary hot plastic deformation on the homogenization and grain size of austenite, which significantly determine the phase composition and morphology of isothermal quenching products in the intermediate temperature area, remains poorly studied for high strength cast iron [1,2]. In the present work the cast and deformed silicon cast irons has studied.

EXPERIMENTAL PROCEDURES:

The experimental meltings of cast iron were carried out in a 50-kg-capacity crucible using an electrical induction furnace of intermediate frequency. The furnace charge consisted of High-Purity Pig Iron: 3.62% C, 2.00% Si, 0.35% Mn, 0.003% S, 0.06% P and up to 10% steel scrap. After melting at 1350°C, the liquid metal was held for 5 min followed by spheroidization operation of graphite inclusions by treatment with metallic Mg. The cast iron was poured at 1430°C into Y block ingots (30 mm). The chemical composition of smelted cast iron is presented in Table 1.

The part of cast ingots were rolling in a laboratory mill at a speed of 0.8 m/sec, with various degrees of deformation (summary $\epsilon \approx 65\%$) after 950°C heating. Ingot and deformed specimens have been isothermal quenching at the temperatures: 280°C and 400°C within 30 minutes in the melt Pb-Sb metallic alloy bath, after austenization at 900°C during 20, 40, 60

and 90 minutes. For study the relation of characteristics structure components of high strength cast iron the metallographic and X-ray structural analyzes were used.

Table 1

Elements	C	Si	Mn	S	P	Mg
Weight , %	3.45	2.30	0.25	0.003	0.05	0.045

According to the data obtained, the studied cast irons, depending on the degree of plastic deformation, differ in the form of graphite inclusions, in the amount of retained austenite and in the dispersity of the metal matrix. In cast irons, which degree of hot plastic deformation does not exceed 30%, graphite inclusions retain in their spherical shape, and at higher degrees of deformations they are elongated to the direction of deformation. A metallographic analysis of studied samples shows that with an increasing plastic deformation degree of ductile iron, the metallic matrix grain size decreases and the volume fraction of bainite increases. An irregular distribution of carbon is determined in the primary austenite at the beginning of austenitization. The isothermal decomposition of the primary austenite, inhomogeneous in composition in the intermediate temperature area is followed by the formation of a bainitic metal matrix with an irregular distribution of the structural components. This is explained by the higher stability of the areas of high-carbon austenite and requires optimization of continuing austenitization, ensuring the homogenization of the metal matrix without intensive growth of austenitic grain. An increase the degree of deformation causes dimensional inhomogeneity of bainitic crystals, the finest of which are located near graphite inclusions. In the course of research it was determined that a change of the deformed state influences multivalued on the processes of formation of the final structure of cast irons during their subsequent thermal treatment. According to the data of X-ray diffraction analysis, the increasing plastic deformation up to 30%, causes increasing the proportion of bainitic constituent in the structure of the metal matrix of studied specimens. The typical X-ray diffractogram of studied austempered ductile irons are presented in the Figure 1. This dependency is evidently due to the grain size refinement of the primary austenite and the increasing of nucleation centers number of bainitic crystals. More significant plastic deformation causes decreasing the completeness of the γ — α transformation regardless of the temperature of isothermal quenching, which is the result of intensification of the carburization processes of austenite due to shape changing of graphite inclusions. As it

seems from the presented data of figure1, with an increase of austenitization time, the amount of retained austenite continuously increases and stabilizes at final homogenization of primary austenite in all isothermally quenched cast irons (fig 2).

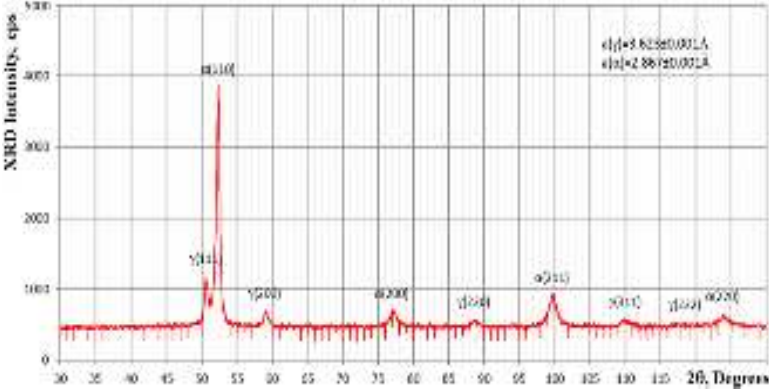
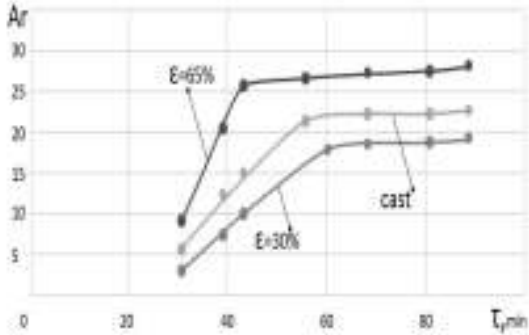
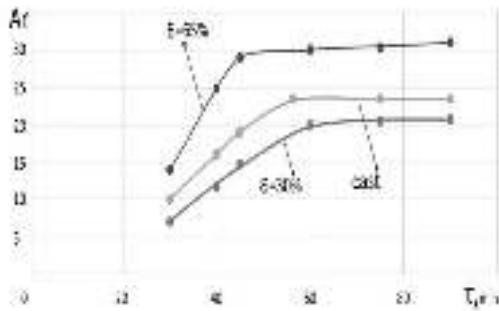


Fig.1. XRD diffractogram of bainitic ductile iron



a



b

Fig.2. Influence of austenitization time on the amount of retained austenite after isothermal treatment within 30 minutes at the temperatures: a) 280°C and b) 400°C.

Typical microstructures of investigated ductile irons are presented in the Fig. 3, Fig.4.

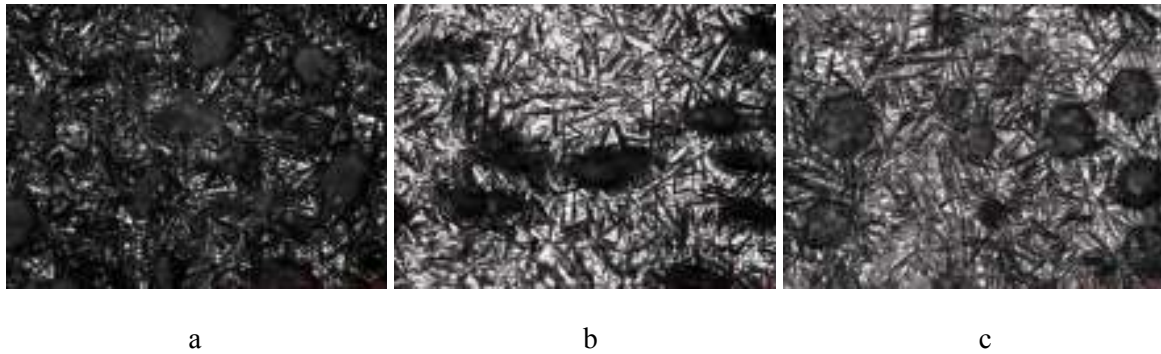


Fig.3. Microstructures (X400) of isothermal quenched (at the 280°C) ductile iron, depending on the degree of plastic deformation: a) $\epsilon \approx 30\%$, b) Ingot, c) $\epsilon \approx 65\%$

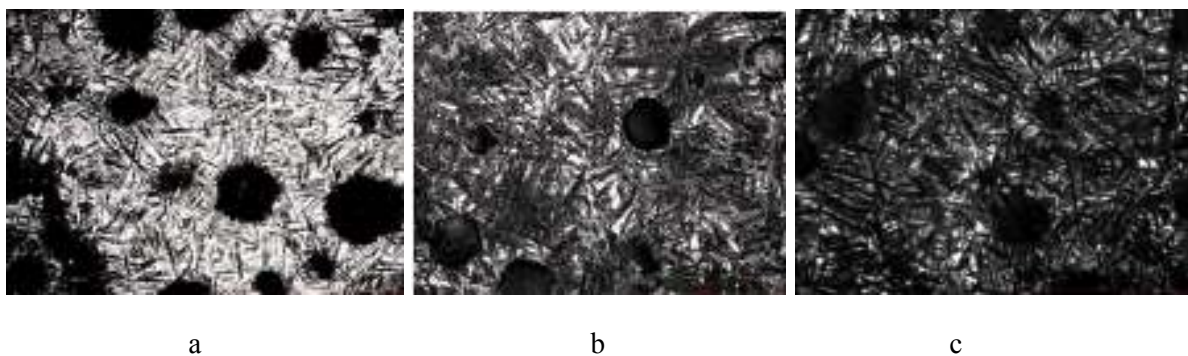


Fig.4. Microstructures (X400) of isothermal quenched (at the 400°C) ductile iron, depending on the austenitization time: a) 30 min, b) 45 min, c) 60 min

CONCLUSIONS

Based on the data obtained, it can be concluded that a combination of hot plastic deformation and isothermal quenching processes allows more wider influence range on the process of structure formation of high-strength cast irons. During the experiments it was determined that hot plastic deformation:

Increases the dispersion of grains of the metal matrix and accordingly microhardness by 4-6 units of HRC;

Increases the degree of decomposition of the primary austenite during isothermal quenching, if the degree of plastic deformation does not exceed 30%;

Causes elongation of graphite inclusions and stabilizes the primary austenite with an increasing degree of deformation over 30%;

Increases the diffusion activity of carbon, accelerates the process of homogenization of the primary austenite and reduces duration of austenitization as whole at a compression degree over 30%.

REFERENCES

1. M. Soliman, A. Nofal, H. Palkowski, Effect of Hot Working Parameters on Microstructure Evolution and Mechanical Properties of Ausformed Austempered Ductile Iron. Materials Science Forum (Volume 925), 2018, pp.218-223;
2. M. Soliman, H.Ibrahim, A. Nofal, H.Palkowski, Effect of Intercritical Annealing on Phase Transformation and Mechanical Properties of Thermo-Mechanically Processed Dual Matrix Ductile Iron. [TMS 2014: 143rd Annual Meeting & Exhibition](#) pp. 959-965.

OBTAINING HEAT AND WEAR-RESISTANT COATING BY ELECTROSPARK ALLOYING

V. Garibashvili, Z. Mirijanashvili, A. Kandelaki, V. Tsiklauri, Z. Tsikaridze

¹Ferdinand Tavadze Metallurgy and Materials Science Institute, 8b E. Mindeli Str., Tbilisi, 0186, Georgia

One of the best methods for hardening and restoring metal products is their processing by electrospark alloying, i.e. the transfer of alloying material to the treated surface by the appearance of sparks during electric discharge. This method allows the alloying of the surface layers of parts using conductive metals, alloys and composite materials. The result is coatings that are closely related to the base metal. The precise selection of alloying electrode materials makes it possible to obtain coatings with the desired properties. It is desirable to cover operating parts at high temperatures, in aggressive environments and in intense wear conditions with heat-resistant, wear-resistant and corrosion-resistant layers. Such a coating is used to select a nickel-chromium alloy hardened by inclusions of particles with high hardness.[1-3].

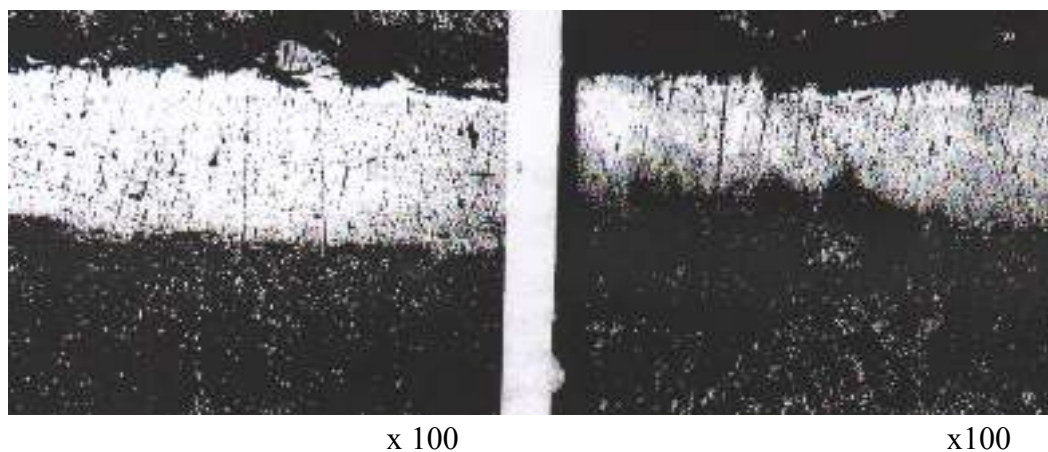
In the F. Tavadze Institute of Metallurgy and Materials Science, the aluminothermic reduction of nickel and chromium chlorides (CrCl_3 , NiCl_2), with the participation of powder reinforcing particles, hardening phases of chromium carbide (Cr_3C_2), involved in the preparation of cermet powder $\text{NiCr-Cr}_3\text{C}_2$, each particle of which is a solid base metal solution (80% Ni - 20% Cr) reinforced with dispersed inclusions of chromium carbide.

For electrospark alloying of metal surfaces, compact electrodes (4X5X40 mm) were obtained by pressing and sintering a $\text{NiCr-Cr}_3\text{C}_2$ powder mixture. To compare wear resistance, U8 steel specimens were coated using standard T15K6 hard alloy electrodes.

The experiments were carried out on electrospark alloying devices "Elitron 10" and "Elitron 12". The thickness of the coating and its quality indicators depend significantly on the short-circuit current. From its optimum value (8A), the thickness reaches 130 μm . Subsequent raising of the short-circuit current does not affect the coating thickness.

The microhardness of the coating, both upon coating with T15K6 hard alloy electrodes and after coating with $\text{NiCr-Cr}_3\text{C}_2$ cermet electrodes, is obtained from the same order and varies in the range of 1000-1400 kg / mm^2 . As for the thickness of the alloyed layers (R.1. A, b), in any case, both standard hard alloys and electrodes are obtained from test powders in the amount of 0.80 - 0.130 mm. The thickness of the coating depends mainly on the power parameters of the electric spark alloying plant.

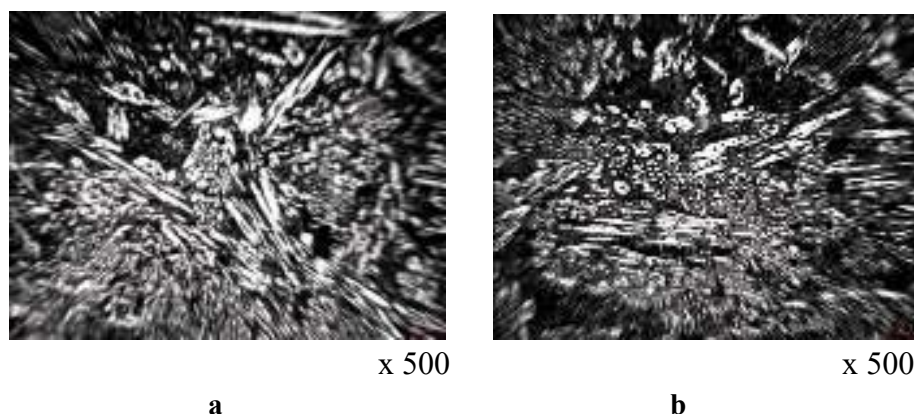
Figure 1 shows microphotographs of the coating obtained by electrospark alloying.



a
 a - alloyed by an electrode of steel T15K6;
b
 b - alloyed by an electrode of NiCr-Cr₃C₂.

Fig. 1 Microphotographs of the coating obtained by electrospark alloying (the main material is steel U8).

Fig. 2 The microstructure of the layers hardened by electrospark alloying.



a
 a - alloyed by an electrode of steel T15K6;
b
 b - alloyed by an electrode of NiCr-Cr₃C₂.

Fig. 2 shows the microstructure of the layers hardened by electrospark alloying.

The results of microstructural analysis and microhardness measurements show that carbide inclusions have a thick, elongated shape. Together with thick carbide inclusions, relatively small particles of different orientations are visible. From the surface of the coating to the boundary of the treated part, the hardness decreases.

The hardness of the alloyed (“white”) layer significantly depends on the appearance of new phases, which are formed by the chemical interaction of the elements of the alloying electrode with the material of the workpiece. It should be noted that the microhardness of the transition

layer is relatively lower than the microhardness of the base metal. This is due to the partial tempering of the transition layer of hardened steel (U8) due to the influence of temperature in the process of electro-alloying.

In order to establish the optimal parameters for obtaining a coating by electrospark alloying, the process modes changed. Under conditions of an oscillation frequency of 100 Hz and a current strength of 5 A (soft mode), the coating thickness was reached 40-60 μm , which was insufficient for the necessary hardening of this surface. Under conditions of a frequency of 200 Hz and a current strength of 8A (enhanced mode). the coating thickness reached 100-130 microns, but the surface was rough. To obtain a smooth surface, alloying was carried out first by enhanced mode, after which the same surface was coated with a relatively soft mode.

Tests on the wear of the rollers, the duration of each cycle of which was 10 min, were carried out on the installation "SMC-2". The wear rate of the lower roller was 15%, the shaft rotation frequency was 300 rpm, and the pressure on the test sample was 60 kgf. The results of the wear tests are shown in Table 1.

The wear resistance of surfaces doped with NiCr-Cr₃C₂ electrodes is obtained in the same order as coatings made of standard hard alloys.

Table 1. Test results of electric spark coating with a pressure of 60 kgf.

#	Anode material	Sample weight, g		Wear test time, min					
		Before alloying	After alloying	10	20	30	40	50	60
1	NiCr-Cr ₃ C ₂	164,6	164,7	164,8	164,7	164,7	164,7	164,7	164,7
		163,5		163,4	163,3	163,2	163,2	163,1	163,1
2	T15K6 (standard)	163,7	163,8	163,9	163,9	163,8	163,8	163,8	163,8
		164,5		164,3	163,3,	164,2	164,1	164,1	164,0

CONCLUSION

Joint aluminothermic reduction of nickel and chromium chlorides (CrCl₃, NiCl₂) with the participation of powder particles of the reinforcing and hardening phases of chromium carbide (Cr₃C₂), a ceramic-metal powder NiCr-Cr₃C₂ was obtained. Each powder particle is a metal base of a solid solution of nickel-chromium (80% Ni-20% Cr) reinforced with dispersed inclusions of chromium carbide.

By compacting and sintering powdered NiCr-Cr₃C₂, compact electrodes (4X5X40 mm) were manufactured for electrospark alloying of the surfaces of metal parts.

The microhardness and wear resistance of surfaces doped with NiCr-Cr₃C₂ electrodes is obtained in the same order as the surfaces coated with electrodes of a standard T15K6 hard alloy.

REFERENCES

1. Paustovsky A.V., Hristov V.G., Alfintseva R.A. “Materials for electric spark hardening and restoration of worn metal surfaces”, *Electronic Materials Processing*, 2016, 52 (1), 13-21;
2. Бажин П.М., Столин А.М., Заринов Н.Г. «Электроискровые покрытия, полученные керамическими СВС- электродными материалами с наноразмерной структурой» *Электронная Обработка Материалов*, 2016, 52 (3), 1-8;
3. R.Schafrik, M.P.Brady etc. “Intermetallic Rain forced Cr-Alloys for High-Temperature Use”. *Materials at High Temperatures*. 1999, 16 (4), 189-193.

REPROCESSING OF MILL SCALE WASTES BY SHS –METALLURGY FOR PRODUCTION OF CAST FERROSILICON, FERROSILICO ALUMINUM AND FERROBORON

D. Ikornikov, V. Sanin*¹, D. Andreev, N.Sahkova, V. Yukhvid

Merzhanov Institute of Structural Macrokinetics and Materials Science Russian Academy of Sciences,
Academician Osipyan str., 8, Chernogolovka, Moscow Region, 142432, Russia.
svn@ism.ac.ru

The metallurgical industry is one of the most massive material-forming industries. High amount of by-products, in the form of mill scale sludge is generated every year in each section of steel making plants due to hot rolled metal processing at elevated temperatures. Mill scale, often called as scale, is the flaky surface consisting of the iron oxides iron(II) oxide (FeO), iron(III) oxide (Fe₂O₃), and iron(II,III) oxide (Fe₃O₄, magnetite). It can be considered as a valuable metallurgical raw material for iron and steel making industry [1, 2]. The strict environmental regulations as well as the valuable metallic content cause the ability to recycle mill scales become an important issue. Currently, many metallurgical plants have accumulated large amounts of mill scale in the dumps, containing oils (4-12 %), moisture (4-18 %). After the removal of oil and water, this material contains up to 70% of iron with the minimum amount of sulfur compounds and can be effectively used in both blast and steel smelting operations. The solution of this task is becoming more effective due to the world deficit and the constant growth of the cost of iron ore, as it allows to reduce raw materials dependence and improve the ecology. So, there has been a big tendency to recover the valuable iron content in the production process.

Accordingly, most used route to recycle the iron content wastes, briquettes are charged into blast furnace due to its reducing atmosphere or into the electric arc furnace (EAF) during the melting of stainless steel scrap [3]. These processes allow the processing of mill scale in the metal product, but the economic efficiency remains at a sufficiently low level.

The most effective approach is the use of energy efficient technologies and the expansion of nomenclature of the products obtained from the recycled scale. In this regard, the present study was conducted to evaluate the possibility, efficiency, and consequences of the reduction of mill scale in combustion mode. A promissory route to production of cast different composition ferro alloys is using technique which was called the “SHS-technology of hightemperature melts” or the “SHS-metallurgy” [4, 5]. This is an energy-saving technique due to the use of internal energy released in high-caloric combustion reactions. Early, the

possibility of preparation on cast ceramic coatings inside metallic pipes firstly was demonstrated by reprocessing of mill scale [6].

In the work the scales generated from steelmaking plants were collected and used for reparation of powder mixtures with the reducing agent (Al) and alloying additives (Si, B). The average particle size was 50–100 μm for the scale and less than 140 μm for aluminum (brand PA-4). The weight of the initial mixture for combustion was constant in all experiments (1200 g). Combustion was carried out in graphite moulds 80 mm in diameter. The inner surface of the graphite molds was laminated with Al oxide (Al_2O_3) to ensure minimal reactive interaction between the form material and metal melt.

Our previous studies have demonstrated that the SHS process carried out under high gravity conditions affords the best separation of the target product (ingot) from the slag (Al_2O_3) and convective mixing of all alloy components, which becomes especially important with an increase in the number and concentration for alloys with an increased number of components and their concentration of components in the alloy. Therefore, the synthesis of the as cast alloy under study was carried out in a centrifugal SHS setup [4].

The main data on the determination of optimal chemical and technological conditions for the production of cast ferroalloys in Fe-Si-Al, Fe-Si-Al (Cr, Mn), Fe-Si-Al-B systems will be presented in the talk. Fig. 1 illustrates composition and the microstructure of SHS produced as-cast ferro alloys by reprocessing of mill scale wastes.

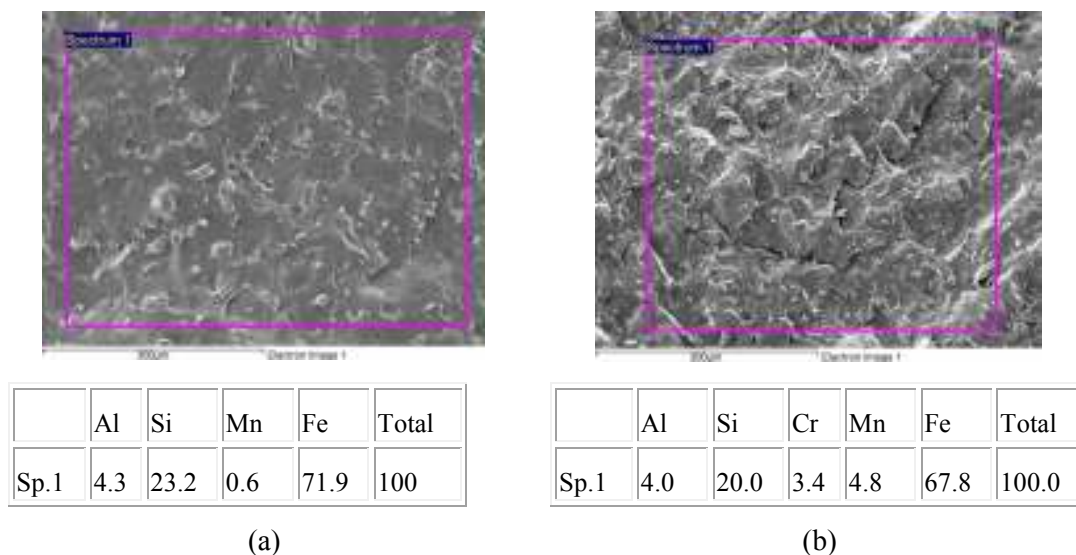


Fig. 1. The microstructure (fissure) and microanalysis of chemical composition (EDS) synthesized cast ferro alloys: (a) – Fe-Si-Al, (b) – Fe-Si-Al (Cr, Mn).

The analysis of the obtained data allows drawing a conclusion about the prospects of the materials under investigation and the method of their production for the formation of volumetric materials for steel making industry. The production of complex alloyed ferroalloys can be realized in combustion mode (SHS) for powder mixtures on the basis of scale. The process of obtaining high-alloy ferroalloys is completely energy independent, which makes it attractive for practical realization.

The study was supported by the Basic Research Program of the Russian Academy of Sciences in priority areas (KP 15).

REFERENCES

1. V. I. Shatokha, O. O. Gogenko, S. M. Kripak, "Utilising of the oiled rolling mills scale in iron ore sintering process", *Res. Cons. and Recyc.*, Vol. 55, 2011, pp. 435-440.
2. D. Cartwright, J. Clayton, "Recycling oily mill scale and dust by injection into the EAF", *Steel Times Int.*, Vol. 24, 2000, pp. 42-43.
3. Q. Yang, N. Holmberg, B. Bjorkman, "EAF smelting trials of briquettes at Avesta works of outokumpu stainless AB for recycling oily mill scale sludge from stainless steel production", *Steel res. Int.*, Vol. 80, 2009, pp. 422-428.
4. Sanin, V.N., Ikornikov, D.M., Andreev, D.E., and Yuxhvid, V.I., Centrifugal SHS metallurgy of nickel aluminide based eutectic alloys, *Russ. J. Non-Ferr. Metall.*, 2014, vol. 55, no. 6, pp. 613–619. doi 10.3103/S1067821214060212
5. V.N. Sanin, V.I. Yuxhvid, D.M. Ikornikov, D.E. Andreev, N. V. Sachkova, M.I. Alymov, SHS metallurgy of high-entropy transition metal alloys, *Dokl. Phys. Chem.* 470 (2016) 145–149. doi:10.1134/S001250161610002X.
6. V. N. Sanin, D. E. Andreev and V. I. Yuxhvid. Self-Propagating High-Temperature Synthesis Metallurgy of Pipes with Wear-Resistant Protective Coating with the Use of Industrial Wastes of Metallurgy Production. *Russian Journal of Non-Ferrous Metals*, 2013, Vol. 54, No. 3, pp. 274–279.

ANCIENT IRON PRODUCTION MONUMENTS OF GEORGIA (XII-I CC B.C.)

G.Inanishvili*¹, T.Badzoshvili

Ferdinand Tavadze Institute of Metallurgy and Materials Science. 8b.E.Mindeli str., Tbilisi 0186, Georgia, Tbilisi.

t.badzo@yahoo.com

Stage-wise depiction of the process of ancient iron metallurgy development might be achieved only after study of archaeological monuments of this category.

The workshops of iron metallurgy exposed and studied on the territory of Lower Bolnisi, Georgia, where relevant material of early antique era metallurgical manufacture was found are significant [4].

Archaeological material of iron metallurgical center of Cholchi covers specific information, which was found in the Black Sea south-eastern region [6]. Four metallurgical centers with some dozen workshops-objects of the period of functioning were revealed which date from the end of the II cc B.C. inclusive antique era. Industrial wastes (forges/furnaces, slag, a set of manufacture equipment) found on those monuments show well a forge construction and technological scheme of pyro-metallurgical process going on in it.

The key device of ironworking found on the territory of Georgia is a metallurgical forge and its construction and operation principle determine prospects of workshop development and possible increase of production scales. Each stage of iron assimilation in the region is characterized by furnaces of corresponding construction and dimension. Proceeding from the production conditions, the furnace undergoes preliminarily designed constructional changes of local character. Their quantitative characteristics were determined as a result of consideration of construction elements of furnaces of ancient iron production metallurgical cycles and at the background of comparison of analyses of production processes going on in those furnaces [1].

Taking into account the dynamics of changes of iron production furnaces, quantitative changes of construction elements, increase of industrial scales and the times of their functioning, we determined the periods of functioning of definite metallurgical centers: 1. Chronologic range of Chorokhi metallurgical center is X-VII cc. B.C. 2. Chronological frames of existence of Choloq-Ochkhamuri metallurgical center is XI-VII cc B.C.. 3. Period of functioning of Supsa-Gubazeuli metallurgical center is from XII c. B.C inclusive antique

era. 4. Khobi-Ochkhamuri metallurgical center functioned in XI-VIII cc B.C. Thus, iron metallurgical centers of Georgia were functioning with the continuous production cycle from the XII century B.C inclusive antique era (Fig. 1).

Iron production forges, while keeping the characteristic form of stationary shaft type forges, undergo constant dynamic changes of construction dimensions, at periodical growth of correspondent production scales. According to archaeological technological data we can distinguish four periods of production and economic development of iron metallurgical workshops in Georgia:

1. Early stage of iron metallurgy assimilation (XII-X cc. B.C.);
2. Stage of technological perfection of production cycle of metallurgy (X-VIII cc B.C.);
3. Period of intense assimilation of metallurgical production (VII-VI cc B.C.);
4. Period of cardinal technical-technological transformations of iron metallurgical production (V-I cc B.C.) [3].

Chorokhi metallurgical center			Choloq-Ochkhamuri metallurgical center			Supsa-Gubazeuli metallurgical center			Khobi-Ochkhamuri metallurgical center		
Object	Date		Object	Date		Object	Date		Object	Date	
	a, C ¹⁴	V		a, C ¹⁴	V		a, C ¹⁴	V		a, C ¹⁴	V
Charnali 1.1	XI	X-VIII	Jikhanjuri 1.1	IX	X-IX	Askana 2.1	XIII-XII	IX-VII	Chogha 2.1.	X-IX	X-IX
Charnali 1.2	X	IX-VIII	Jikhanjuri 1.2	VIII	XI-IX	Askana 2.2	XIII-XII	XII-X	Chogha 3.1	X-VIII	XI-X
Charnali 2.1	VIII	VIII-VII	Jikhanjuri 1.3	IX	IX-VIII	Askana 3.3	Anc.	Anc.			
Charnali 2.2	IX-VIII	VIII-VII	Jikhanjuri 2.1	VIII-VII	VIII-VII	Askana 4.1	IX	XII-X			
Charnali 3.1	IX-VIII	IX-VIII	Jikhanjuri 3.1	VIII-VII	X-IX	Mziani 2.1	XI-VII	IX-VII			
Charnali 3.2.	VIII-VII	VIII-VII	Jikhanjuri 4.1	IX	VIII-VII	Mziani 3.1	XI-VII	XII-X			
			Tsetskhauri 1.1	X-VIII	IX-VIII	Mziani 4.1	XIII-XII	VIII-VII			
			Tsetskhauri 2.1	IX	XI-IX	Mshvidobauri 1.1	X-VIII	X-VIII			
			Leghva 1.1	X-IX	XI-IX	Mshvidobauri 2.1	XIV-XIII	X-VIII			
			Leghva 1.2.	XI-X	XI-IX	Mshvidobauri 4.1	XV-XIV	XII-X			
						Nagomari 1.1	X-IX	XI-IX			
						Nagomari 1.2	XIV	XII-XI			
General date	XI-VII	X-VII	General date	XI-VII	XI-VII	General date	XIV-anc.	XII-anc.	General date	X-VIII	XI-IX

Fig.1. Chronological groups of forges functioning on the territory of Georgia

a, C¹⁴ – Archaeological and radio-carbon dates;

V – Dates of relevant constructional changes.

On the territory of Georgia the iron culture genesis from the moment of its assimilation till global spreading of iron-steel products covers transitional stages of using the production organization conditions and technical-technological facilities, which depend on distribution of raw material, products necessary for metallurgical process, for their further assimilation-processing and on the order of differentiation of the work process [2].

By IX-VII cc B.C. swift growth of total production cycle of metallurgical centers reaches its highest indices by VII-VI centuries and it is connected with active functioning of Chorokhi and Supsa-Gubazeuli metallurgical centers working on poly-metallic and magnetite ores. Maximum loading of production process is conditioned by assimilation of the Black Sea

shore magnetite sands, as one of the main ore bases. By VIII-VI cc B.C. increase of corresponding iron production indices, compared to the previous periods is determined according to the proportion: 1 : 1.5 :3.

Differentiation process undergoes still more deepening and refining in antique era. After separation of professional universal metalworking masters from metallurgical manufactures, smith's shops were created as independent units. Specialists of relatively narrow, but highest qualification, forgers, use to amalgamate in the new type production/manufacturing nuclei.

District urban workshops of antique era unite the system of highly skilled masters of metallurgist – metalworkers, whose works are the etalons of commodity goods. The goods produced in urban workshops show the limit of perfection.

Results of historic-metallurgical study offered in the present article, considering the chemical-technological analysis of products of iron manufacture and production wastes and the data of dynamics of development of construction elements of forges, determine the general scheme of iron culture assimilation on the territory of Georgia [5-7].

Dynamics of assimilation-spreading of iron culture in the XII-I cc B.C. on the territory of Georgia obeys the ascending principle of progress of creativity. At the same time, at definite stages of civilization it undergoes qualitative and quantitative changes, together with corresponding technical-technological fluctuations, impulse upheavals, which determine achievements of ferrous metallurgy and metalworking in the South Caucasus region.

REFERENCES

1. Tavadze F., Sakvarelidze T., Abesadze Ts., Dvali T. Cold-blowing Process in Iron Production in Old Georgia. *smamish*, 11, 1961, pp. 95-108;
2. Inanishvili G. For the Issues of Chronology of Colchis Metallurgy. *Guria*, III. Tbilisi, 2001, pp. 45-61;
3. Inanishvili G., Maisuradze B., Gobejishvili G. Mining and Metallurgical Activity in Ancient Georgia (3rd – 1st millennium B.C.). Tbilisi, 2010. P.224;
4. Gzelishvili I.A. Iron Smelting in Ancient Georgia, Tbilisi,1964;
5. Tavadze F., Inanishvili G., Sakvarelidze T., Zagju T. Investigation of Ancient Slag of Iron Manufacture on the Territory of Georgia. *History of Science*, Tbilisi, 1984, pp. 20-25;
6. Khakhutaishvili D.A. Iron Production in Ancient Colchis. Tbilisi,1987;
7. Inanishvili G. About the History of Iron Production in Georgia. *Metalla*, 14. 1/2. Bochum, 2007. P. 62.

GRAPHENE DERIVATIVES INFLUENCE ON MECHANICAL PROPERTIES AND MICROSTRUCTURE OF ALUMINA BASED CERAMIC MATERIALS

N.Jalagonia*, T.Kuchukhidze, T.Archuadze, L.Kalatozishvili, N.Darakhvelidze, M. Mumladze, G.Bokuchava

Ilia Vekua Sukhumi Institute of Physics and Technology, 7 Mindeli Str., 0186, Tbilisi, Georgia
sipt@sipt.org

Abstract. In this study obtaining methods of matrix ceramic composites with different compositions by high temperature pressing technology have been discussed. Following ceramic composites have been obtained α -Al₂O₃, α -Al₂O₃-GO, α -Al₂O₃-RGO. Ceramic composites are obtained in high temperature vacuum furnace with different temperature and pressure conditions. Received ceramics do not have open pores and their density reaches 99.5 % of TD.

INTRODUCTION

Ceramic materials are widely used in many fields of science because they have excellent chemical, mechanical and thermal properties. Alumina (Al₂O₃) is remarkable example of ceramic materials. Due to its outstanding characteristics, alumina is used in autoindustry, aerospace and biomedical activities also as cutting materials. Alumina in its various levels of purity is used more often than any other ceramic materials. Alumina-based ceramic materials are the cheapest, because aluminum is one of most abundant elements on Earth and the methods of its production are well developed. Nevertheless, alumina-based ceramics have some disadvantages, such as low resilience and fracture toughness [1-3]. Improvement of the physical-mechanical properties of ceramics to a certain degree became possible by reducing the size of particles of sintered powders to nano sizes, using different dopants and reduction of sintering time, because during consolidation process the grain sizes dramatically increase, which negatively affects to final product properties. Recently special attention is paid to reinforced ceramic composites with carbonaceous materials. Considering the unique physical-mechanical properties of carbon nanostructures, they are widely used as reinforcement for alumina ceramic composites [4].

The aim of this work is to prepare and to study the mechanical properties and microstructure of alumina matrix composite material reinforced by (1.5 wt.%) graphene oxide (GO) and reduced graphene oxide (RGO) using hot pressing method.

EXPERIMENTAL PROCEDURE AND SAMPLE PREPARATION

Synthesis of graphene oxide and reduced graphene oxide. Synthesis of graphene oxide have conducted by intercalation method from graphite. Graphite flakes (2 g) mixed in 50 mL of H₂SO₄ (98%) and potassium permanganate (6 g) very slowly during 1 h. The flask kept under at ice bath (27-35°C) with continuous stirring. After 1 h 100 ml water was added in the mixture. Then continue stirring again about 1 h and 20 mL H₂O₂ was added. After washing and filtration, the mixture centrifugation has done. Stable graphene oxide suspensions have obtained which used as reinforcement materials in ceramic composite.

Synthesis of reduced graphene oxide. A weighed amount of GO and distilled water were placed in ultrasonic bath. The mixture was held for 3 h. The resultant black substance was then heated in a commercial microwave oven for 2 minutes at 800 watts. The solution was then filtered and washed with ethanol. The obtained residue was dried using an oven at 110°C for 6 hours. The obtained rGO solid were then characterized.

Preparation of pressing powdery composite. 65 g α -Al₂O₃ was mixed to graphene oxide (1.5% mas.) and in the other hand to reduced graphene oxide. 100 mL H₂O was added into mixture and homogenization carried out by nanomill during 24 h. Then the mixture dried and placed in press form.

SEM. Structural-morphologic investigation of ceramic composites has been performed by JEOL JSM-6510LV and Nikon ECLIPSE LV 150 microscope. Chemical content of these samples has been measured simultaneously with energy dispersive micro XRD analyzer.

Determination of microhardness. Microhardness and modulus of Al₂O₃ have been studied according to ISO-14577 international standard at dynamic ultra microhardness tester DUH-211S.

RESULTS

Alumina is material which widely used for obtain of matrix ceramic composites. High temperature vacuum furnace (OXY-GON) has been used for obtaining of them [5-6]. Alumina based ceramic composites have obtained in the OXY-GON furnace: α -Al₂O₃, α -Al₂O₃-GO, α -Al₂O₃-RGO. Sintering temperature–1400-1600°C, sintering time was 20-60 min at maximum temperature. Refrigeration of graphite pressure-shape has been in inert atmosphere. Obtained corundum product has black color, because there have been thermal dissociation and formation defect lattice of Al₂O₃ in vacuum. For purpose, relaxation (whiten) of product with defect structure have been annealing in high temperature furnace at air

(1600°C, 1 h). Physical-mechanical and structural-morphological study has been conducted for obtained materials.

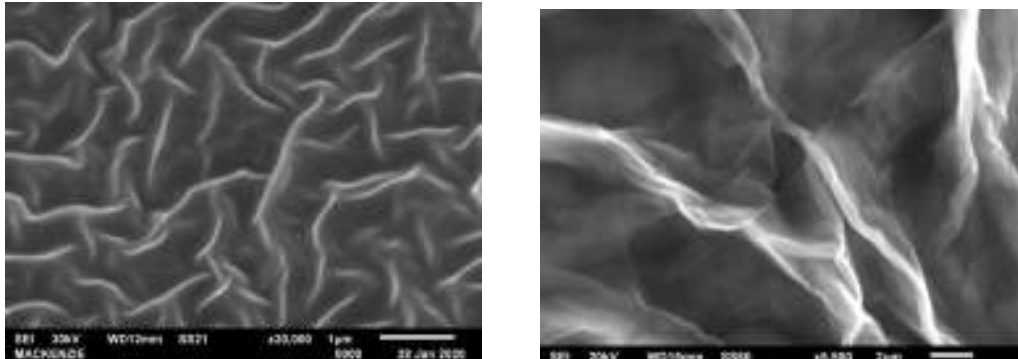


Fig. 1. SEM of GO and RGO

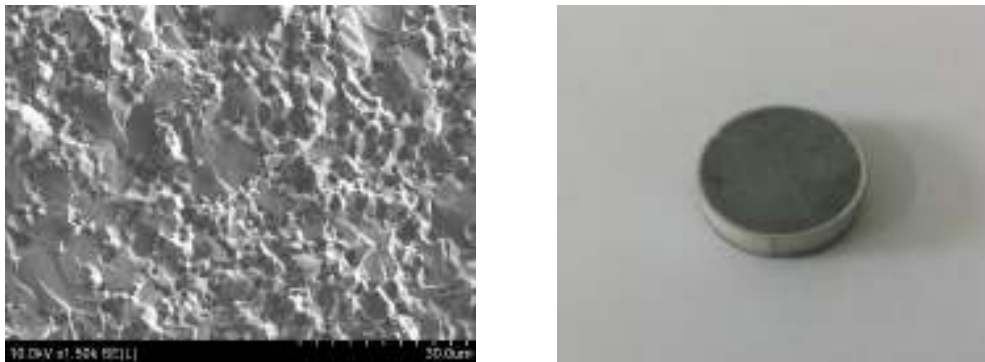


Fig. 2. SEM of alumina based ceramic composite

As an electronic micrographs (Fig. 1) showed, average number of GO or RGO layers are 10-30 nm and graphene oxide particles sizes are approximate 50-70 nm in suspension.

As above mentioned, Obtained ceramic samples with various thickness and cylindrical diameter forms (Fig.2) their microhardness was established at dynamic and static conditions. Microhardness is relatively high at small depth (load) and its value falls when depth (load) increases and goes at stationary value. Reason may be is obtaining condition of ceramics. Also some physical-mechanical parameters of obtained composite materials are given in table 1.

Table 1. Physical-mechanical properties of composite ceramics which is reinforced with graphene oxide and reduced graphene oxide.

Sample	Density g/cm ³	Open porosity, %	Water absorption %	Microhardness, GPa (200 g)	σ -bending strength GPa
α -Al ₂ O ₃	3,94-3,96	0,08-0,11	0,03-0,05	12	300
α -Al ₂ O ₃ -GO (1.5% mas.)	3,98-4,00	0,02-0,04	0,03-0,05	16,9	385-410
α -Al ₂ O ₃ - RGO (1.5% mas.)	3,95-4,00	0,01-0,03	0,03-0,05	18,4	380-400

CONCLUSIONS

In this works, obtaining ceramic matrix composites was investigated, which is based on consolidation of powdery composites in high temperature vacuum furnace OXY-GON. Following pressing powdery composites α -Al₂O₃, α -Al₂O₃-GO, α -Al₂O₃-RGO have been obtained by ball milling. Ceramic products were obtained by sintering at 1400-1600°C (1 hr, 50 MPa), which is characterized by high flexural strength (380-450 MPa), microhardness and fracture toughness and without of open porosity. Their relative density achieves 99.5% of the TD.

REFERENCES

1. A. Kmallik, S. Gangadharan, S. Dutta and D. Basu. Bull. Mater. Sci., 33(4), 2010, pp.445–449;
2. V. Lysenko, V. Mali, A. Anisimov. Athens J. of Sciences, 2014, pp.269-279;
3. R. Benavente, A. Pruna, A. Borrell, M.D. Salvador, D. Pullini, F. Penaranda-Foix, D. Busquets. J. Materials Research Bulletin, 2015, 64, pp.245-251;
4. Ha.Porwal, P. Tatarko, S. Grasso, J. Khaliq, I. Dlouhy, M. J. Reece. Carbon, 2013, 64, pp.359-369;
5. T. Kuchukhidze, N. Jalagonia, E. Sanaia, K. Barbakadze, F. Marquis, G. Bokuchava. Proceedings of ICMSF 2018: 20th International Conference on Materials Synthesis and Fabrication, 2018, pp.1659-1662;
6. N.Jalagonia, F. Marquis, K. Barbakadze, E. Sanaia, G. Bokuchava, T. Kuchukhidze. Materials Science Forum, ISSN:1662-9752, Vol.900, pp.101-104; doi:10.4028/www.scientific.net/MSF.

FABRICATION OF MEMRISTOR ON THE BASES OF ZrO₂ AND HfO₂ DIOXIDES AND RESEARCH OF ITS PHYSICAL CHARACTERISTICS

L.Jibuti^{*1}, A.Bibilashvili^{1,2}, Z.Kushitashvili²

1 Ivane Javakhishvili Tbilisi State University, 1, Chavchavadze Ave., 0179 Tbilisi, Georgia

2 LEPL Institute of Micro and Nanoelectronics, 13, Chavchavadze Ave., 0179 Tbilisi, Georgia

* ladojibuti@gmail.com

INTRODUCTION

In our work is considered fabrication of double-layered ZrO₂-HfO₂, using modernized reactive magnetron sputtering technology. We studied the influence of the pulse photon treatment (PPT) and annealing in the N₂ ambient on the physical characteristics of fabricated structure.

It has been shown that the PPT and annealing in the N₂ ambient significantly improve the electro-physical characteristics of the dioxide layers. As a result of additional treatments, transition metal dioxides with improved physical properties were obtained and used to improve the electro-physical characteristics of the memristor. Nanostructure of Si-ZrO₂-HfO₂-Al was fabricated on p-type silicon substrates using reactive magnetron sputtering. Various measurements are conducted to study their electro-physical and structural characteristics. Dioxide layers with improved properties were then used in the Si-W-ZrO₂-HfO₂-Mo-Al metal-insulator-metal structure to study the resistive switching effect.

EXPERIMENT AND MEASUREMENTS

For fabricating MOS structures p type silicon was used as a substrate with the following parameters: Thickness ~300μm; diameter 65mm; surface orientation [100]. For studying optical properties of the dioxide layers Al₂O₃ was used as a substrate with the following parameters: Thickness ~300μm; diameter 75mm; surface orientation [0002]. Dioxide layers were fabricated in the Ar and O₂ ambient using reactive magnetron sputtering technology. Concentration of Ar and O₂ gases was controlled using SRS RGA200 mass spectrometer [1]. In the vacuum chamber, sputtering targets of Zr and Hf metals were placed so that ZrO₂ and HfO₂ dioxide layers were obtained without breaking the vacuum.

Experiment results showed that optimum technological conditions for fabricating dioxide layers are following:

Pressure in vacuum chamber, $P=3.7\div 4.9\cdot 10^{-2}$ Pa; process duration, $t=7.5$ min; substrate temperature, $T=550^{\circ}\text{C}$; Ar:O₂ = 20:70; voltage on magnetron, $U \approx 300\text{V}$; current, $I=300\text{mA}$.

Thickness of each dioxide layer fabricated in abovementioned conditions was $\sim 45\text{nm}$. For improving physical characteristics of the dioxide layers we studied the influence of the pulse photon treatment (PPT) and annealing in the N_2 ambient on fabricated structures. The PPT process was conducted in two modes: 1) Power density $50\text{W}/\text{cm}^2$, 2 pulses with 0.5sec duration each and 2) Power density $70\text{W}/\text{cm}^2$, 1 pulse with 1sec duration. Power density of PPT device can be modified continuously to $100\text{W}/\text{cm}^2$ and duration of pulse from 0.1sec to 100sec with 0.1 step.

Thermal annealing of fabricated structures was carried out in thermal annealing oven. Annealing temperature was $(500\div 800)^\circ\text{C}$ and process duration 15 minutes. For obtaining MOS structure, $\text{Si-ZrO}_2\text{-HfO}_2$ was coated with Al using vacuum-thermal evaporation technology [2].

For studying electro-physical characteristic of the fabricated MOS structure, C-V and G-V measurements were conducted. Fig.1a and b show the measurement results.

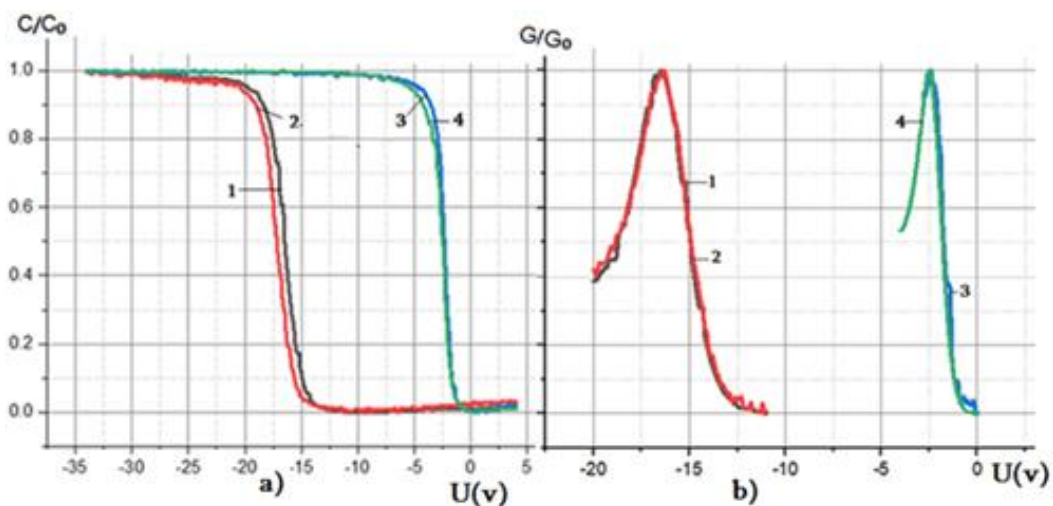


Fig.1. Normalized C-V(a) and G-V(b) characteristics of Si- $\text{ZrO}_2/\text{HfO}_2\text{-Al}$ structure, 1) Without additional treatment; 2,3) After PPT and 4) After thermal annealing

As seen in figure 1 a and b, 1sec. , $70\text{W}/\text{cm}^2$ PPT and thermal annealing significantly decrease charge in oxide (Fig.1a) and density of states on the Si-oxide border (Fig.1b).

Figure 2 shows $\text{Si-ZrO}_2/\text{HfO}_2$ XPS curves without additional treatment (---) and after PPT (-).

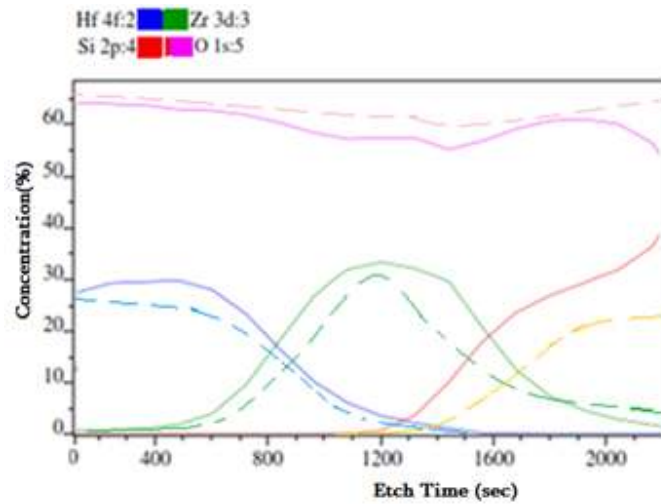


Fig.2. -ZrO₂/HfO₂ XPS curves,
 (---) without additional treatment; (-) after PPT.

Figure 3 a and b shows optical transmission spectrums of ZrO₂ and HfO₂ dioxide layers without additional treatment and after PPT in 1sec. 70W/cm² mode. As seen in curves, PPT has influence only on ZrO₂ layer.

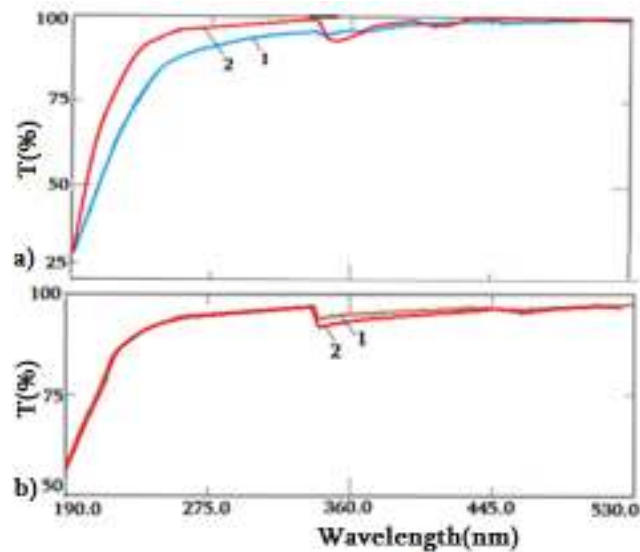


Fig.3. Optical transmission spectrum of a) ZrO₂ (1) before and (2) after PPT
 and b) HfO₂ (1) before and (2) after PPT

On the bases of experimental results, dioxide layers with improved physical characteristics were used in the Si-W-ZrO₂-HfO₂-Mo-Al metal-insulator-metal structure to study the resistive switching effect. Total thickness of both dioxide layers was ~55nm.

Figure 4 shows I-V characteristics of memristor before and after PPT in 1sec. 70W/cm² mode. Measurement results showed that in Si-W-ZrO₂-HfO₂-Mo-Al structure before additional treatment $R_{off}/R_{on}=1,4 \cdot 10^{-5}$ and after PPT $R_{off}/R_{on}=2,3 \cdot 10^{-6}$. Hysteresis loop area divided by the rectangle area where the loop is placed was 0.23 before additional treatment and after PPT it has become 0.63.

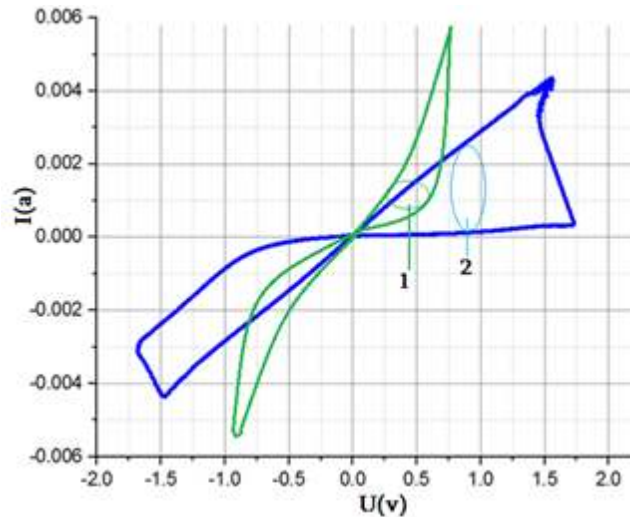


Fig.4. Si-W-ZrO₂-HfO₂-Mo-Al memristor I-V curves,
(1) without additional treatment and (2) after PPT

CONCLUSION

1. Optimum modes of PPT and thermal annealing of dioxides layers was selected.
2. Technological route of resistive memory fabrication was selected.
3. Memristor I-V measurements showed that after PPT in 1sec. 70W/cm² mode, R_{off}/R_{on} value decreases ~ 10 times and hysteresis loop increases $\sim 2,74$ times.

REFERENCES

1. Z. Kushitashvili, A. Bibilashvili, N. Biyikli, IEEE Transactions on Device and Materials Reliability, 2017, v.17, pp.667-671, Issue:4;
2. Erik C. Garnett et al., Nature Nanotechnology, 2009, v.4, pp. 311-314.

SYSTEMS OF PULSED PHOTON IRRADIATION (PPI) OF MATERIALS AND STRUCTURES IN ELECTRONICS

Z.Jibuti^{1*}, A.Bibilashvili^{1,2}, L.Jibuti^{1,2}, Z.Kushitashvili¹

¹Institut of Micro and Nanoelectronics,13, Chavchavadze Av., 0179 Tbilisi, Georgia

² Ivane Javakhishvili Tbilisi State University, 1, Chavchavadze Ave., 0179 Tbilisi, Georgia

*z.jibuti@gmail.com

To date, a number of PPI systems of various modifications are used in electronics technology. These systems were created to provide faster (than diffusion furnaces), but still thermal heating due to the use of various lamps as a heat source. These are closed and maximally heat-insulated systems. In such systems, to reduce heat removal from the samples, the holders are made of materials with low thermal conductivity[1-10].

With allowance for the important role of the ionization factor in the technological activation - diffusion processes [11-16], we developed a series of PPI 1-8 systems, in which, on the contrary, conditions are created for maximum reduction of sample heating, and attention is paid to the spectral composition of photon radiation. When developing this series, the task was to create such systems that would allow a controlled change in the duration, spectral composition and intensity of irradiation as well as in the sample heating temperature. In this paper, four of them are presented.

The first PPI-1 system (Fig.1) of this series consists of two units: a control unit and a radiation unit. The use of the Π -shaped reflector design, and the radiation source of a set of 19 KG 1000x220 halogenic lamps arranged in two rows, ensures uniform irradiation of the samples throughout the area of 100 cm². The system allows a smooth change in the irradiation power density up to 190 W. cm⁻², and the pulse duration from 0.1 to 1000 sec in 0.1sec increments. The reflector is made of special ceramics, characterized by stable optical properties. The temperature of the samples, depending on the physical or technological task, is controlled by selecting holders and venting heated air. In order to avoid uneven heating of the sample over the entire area, to reduce the local places of heat removal, the contact of the sample with the holder should be minimal or continuous over the surface. This is achieved by placing the samples in the reflector block on quartz needles or on a copper holder with a polished surface. The design of the copper holder provides its cooling with running water or liquid nitrogen vapor.

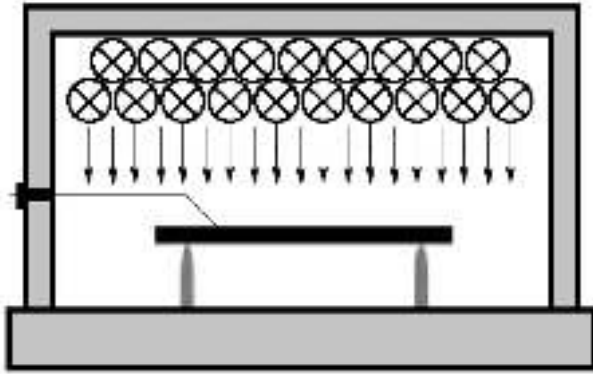


Fig.1 PPI-1, radiation unit.

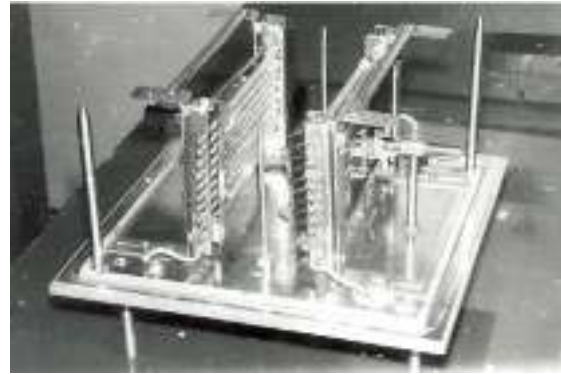


Fig.2 PPI-2, radiation unit.

Later, to solve a number of research and technological problems, the need arose to develop PPI-2 systems, where the radiation unit (Fig.2) is designed to provide photon effects on the samples simultaneously from both sides, and PPI-3 (Fig.3), designed for photon exposure of the plates in a vacuum or inert medium. The reflectors in these systems are made of polished stainless steel.



Fig.3 PPI-3, radiation unit.

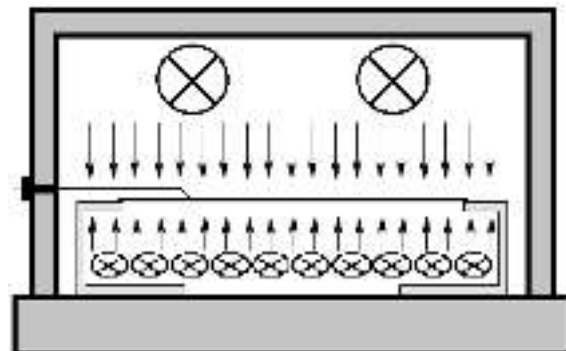


Fig.4 PPI-4, radiation unit.

According to its characteristics, the PPI-4 system (Fig.4) is somewhat different. Its creation was caused by the need to better vary the spectral composition of the radiation in the visible and ultraviolet spectral regions, which turned out to be especially important for wide-band gap materials and structures. This system has two photon sources. The first of them is the DRT 1000 mercury lamps, located in the upper part of the reflector unit. The source operates in a continuous mode. The rated power of each lamp is 1 kW. The second source is located at the bottom of the reflector and consists of a set of 10 halogen lamps KG 1000x220. The source operates in a pulsed mode. The system allows smooth and stepwise change of the radiation power. The pulse duration can be changed from 0.1 to 10 s, in increments of 0.1 s. The reflector is also made of ceramic. The sample is placed on quartz stands between two

lamp sections. To avoid uneven heating of the sample throughout the area, the contact of the sample with the holders is minimal. The heated air is vented through the air offtake. The arrangement of the lamps and the shape of the reflector provide uniform processing of samples with an area of 100 cm². During irradiation, the sample is placed in such a way that the working side of the sample is directly exposed to radiation of the DRT 1000 lamps. The greater number of photons emitted by the lamps energetically exceeds the band gap of semiconductor materials used in electronics. Therefore, the main absorption of photons occurs in a thin surface layer of the material, which leads to the excitation of its electronic subsystem. The radiation intensity of the DRT 1000 lamps is insufficient for annealing defects and activating the implanted impurity. To create conditions for diffusion processes, the back side of the sample is subjected to pulsed photon exposure from KG 1000x220 lamps. The emission spectrum of the lamps provides resonance absorption of photons at the energy levels of defects, thereby reducing their chemical bond in the sample. The simultaneous use of both radiation sources can significantly reduce the heating temperature of the sample. In this case, undesirable redistribution of the impurity can be avoided. If necessary, the diffusion dispersal of an impurity can be controlled by its depth distribution by changing the operating modes of the KG 1000x220 lamps.

The use of these systems in electronics technology made it possible, keeping high quality, to significantly reduce the duration and temperature of the processes.

REFERENCES

1. C. Gao, Y. Lu, P. Dong, J. Yi, X. Ma, and D. Yang, *Applied Physics Letters*, 104, 032102,2014.
2. V. V. Voronkov, R. Falster, T.H. Kim, S.S. Park, and T. Torack, *Journal of Applied Physics*, 114, 043520, 2013.
3. D. C. Walter, B. Lim, K. Bothe, V. V. Voronkov, R. Falster, and J. Schmidt, *Applied Physics Letters* 104, 042111,2014
4. S.C. Chang, J.M. Shieh, B.T. Dai, M.S. Feng, and Y.L. Wang, *Journal of Vacuum Science & Technology B*, 21,2003,pp.858 -861
5. D. Kot, G. Kissinger, M. A. Schubert, and A. Sattler, *Applied Physics Letters* 104, 182101,2014.
6. Jorge Garagorri, M. Reyes Elizalde, Matteo C. Fossati, David Jacques, and Brian K. Tanner, *Journal of Applied Physics*, 111, 094901,2012.

7. L. Li, Z. Yang, Z. Zuo, J. Y. Kong, and J. L. Liu, *Journal of Vacuum Science & Technology B*, 28, 2010, pp. C3D13- C3D16.
8. Yulu Chen, Shan Wu, Yinjie Ma, Yongliang Fan, Xinju Yang, Zhenyang Zhong, and Zuimin Jiang, *Journal of Applied Physics*, 115, 233502, 2014.
9. R. Singh, M. Fakhrudin, K.F. Poole, *Applied Surface Science*, 168, 2000, pp. 198-203.
10. R. Singh, K.C. Cherukuri, L. vedula, A. Rohatgi, S. Narayanan, *Appl. Phys. Lett.*, 70, 13, 1997, pp. 1700-1702.
11. Z.V. Jibuti, N.D. Dolidze and B.E. Tsekvava, *New Developments in Material Science*, New Science publishers, Inc. New York, Chap. 6, pp. 2011, 43-54.
12. Z. Jibuti, A. Bibilashvili, L. Jibuti, N. Dolidze, *IOP Conf. Series: Earth and Environmental Science* 362, 012077, 2019, p. 1-7.
13. D. Daraselia, D. Japaridze, Z. Jibuti, A. Shengelaya, *Bull. Georg. Acad. Sci.*, 5, 1, 2011, pp. 116-118.
14. D. Daraselia, D. Japaridze, Z. Jibuti, A. Shengelaya, K. A. Müller, *J. Supercond. Nov. Magn.*, 26 2013, pp. 2987–2991.
15. Z. Jibuti, D. Daraselia, D. Japaridze, A. Shengelaya, *Proc. of International Conference Advanced Materials and Technologies*, Tbilisi, Georgia, 21 -23 October, 2015, pp. 47 – 51.
16. D. Daraselia, D. Japaridze, Z. Jibuti, A. Shengelaya, and K. A. Müller, Nonthermal effects in photostimulated solid state reaction of Mn doped SrTiO₃, *Journal of Applied Physics* 121, 2017, pp. 145104 1-6.

ALLOY DISORDERS IN $\text{InP}_x\text{As}_{1-x}$ SOLID SOLUTIONS

E.Khutsishvili*, T.Qamushadze, N.Kobulashvili, Z.Chubinishvili, R.Razmadze,

Ferdinand Tavadze Institute of Metallurgy and Materials Science, Tbilisi, Mindeli str.8b, 0186, Georgia

* elzakhutsishvili@yahoo.com

Investigation of the transport properties of semiconductors have shown that there might be observed inhomogeneities of different origin [1-3]. One of the type of inhomogeneity connected, with random space fluctuations of the composition [4] in so-called inhomogeneous semiconductor alloys. The semiconductors crystals contained disordered areas of different origin usually have the low values of carriers mobility. Sufficient attention has to be given to the effects of inhomogeneities blocking current carriers flow. At certain conditions the properties of these disordered areas can be surprisingly distinguished from the properties of matrix and have strong effect on their properties. Nowadays, experimental knowledge concerning such materials is quite rudimentary with a few exceptions. This paper is devoted mainly to researching of electrical properties of $\text{InP}_x\text{As}_{1-x}$ semiconductor alloys. The purpose of presented work is to reveal the contribution of disorder scattering of charge carriers to the electrons mobility of semiconductor alloys, particularly for $\text{InP}_x\text{As}_{1-x}$ solid solutions.

Composition dependences of current carriers' mobility data at 300 K for $\text{InP}_x\text{As}_{1-x}$ solid solutions with nearly the same carriers concentration $n \sim 10^{16} \text{ cm}^{-3}$ and 10^{18} cm^{-3} are presented in Fig. 1.

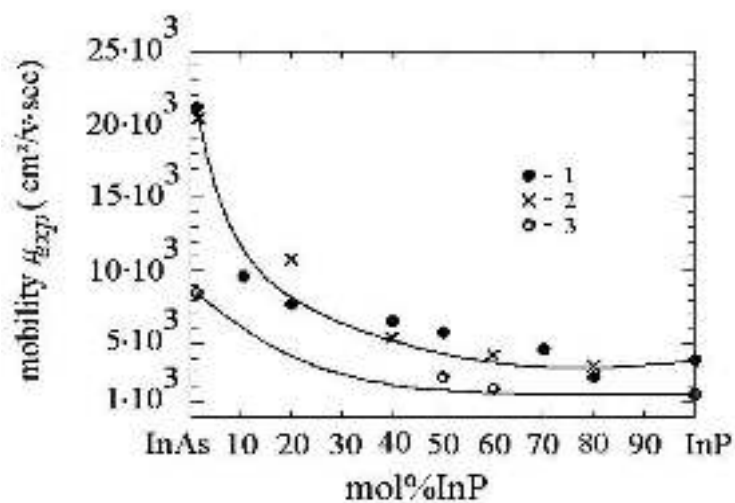


Fig. 1. Composition dependences of the current carriers mobility (μ_{exp}) for $\text{InP}_x\text{As}_{1-x}$ solid solutions at 300 K: 1,3—our data and 2—data [5], n : 1, 2- 10^{16} cm^{-3} ; 3- 10^{18} cm^{-3}

This Fig.1. reveals the weak minimum in composition dependence on the InP-rich side of solid solutions system. Such character of composition indicates the appearance of the additional, so-called “alloy” scattering, mechanism of the current carriers scattering relatively to existing mechanisms in InAs and InP. First the “alloy” scattering of current carriers was observed in SiGe semiconductor alloys [7].

The main question at theoretical consideration of current carriers scattering is to analyze inhomogeneity electrostatic potential $V(r)$ modulating the energy bands in semiconductors. The general characteristics of potential $V(r)$ are inhomogeneity amplitude, potential distribution function and characteristic spatial extent of inhomogeneity. The most important is how the inhomogeneity general characteristics of potential $V(r)$ depends on and under what conditions they will be large enough to change considerably the semiconductors properties compared with a homogeneous material [6].

The “alloy” scattering mechanism of current carriers have been originally derived by Brooks [4]. According to Brooks in disordered alloy the composition changes from one region to other one at the expense of statistical fluctuations. This causes energy bands deformation, peaks and dips at the edge of bands, which looks like deformation potential in theory of scattering by thermal vibration of lattice atoms (Fig.2).

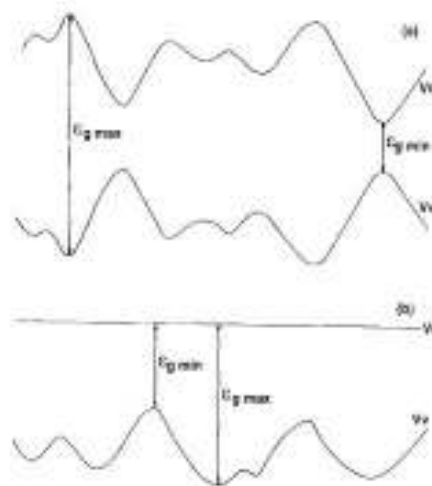


Fig.2. A schematic band diagram of an inhomogeneous semiconductor alloy with small-scale (a) and large-scale (b) composition fluctuations [6].

So “alloy” scattering can be considered as “frozen” scattering by thermal vibration of lattice. The feature of “alloy” scattering is that at low level of carriers concentration its contribution to the mobility increases with increase of alloy components content. At high level of carriers

concentration the mobility depends on alloy components content weakly and scattering is defined by ionized impurities.

We carried out appropriate analysis of the mobility on the basis of reasonable theories [8]. It is necessary to consider simultaneous action of all kinds of carriers scattering in $\text{InP}_x\text{As}_{1-x}$ semiconductor alloys: the “alloy” disorder scattering, scattering on acoustic lattice vibrations, scattering on impurity ions. The net mobility (μ) depends on the various mobility components, associated with each scattering mechanism, as:

$$1/\mu = 1/\mu_{dis} + 1/F (1/\mu_L + 1/\mu_I)$$

where μ_L , and μ_I are the components related to the lattice vibrations and ionized impurity scattering respectively, μ_{dis} is the component related to disorder scattering and F is a correction factor, which takes into account the combined effect of different scattering processes.

Comparison of experimental dates of mobility with theoretical predictions in $\text{InP}_x\text{As}_{1-x}$ solid solutions with $n \sim 10^{16} \text{ cm}^{-3}$ has shown, that at temperatures near 300 K the prevailing mechanism is the scattering on optical phonons. Contribution of the disorder scattering increases with increasing of InP composition in solid solutions system at fixed temperatures and weakens with lowering of temperature in the range of 4.2–300K and never dominates. Assumption of the existence of an additional mechanism of the current carriers scattering due to the disordered arrangement of solid solution atoms allows achieving the full agreement of experimental mobility with the theory.

Obtained composition dependence of current carriers mobility for $\text{InP}_x\text{As}_{1-x}$ alloys (Fig. 1) differs from the similar dependence for $\text{Si}_x\text{Ge}_{1-x}$ alloys [7] with well-defined minimum in the middle of alloys system. The data for alloy scattering in $\text{InP}_x\text{As}_{1-x}$ solid solutions do not reveal such tendency. An estimate of maximal share of disorder scattering in $\text{InP}_x\text{As}_{1-x}$ solid solutions results in the value which does not exceed ~20% of total magnitude of determinative scattering at 300K and ~10% at lower temperatures. The reason of absence of clear minimum in the composition dependence of mobility for $\text{InP}_x\text{As}_{1-x}$ solid solutions, as for $\text{Si}_x\text{Ge}_{1-x}$ alloys, may be apparently connected with the specific properties of $\text{InP}_x\text{As}_{1-x}$ caused by fact, that sublattices of InP and InAs retain a certain natural properties in contrast to Si and Ge in $\text{Si}_x\text{Ge}_{1-x}$ alloys. Model of inhomogeneities, describing disordered regions and applying for explanation of experimental results, was found to be in fair agreement with

experimental data. The “alloy “ disorders in $\text{InP}_x\text{As}_{1-x}$ practically do not disturb the crystal lattice in tangible way at temperatures in the range of 4.2-300 K.

REFERENCES

1. B. Shklovski and A. Efros, *Electronic Properties of Doped Semiconductors*, Springer, Berlin, 1984, p.136.
2. H. Brooks, *J. Appl. Phys.*, **30**, 1959, pp 1118-1124.
3. E. Khutsishvili, M. Kekua, M., *Phys. Stat. Sol. (a)*, 61, 1980, pp. K1-K2.
4. L. Makowski, M. Glicksman, *J.Phys. Chem. Solids.*, **34**, 1973, pp. 487-492.
5. H. Weiss, *Zeitschrift Naturforschung, Teil A* 11, 1956, pp.430-434.
6. A. Y. Shik, *Electronic Properties of Inhomogeneous Semiconductors*, Electro Component Science Monographs, Gordon & Breach Science Pub., 1995, p.153.
7. M.Kekua, E.Khutsishvili, *Germanium–Silicon Semiconductor Solid Solutions*, Metsniereba. Tbilisi, 1985, p.175.
8. A. Anselm, *Introduction to the Theory of Semiconductors*, Nauka, Moscow, 1978.

BIODEGRADABLE POLYMER COMPOSITE MATERIALS MADE FROM INORGANIC FILLERS AND FIBERS

S. Kvinikadze*^{1,2}, N. Chikhradze², A. Vanishvili², G. Abashidze², R. Katsarava^{1,3}

¹ Georgian Technical University, 77, Kostava Str., Tbilisi 0160, Georgia

² LEPL. G. Tsulukidze Mining institute, 7, E.Mindeli Str., Tbilisi 0186, Georgia

³ Institute of Chemistry and Molecular Engineering, Kakha Bendukidze University Campus, 240 David Aghmashenebeli Alley, 0159, Tbilisi, Georgia

* sophi.kvinikadze@gmail.com, tmi@mining.org.ge

Polymer composites (PCs) made of polyester resins have gained increased attention as construction materials. The construction of bridges and concrete repair are new areas where the use potential of polyester resins has increased drastically[1]. Different inorganic fillers, including various fibrous materials (FM), are used for the production of PCs. The FMs substantially enhance the mechanical properties of PC. Basalt and metal fiber are unique fibers having high density and specific rupture properties at a certain load. Above mentioned properties allow its use in many applications [2].

One of the significant components of PC is the andesite filler of Bakuriani mine which we successfully used for making PCs [3]. For obtaining highly filled PCs of enhanced mechanical strength we decided to use two fractions of andesite. The first fraction is a coarse fraction with the particles size up to 1,5 mm and the second fraction is a fine micro and nano fraction. The coarse fraction was obtained by using of “Retsch” crusher, and fine micro and nano fraction (so-called “andesite powder”) – by grinding of coarse fraction in the “Fritsch“ mill. The PC samples of armoplastoconcrete (type of PC) were also produced. Graphite was selected as armoplastoconcrete aggregate. Graphite with its mechanical characteristics is acceptable and non-deficit raw material. The optimal size of Graphite riprap is considered 10-12mm. Duramax-type steel fibers with hooked ends were used for reinforcement. Dramix type basalt fiber length is 3,5 cm and its diameter is 0,6 mm. Metal fibers (TurboBuild integral) with a length of 2cm and with diameter of 15mkm; linear density 550 tacks. Above mentioned fibers are shown in Figures 1-2.

A producer of basalt fibers is Basalt Fibers LLC, Rustavi. To determine metal fiber corrosion resistance those were placed in the area of plastconcrete. The fibers did not reveal the significant signs of corrosion because weight loss was only 0.03%.



Fig. 1. Metal fibers



Fig. 2. Basalt fibers

Cylindrical and cubic-shaped samples were fabricated by using of andesite filler, Graphite riprap, and metal basalt fibers. Polyester resin was used as a binder of the above-mentioned components. Diameter of the armoplastoconcrete (cylindrical shaped) samples was 10 cm and the length of this sample was 9-10 cm. The side length of cubic shaped armoplastoconcrete sample was 10 cm. Therefore, we have explored the characteristics of cubic shape and cylindrical shaped armoplastconcrete .

1. The process of hardening of fine-grained plastoconcrete (fabricated on a base of polyester resin) is studied according to the increase in time of the indicators of durability on tension and compressing, as well as hardness. It was determined that after 3-7 days, the durability on the tension of plastoconcrete is approximately 60% of the maximum durability, on compressing – 95%, and hardness – 58% of the maximum hardness;
2. The average weight of the produced armoplastoconcrete is 2,29 gr/cm³, specific weight - 3,09 gr/cm³, general porosity – 25,8%, open porosity – 5,7%, closed porosity – 21,0%, water absorption – 0,32%;
3. The durability limit of plastoconcrete on compressing is 57,0MPa, armoplastoconcretes - 72,6-76,0MPa. Reinforcing by fibers gives a 27-33 % increase of the durability limit on compressing of plastoconcrete. There is no big difference between the durability limits of plastoconcrete reinforced by steel and basalt fibers. The diagram presented below (see Figure 3) reflects the comparative durability of cement-concrete and reinforced polymer concrete on compressing;
4. The durability limit of plastoconcrete is 7,35MPa, armobasalt –plastoconcrete -10,4MPa, and armosteel – plastoconcrete - 8,42MPa. So, The durability of plastoconcrete on tension compared to cement concrete’s durability is approximately 7 times higher. Reinforcing of plastoconcrete by basalt and steel fibers gives the increase of durability accordingly by 41

and 14%. In this case, a basalt fiber not only equals but also exceeds with its efficiency a steel fiber;

5. The preference of plastoconcrete at shocking compared to cement concrete was increased. The indicator of shock resistance of cement concrete is $3,3\text{kgf.cm/cm}^3$, the analogue indicator of plastoconcrete - $36,2\text{kgf.cm/cm}^3$. Unlike cement concrete, basalt, as well as steel fibers (inserted in plastoconcrete) do not increase a shock resistance indicator seriously.

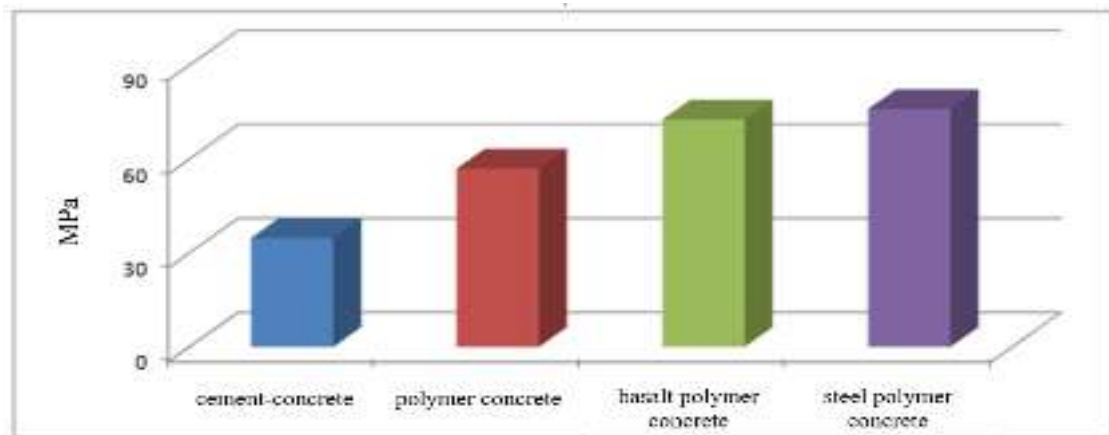


Fig. 3. The comparative durability of cement-concrete and reinforced polymer concrete on compressing

It is clear from above mentioned data that armpolymerconcrete is highly recommended because of it many positive mechanical properties but most importantly it is not biodegradable.

Nowadays, one of the most important and rapidly developing fields of a modern macromolecular chemistry is a chemistry of biodegradable polymers and technology. It is widely recognized fact that chemistry of biodegradable polymers and technology is fast developing and crucial field of chemistry. Nowadays we have a lot of biodegradable polymers available produced by several scientific societies and one of them is homo-PEUs.

In 1997, Katsarava et al. [4] published a synthesis of homo-PEUs (1-L6), without using diisocyanates, via active polycondensation. In this procedure, active carbonates (e.g. di-p-nitrophenyl carbonate) interact with di-p-toluenesulfonic acid salts of bis (α-amino acid)-α,ω-alkylenediester. They have developed a novel class of amino acid-based poly (ester urea)s (PEU) materials which are biodegradable in vivo and possess mechanical properties superior

to conventionally used polyesters (<3.5 MPa) [5]. Table 1 below summarizes the properties of exemplary PEUs.

Table 1

Polymer designation	Tensile Stress at Yield (MPa)	Percent Elongation	Young's modulus (MPa)
1-L-Leu-6	21	114	622

Homo-PEU (1-L6) was used as a biodegradable component of PC and round-shaped samples were made. PC with above mentioned biodegradable components are shown in Figures 3-4. The biodegradability and mechanical characteristics of the samples shown in Figures 4 and 5 are under exploration. It is noticeable that we are exploring biodegradability characteristics in natural conditions



Fig. 4. The sample prepared for biodegradability study

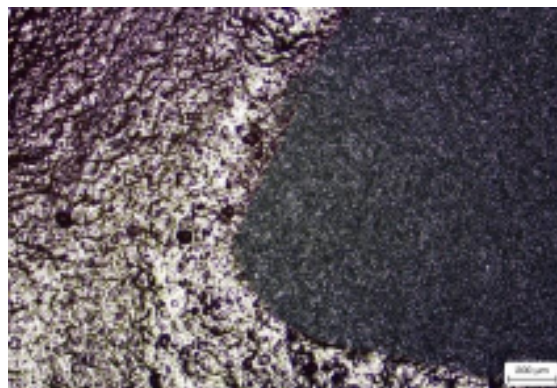


Fig. 5. The sample's morphology, Zeiss (x50)

The innovative idea of this research is to make a composite, which would be strengthened by fibers and solid nanoparticles. It should be noted that this sort of polymer would satisfy a wide range of requirements. we are able to insert the biodegradable components into polymer material that would convert polymer material into biodegradable material and therefore our planet would be protected from potential pollutants.

ACKNOWLEDGMENT(S)

This work was supported by the Shota Rustaveli National Science Foundation (SRNSF) [Grant CARYS19-836, Title: “Development of shock-resistant and biodegradable polymeric composites and provision of a technology transfer”].

REFERENCES

1. Unsaturated Polyester Resins, Jürgen H. Aurer, Ab Kasper;
2. Basalt - A technical fibre for civil applications; R.Turukmane, S. S Gulhane, A. Daberao; Chemical Fibers International, 2018;
3. Production of disperse reinforced cement-free concrete; G. Tsulukidze Mining Institute, 2016;
4. Amino acid-based bioanalogous polymers. Synthesis, and study of regular poly(ester amide)s based on bis(alpha-amino acid) alpha, omega-alkylene diesters, and aliphatic dicarboxylic acids; R. Katsarava, V, Beridze, N, Arabuli, D, Kharadze, Chu CC, Won CY. J Polym Sci Part A: Polym Chem 1998;37:391;
5. Poly(ester urea) Polymers And Methods of Use; R. Katsarava, D. Tugushi, Z. D. Gomurashvili; United States Patent; Patent No.: US 8,765,164 B2.

DETERMINING AMOUNT OF NITROGEN DIOXIDE (NO₂) IN THE ATMOSPHERE BY USING OF THE COST-EFFECTIVE SENSORS AND ANALYSIS OF THE COLLECTED DATA

L. Kirtadze*¹ G. Jibuti²

¹ San-Diego State University Georgia, Tbilisi, Kostava str., 3, Georgia

² Tbilisi State University, Tbilisi, Chavchavadze str., 3, Georgia

* lkirtadze4594@sdsu.edu

giorgi.jibuti@tsu.ge

Anthropogenic activities, such as rising energy usage and production, as well as natural processes, release enormous amount of trace pollutants into the atmosphere, affecting Earth's living environment. After beginning of the industrialization process in 19th century, number of different types of pollutants had been increased in the atmosphere. It should be noted that effects of the increased number of pollutants are severe, because huge amount of greenhouse gases changed energy balance on the Earth and several pollutants affected human and ecosystem health. Therefore, it is crucially important to investigate ongoing physical and chemical processes in the atmosphere and that is why the research of the atmosphere pollution is one of the most important research topics. Nitrogen Dioxide (NO₂) is considered as one of the most widely spread pollutants, among several different pollutants. The source of that pollutant might be different, but primary source is fuel combustion processes. NO₂ possess ability to undergo transformation process and that is why it can be precursor of several pollutants such as acid rains and Ozone (O₃). Based on the above provided information, it can be concluded that it is important to have improved methods to control NO₂ emission and accumulation process.

The aim of this research is to determine amount of the nitrogen dioxide into the atmosphere by using of the cost-effective sensors and expensive Teledyne NO₂ instrument and compare results of these two instruments and determine how close these results are. Widely spread method for measuring nitrogen dioxide is chemiluminescence method, which is based on the principle of chemiluminescence reaction. The process happens in the reaction vessel between NO₂ and O₃. During that reaction high energy state NO₂* is formed. The energy emitted by the NO₂* is proportional to the amount of the Nitrogen dioxide. The principle based on which cost-effective sensor works is electrochemical. The target air is oxidized or reduced on the electrode and produced current is measured. The amount of current produced by the sample is proportional to the amount of sample that has been oxidized or reduced.

In this research we used both sensor and chemiluminescence methods for determining amount of the Nitrogen Oxides. The research has been conducted by using of the sensor “Flying Laboratory SOWA” from the SMART|AtmoSim_LAB of Tbilisi State University and by using of the National Environmental Agency’s instrument that works based on the chemiluminescence principle (“Teledyne NOx +O3 analyzer-Model T204”). Sensor was placed on the National Environmental Agency’s station and data was collected for two months. Collected data was analyzed by using of the MathWorks MATLAB and Microsoft Excel.

Nitrogen Dioxide concentration vs time plots had been plotted and various trends has been evaluated. It should be noted that, station measured NO₂, and sensor measured NO₂ has been plotted together on the graph.

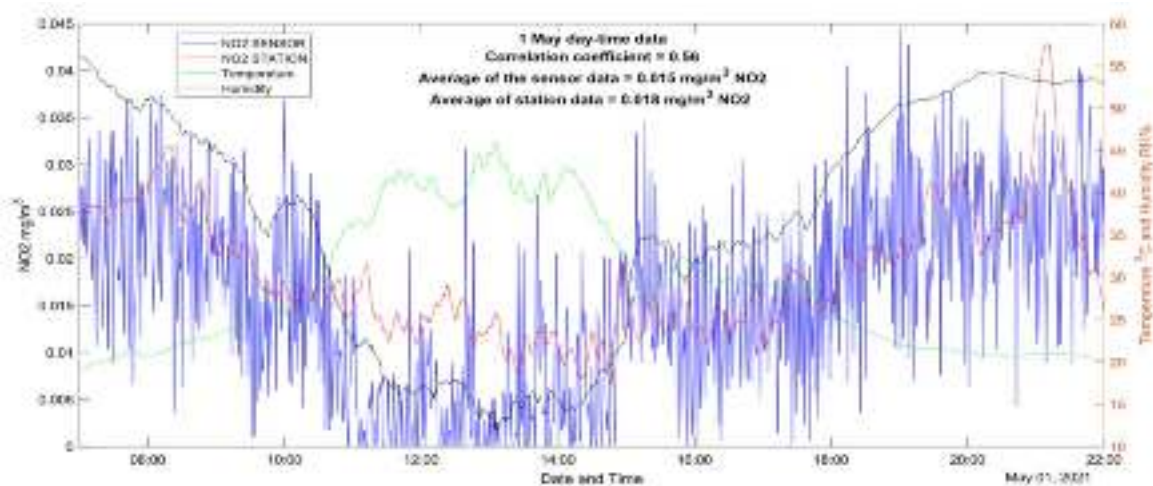


Fig. 1: 1st May, day-time data

Sensor data has noticeable noise and that is why the data had been smoothed by using of the moving average smoothing method.

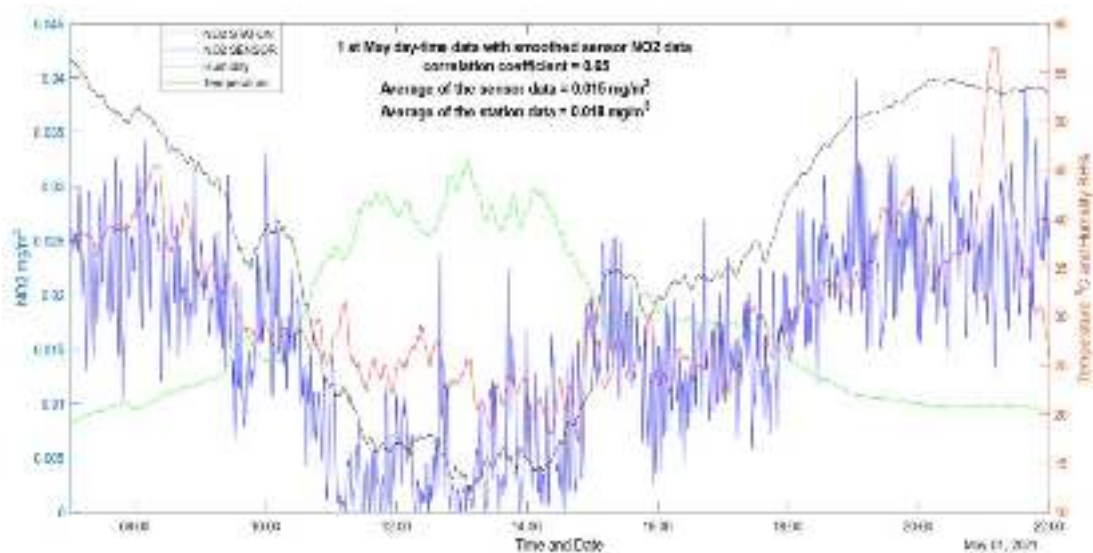


Fig. 2: 1 May day time with smoothed sensor data

Based on the correlation coefficient value, it can be concluded that the data collected by the sensor and the data collected by the station chemiluminescence apparatus are quite close. It is noticeable that during three-month, sensor was working without any kind of problem while it is not created to work in this kind of regime.

Based on the collected results it can be concluded that, amount of the nitrogen dioxide is increased during the daytime period and decreased during the nighttime period. This fact most likely is the result of the transport traffic which is more intensive during the day and less intensive during the nighttime period especially due to the current corona virus pandemic restrictions. It should be also noted, that given station is located in recreation area and is away from heavy traffic, but it still has main influence on NO₂ concentration in air.

REFERENCES

1. Alsobaai, A. "Storage of Nitrous Oxide (NO_x) in Diesel Engine Exhaust Gas Using Alumina-Based Catalysts: Preparation, Characterization, and Testing." *The Journal of Engineering Research (Print)* 14.1 (2017): 64-73. Web.
2. Chen, Chun-Han, and Li, Yueh-Heng. "Role of N₂O and Equivalence Ratio on NO_x Formation of Methane/nitrous Oxide Premixed Flames." *Combustion and Flame* 223 (2021): 42-54. Web.
3. Brune, William H. "Atmospheric Chemistry in a Changing World." *Eos, Transactions American Geophysical Union* 84.45 (2003): 494. Web.
4. Letcher, and Letcher, T. M. *Climate Change: Observed Impacts on Planet Earth*. 1st ed. Amsterdam: Elsevier, 2009. Web.
5. Bigazzi, A.Y. and Figliozzi, M.A. (2014) Review of urban bicyclists intake and uptake of traffic-related air pollution. *Transport Reviews* 34(2), 221–245.
6. Davis, L.W. (2008) The effect of driving restrictions on air quality in Mexico City. *Journal of Political Economy* 116(1), 38–81.
7. Fiore, A.M., Naik, V. and Leibensperger, E.M. (2015) Air quality and climate connections. *Journal of the Air & Waste Management Association* 65(6), 645–685.
8. Grant, U. (2012) *Urbanization and the Employment Opportunities of Youth in Developing Countries*. UNESCO Report. Available at: <http://unesdoc.unesco.org/images/0021/002178/217879e.pdf> (accessed 2 July 2018).
9. Heck, W.W., Taylor, O.C. and Tingey, D.T. (eds) (1988) *Assessment of Crop Loss From Air Pollutants*. Springer, Dordrecht, The Netherlands.
10. Omidi, Y., Goudarzi, G., Heidari, A. M., & Daryanoosh, S. M. (2016). Health impact assessment of short-term exposure to NO₂ in Kermanshah, Iran using AirQ model. *Environmental Health Engineering and Management Journal*.

DETERMINATION OF TECHNOLOGICAL PARAMETERS FOR THE PRODUCTION OF ALUMINUM ALLOYS (8-22 MM) BY THE METHOD OF "WITHOUT INGOT ROLLING"

G. Kevkhishvili*, T. Namichishvili, I.Jordania, J. Loria, V. Ramishvili, J. Gamsakhurdia

Ferdinand Tavadze Metallurgy and Materials Science Institute, 8b E. Mindeli Str., Tbilisi, 0186, Georgia

gkevkishvili@mail.ru

ABSTRACT. For several years Georgian Institute of Metallurgy and Materials Science has been actively working now to develop the technology of "without ingot rolling". where casting and rolling plant was designed and pilot version constructed. The method is a combination of two independent processes (continuous casting, hot rolling). This work discusses in detail the mechanism for the formation of the primary billet in a combined mold. The article discusses the methodology for determining the basic technological parameters of the process "without ingot rolling " of their relationship with structural, powerful energy parameters and mechanical properties of the work pieces. The values of all parameters and their interdependence are provided in the paper as nomogram. The experiments show that the difference between theoretical computations and experimental data is no more than 5-7%. The specified method has mastered the technology of producing aluminum leaves with a thickness of 8,10,16,22 mm by the method "without ingot rolling."

Key words: crystallizer, roll, billet, crystallization front, meniscus of the liquid metal, deformation.

Today, the world leading steel manufacturers pay great attention to development of the highly efficient modular equipment and plants for low-productive companies. Against the background of the world energy crisis, great emphasis is placed on significant reduction of energy carriers and capital investments per ton metal production. In that direction the priority is given to metal sheets production using compact casting and rolling plants (so-called direct method). The mentioned method permits 6-7-fold reduction of energy resources, reduction of steel loss by 5-7%, and moreover, it allows to cut out 60-70% of expensive equipment and plants from the technological processes (casting and rolling plants), which, in its part, leads to significant reduction of production space and capital investments. All of these together with the highly ecological factors show clearly why the mentioned method is considered to be the most actual and prospective today.

The method of direct rolling is quite simple. Liquid metal is poured between a pair of rotating rolls equipped with cooling system and placed in a horizontal plane at a certain distance

from each other. Rotation velocity is such that the billet coming out of the rolls has enough time for crystallization. By means of the rolls rotation velocity variation the metal crystallization front can be shifted to the line joining the centers of the rolls to regulate the hot rolling process necessary for producing a strong fine-grained structure. Georgian Institute of Metallurgy and Materials has been actively working for several years now to develop the technology of “casting and rolling” process. According to the detailed analysis of the available sources a pilot casting and rolling plant construction was developed and fabricated in metal. At the first stage, the values of minimum tensile stresses, which provide the mechanical and structural properties characteristic of rolling, were studied during hot rolling.

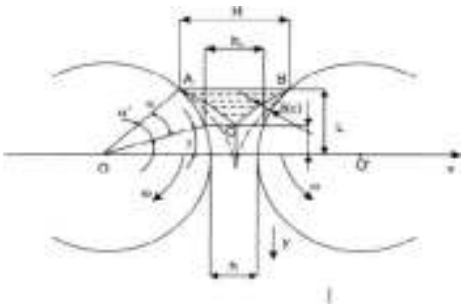


Fig. 1. Scheme of the billet shaping process in direct rolling

They were processed aluminium billets in hot rolling (500-550°C) Ø16mm were casted at different strains ϵ 20-60%. It was estimated that at 35-40% strain the samples completely satisfy properties of the rolled metal. The forces generated on the rolls at 0-60% strain were theoretically calculated (with account of the billet size, the temperature and chemical composition of the metal, the diameter and rotation velocity of the rolls). Relation between the forces generated on the rolls.

As it was mentioned above, by means of the rolls rotation velocity variation the liquid metal crystallization front (point C, Fig. 1) can be shifted to the line OO' joining the centers of the rolls. The higher the point the more is the billet strain in hot rolling, and consequently, the greater are the forces generated on the rolls. These are the forces regulating the process of casting. Theoretical calculation estimates the force to be maintained throughout the process of casting in order to avoid the metal crack (due to insufficient cooling) and the billet jam between the rolls due to the greater strain than admissible.

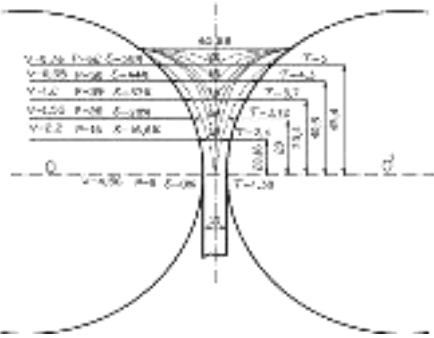


Fig. 2. Nomogram of relation between the billet crystallization velocity and the forces Generated on the rolls in the process of direct rolling. h=10mm ,

“without ingot rolling” process, a combined mold is used, two movable (wolves) and two fixed (side blocking plates) walls. during hot rolling from the crystallizer, the resulting billet is subjected to resistance both on the roll and on the side plates,

due to the acting forces. on the side plates, these forces are caused firstly by the ferrostatic pressure of the molten metal, and secondly by hot rolling of the work piece caused by the transverse deformation process due to friction end by slipping. Both values are so small that they can be neglected when calculating the energy parameters. Thus, we know the location of the metal meniscus with respect to the axial line 00^1 (angle α is taken from the recommendation in the literature [4.5.]), And in the case of 35–40% of the tension point C, using the proposed empirical formula, we calculate the time required for obtaining thickness $1/2h$, and the speed of rotation of the rolls which is equal to:

$$w = \frac{(\alpha - \gamma)2k\cos^2\gamma}{R^2} \left[\left(1 + \frac{h}{2R}\right) - \cos\gamma \left(2 + \frac{h}{R} - \frac{x_0}{R} - \frac{bx_0}{R^2}\right) + \cos^2\gamma \left(1 - \frac{x_0}{R}\right) \right]$$

W-is the angular velocity of rotation of the rolls; α -A angle point value; R-radius of the rolls, m; γ -C- is the angle at the point; h -is the thickness of the work pieces, m; K-value crystallization characteristic in measurement m^2 / min .; X_0 - the growth rate of the crust thickness at the initial stage of crystallization is m. On the basis of the method described above the optimal velocity for the rolls with 420mm diameter was established to be 0.7rot/min ($V=0.92 \text{ m/min}$) for casting an aluminium sheet of 10mm thickness and 240mm width at 35-40% strain. Certainly, in real process of casting the crystallization front is not uniformly distributed throughout the cross section, which is due to the method of liquid metal delivery to the crystallizer. The metal flows derived at that moment break the integrity of the crystallization front. Therefore, in real casting the forces derived on rolls are admissible to be 5-10% more compared to the optimal one, the more so if the forces of friction coefficient on the lateral closing plates are neglected. As our experiment shows, during casting the forces change to 35-65t in great interval, but it is well regulated by means of the rolls rotation velocity providing a stable process. Such a change of forces is caused by fluctuation of the level of liquid metal in crystalizer because casting from the intermediate ladle is manu ally done. In conditions of 420 mm diameter crystallizer when $\alpha=30^\circ$ the height of the metal pole in the crystallizer is just 110 -115mm, while 10-20mm variation of the metal has a great influence on crystallizaion process. Experimental casting proceeds in quite a short period (3) and since the velocity variation process is easily regulated this is not a great problem. How- ever, in conditions of manufacture the all-around automation of the process will be necessary. The same method was used for estimating the velocity for aluminium sheets of 8-9 mm thick.As the experiments showed, technological parameters computed theoretically do not greatly differ from the parameters estimated experimentally.

The method is a combination of two independent processes (continuous casting, hot rolling). First of all, we assessed the minimum strains providing properties of the rolled metal for the billet produced by the method. Examination of metallographic and mechanic properties of the samples produced with different strains show that the strain of 35-40% is quite sufficient for the billet to gain the properties of rolled metal. Under such strain proper time and velocity necessary for production of the metal sheet of $h/2$ thickness were theoretically calculated. The values of all parameters and their interdependence are provided in the paper as nomograms. The experiments show that the difference between theoretical computations and experimental data is no more than 5-7%. The mentioned method, i.e., the so-called direct method was used to develop the technology for production of aluminium sheets of 8, 10,16 and 22 mm thickness.

CONCIUSIONS

1. Technology Mastering and manufacturing of aluminum alloy sheets with a thickness of 8-22 mm. method " Without ingot rolling ". The optimal values of all the basic technological parameters of the process, their relationship with structural, powerful energy parameters and the mechanical properties of the work pieces are determined.

3.reconstruction of test equipment to move to a new stage. Which concerns the technological process for the manufacture of composite plates with a thickness of 25-45 mm based on aluminum alloys. This work has already been submitted and obtained Patent: P 2018 6913 B.

4.Iron-aluminum, like titanium-aluminum, belongs to the group of incompatible metals in the manufacture of the composite. A method has been developed to establish additional mechanical bonding between composite layers during molding. The application is currently under consideration by the National Intellectual Property Center of Georgia.

REFERENCES:

1. Brovman M. Ia., Marchenko I. K., Kan Yu. (1976) Usovershenstvovanie tekhnologii I oborudovaniia mashin nepreryvnogo lit'a zagotovok. M., 136 (in Russian);
2. Ramishvili Sh. D., Tkhelidze N. D., Kevkhishvili G. Sh. (1984) Opredelenie usilii vytiagivaniia polei zagotovki iz kristallizatora. Sb. stat'ei, Tbilisi, 70 (in Russian);
3. Ramishvili Sh. D. (1985) Nepreryvnoe lit'e polykh chugunnykh zagotovok. Tbilisi, 36 (in Russian);
4. Brovman M. Ia. (2007) Nepreryvnaia razlivka metallov, M., 482 (in Russian);
5. Tselikov A. I., Tomlenov A. D., Zyuzin V. I., Tretyakov A. V., Nikitin G. C. (1982) Teoriia prokatki Metallurgii, M., 335, 4 (in Russian).

INFLUENCE OF γ -RAYS IRRADIATION ON THE PHYSICAL-MECHANICAL PROPERTIES OF MONOCRYSTALLINE p-Si

I.Kurashvili*¹, T.Kimeridze^{1,2}, G.Chubinidze¹, D.Mkheidze¹, M.Kadaria¹, T.Melashvili¹, N.Gogolashvili¹, V.Kirtskhalia^{1,2}, G.Darsavelidze¹

¹ Ilia Vekua Sukhumi Institute of Physics and Technology, Tbilisi, Georgia

²Sokhumi State University, Tbilisi, Georgia

* i.kurashvili@sipt.org.ge

Investigations of structural defects in silicon introduced with high energy particles or γ -rays have achieved remarkable progress in recent years. Radiation in the room temperature forms numerous vacancies and matrix interstitials in silicon, that can take part in the formation of stable complexes. At present, there is extensive information on changes in the electrophysical properties of irradiated silicon, but further complete studies are required to establish a firm understanding of their microscopic mechanisms. This information is necessary to create new semiconducting materials and equipment based on Si with controllable parameters. There is very little information about the relationship between the electrophysical properties of neutrons-irradiated silicon and the characteristics of the internal friction temperature spectra [1]. Obtained results show wide application possibilities of the internal friction in the investigations of radiation defects.

In the experiment boron doped monocrystalline silicon grown by Czochralski method in [111] direction was used. Double-side polished plates with (111) orientation and 0,5-1 mm thickness and rods: 0,8x0,8x30mm³ with [111] direction were prepared for the investigations. The investigated samples are characterized with resistivity 200ohm.cm and dislocation density $\sim 10^4\text{cm}^{-2}$.

Electrophysical characteristics were determined in the constant magnetic field of 0.5 Tesla induction on the Ecopia HMS-3000 device by Hall effect measurements. Optical absorption spectra of IR irradiation were studied on Cary 660 FTIR Spectrometer. Dynamic mechanical characteristics were determined by internal friction method at torsion oscillations frequency $\sim 1\text{Hz}$ and in the ranges of $5 \cdot 10^{-5}$ - 10^{-3} strain amplitude. The samples were irradiated at room temperature with γ -rays from a ⁶⁰Co source (E=1,25MeV) to a fluence of $2 \cdot 10^{17}\text{cm}^{-2}$ photons (Irradiation by γ -rays from ⁶⁰Co was conducted on the Agat-Metrology radiation device at Georgian National Agency for Standards and Metrology).

Electrophysical characteristics of highly polished Si:B substrates in initial, γ -rays irradiated and annealed (at 300^oC, 0,5 hrs.) states were studied at room temperature. Current carriers' mobility is sufficiently high in the initial state that indicates homogeneous distribution of dopant B atoms and dislocations formed during growth in monocrystalline Si structure. Noticeable increase of electrical resistivity and slight decrease of current carriers' mobility and concentration is observed in γ -rays irradiated state.

Table 1. Electrophysical characteristics of p-Si:B monocrystals

p-Si:B (111)	Resistivity, ohm cm	Holes concentration, cm ⁻³	Holes mobility, cm ² ·V ⁻¹ ·sec ⁻¹
Initial state	200	8·10 ¹³	450
After γ -rays irradiation, 2·10 ¹⁷ cm ⁻²	235	6·10 ¹³	445
After annealing at 300 °C, 0,5hrs	130	1·10 ¹⁴	455

Effect of thermal annealing at 300 °C temperature on the electrophysical characteristics was studied. Radical changes in the structure of radiation defects are expected at these temperatures. In particular, dissolution of divacancies and vacancy-oxygen pairs and formation of new, thermally stable complexes [2-3]. Actually, annealing in vacuum at 300^oC temperature for 0,5 hrs cause significant decrease of resistivity, slight increase of holes mobility and concentration. It is supposed, that these changes of electrophysical parameters are stipulated by decrease of concentration of electrically active radiation defects, formation of new complexes and shift of important part of thermal and radiation origin defects in the core and atmospheres of dislocations.

Abundance of overlapping maxima stipulated by the interactions of current carriers, lattice oscillations and electronic transitions have been revealed in a wide range of wave number of IR irradiation optical absorption spectra. As expected, maxima related to optically active oxygen (1105cm⁻¹) and carbon (505cm⁻¹) are distinguished with high absorption intensity. In the optical absorption spectrum after γ -rays irradiation maximum has been revealed in a wave number region of 2360cm⁻¹.

Thermal annealing causes a weak reduction of intensity of maximum related to the optically active oxygen atoms. It is supposed, that oxygen atoms react with radiation defects during annealing and forms complexes. This assumption is confirmed by the fact that intensity of

maxima in 885-890 cm^{-1} region related to the optically active, electrically neutral VO_2 complexes increases by 15-20% in the annealed state. According to the literature [3-4], this transformation is stipulated by recombination of divacancy dissolution products- vacancy and oxygen atoms. The formation of VO_2 complex should also be associated with a weakening of the negatively charged divacancy maximum at 2360 cm^{-1} . It should be noted, that the dislocations together with their atmosphere, is a very effective source of radiation defects capture and subsequent transformation. Dislocation can make a significant contribution in modifying an influence of γ -rays irradiation[5].

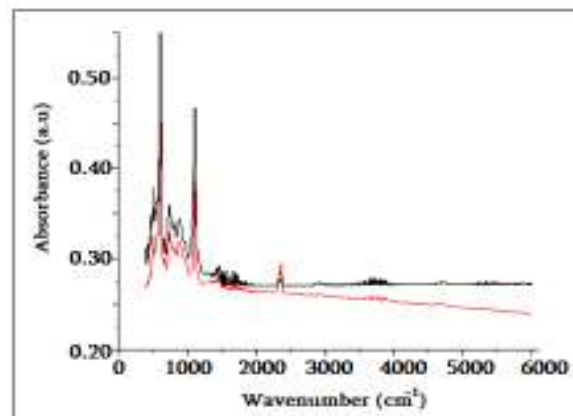


Fig.1. IR irradiation optical absorption spectra of Si plates with (111) orientation
1-initial, 2- after γ -rays irradiation

Internal friction and shear modulus amplitude dependences have been investigated at room temperature. In initial state Si is characterized with unchanged internal friction intensity in a range of $5 \cdot 10^{-5}$ - $1 \cdot 10^{-4}$ strain amplitude. Linear increase of internal friction begins from the critical point $1 \cdot 10^{-4}$ and continues up to $1 \cdot 10^{-3}$ strain amplitude (fig.2 a). Internal friction change is reversible in a range of $5 \cdot 10^{-5}$ - $1 \cdot 10^{-3}$ strain amplitude, which indicates absence of plastic deformation in sample structure under such conditions. γ -rays irradiation causes an increase of critical strain amplitude up to $4,5 \cdot 10^{-4}$, significantly reduces an inclination of internal friction linear branch on the $Q^{-1}(\epsilon)$ curve. In a wide range of strain amplitude internal friction change is still characterized by complete reversibility. Annealing of γ -irradiated sample causes further increase of critical strain amplitude up to $5 \cdot 10^{-4}$. For comparison it should be noted that annealed (at 300 $^{\circ}\text{C}$) non-irradiated silicon is characterized with critical strain amplitude increased only by 15%.

Torsional oscillations frequency squared (f^2) proportional to the shear modulus decreases monotonically by increasing strain amplitude. Shear modulus reduction rate increases sharply

at the critical point of strain amplitude. Fig.2.b shows regularities of changes in dynamic shear modulus under the influence of γ -irradiation and thermal annealing.

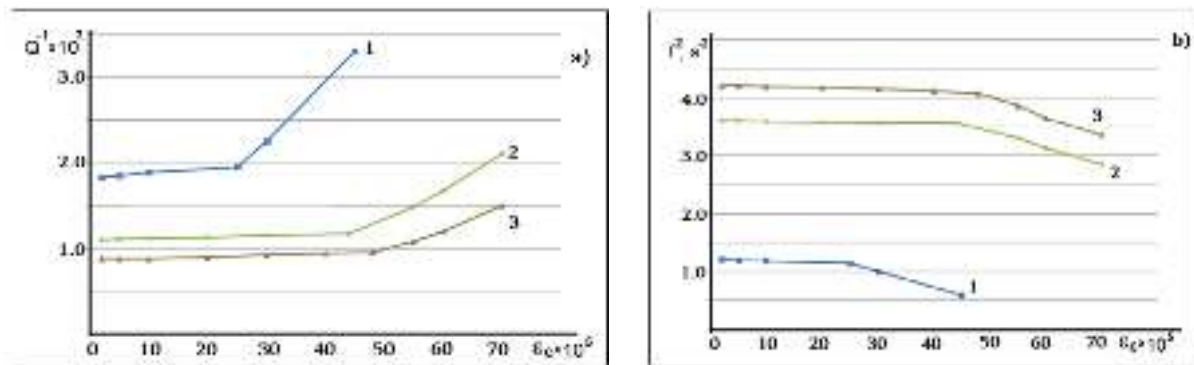


Fig.2. Amplitude dependences of internal friction (a) and shear modulus (b) of monocrystalline Si [111] in initial state (1), after γ -rays irradiation (2), after thermal annealing at 300°C, 0,5 hrs (3).

Changes of electrophysical characteristics and IR irradiation optical spectra stipulated by γ -irradiation and thermal annealing of monocrystalline Si have revealed transformations in the structure of radiation defects. It is supposed, that as a result of transformation high thermally stable complexes containing vacancies and oxygen atoms have been generated.

Migration of defects towards dislocation nuclei is stimulated in a deformation field localized with dislocations existing in Si structure. Respectively their effective blocking takes place, which is reflected in an increase of the main characteristic of dislocation-pinning center, critical amplitude, by 3-4 times in γ -rays irradiated monocrystalline Si.

REFERENCES

1. L.N. Aleksandrov, M.I.Zotov, V.F.Stas, B.P.Surin. J. Physics and Technology of Semiconductors, 18, #1, 1984, pp.72-75 (in Russian)
2. A. Chroneos, C.A.Londos, E.N. Sgourou, P.Pochet. J. Applied Physics Letters, 99, 2011, 241901 doi: 10.1063/1.3666226
3. C.A.Londos, E.N. Sgourou, D.Hall, A. Chroneos, J. Material Science: Materials in Electronics 25, 2014, pp.2395-2410
4. N.V.Sarlis, C.A.Londos, L.G.Fytros. J.Applied Physics, 81 (4), 1997, pp.1645-1650
5. L.A.Kazakevich, P.F.Lugakov. J. Phys. Stat. Sol (1), 71, 1982, pp.99-108.

ADVANCED SHS COMPOSITES AND COATINGS FOR THE HIGH-TEMPERATURE FIELDS OF APPLICATIONS

E. Levashov*, S. Vorotilo, V. Kurbatkina, Yu. Pogozev

National University of Science and Technology «MISIS», Leninsky prospect 4, 119049, Moscow, Russia

* levashov@shs.misis.ru

Elemental and magnesium-thermal self-propagating high-temperature synthesis (SHS), hot pressing and spark plasma sintering were used to produce ultra-high temperature ceramics (UHTCs) based on the solid solutions of carbides (Ta,Zr)C, (Ta,Hf)C and borides (Ta,Zr)B₂, (Ta,Hf)B₂. UHTCs demonstrated high resistance against the impact of high-enthalpy oxidative gas flow. Sequences of chemical and structural transformations were investigated. At 3000 °C, the rate of thermochemical corrosion of carbide-based UHTCs was 15-20% lower as compared to the basic composites, whereas the boride ceramics based on (Ta,Zr)B₂, (Ta,Hf)B₂ demonstrated decomposition enthalpy up to 390 kJ/g, which is an order of magnitude higher than the enthalpy of analogous materials. To enhance the oxidation resistance, silicides MoSi₂, ZrSi₂ and TaSi₂ were added to the UHTCs.

SHS in the ZrB₂-MoSi₂-ZrSi₂ and HfB₂-MoSi₂-HfSi₂ systems was employed to obtain heterophase powders with 1-2 μm boride grains and 2-4 μm silicide grains. Eutectic colonies Me^{IV}Si₂-MoSi₂ were present within the molybdenum disilicide grains. The peculiarities of infiltration of carbon framework by Me^{IV}-Me^{VI}-B-Si melt were studied.

Hierarchically-structured TaSi₂-SiC ceramic reinforced with discrete SiC and Si₃N₄ fibers was synthesized. This ceramic combined high hardness and fracture toughness and was used for plasma-ionic sputtering of high-temperature coatings.

This study proposes a combustion-based ceramic matrix composite processing technique intended on single-step *in situ* deposition of single-crystal SiC nanowires (SiC_{nw}) on the surface of carbon fibers (C_f) and formation of SiC_{nw}-reinforced SiC matrix. This was accomplished by Ta-catalyzed combustion of poly-(C₂F₄)-containing reactive mixtures with pre-mixed chopped C_f. Depending on the combustion conditions, carbon fiber surface is subjected either to formation of diffusion layers, ceramic particle incrustation or growth of continuous arrays of carbon-coated single-crystal SiC_{nw} with a nearly defect-free lattice, 10-50 nm diameter and 15-20 μm length. Thermodynamics, phase and structure formation mechanisms were explored, and the optimal conditions were outlined for reproducible C_f/in

situ SiC_{nw} dual reinforcement of SiC-based ceramics. Hot pressing at 1500 °C produced C_f/in situ SiC_{nw}-reinforced ceramic SiC-TaSi₂ specimens with a relative density of 97%, 19 GPa Vickers hardness, 3-point flexural strength $\sigma = 420 \pm 70$ MPa and fracture toughness $K_{IC} = 12.5$ MPa·m^{1/2}.

The coatings consisted of amorphous phase with the inclusion of nanoparticles of fcc solid solution Ta(Si,C,N). Coatings had the hardness of 26 GPa and Young modulus of 268 GPa and were characterized by thermal stability up to 800°C and friction coefficient of 0.2 (at 800°C). Low friction coefficient was caused by formation of thin oxide layer consisting of TaSi_xO_y nanofibers in the contact zone.

The work was supported by the Russian Science Foundation (Agreement No. 19-19-00117).

REFERENCES

1. S. Vorotilo, E.A. Levashov, et al. *Ceramics Intern.*, [Vol. 45, Is. 2](#), 2019, pp. 1503-1512
2. V.V. Kurbatkina, E.I. Patsera, et al. *Ceramics Intern.*, 45, 2019, pp. 4067-4083
3. S. Vorotilo, A.Yu. Potanin, et al. *Ceramics Intern.*, Vol. 45, Iss. 1, 2019, pp. 96-107,
4. A.N. Astapov, et al. *Ceramics Intern.*, [Vol. 45, Is. 5](#), 2019, pp. 6392-6404
5. A.N. Astapov, et al. *Inter. J. of Heat and Mass Transfer*, 140, 2019, pp. 12–20
6. A.Yu. Potanin, S. Vorotilo, *Corrosion Science*, Vol. 158, 2019, 108074
7. A.Yu. Potanin, et al. *Ceramics Intern.*, Vol. 45, Is. 16, 2019, pp. 20354-20361
8. Kiryukhantsev-Korneev Ph.V., et al. *Ceramics Inter.*, Vol. 46, Is. 2, 2020, pp. 1775-1783
9. A.V. Bondarev, et al. *Surface & Coatings Technology*, 359, 2019, pp. 342–353

ELECTROCHEMICAL BEHAVIOUR OF GOLD IONS ON CARBON ELECTRODES PRODUCED FROM RICE HUSK

Z. Mansurov ^{1,2}, Zh. Supiyeva*^{1,2}, G. Smagulova ^{1,2}, V. Pavlenko ^{1,2}

¹ Institute of Combustion Problems, 172, Bogenbai Batyr str., Almaty, Kazakhstan

² al-Farabi Kazakh National University, 71, al-Farabi ave., Almaty, Kazakhstan

* zhazyra@mail.ru

ABSTRACT

The gold electrodeposition process from a chloroauric solution on carbon electrodes obtained on the basis of rice husk was investigated by means of cyclic voltammetry. The morphology of electrodeposits was analyzed by means of scanning electron microscopy. It has been shown that electrochemical reduction of AuCl_4^- on carbon electrodes occurs until its full recovery, i.e. Au^0 . The scanning electron microscopy allowed to obtain the images of gold adsorbed on the carbon surface, while the morphology of the deposits was described. In particular, it is clearly seen that the surface of carbon has a relief structure and gold has grown in the form of clusters. The smallest gold nanoparticles adsorbed on the surface of carbon electrode that could be examined were 100-250 nm in diameter.

KEY WORDS: gold electrodeposition, carbon electrode, rice husk, cyclic voltammetry

INTRODUCTION

Activated carbons (AC) have a set of unique properties: electrical conductivity, high specific surface area, resistance to many chemical reagents, due to which their practical applications are constantly expanding [1-3].

High interest in gold is associated with various fields of application of this metal and its value as an asset in the financial market. Gold is the subject of numerous studies of electrochemical processes occurring at the surface of various materials. The purpose of this work is to study the anodic oxidation and cathodic reduction of gold ions using carbon-based materials, which were obtained by carbonization and activation of rice husk (RH).

In the present work, gold electrodeposition process on the carbon electrode was studied by means of voltammetry, while the morphology of the electrodeposits was analyzed by scanning electron microscopy (SEM).

EXPERIMENTAL

The cleaned and dried RH was collected from local farms of Almaty region, Kazakhstan, and subjected for carbonization at 500°C in the argon atmosphere. Carbonized RH was mixed with potassium hydroxide by use the weight proportion of 1:5 (carbonized rice husk to KOH) and activated at 850°C under argon atmosphere. The resulting mixture was subjected to washing by distilled water until the neutral pH.

Specific surface area of resulting carbon materials was investigated by use of “Sorbtometer-M”. Microstructural and elemental analysis was carried out using the Quantum 3D 200i Dual System SEM, JEO JSM-6490LA scanning electron microscope and Raman spectroscopy (“NTEGRA Spectra Raman”) with laser wavelength of 473.0 nm, signal with an area diameter of 80 nm. The electrochemical investigations were conducted by using Autolab Potentiostat/Galvanostat Model AUT83945 (PGSTAT302N).

A working solution with the concentration of 100 mg·L⁻¹ were prepared by diluting the standard samples of Au³⁺ ions (“IRGIREDMET”) with distilled water. The basic background electrolyte was a solution of 0.1 mol·L⁻¹ hydrochloric acid.

RESULTS AND DISCUSSION

In order to identify the surface morphological features of synthesized samples, the SEM has been used. As it can be seen from Figure 1 a,b, the samples have a complex structure. Surface macrostructure represent typical macropores with diameter of 4-22 μm (Figure 1a,b). The typical Raman spectrum of graphene exhibit three peaks: peak D at 1351 cm⁻¹, peak G at 1580 cm⁻¹, and peak 2D at 2700 cm⁻¹. The ratio between the intensities of peak G (I_G) and peak 2D (I_{2D}), I_G/I_{2D} gives an estimate of the number of layers [4]. Analysis of Raman spectra (Figure 1c) of carbon material obtained from RH showed the content of graphene films with three or more layers (I_G/I_{2D}= 0.63; 0.50; 0.43; 0.30).

The obtained adsorbents composed of amorphous silica and carbon. Specific surface of annealed RH was determined by BET method; it was 2818 m² g⁻¹, pore specific volume was 1.59 cm³ g⁻¹ and average pore size was within 1.0 ÷ 2.0 nm.

The carbonized and activated rice husk (CARH) have a rather low redox potential and the stationary potential is 0.05 V (Ag/AgCl). The measured stationary (real) potential of gold in a hydrochloric acid medium is equal to 0.47 V (Ag/AgCl). The potential difference between

gold (oxidizing agent) and sorbent (reducing agent) is 0.42 V relative to the reference electrode.

Cyclic voltammetry curves of gold ions in 0.1 M HCl measured on carbon-capped electrodes are illustrated in Fig. 1d (curve 1) [5]. This curved represents an oxidative peak (0.8 V) in the reverse scan and a reductive peak (0.55 V) in the forward scan. The background electrolyte based on 0.1 M HCl measured on a carbon electrode was also examined in this potential region (Fig. 1d, curve 2). However, no clear redox processes were observed. Since activated carbon has a large surface area, large charge-discharge currents of the double electric layer (non-Faraday currents) were revealed.

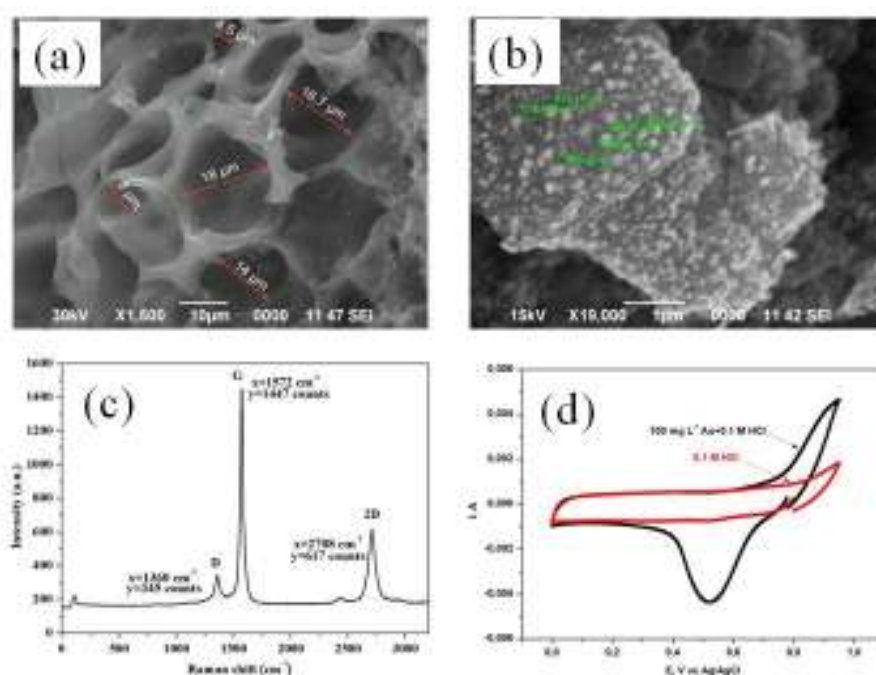


Fig. 1. (a) SEM images of the surface of the carbon electrode before and (b) after adsorption of gold, (c) Raman spectra of activated carbon, (d) Cyclic voltammograms on carbon electrode in (curve 1) 0.1 M HCl + 100 mg·L⁻¹ HAuCl₄ and (curve 2) 0.1 M HCl at 5 mV·s⁻¹.

In turn, charge-discharge currents are due to the large surface area of electrode, which is reflected on the voltammograms. Thereby in order to calculate the kinetic data on the gold electroreduction reaction on this material, compensation should be made for a non-Faraday current. For this purpose, the currents of a double electric layer were taken from the value of the cathodic current peak. Finally, the resulting peak current values were used to calculate the diffusion coefficient which will be discussed during the Conference.

CONCLUSION

The resulting material obtained on the basis of RH was studied by modern and informative methods of physico-chemical analysis including scanning electron microscopy, Raman spectroscopy and BET analysis. It was demonstrated that the resulting material has a developed macroporous structure and possesses a high specific surface area. The electrodeposition of gold was studied in solutions containing HAuCl_4 forming AuCl_4^- ions. When current density was equal to zero, the system exhibited a constant open circuit potential of about +420 mV vs. Ag/AgCl. The diffusion coefficient which will be discussed during the Conference. The features of diffusion coefficients and adsorption capacity will be discussed during the Conference.

ACKNOWLEDGMENTS

Ministry of Education and Science of the Republic of Kazakhstan financially supported this work, Project No. AP05134691.

REFERENCES

1. S. Azat, V. Pavlenko, *Applied Mechanics and Materials*, 467, 2014, pp. 49-51.
2. V. Pavlenko, Zh. Supiyeva, *Eurasian Chemico-Technological Journal*, 20, 2018, pp. 99-105.
3. S. Azat, V. Pavlenko, *Advanced Materials Research*, 535-537, 2012, pp. 1041-1045.
4. S. Nanda et al., *Trends in Analytical Chemistry*, 80, 2016, pp. 125–131.
5. Z. Mansurov et al., *Eurasian Chemico-Technological Journal*, 4, 2019, pp. 283–289.

SYNTHESIS OF NANOCOMPOSITION CERAMICS BASED ON A SYSTEM WITH MODIFIED WOLLASTONITE

Z. Mansurov ^{*1}, N. Mofa, A. Zhapekova

Institute of Combustion Problems, 172 Bogenbai Batyr St., Almaty, Republic of Kazakhstan

[*zmansurov@kaznu.kz](mailto:zmansurov@kaznu.kz)

During synthesis of ceramic and metal-ceramic systems under the conditions of theological combustion (SH-synthesis), the phase composition of the reaction products, the structure and properties of the material being obtained are largely determined by the thermokinetic characteristics of the combustion process. Combustion parameters, in their turn, depend not only on the composition of the charge, but also on the dispersion of the reagents, density and uniformity of the pre-requisites of the samples being synthesized [1]. An effective way to influence the formation of the microstructure and phase composition of the final products is to introduce "inert" and "active" additives introduced into the charge [2]. Mechanochemical treatment (MCT) of powder materials in activator mills is an effective way to obtain active components for SHS-charge systems. By varying the MCT modes and introducing various organic modifiers into the processed powder, particles of a composite structure consisting of inorganic and organic parts (an inorganic core encapsulated in an organic shell) can be obtained [3]. Each of the components of the modified powder material performs its role in the subsequent SH-synthesis process [4]. Wollastonite is one of the promising filler materials widely used in the world practice when creating various composite systems [5]. MCT of wollastonite, as well as other minerals, leads to changes in the dispersion, defect and structural arrangement of the particle surface, which is a prerequisite for obtaining, in this way, the material of microadditives in the SHS-charge mixture.

In this paper, wollastonite was chosen as an additive for conducting SH-synthesis of quartz-based systems with a stoichiometric ratio of it to APS-grade aluminum. The modifying additives of wollastonite were polyvinyl alcohol ($(C_2H_3OH)_n$), silicon $H_2SiO_3 \cdot n(H_2O)$ and succinic acid ($C_4H_4O_6$). Mechanochemical treatment (MCT) of powders was carried out in a planetary centrifugal mill (PCM) at an acceleration of 40 g. Activated powders were pressed into cylindrical samples with a diameter of 20 mm and a height of 20 mm with the introduction of a binder in the amount of 5%. The subsequent combustion was carried out at 900°C.

In the course of MCT, there takes place not only destruction of particles, but also accumulation and redistribution of defects in the volume of the particle. The change in

particle defects can be estimated by the size of the crystallites. As the time of MCT increases, there occurs accumulation of defects and the size of wollastonite particle crystallites decreases (from 910 to 740 Å). However, in the presence of modifiers in the course of MCT, an increase in the size of crystallites is observed (up to 1100 Å). Such changes may be associated with the flow of defects to the surface, where the chemical processes of interaction of surface layers with additives-modifiers begin to proceed.

The changes in morphology and the formation of surface structures on wollastonite particles as a result of MCT are illustrated by images obtained using a transmission electron microscope. Figure 1 shows wollastonite particles in the initial state, having a needle like shape. After the MCT of wollastonite powder, an organic film is formed on the surface, which increases as the processing time increases. When using succinic acid and polyvinyl alcohol as a modifier, the polymer formation on the particle surface is more intense (Figure 1 b,c). Wollastonite particles retain their needle-like shape and are encapsulated in a structured organic film of various thicknesses.

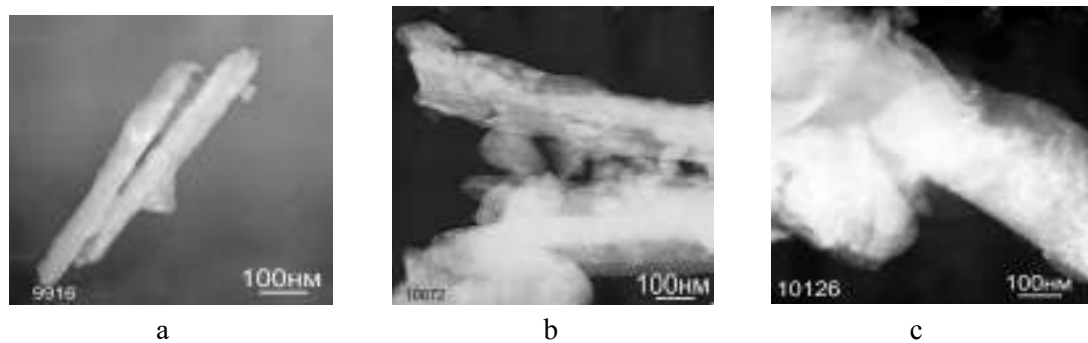


Fig. 1. Electron microscopic images of wollastonite samples in the initial state (a) and after MCT in the presence of succinic acid (b) and polyvinyl alcohol (c) for 20 minutes

The obtained modified particles showed high activity, that is evident in the change of kinetic characteristics of combustion mode of SHS systems into the charge of which wollastonite was introduced in different conditions. Introduction of wollastonite powder in the initial state into the charge mixture ($\text{SiO}_2 + 37.5\% \text{ Al}$), first of all, increases the induction period and reduces the combustion rate, as well as the maximum process temperature (Figure 2). Wollastonite plays the role of ballast, which takes part of the heat of the exothermic reaction between quartz and aluminum, resulting in a slower combustion process (from 50 deg/sec.) up to 10 deg / sec.) and the maximum combustion temperature somewhat decreases. The higher the content of wollastonite in the charge mixture, the lower these characteristics are. When wollastonite additives are introduced to the charge mixture, after MCT, the thermokinetic parameters of SH-synthesis change. If the induction period decreases after 10 minutes of

treatment and the combustion rate increases, then the reverse changes are observed for these two parameters with the increase in MCT time (Figure 3).

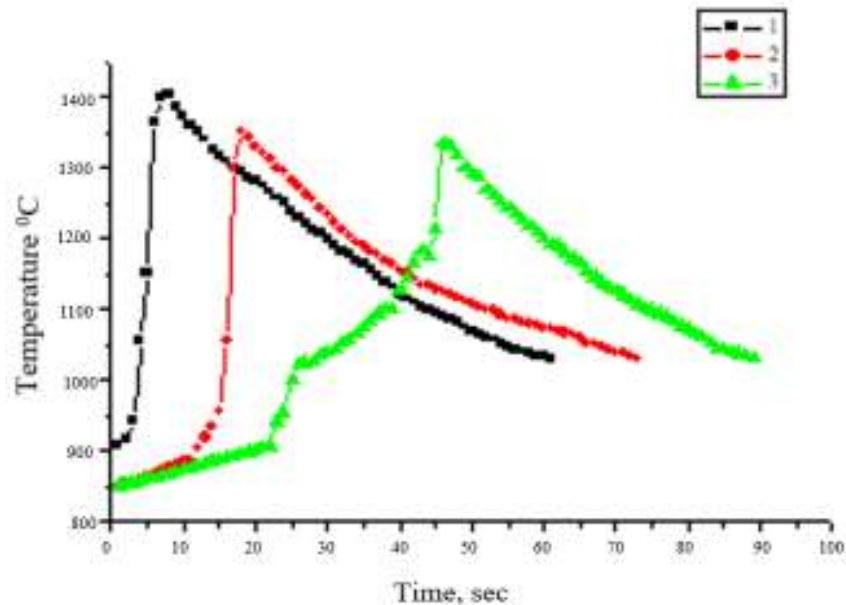


Fig. 2. Thermograms of the system [(SiO₂ +37.5%Al)] combustion without (1) and with wollastonite additives in the amount of 5(2) and 10% (3)

The decrease in the temperature of combustion of the mechanically activated mixtures can be related to a decrease in the temperature of the reaction due to the stored energy of mechanical activation, as well as the loss of chemical energy of the system as results of the interaction of components during MCT. The increase in the combustion temperature is primarily due to a significant increase in the level of particle energy stored during MCT.

At the next stage, wollastonite, processed in a mill with modifiers, was introduced into the mixture (SiO₂+Al). Figure 4 shows that after 10 minutes of MCT of wollastonite with modifiers, its introduction in an amount of 5% in the charge leads to a decrease in the induction period and an increase in the combustion rate.

X- ray phase analysis of samples showed that after the introduction of activated wollastonite into the charge mixture, highly dispersed phases of Ca₂Al((AlSi)O₇) and Fe₂SiO₄ are formed in the synthesis products, which increase the strength of the material from 28 to 35 MPa. Phase formation occurs under high-speed and high-temperature conditions, therefore they have a high degree of dispersion. Modification of wollastonite with succinic and silicic acid within 20 minutes contributes to the formation of aluminum nitride in the synthesized sample, which in its turn strengthens the material (up to 40-52 MPa). After 40 minutes of processing wollastonite with silicic acid, the fraction of reduced silicon decreases, but particles of

gelenite - $\text{Ca}_2\text{Al}((\text{AlSi})\text{O}_7)$, which strengthens the material, are formed. A similar pattern in phase formation is observed when using wollastonite modified with polyvinyl alcohol and succinic acid for 40 minutes of MCT.

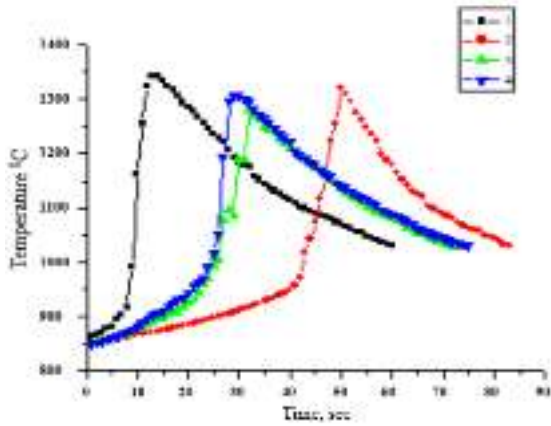


Fig. 3. Thermogram of the combustion system $[(\text{SiO}_2 + 37.3\% \text{Al})]$ with wollastonite additives in an amount of 10% after MCT during 10 (1), 20 (2), 30(3) and 40 minutes (4)

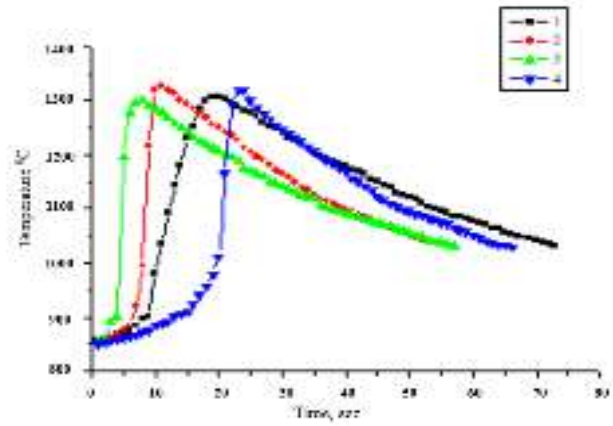


Fig. 4. Thermograms of the system $[(\text{SiO}_2 + 37.3\% \text{Al})]$ with 5% wollastonite activated for 10 minutes with flint (1), succinic acid (2), polyvinyl alcohol (3) and without modifier (4)

Thus, by introducing activated and modified wollastonite into the charge mixture in an amount of 5%, it is possible to purposefully influence the thermokinetic characteristics of the combustion process and, as a result, control the phase formation and properties of the synthesized material.

REFERENCES

1. G. Merzhanov, Self-propagating high-temperature synthesis. Physical chemistry: Modern problems, ed. by Y. M. Kolotyrlin. - M. Chemistry, 1983, pp.5-44.
2. N.Z. Lyakhov, T. L.Talako, T. F. Grigorieva, Influence of mechanical activation on structure formation in self-propagating high-temperature synthesis, Novosibirsk: Parallel, 2008, p.168.
3. Z.A. Mansurov, N.N. Mofa, Mechanochemical synthesis of composite materials, Almaty: Kazakh University, 2016, p. 376.
4. Z.A. Mansurov, N.N. Mofa, B. S. Sadykov, Zh. Zh. Sabaev, A. E. Baccara, Engineering and physics journal, 2016, V. 89, №1, pp. 221-228.
5. Z.A. Mansurov, N.N. Mofa, T. V. Chernoglazova, Wollastonite is a universal reinforcing filler of composite materials, Almaty: Kazakh University, 2018. p, 308 .

RESEARCHING OF SHS ELECTRICAL-ROLLING PROCESS OF METAL-CERAMIC MATERIALS ON BASE OF Ti-B SYSTEM

Z.Melashvili*, T.Namicheishvili, G.Tavadze, A.Tutberidze, G.Parunashvili,
Z.Aslamazashvili, J.Gamsakhurdia

Ferdinand Tavadze metallurgy and materials science institute. 8b.E.Mindeli str., Tbilisi 0186, Georgia, Tbilisi.
metalurgi@mail.ru*

Evolution of modern techniques requires development and production of metal-ceramic materials with high physical-mechanical properties, among which, exceptional methods of obtaining unlimited longitudinal dimension products by SHS electrical-rolling process method are developed at the Ferdinand Tavadze Metallurgy and Materials Science Institute. [1].

Heating current at the deformation core causes the initiation of synthesis and continuous compensation of heat losses during hot deformation of the product, while maintaining equality of rolling and combusting front transfer speed ensures to form viscous-plastic mass in the hot core of the deformation.

In order to obtain high quality nonporous materials, it is necessary to study the dependence of the degree of relative deformation on the material density. For this purpose, the process of rolling a cone-like specimen was studied, where the rolled one represents material obtained by variable shrinkage. For each intersection of this material, the corresponding shrinkage (relative deformation), current angle of bite, density, and other rolling parameters are determined. The relative deformation carried out from the beginning to the end of the rolling stock was 0-65%.

According to the Law of Mass Conservation, an image is obtained by which the location of the cross-section of the wedged material corresponding to any point chosen at the length of the rolled material can be determined:

$$L_{0x} = \frac{-h^0 + \sqrt{(h_0)^2 + 4L_{1x}h_0 \frac{B_1 + B_{1x}}{2B_1} K_x t g \acute{\alpha}}}{2tg \acute{\alpha}}, \quad (1)$$

And given the cone-likeness of the product, its height equals to:

$$H_{0x} = h_{0x} + 2L_{0x}tg \acute{\alpha}, \quad (2)$$

Where: L_{0x} is the length of the wedge-type target billet; h_0 and H_{0x} are the height of wedge-type billet and section height of wedge-type billet; B_1 is the width of front of the prepared or rolled material; B_{1x} - is the width of the target section; L_{1x} - x is the length of section-rolled

target; $K_X = \rho_0 / \rho_{1x}$ - x is the hardening coefficient at the section; ρ_0 and ρ_{1x} - are the densities of the material in the cross section X and mixture; α - Wedge-type target's cone-likeness.

During the experimental studies, flat specimens of briquetting charge with same thickness were rolled and put in containers (with different shrinkage) ($\Delta H = 3$ mm, 6 mm, 9 mm, 12 mm, 14 mm). The length of the deformation core were conventionally divided into aisles. The initial and final intersections of each site were considered as the entry and exit intersections at the deformation core, for which, according to the law of mass conservation, mathematical transformations made possible to obtain image which determines: billet's transfer velocity.

$$U_1 = \pi D n \left(1 - \frac{\Delta h}{D}\right) K H_0 B_0 / 60 H_1 B_1 \quad (3)$$

Where: $H_0 B_0$ and $H_1 B_1$ are the height and width of the charge and rolled stock; ρ_0 and ρ_1 - specific densities; U_0 and U_1 - Velocities of movement of the charge and material, in aisles located at the core of deformation (at the entering and leaving sections); $U_0 = \pi D n (1 - \frac{\Delta h}{D}) / 60$ - horizontal constituent of roll's circular velocity, D - diameters of rolls; n - number of turns of rolls; Δh - shrinkage; $K = \rho / \rho_1$ - coefficient of hardening.

Billet derived from SHS (self-propagating high temperature synthesis) process, appears to be porous material, from which, after further hot-pressing (rolling) it, material with intended mechanical properties and measurements is obtained. In the deformation core, the formed grains of the synthesized charge approach each other, and at the exit of cross section, hardened material is obtained; Porous empties are significantly reduced and the relative porosity decreases to 2–5% at certain shrinkage. As a result of material's shrinkage at the cross-section, compression takes place predominantly, the grains move in a vertical direction. Reaching some kind of adhesion, the charge begins to flow in a longitudinal direction. Thus, SHS electro-rolling process involves intergranular and interparticle shear deformation. Increase of material density along the deformation core depends on charge compaction degree.

On the basis of experimental data, the density of the material depending on the whole length of the rolling or the relative deformation can be calculated by the following empirical image:

$$\rho_x = \rho_0 + (\rho_1 - \rho_0) (l_{1x} / l_1)^m, \quad (4)$$

or

$$\rho_x = \rho_0 + (\rho_1 - \rho_0) (\varepsilon_x / \varepsilon)^m, \quad (5)$$

Where: ρ_0 and ρ_1 - are the densities of the synthesized charge and the rolled material; m - is the coefficient, depending on the relative deformation, specifically: when $\varepsilon = 9-30\%$, $m = 1$;

when $\varepsilon = 30-45\%$, $m = 0.75$; when $e = 45-60\%$, $m = 0.5$; l_x, l - is the lookup of the expanded material at the cross section and the total rolling, or the lookup of deformation core and the lengths of the whole aisles; $\varepsilon_x, \varepsilon$ - are relative deformations corresponding to l_x, l arcs in the search section of wedge-type rolled material or in the deformation core.

(4) and (5) allow us to calculate the density values for any intersection of the rolled material, or the density-dependent values of relative deformation along the deformation core. Reliability of the empirical images was tested by experiments. Relative error between experimental and empirical values was 2-4%. Dependence of the material density change on the length of the rolled material is shown in Fig. 1, and the values of the initial and final densities of the deformation core were determined experimentally and computed (5), (Fig.2).

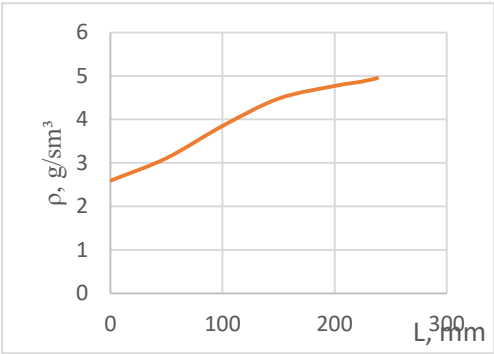


Fig.1. TiB₀₆ material density change over rolled material length.

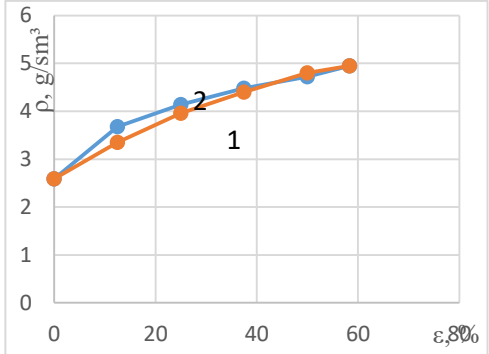


Fig. 2. TiB₀₆ material density change in relative deformation change: 1 - Experimental data; 2 - (5) Computed by the image;

As it can be seen from Figure 2, except for the initial and final cross-sections of the deformation core, the density values obtained experimentally and calculated empirically along the entire deformation core are 4.4% with average relative error. From the above we can conclude that the curves obtained by image (5) are more or less close to the experimental density change curve. Therefore, the empirical images (4) and (5) may be applied to the base of the Ti-B system for the SHS electro-rolling of the metal-ceramic material.

Thus, as we know what rolled billet dimensions are, it is possible for any of its carving points to determine the carving size before proper rolling, which will allow us to determine shrinkage magnitude and angle of bite on the rolling mill.

Theoretical calculations show that in the case of TiB₀₆ box groove rolling, the relative porosity of the initial synthesized charge is 50%, depending on the relative porosity and the

relative deformation of the rolled material. In the deformation core aisles' inlet and outlet sections, comparison between billet and roll velocities and its incensement change is shown in Figure 3.

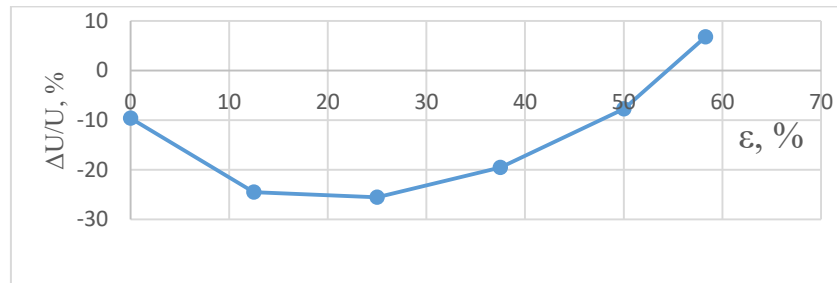


Fig.3. Comparison between billet and roll velocities in the deformation core aisles' inlet and outlet sections.

As it is shown in Fig. 3, growth of deformation (along with porosity decreasing), increases container and roll velocities relative growth when entering the deformation core. This is due to the fact that as shrinkage increases, intensity of compaction falls. Synthesized charge flows in a predominantly transverse direction, despite that the horizontal constituent of the circular velocity vector increases. Although no sharp increase in friction forces is observed, which itself ensures longitudinal displacement of the billet. From $\varepsilon = 25\%$ to some degree of deformation (54-55%), lag between billet velocity and roll velocity decreases. At this time, intensive compaction is taking place, that is, the synthesized TiB_{06} grains move predominantly in vertical direction and elongation is minimal. As the deformation increases ($\varepsilon = 54-55\%$), shrinkage of TiB_{06} grains and titanium phase increases, thus, decreases porosity. Thereby, we can conclude that rolling process should be carried out at $\varepsilon > 54\%$ relative shrinkage conditions. $\varepsilon = 54-58\%$ can be applied as optimal mode, with relative porosity decreasing to 2-3%. Further growth of deformation slightly affects to the material compacting. Also it worsens rolling mill's effectiveness (energy-force parameters is increasing dramatically), biting conditions and rolling stability in general. In the event of breaching a TiB_{06} fastening condition, if angular velocity of the rolls is reduced, total forces increase due to the separation of deformation core from the combustion front, i.e. growth of holding time, which itself increases the slip between the combustion front displacement and the billet displacement. The charge becomes cold, increasing resistance to deformation and danger of cracking. If the speed of rolls is above the optimum speed, difference between the combustion front and the billet displacement velocity slip is reduced, i.e, the combustion front is approaching the starting point of deformation core, amount of liquid phase in SHS

products increases and billet structure remains unformed. Full compacting process does not take place and porosity increases.

Thus, technological regime disruption, particularly in the case of non-optimal delay of synthesized specimens and missing rolling and SHS velocities prior to begin rolling process, porous materials and cracks are formed during compacting.

Based on aforementioned studies, optimal technology of TiB_{06} material for SHS electro-rolling has been established, which allows constant distance formation from deformation center to combustion front. Also we can obtain equal compacted materials on the whole length of billet.

CONCLUSION

The work deals with the TiB_{06} SHS electro-rolling process of selected charge in order to obtain metal-ceramic protective and corrosion-resistant tiles. In particular, during the process of SHS electro-rolling, according to experimental data and theoretical calculations, we have obtained searching section of rolled products and wedge-type billet's matching point calculation image that corresponds to the rolled products. Billet's movement velocity and density value of charge and rolled products change due to different values of relative deformation. Obtained results can be used during SHS electro-rolling of Ti-B system charges.

We have developed SHS electro-rolling technology of material, which ensures speed equality of rolling and synthesis process throughout the whole work, as well as the means for obtaining compacted materials. TiB_{06} metal-ceramic tiles that are developed through that technology meet the required properties.

REFERENCES

1. T.Namicheishvili, A.Tutberidze, Z.Melashvili, G.Tavadze, Z.Aslamazashvili, G.Oniashvili, G.Zakharov. Method for obtaining inorganic product from powder exothermic chasm, Saqpatenti. Patent P 6541 . LEPL Ferdinand Tavadze Metallurgy and Materials Science Institute, 2016;
2. Porous Material Deformability in Four-Roll Pass Rolling / L.A. Barkov, Yu.I. Kamenshchikov, M.N. Samodurova, Yu.S. Latfulina // Bulletin of the South Ural State University. Ser. Metallurgy, 2017, vol. 17, no. 1, pp. 89–92. DOI: 10.14529/.

OBTAINING COMPOSITE POWDERS STRENGTHENED WITH HIGH-MELTING COMPOUNDS

Z. Mirijanashvili, V. Gharibashvili*, A. Kandelaki, V. Tsiklauri, K. Ukleba
Ferdinand Tavadze Metallurgy and Materials Science Institute, 8b E. Mindeli Str., Tbilisi, 0186, Georgia
v.garibashvili@gmail.com

RESUME

Along with combined results of studying basic kinetic properties of thermo-graphical, radiographic-phase and charge's metal chloride-oxide reduction processes, we have developed the scheme of obtaining composite powders (NiCr-Cr₃C₃; NiCr-Cr₃C₃-Co-Cu; CrB₂-Al₂O₃; (TiCr)B - Al₂O₃; CrNi -B₄C; WC-FeNi; FeCr-Ni₃Al; CrNiCo-Al₂O₃) strengthened with high-melting compounds.

It was found that the maximum fraction of the obtained composite powders varies within 100-125 μm and does not exceed 5%, while remaining fractions of particles are 5-20 μm within 30-35%, 20-50 μm - 35-40%, 55-100 μm - 15-20%. Powder particles (oxides, carbides) of the solidifying, hardening phase are evenly distributed throughout the powder and their fraction does not exceed 5 μm. Researching of composite powder's technological properties has revealed: Density varies from 4.6 to 4.95 g/cm³; Free dump specific weight 1,05-1,2 g/cm³; Judder specific weight 1.5-1.65 g/cm³ and fluidity 39-42 sec.

One of the promising methods to obtain metal-ceramic powders is the joint Aluminum recovery of corresponding metal's chloride-oxide-carbide charge - by formation of reinforcing, strengthening phase powder particles (Al₂O₃) or by collaboration of fine-disperse carbides and other high-melting compounds. This task can be resolved only by using powder metallurgy methods that gives the opportunity to create composite materials and powder alloys with unique properties [1-3].

Metal-ceramic powders with improved exploitation features are used for manufacturing special-purpose products and for restoration and reinforcement of detail surfaces as well. Wide range of customers for such products include: machinery, stone processing and mining-concentrating factories, aviation, metallurgical factories, oil-processing companies, private working objects and etc.

In order to determine the nature of thermal effects running in the process of obtaining powdered composite material with relevant burden and its recovery through the Aluminum, initial raw material was used: nickel chloride (NiCl_2). Chromium chloride (CrCl_3), chromium carbide (Cr_3C_2), cobalt oxalate (CoC_2O_4), boron anhydride (B_2O_3), titanium oxide (TiO_2) and metal aluminum powder.

Summarizing the results of thermographic and radiographic-phase studies, nature of thermal effects in current chloride-oxide charge's aluminum recovery was explained. Interaction of nickel and chromium chlorides with aluminum is highly exothermic, rapidly going process, and it begins at 650°C . During the reaction, temperature of charge increases arbitrarily throughout the whole mass and reaches $900\text{-}950^\circ\text{C}$. At this time, secondary product, that'd been resulted from the reaction - AlCl_3 , can be easily removed from reaction zone (its evaporation temperature is 180°C).

In case when large aluminum granules are used for reduction, molten aluminum will restore its surrounding nickel and chromium chlorides. Metallic nickel and chromium are being produced. High-melting nickel (NiAl , Ni_2Al_3) and chromium (Al_7Cr , Al_{11}Cr , $\text{Al}_{11}\text{Cr}_2$, Al_4Cr , Al_3Cr , Al_9Cr_4 , Al_8Cr_5 , AlCr) compounds can also be formed. The latter are involved in the process of charge recovery.

Reduction of metal aluminum particles size results in an increase of reducing agent's reaction surface. This helps to fasten recovery process. Thermographic study revealed that reduction of nickel and chromium chlorides with metal aluminum (with NaCl addition into the charge, (relatively $\text{NaCl}:\text{CrCl}_3 = 1:1$)) initiates the reaction at 560 and 475°C respectively.

After completion of reduction reaction aluminum content in the obtained product is $3.5\text{-}5.0\%$, and with the addition of charge in NaCl , rate decreases to $0.015\text{-}0.3\%$. This event can be explained by the fact that in the first case, contact of the reduction agent is less with the restoration component and that the arising chromium forms above-mentioned compounds with residual aluminum. In the second case presence of relatively low temperature salt defrosting ($\text{CrCl}_3:\text{NaCl}$) impedes interactive solubility of metal chromium and aluminum.

Thermal dissolution (dissociation) cobalt oxalate, with temperature influence, revealed that at 415°C cobalt oxalate decomposition begins, and the obtained cobalt powder only accords with high temperature modification.

Thermographic research made it possible to study thermal effects resulted from aluminum reduction of components (NiCl_2 , CrCl_3 , CoC_2O_4 , NaCl) inside the charge. Ratio of the

chromium chloride mixture with sodium chloride corresponds to 1:1 thermogram. Fixed thermal effect 225⁰C corresponds to the beginning of crystalline water removal temperature from cobalt oxalate and it is endothermic in nature.

The following effect of 415⁰C corresponds to the beginning of the cobalt dissociation as well as the eutectic melting of NiCl₂- CrCl₃ - NaCl. However, its exothermic nature is explained by initiation of dissociation-induced reduction reaction. In this case, endothermic effect of reagent dissociation is significantly behind the exothermic effect of reduction reaction, and total exothermic-character effect is displayed on the thermogram. The third effect at 650⁰C can be explained by aluminum melting and by effective reduction process, which is exothermic in nature and the temperature throughout the reactive mass can be increased arbitrarily up to 800⁰C. Upon reaching this temperature, produced complex salt N NaAlCl₄ begins to melt and the endothermic effect is observed on the thermogram.

The nature of thermogram temperature difference curve of aluminum oxide compounds B₂O₃ and TiO₂, showing that the endothermic effect 425⁰C corresponds to the boron oxide melting temperature, and the exothermic effect 650⁰C corresponds to the beginning of the titanium oxide reduction process. It should be noted that with the use of other oxides (Fe₃O₄, CoO) as charge components, reduction temperature always corresponds to melting temperature of aluminum and it is exothermic in nature.

During reduction processes, addition of high-melting compounds to the charge does not alter the nature of temperature differential curves, indicating that these components do not participate in chemical procedures involved in the process.

By combining results of the research on thermographic, volumographic, radiographic-phase and basic kinetic characteristics of the procedure, a process scheme to fabricate composite powders reinforced by high-melting compound was developed (Figure 1), including: mixing of charge in rotary mixer → charge briquetting → charge-type oven reduction in argon atmosphere → condensation of secondary product (AlCl₃) → wet grinding of sinter cake in ball mill → drying powders → riddling → prepacking. Throughout the whole cycle, loss of suitable powder does not exceed 5%.

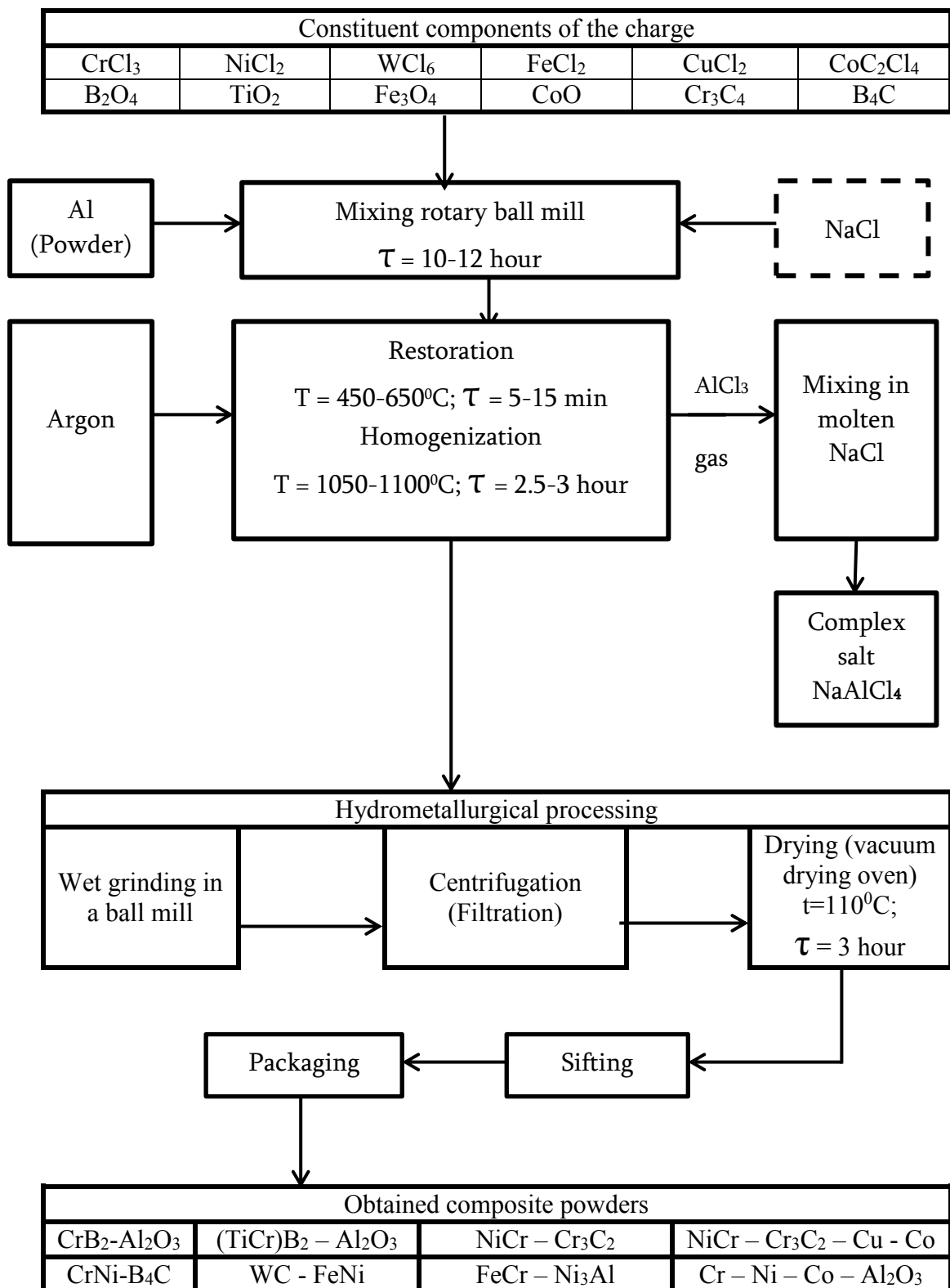


Fig. 1. Scheme of the process for producing composite powders hardened by refractory compounds

Reduced briquettes retained their shape due to the solidification of residual secondary product (NaAlCl_4). It resembles a cloudy mass (Fig. 2) and the briquettes reduced for complete removal of the latter are subjected to hydrometallurgical processing in accordance with the following scheme: Briquette's grinding mass processing in a rotary ball mill with wet (water) method; Centrifugation and complete removal of chlorine-ion with water; Drying powder in a vacuum-drying oven at 100-110⁰C (0.0133 MPa – 100 Hg).

The powder was riddled through a vibro sieve. Particle shapes of obtained composite powders are different (Fig. 2 a, b, c). Dendritic structure (Fig. 2b) varies between 2-5 μm in accordance with axis and branch diameter, with a length not exceeding 100 μm . Dispersion of dried powders are determined by "Coulter Model TA-II" - particle size analyzer, and, it was found that its maximum fraction range was between 100-125 μm and not more than 5%, but remaining fractions of the particles were 5-20 μm within 30-35 %, 20-50 μm - 35-40% and 55-100 μm - 15-20%. It's worth noting that the powder particles of the reinforcing, hardening phase are evenly distributed throughout the powder, not exceeding 5 μm .

Researching of composite powder's technological properties has revealed: Density varies from 4.6 to 4.95 g /cm³; Free dump specific weight 1,05-1,2 g /cm³; Judder specific weight 1.5-1.65 g /cm³ and fluidity 39-42 sec.

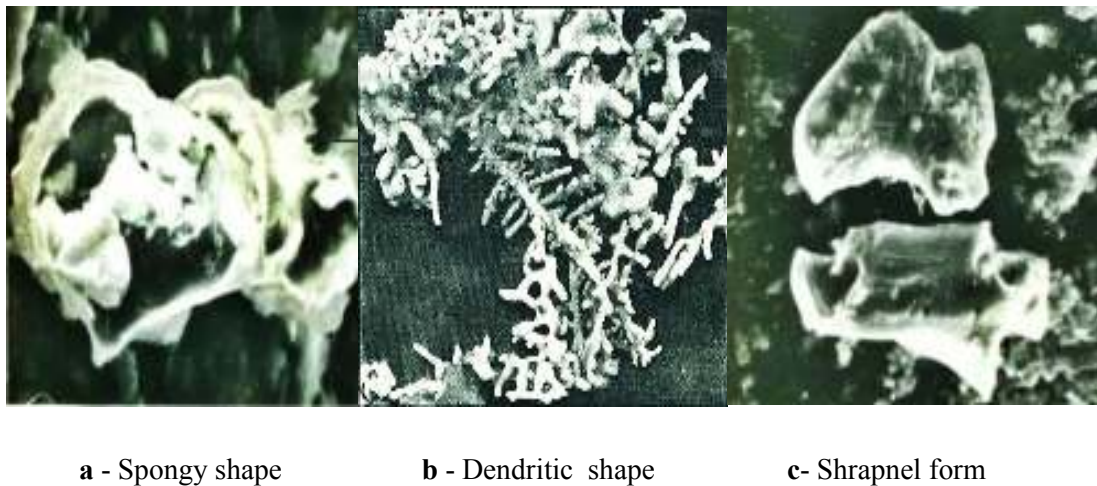


Fig 2. Forms of composite powders particles

REFERENCES

1. Паустовский А.В., Ткаченко Ю.Г., Кириленко С.Н. и др. «Оптимизация состава, структуры и свойства покрытий» Электронная Обработка Материалов, 2013,49(1);
2. R.Schafrik, M.P.Brady etc. “Intermetallic Reinforced Cr-Alloys for High-Temperature Use”. Materials at High Temperatures. 1999, 16 (4), 189-193;
3. Al. Kandelaki, Z. Mirijanashvili, G.Tavadze; International Symposium “Preparation of Nanocrystalline Hardmetal Powders From Tungsten-containing Wastes”. Cancun, Mexico, 2014.

RADIAL FORGING MACHINE FOR PROCESSING POROUS SINTERED WORKPIECES

S. Mebonia*¹, J. Sharashenidze², A. Shermazanashvili¹

¹R. Dvali Institute of Machine Mechanics, Tbilisi, Mindeli str., 10, Georgia

²Ferdinand Tavadze Metallurgy and Materials Science Institute, 8b E. Mindeli Str., Tbilisi, 0186, Georgia

*meboniaslava@mail.ru

ABSTRACT: Based on the analysis of the designs of rotary and radial-forging machines, it is shown that hydraulic crimping machines are most suitable for processing porous sintered workpieces. The design of a gas-hydraulic radial forging machine is proposed, which makes it possible to increase the degree of deformation of the work piece and increase the intensity of the forging process, which increases the productivity of the forging machine.

KEYWORDS: radial-forging machine, porous sintered workpieces, receiver.

BASIC PART. Using the radial forging method in mechanical engineering is particularly advantageous for processing long axisymmetric parts of complex configurations, such as stepped shafts and axles. The complex shape of the inner surface is also distinguished by a group of axisymmetric parts with an internal stepped profile, in particular, adapter sleeves, nipples and stepped couplings, as well as parts with internal straight and spiral slots[1- 3].

Obtaining the above parts by mechanical processing on metal-cutting machines is uneconomical, since during processing there are large losses of metal [1,2].

In addition to the above, the radial forging method improves the structure and mechanical properties of the metal. The pulsating nature of the load characteristic of radial forging makes full use of the metal's plasticity resource, reducing the deforming forces, and makes it possible to manufacture parts from low-plastic and hard-to-form steels and alloys [3].

The radial forging process is implemented on radial forging machines of various designs. The leading manufacturer of modern rotary and radial forging machines is the Austrian company GFM [1].

Existing rotary forging machines are divided into three groups [3-5]:

1) Circular machine; 2) Drum of the machine; 3) Spindle of the machine. Radial forging

machines are also divided into three groups: 1) Roller machines; 2) Lever machines; 3) Connecting rod machines. In addition, the metallurgical industry uses hydraulic crimping machines of various designs, such as hydraulic presses, devices with a forming punch and multi-punch machines [6,7].

On fig. 1 the classification of existing rotary and radial-forging machines is given.

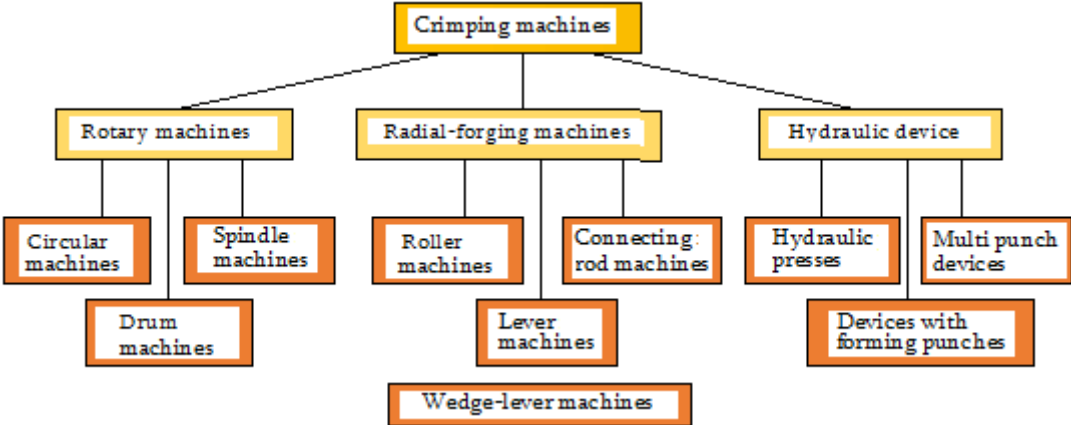


Fig. 1. Classification of radial forging machines

Analysis of the designs of rotary and radial forging machines has shown that hydraulic crimping machines are most suitable for processing hard-to-form metals, their alloys and porous sintered workpieces [6,7]. Therefore, we developed a gas-hydraulic radial forging machine.

We believe that the proposed machine design and material processing conditions will significantly facilitate the production of products of the desired shape, with a density almost close to the theoretical one, from porous sintered blanks, since deformation occurs under conditions of comprehensive compression. This is a completely new direction in the plastic processing of porous work pieces. The scheme of its construction is shown in Fig. 2.

The machine contains working cylinders 1 with piston rings 2, which are connected by means of shock absorbers 3 to the shock mass 4, to which the striker 5 is attached. Each working cylinder 1 is tightly connected to the upper part of the high-pressure gas receiver 6 of an annular shape, which at the same time is a machine body. The high-pressure gas receiver is common to all working cylinders. The lower cavity of the working cylinders 1 is closed by covers 7 and connected to the high-pressure hydraulic system via a pipeline. The working cylinders are arranged radial in a circle.

Toothed rails 8 are attached to the side surfaces of the shock masses, which are engaged with the synchronizing gears 9 and 10. The gears 9 and 10 are located in the cylindrical recesses of the machine body.

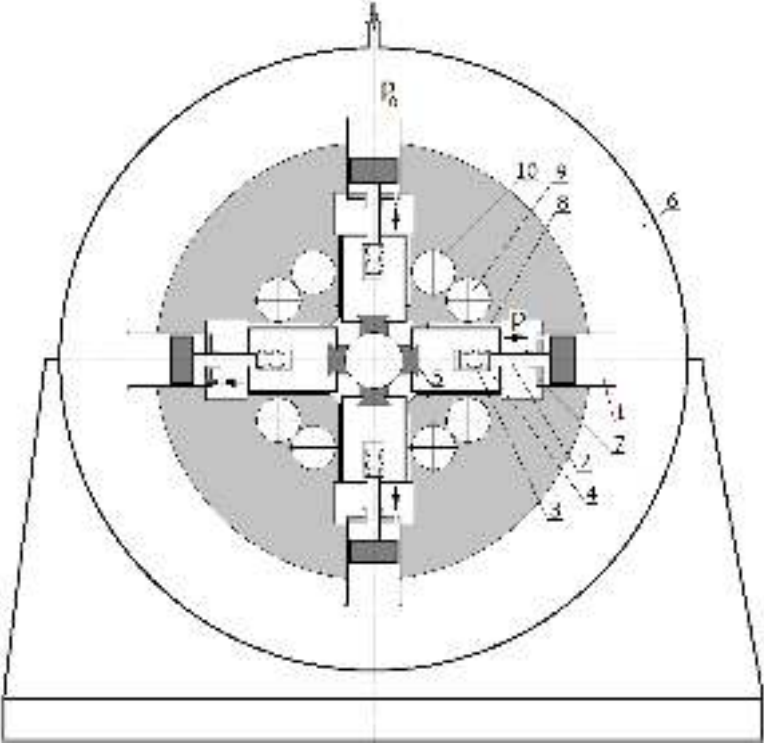


Fig. 2. Scheme of machine

The principle of operation of the machine is as follows. From the hydraulic system, the high-pressure (p , ATM) liquid enters the lower chamber of the working cylinders 1, as a result of which the cylinder pistons overcome the resistance of the high-pressure gas (p_0 , ATM) in the receiver 6, and radial move the shock masses 4 together with the strikers 5 to the periphery of the installation. This action prepares the machine for the job.

When the feed mechanism feeds the work piece between the strikers, the lower part of the working cylinders 1 is abruptly disconnected from the high-pressure system and connected to the atmosphere, which causes a sharp drop in pressure in this cavity. At the same time, under the influence of high-pressure gas of the receiver 6 in the upper cavity, the pistons of the cylinder 1, together with the shock mass 4 and the strikers 5, are rapidly accelerated from the periphery to the center of the machine and strike the work piece, which leads to its plastic deformation.

The toothed rails 8 attached to the shock masses 4 together with the gear wheels 9 and 10 provide a coordinated shock movement of the shock of all four masses, which is necessary in order for the strikers to simultaneously carry out shock effects on workpiece.

After the end of one working cycle, the lower areas of the working cylinders are re-connected to the high-pressure system, and the machine is ready to perform the next cycle when it returns to its original state.

CONCLUSION.

The positive effect of the presented machine is due to the fact that its design scheme contains radial arranged in a circle working cylinders, the upper part of which is constantly connected to the high-pressure gas receiver, which is common to all working cylinders. In this case, it becomes possible to influence the work piece simultaneously from four sides, which creates a favorable deformation scheme and a stress-strain state of all-round compression. This dramatically reduces the probability of occurrence and development of cracks in the work piece, which increases the possibility of producing high-quality products and greatly facilitates the process of plastic deformation of sintered porous workpieces. Besides that the intensity of the forging process is not limited, since the stresses in the longitudinal section of the work piece are far from critical, which makes it possible to increase the degree of deformation and intensity of the forging process, resulting in increased productivity of the machine.

REFERENCES

1. V. A. Tyurin, V. A. Lazorkin, I. A. Pospelov, Kh. P. Pluhowski. Forging on radial-shaped machines. M., Mechanical engineering, 1990. Pp. 12-13.
2. V. A. Boguslaev, V. V. Borisevich, V. K. Borisevich, and others. processing of metals by pressure. Educational. in 2 kN., kN.1. Kharkiv: NAT. Aerospace UN-t, Kharkiv aviation Institute, 2002. 419 PP.
3. Y. S. Radchenko. Rotary compression. M., Mechanical engineering, 1972.Pp. 148.
4. Y. S. Radchenko. Rotary forging - processing of parts on rotary and radial crimping machines. M., Mashgiz, 1962. 187 PP.
5. V. I. Lyubvin. Processing of metals by radial compression. M., Mechanical engineering, 1972. 248 p. M
6. Forging and stamping equipment. Ed. A. N. Banketov and doctor of Sciences, Professor E. N. Lansky. M., Mechanical engineering, 1982. Pp. 412-414.
7. Persikov Z. I. Drawing machines. Moscow: Metallurgy, 1986. 208 p.

LIQUID CHARGE PRECURSORS FOR PRODUCTION OF B_4C - MeB_2 FINE COMPOSITE POWDERS

A. Mikeladze¹, R. Chedia², L. Chkhartishvili*^{1, 3}, O.Tsagareishvili¹, N. Barbakadze², K. Sarajishvili², T. Korkia², M. Darchiashvili¹, V. Ugrehelidze⁴

¹ Ferdinand Tavadze Metallurgy and Materials Science Institute, 8b E. Mindeli Str., Tbilisi, 0186, Georgia

² Peter Melikishvili Institute of Physical and Organic Chemistry, 31 A. Politkovskaya Str., Tbilisi, 0186, Georgia

³ Georgian Technical University, 77 M. Kostava Ave., Tbilisi, 0175, Georgia

⁴ National High Technology Center of Georgia, 21 P. Kavtaradze Str., Tbilisi, 0186, Georgia

levanchkhartishvili@gtu.ge

ABSTRACT An effective method of production of boron carbide / metal diboride nanocomposites, the in prospective hard materials with improved mechanical properties, is their chemical synthesis from corresponding liquid charge. Here is reported on the initial stage of the technology – preparing liquid charge precursors.

Among current commercial hard materials, boron carbides (B_4C) possess the highest hardness-to-density ratio. For this and other unique properties, boron carbide based composites are widely used in various technologies. However, boron carbides' brittleness and, therefore, relatively low stability against crack formation hamper further extension of the sphere of their industrial applications. As is believed, this problem can be resolved by creation boron carbide based composite materials in nanocrystalline state.

Original technology suggested by authors includes obtaining of the B_4C - MeB_2 (metal diboride) nanocomposite powders from liquid charges in form of B- and Me-compounds dissolved in organic solvents by their multi-stage thermal treatment at relatively moderate temperatures. Organic solvents serve for C-source as well. Studies show that a powder obtained from such kind of liquid charge should be fine and truly composite, not a mixture of components' powders. These are two important factors for retaining nanostructure and, consequently, achieving high mechanical properties of solid materials and / or goods obtained by further compacting of powders.

In the literature, there are number of reports on synthesis of B_4C and MeB_2 powders separately, as well joint synthesis of these component-powders. Their review and references to original works will be given elsewhere [1] (see also [2]).

We try to answer the question: How to combine in novel technologies the methods of obtaining boron carbide, titanium and zirconium diborides in a single technological cycle in

order to obtain true powdered ceramic composites of B_4C-TiB_2 and B_4C-ZrB_2 ? Here, we are focused on preparing corresponding precursors in form of liquid charge.

Earlier it has found the possibility of receiving the same composite from the system that consisted of amorphous boron and TiO_2 -glycerin- H_2O or H_3BO_3 - TiO_2 -glycerin- H_2O systems. On mechanisms occurring in the preparation of ceramic compositions containing boron carbide and titanium diboride, one can see our previously released projects [3, 4] and also recent patent [5] and papers [6 – 12]. In particular, the data have been presented, which confirms the possibility of obtaining nanoscale powder B_4C-TiB_2 composite at relatively moderate temperatures.

From the analysis of the literature in field, one can conclude that in the synthesis of metal (e.g. titanium and zirconium) diborides are often used organic compounds of different classes. And amorphous boron, boron oxide, boric acid and its compounds, boron halides, bororganic compounds, borates and its derivatives are used as boron sources. From commercial point of view, it is better to use available – cheap compounds (B_2O_3 , H_3BO_3 , and $B(OR)_3$). The sol-gel and co-precipitation methods are often used to obtain precursors and preceramic powders of metal borides and boron carbides. General analysis of the approach (see the scheme presented in Figure 1) of obtaining boron carbide and metal (e.g. titanium and zirconium) diborides shows that the final products are obtained using actually the same technological processes. For example, sources of boron, zirconium, and carbon are necessary for obtaining zirconium diboride and in this case it needs to implement technological processes in accordance to Direction I (Figure 1). The main problem is optimization of $B_2O_3:ZrO_2:C$ ratio during the pyrolysis. There are various literature data on pyrolysis of precursors under controlled conditions (ensuring the removal of excess carbon) showing that optimal temperature is within 500 – 800°C and it depends on the nature of used organic compound. In case of using carbohydrates, pyrolysis is finished up to 500 °C. And when using carbon-chain polymers, a temperature of 700 – 800 °C is sufficient to form active carbon. For the preparation of B_4C-ZrB_2 or B_4C-TiB_2 composites, boron, zirconium and carbon-containing compounds are also necessary. These composites are mainly obtained by mixing the preprepared powders of borides or interaction of appropriate oxides and boron carbides. As shown in Figure 1, when implementing the method for producing zirconium boride by the Direction II, it is possible to obtain a composite B_4C-ZrB_2 (or B_4C-TiB_2) from the same initial compounds that are necessary to obtain ZrB_2 (or TiB_2). Only difference is the $B_2O_3:ZrO_2:C$ molar ratio change in way to obtain boron carbide and metal diborides as well.

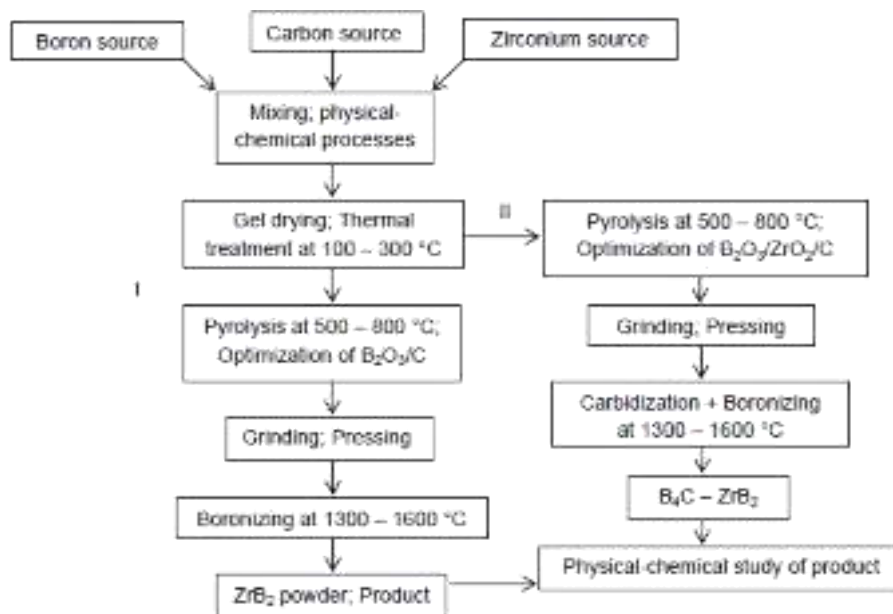


Fig. 1. General technological route of obtaining of B_4C-ZrB_2 using organic compounds as carbon source.

Preliminary studies have established the reality of the implementation of this technological route. For this purpose it was used different composition systems: amorphous boron–PVA– H_2O , amorphous boron–sucrose– H_2O , amorphous boron–PVA– ZrO_2-H_2O , H_3BO_3 –PVA– TiO_2-H_2O , H_3BO_3 –sucrose– ZrO_2-H_2O , H_3BO_3 –sucrose– TiO_2-H_2O , H_3BO_3 –sucrose– $Zr(OR)_4$ –propanol– H_2O , H_3BO_3 –PVA– $Zr(OR)_4$ –propanol– H_2O , H_3BO_3 –PVA– $Ti(OR)_4$ –propanol– H_2O , etc. Some of these versions of the technology will be described elsewhere in more details in subsequent subsections together with corresponding SEM, EDX spectroscopy, and XRD data.

For all the composites presented here, the precursor consisted of sucrose – 37, boric acid – 34, and titanium oxide – 2 g. Final product contained 18 – 20 % of titanium diboride. In particular, the synthesis of boron carbide precursor was carried out according to the following route. 120 ml of water and 25 g of sugar were placed in a porcelain cup. The resulting solution was heat-treated at 90 – 100 °C and under stirring 31 g of boric acid was added in portions until complete dissolution (solubility of boric acid in methanol at 100 °C is 29.53 g / 100 ml). Due to reaction between boric acid and sucrose, various types of compounds should be obtained (e.g. esters). From the resulting solution, water was removed (at ~ 90 °C) under stirring and viscous mass obtained. Then the temperature was raised to 145 – 150 °C. Within 120 min, charge maintained at this temperature until the formation of a black porous mass.

Porous mass was cooled and grinded in porcelain mortar. Black powder is obtained. For pyrolysis of the precursor powder, the powdered sample was placed into quartz pipe under argon flow. The pipe was heat-treated up to 550 – 600 °C. During the pyrolysis following processes occur: sucrose melting (at 185 °C) and intensive destruction (starting from > 225 °C). In the inert atmosphere up to 325 °C, about 30 % of the initial mass was left and mass loss at 500 °C was 78.55 %.

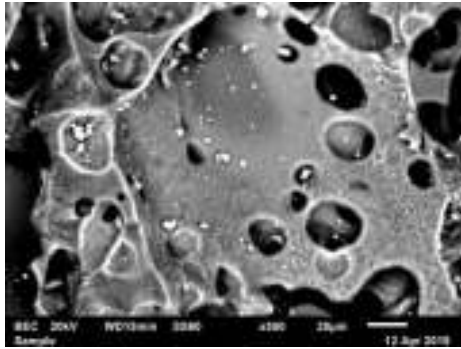


Fig 2. SEM image of pyrolyzed B₄C precursors.

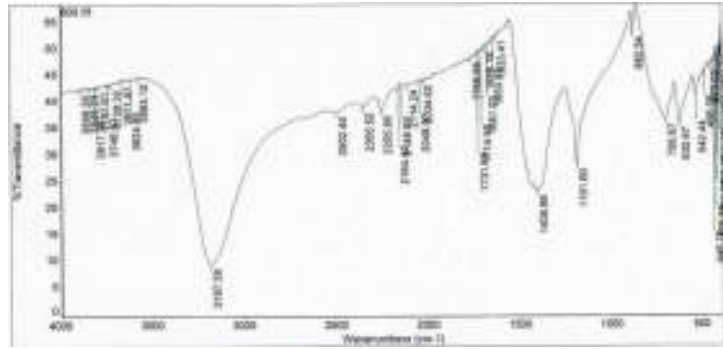


Fig 3. IR transmittance spectrum of pyrolyzed organic precursor.

Herewith, obtained boron oxide was melted (at 450 °C) and homogeneously distributed in the resulting amorphous coal matrix. There occurs the homogenization of boric oxide in carbon obtained from sugar. When conducting the pyrolysis at a relatively low temperature, more amorphous coal was obtained than at high temperature (> 600 °C). Pyrolysis lasted in 120 min. Low sintered large-porous black mass was obtained (**Figure 2**), which can be easily grinded both in mortar or ball mill. Infrared (IR) transmittance spectrum of a pyrolyzed organic precursor is shown in **Figure 3**. The bands were registered at around wavelengths of 406, 409, 412, 417, 421, 424, 436, 447, 470, 496, 542, 633, 707, 883, 1633, 1651, 1682, 1698, 1715, 1732, 1770, 2035, 2049, 2114, 2149, 2164, 2256, 2356, 2502, 3188, 3583, 3625, 3672, 3728, 3747, 3798, 3817, 3849, and 3998 cm⁻¹. That powder was pressed (40 – 50 MPa) into pills and carbidized at 800 – 1500 °C in argon or vacuum for 1 – 5 h.

Summarizing we can conclude that obtaining of fine powders of boron carbide and boron carbide based nanocomposites using liquid charge in form of aqueous plus organic compounds solutions and suspensions is highly prospective route to develop novel hard materials with advanced mechanical properties.

This work was supported by Shota Rustaveli National Science Foundation of Georgia (SRNSFG) – Grant # AR-18-1045: “Obtaining of boron carbide-based nanostructured heterophase ceramic materials and products with improved performance characteristics”.

REFERENCES

1. N. Barbakadze, K. Sarajishvili, R. Chedia, L. Chkhartishvili, O. Tsagareishvili, A. Mikeladze, M. Darchiashvili, V. Ugrekhelidze. Obtaining of ultrafine powders of some boron carbide based nanocomposites using liquid precursors. *Nanotechnology Perceptions: A Review of Advanced Technologies and Their Impacts*, 2020 – *in press*
2. L. Chkhartishvili, A. Mikeladze, O. Tsagareishvili, A. Gachechiladze, A. Oakley, B. Margiev. Ch. 2: Boron-containing nanocrystalline ceramic and metal–ceramic materials. In: *Handbook of Nanomaterials for Industrial Applications* (Ed. Ch. M. Hussain), 2018, Amsterdam, Elsevier, 13-35.
3. ISTC Project # G-462: New Hard Alloys with Nanocrystalline Components (2001 – 2003).
4. STCU Project # 4600: Tungsten, Titanium, and Boron Carbide-Based Nanocrystalline Hardmetals (2009 – 2011).
5. O. Tsagareishvili, A. Mikeladze, R. Chedia, L. Chkhartishvili. Method of obtaining boron carbide based hard nanocomposite materials. National Center for Intellectual Property of Georgia “Geo Patent” – Patent # GE P2018 6709 B (2018 October 11). – *in Georgian*
6. A. Mikeladze, O. Tsagareishvili, L. Chkhartishvili, R. Chedia. Obtaining B_4C – TiB_2 ceramic nanostructured alloys. *Proc. Georg. Natl. Acad. Sci. (Ser. Multi-Disciplinary Studies)*, 2017, 2, 37-44. – *in Georgian*
7. A. Mikeladze, L. Chkhartishvili, O. Tsagareishvili, R. Chedia, M. Darchiashvili. Ceramic composites B_4C – TiB_2 in nanocrystalline state: Production, structure, and mechanical properties. In: *Book of Abstracts of 3rd International Conference “Inorganic Materials Science Modern Technologies and Methods”*, 2018, Tbilisi, Georg. Natl. Acad. Sci. Press, 62-65.
8. A. Mikeladze, O. Tsagareishvili, L. Chkhartishvili, R. Chedia, M. Darchiashvili. Production of titanium-containing metal-ceramic composites based on boron carbide in the nanocrystalline state. *Adv. Appl. Ceram.*, 2019, 118, 4, 196-208.
9. A. Mikeladze, O. Tsagareishvili, L. Chkhartishvili, R. Chedia. Obtaining of some boron-containing and related nanocrystalline systems from solutions and suspensions. In: *Proceedings Book of International Symposium on Boron*, 2019, Nevsehir, Boren, 181-191.
10. A. Mikeladze, O. Tsagareishvili, L. Chkhartishvili, R. Chedia, R. Tsiskarishvili. Method for manufacturing nanocrystalline systems from liquid charge. *Nano Studies*, 2019, 19, 15-36. – *in Russian*
11. L. Chkhartishvili. On obtaining boron carbide based nanocomposites. In: *Proceedings of International Conference on Materials Science, Mechanical and Automotive Engineerings and Technology in Cappadocia* (Eds. B. Kurt, C. Carboga, Z. Bayer Ozturk, N. Kuckdeveci), 2019, Nevsehir, Bektas Veli Univ., 17-21.
12. N. Barbakadze, K. Sarajishvili, R. Chedia, L. Chkhartishvili, O. Tsagareishvili, A.

Mikeladze, M. Darchiashvili, V. Ugrekheldze. Obtaining of ultrafine powder composites of tungsten, molybdenum, titanium and boron carbides using liquid precursors. In: Book of Abstracts of 11th Japanese–Mediterranean Workshop on Applied Electromagnetic Engineering for Magnetic, Superconducting, Multifunctional & Nanomaterials, 2019, Batumi State Univ., 114-115.

CORROSION RESISTANCE OF STEEL MIILUX -500 IN SALT SPRAY CHAMBER AND SUBTROPICAL CLIMATE OF THE ATMOSPHERE

M.Mikaberidze*¹, D.Ramazashvili¹, S. Gvazava¹, V.Tediashvili¹, G.Tavadze¹, V.Tsintsadze¹, R.Bagrati¹, A.Chkhikvadze², O.Gurushidze²

¹ Ferdinand Tavadze Metallurgy and Materials Science Institute, 8b E. Mindeli Str., Tbilisi, 0186, Georgia

²State Military Scientific-Technical Center "DELTA"

mananamikaberidze@yahoo.com

It is known that due to the climate factors, corrosion causes damage or complete failure of combat vehicles, weapons and equipment. In addition, corrosion has a negative impact on the accuracy and security of weapons. According to studies conducted by US, UK, Canada, Australia, the Netherlands and other countries, corrosion is considered to be a major problem for land, air and naval forces. These countries are constantly performing versatile studies to determine and analyze costs caused by corrosion. From this point, the great interest appears to be towards the development of the new corrosion-resistant armor steels and their use in the field of defense [1-3].

The goal of the work was to study corrosion-resistance of armor steel - MIILUX 500, with both accelerated methods in salt spray chamber, as well as its long-term examinations in Batumi subtropical climate of the atmosphere [4].

The object of the research was the armor steel MIILUX-500; it's welded and non-welded samples. Also samples coated with polyurethane (one and two layer). [5]. Chemical composition of the samples of armor steel MIILUX- 500 is set: (mass%): C - 0.3; Si - 0.7; Mn - 1.7; Cr - 1.5; Ni - 0.8; Mo - 0.5; B - 0.004; P - 0.003; S - 0.015; Hardness was measured by the Rockwell installation and it fluctuates in range of 48 ÷ 50HRC. Metallographic examination revealed that the steel has loosened Martensite-Troostitic microstructure.

According to modern literature the research methods are selected in the subtropical atmosphere and salt spray (fog) chamber [6 – 9]. Salt spray chamber test method was based on ASTM B117 and SAE J2334 standards. One cycle consists of three phases: 1. The relative humidity - 100%, temperature - 50°C, duration - 6 pm; 2. Spraying (0,5% NaCl + 0,1% CaCl₂ + 0,075% NaCO₃), temperature - 25°C, duration - 15 min; 3. Drying process - relative humidity - 50%; temperature - 60°C; Duration - 17.75h.

In salt spray chamber corrosion examinations of steel MIILUX-500 revealed: after 100 hours the uncoated samples have been strongly oxidized. Black and brown layer are covered with laps and it's flaking. Samples coated with single layer polyurethane are oxidized in some

places on the ribs and alloy stitches. The rust spots are red in color. In some places, the paint is (point-like) greasy. After 200 hours of viewing, the state of the dyed samples coated with a single layer of polyurethane was significantly deteriorated. The number of red dot rusts increased. Damage to non-stained samples is particularly noticeable on welded stitches. After 500 hours of viewing, strong corrosive decomposition of non-welded samples is observed throughout the surface. A large number of corrosion products fall off the surface without any force modifications. Corrosion centers (in the form of iron rust) are abundant on the sides and face of all coated samples. Welded samples coated with a single layer of polyurethane are particularly susceptible to damage - the welding strip is worn, indicating that the coating on the welded structure is defective, that the solution has percolated and that the paint has peeled. The picture clearly shows that the coating contains microforms in which the salty fog penetrates and under the paint, corrosive processes develop in conditions of limited oxygen supply. Iron oxides with low protective ability arise. As their volume increases, the paint layer breaks down and the rust releases to the surface.

Electrochemical study was conducted of MIILUX - 500 coated steel with one - layer polyurethane in room temperature with 3% sodium chloride solution. The starting potential was 0.001 volts. Within 600 hours, the potential did not change. Then a slight break in the paint layer occurred and the potential value varied from -0.001 - -0.06 volts. After 1150 h, due to the pore elongation, the potential value changed in the positive direction to 0.036 - 0.068 V. At 1800 h the potential was stabilized and after 2200 h. it did not exceed -0.44 V, indicating that the steel was being measured, not the dye. Although, the oxidation process was not active under the paint and no oxidation was observed on the surface. If we compare the corrosive tests in the salt spray chamber and the electrochemical tests at room temperature, it is obvious that the activity of the corrosive processes, except for humidity, significantly is affected by temperature. The obtained results allow us to conclude that one layer of coating is insufficient and additional coating is required. Two-layer polyurethane-coated MIILUX-500 samples showed no changes and no damage.

Long-term tests of samples of the armor steel MIILUX-500 were carried out at the Batumi Corrosion Research Polygon at the open atmospheric stand. There were exhibited: Samples welded and non-welded. Also polyurethane coated samples: unwelded (6 samples coated with one layer of polyurethane, 6 coated with two layers of polyurethane) and welded (6 samples coated with one layer of polyurethane, 6 coated with two layers of polyurethane). Meteorological data were monitored and processed throughout the exposition. According to program timeframe, within 30 days, 3, 6, 10 and 12 months, visual analysis of the removed

samples - description, photography, corrosion type determination and speed calculation, chemical analysis of corrosion products were conducted. Samples of polyurethane-coated MIILUX - 500, welded and without welding, suffer from equal corrosive degradation from the first days. Their surface is covered with Fe₂O₃ iron oxides, the number of which increases with time. The corrosion rate of welded samples after 1000 hours' tests is $K = 0.35 \text{ g} / \text{m}^2 \cdot \text{h}$. The corrosion rate of non-welded samples is less than one order. $K = 0.022 \text{ g} / \text{m}^2 \cdot \text{h}$, (Fig. 1,2). Visual inspection made clear that after one month single-layer samples showed changes - spots and rust spots occurred, that gradually deepened. The samples coated with two layers, after 12 months of testing, despite high humidity and severe meteorological conditions, experienced no changes or damage. The exams continued and after one year the surface condition of the samples did not change – results were completely satisfactory. Despite severe meteorological conditions, no change or damage to the surface was observed. It is established, that the studied armor steel MIILUX-500 has been found to be compatible with its chemical composition, mechanical properties and corrosive properties. The results of our MIILUX-500 tests in salt spray chamber and in natural conditions are correlated with each other. Steel MIILUX-500 coated with two layers of polyurethane is recommended in order to use in the humid subtropical atmosphere. The thickness of the paint should be equal on the entire surface and should not have mechanical damage.

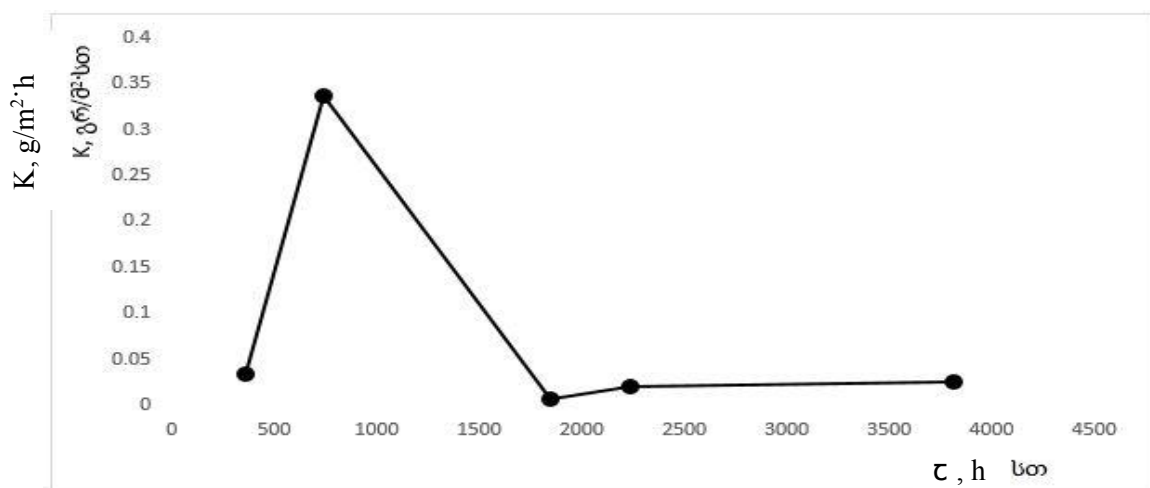


Fig.1 Corrosion rate of welded steel MIILUX-500

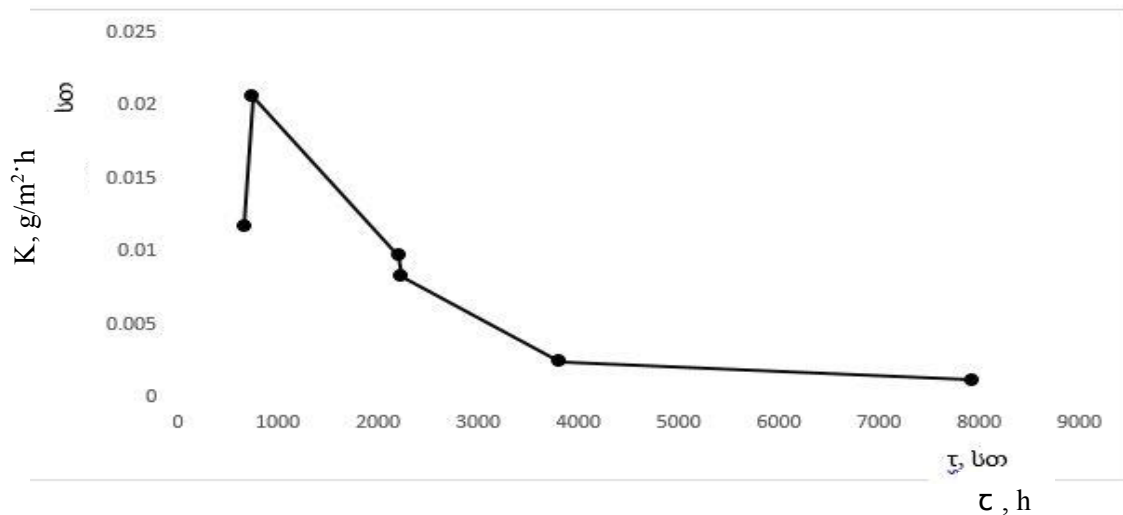


Fig.2. Corrosion rate of non-welded steel MIILUX – 500

REFERENCES:

1. U.S. Army TARDEC Accelerated Corrosion Test for Complete Vehicles 7/12/07;
2. Military Vehicle Development Testing & Engineering NATC. Nevada Automotive Test Center. Corrosion and Fungus Tests, Environmental Chamber Test, 2007;
3. Corrosion-doctors.org/corrosion atmospheric tests.htm;
4. Adjara Climate Change Strategy. Tbilisi, National Document 2013;
5. MIILUX Ltd, www.miiluxproection.fi;
6. ASTM B117 The standard in salt spray testing;
7. BS EN ISO 12944 Atmospheric corrosivity categories and examples of typical environments;
8. ISO 9223;201 Corrosion of metals and alloys – Corrosivity of atmospheres. Classifications, determination and estimation. Second edition 2012;
9. Corrosion of metals; Wear and Erosion. ASTM V.03.02. August 2014.

ELECTROCHEMICAL INVESTIGATIONS OF TiB_{0.6} ALLOYS OBTAINED BY SHS-ELECTRIC ROLLING METHOD

M. Mikaberidze*, Z.Melashvili, V. Tediashvili, S. Gvazava, D. Ramazashvili, N.Kvataia

Ferdinand Tavadze Institute of Metallurgy and Materials Science. 8b.E.Mindeli str., Tbilisi 0186, Georgia, Tbilisi.

mananamikaberidze@yahoo.com

One of the promising methods for making metal ceramic plates is an innovative SHS (self-propagating high-temperature synthesis) followed by electric rolling combined process adopted by Ferdinand Tavadze Metallurgy and Materials Science Institute. This method ensures deformation of hot viscous plastic mass in the deformation core and continuous compensation of thermal losses.

The SHS- electric rolling method is distinguished by its energy efficiency, low cost, efficient process management and ecological purity. It makes it relatively easy to obtain materials with planned properties. By using that method, it is possible to obtain special, different structural ready-made metal ceramic composite materials from pre-selected burdens. In particular: protective gradient, corrosion resistant, worn-resistant, scaling-resistant plates. The principle of SHS- electric rolling method: a pre-compact, burden briquette-filled container is delivered to rolling mill in the deformation core. Electrical chain provides deformation core with electricity: with burden roll – container-roll and with the use of joule heat SHS process starts to initiate, drive powers on and electric rolling process begins, at which point thermal SHS product with viscous plastic mass is delivered to the rolls. [Patent P6541.F. Tavadze Institute of Metallurgy and Material Science, 2016].

TiB_{0.6} alloy samples, wedge-shaped with compression of 25–62% and longitudinal with compression of 55%, were obtained by the SHS method followed by electric rolling.

The aim of the work was the study an influence of compression degree of the wedge-shaped and longitudinal Ti-B_{0.6} alloys on their corrosion resistance in 10% solutions of NaCl, HCl and NaOH.

Electrochemical studies of wedge-shaped (with compression of 25–62%) and longitudinal (with compression of 55%) TiB_{0.6} samples were carried out in 10% solutions of NaCl, HCl and NaOH.

Potentiodynamic curves were taken using a potentiostat at a speed of 50 mV / min. Polarization curves were constructed in the coordinates "potential - the logarithm of current density."

Dissolution and passivation areas are clearly expressed on the potentiodynamic curves in all the solutions studied by us. It was found that 25 - 62% compression of wedge-shaped alloys in a solution of sodium chloride does not significantly affect the electrochemical properties of TiB_{0.6}. In solutions of hydrochloric acid and sodium chloride, the passivation areas are much longer than in the sodium hydroxide solution, which indicates their lower resistance in this solution (Fig1-3). On the potentiodynamic curves of longitudinal TiB_{0.6} samples with 55% compression, almost the same dependence is observed as for wedge-shaped samples - the passivation area is much less in sodium hydroxide solution than in solutions of sodium chloride and hydrochloric acid. (Fig. 4)

It can be concluded that the studied TiB_{0.6} samples have high corrosion resistance in these solutions.

The corrosion currents of the alloys were calculated by extrapolating the intersection points of the Tafel sections on the ordinate of the current density of the potentiodynamic curves recorded in 10% HCl, NaOH, and NaCl solutions. Corrosion rates were determined by the formula: $K = \frac{i \cdot A}{26,8 \cdot n \cdot S} \text{ g/m}^2\text{h}$ The calculation results are shown in table.

Table: Influence of compression ratio on stationary potentials and corrosion rate of wedge-shaped and longitudinal samples of TiB_{0.6} alloy

compression,%	10% NaCl		10% HCl		10% NaOH	
	Est.,v.	K, g/m ² h	Est.,v.	K, g/m ² h	Est.,v.	K, g/m ² h
wedge-shaped						
25	-350	0,007	-400	2,12	-300	0,0614
40	-400	0,024	-500	1,53	-500	0,049
50	-450	0,003	-450	1,43	-600	0,038
longitudinal, 55%	-400	0,00063	-500	0,85	-500	0,268

As shown in the table, the corrosion rate of wedge-shaped TiB_{0.6} samples in solutions of hydrochloric acid and sodium hydroxide decreases with increasing of compression rate of the alloy, which is associated with a decrease of the porosity of the material. This effect is not observed in a sodium chloride solution, but the corrosion rate of TiB_{0.6} alloy is much lower. The highest corrosion resistance was revealed by longitudinal TiB_{0.6} samples with compression of 55% in the 10% solution of sodium chloride. In general, we can conclude that the studied compressed TiB_{0.6} samples, both wedge-shaped and longitudinal, showed high corrosion resistance in 10% HCl, NaOH, and NaCl solutions, especially in solution of sodium chloride.

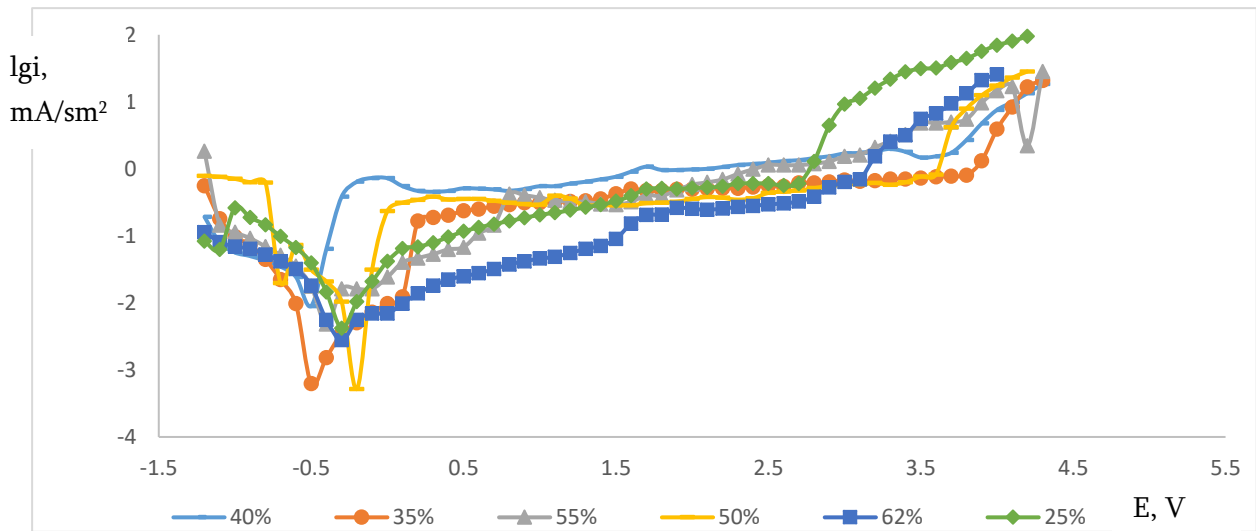


Fig. 1. Potentiodynamic curves of wedge-shaped $TiB_{0.6}$ samples with different compression ratios in a 10% NaCl solution

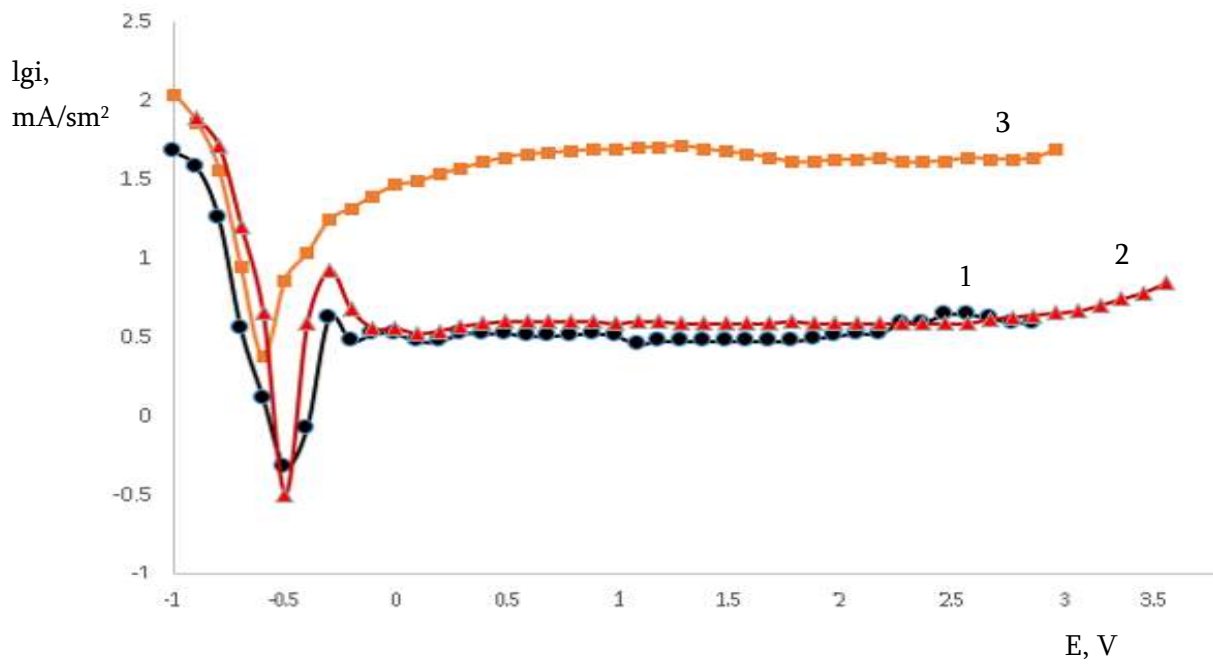


Fig.2. Potentiodynamic curves of wedge-shaped $TiB_{0.6}$ samples with different compression ratios in a 10% HCl solution: 1– 50 %; 2 - 40%; 3– 25%

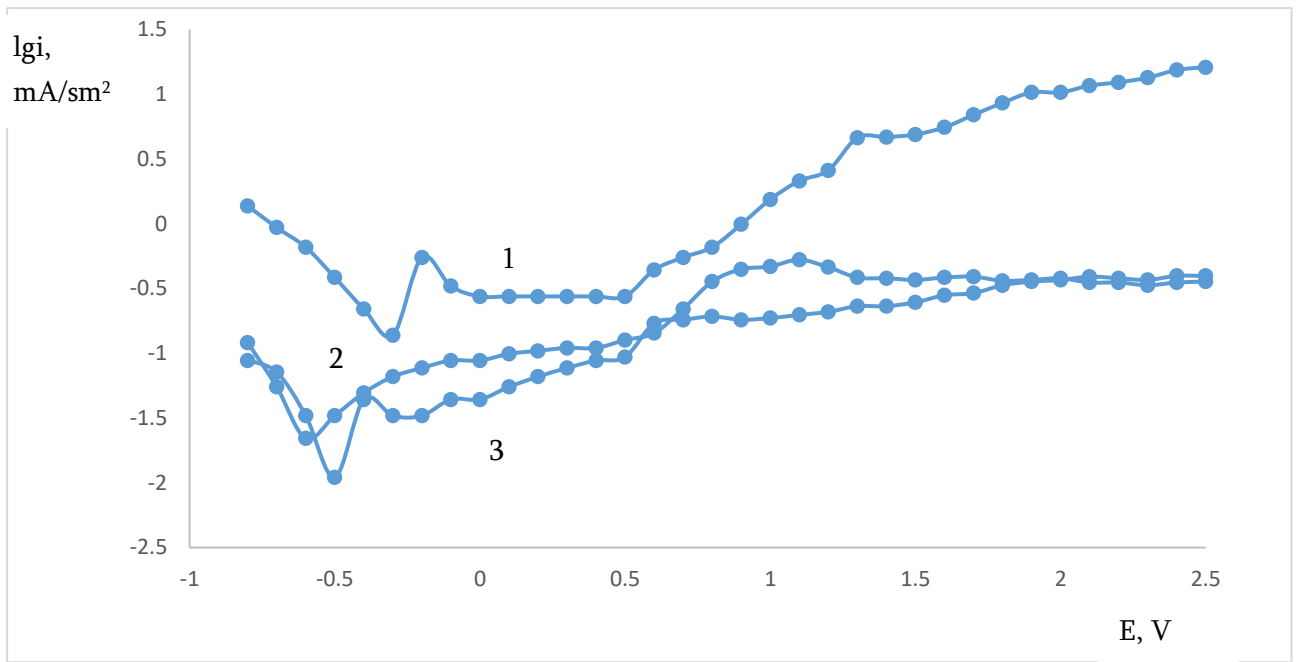


Fig. 3. Potentiodynamic curves of wedge-shaped $\text{TiB}_{0.6}$ samples with different compression ratios in a 10% NaOH solution: 1-35%; 2-50%; 3- 40%

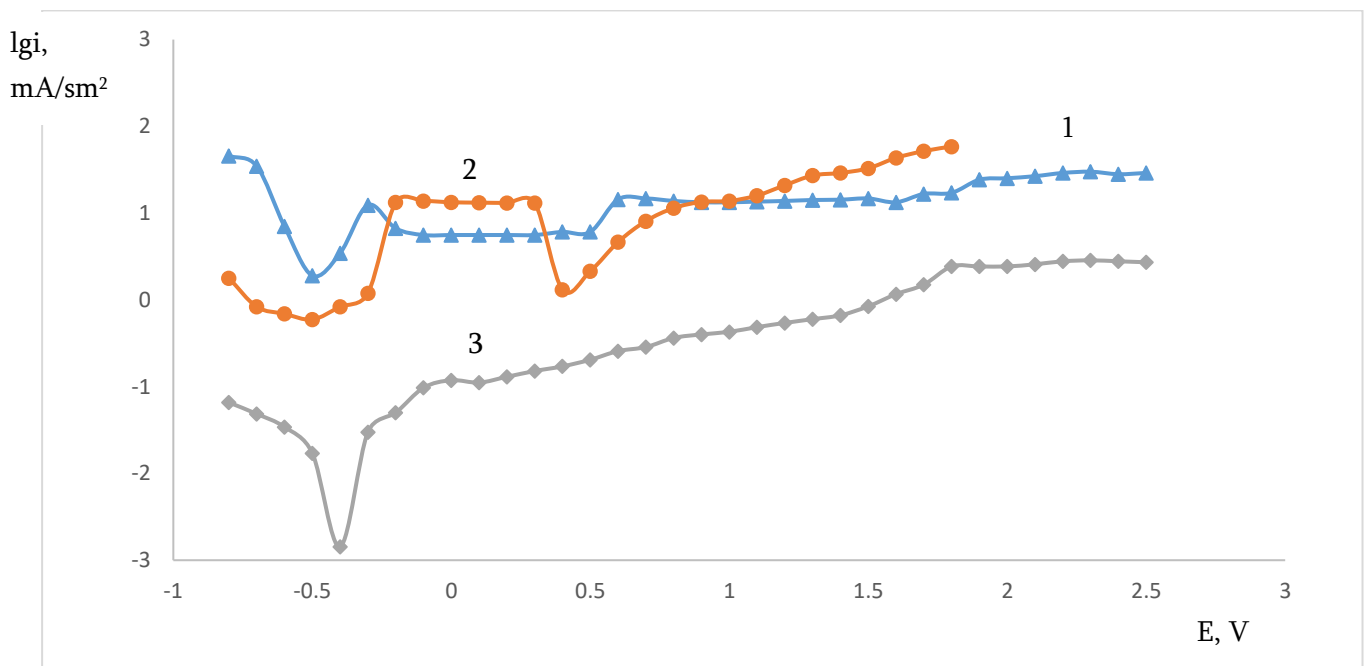


Fig. 4. Potentiodynamic curves of 55% longitudinal $\text{TiB}_{0.6}$ samples in the 10% solutions of: 1-HCl, 2 -NaOH, 3 - NaCl

COMBUSTION SYNTHESIS OF CERAMICS: FUTURE DIRECTIONS

A. Mukasyan *

University of Notre Dame, Notre Dame, IN, 46556, USA

* amoukasi@nd.edu

Researchers in more than 100 countries are currently using self-sustained reactions for material synthesis. Analysis of the Web of Science database shows that the number of publications on the topic of combustion synthesis (CS) has rapidly increased in recent years, with more than 2000 papers published in each year from 2018 to 2020. Several examples of industrial applications of CS are known, including production (40 tons per year) of titanium diboride powders (Hubei DoBo Advanced Ceramics Co., Ltd., China), ferrosilicon nitride (100 tons per year) by NTPF Etalon (Russia), high performance LED phosphors (Ellim Advanced Materials South Ltd., Korea) for LG display, and others (Fig. 1).



Fig. 1: bulk materials and net shape articles fabricated by CS route

The goal of this mini review is to summarize and critically discuss the specifics for direct CS of the ceramics, including synthesis conditions, mechanism of microstructure formation, as well as material's properties. Special attention is paid to the last achievements in the field, including analysis of such novel synthetic routes as reactive spark plasma sintering, combustion synthesis with mechanical stimulation, as well as CS of nanostructured ceramics and composites.

The world market on advanced ceramics is continuously growing. While other technologies exist for the production of ceramic powders, it is logical to assume that some novel ceramics

will be difficult or essentially impossible to fabricate by such conventional approaches. Taking into account the novel routes to control powder morphology and the flexibility of energy-efficient CS, which is easy to scale up (cf. [1-4]), it may be expected that CS technologies will find their place in the market. The production of *nano-scaled and sub-micron* spherically shaped carbides, borides, carbonitrides, and other ultra-high temperature powders using *combination of the mechanically induced nanostructured composite* particles and self-sustained reactions is among the first candidates for such applications [3, 5].

Combination of CS and Spark Plasma Sintering (SPS) for synthesis of monolithic ultra-high temperature bulk ceramics is another promising direction. Indeed, since these compositions possess very high melting points, it is in principle difficult to consolidate the powders to pore-free bulk materials. Recent experiments showed that rapid SC reactions during SPS intensify mass transport in such systems, and thus enhance their sinterability (cf. [2, 4]. Additional investigation is required to optimize this method, but it has substantial potential as a substitute for conventional powder metallurgy approaches used to produce dense *ultra-high temperature ceramics*.

The recent breakthrough results that demonstrate the ability of *CS methods to fabricate metastable compounds* are very promising [6-8]. The near future will show whether or not scientists are able to broaden the list of CS-produced metastable phases and raise the output of products to the laboratory (~kg) scale. If successful, CS may become the go-to method for synthesis of such unique materials.

It is worth noting that self-sustained reactions can also be used *for joining materials*. This method should be used when conventional approaches do not work. Such special cases include the joining of refractory materials (high-temperature ceramics) or dissimilar materials where the issue of CTE mismatch is critical. The reported examples of joining carbon-carbon composites [9,10] and silicon carbide to an aluminum alloy [11] demonstrate the effectiveness of CS-based approaches.

Finally, many fundamental questions should be addressed to provide deeper understanding into the phenomenon of self-sustained reactions:

Can the majority of such reactions can be accomplished in the solid flame mode that is essentially through solid-state diffusion? What mechanisms might be responsible for the occurrence of solid-state reactions within the microsecond time scale? What is the mechanism

leading to formation of metastable phases during SCS? Do SPS conditions influence the kinetics of the self-sustained reactions?

In order to answer these and numerous other questions, novel *in-situ and operando diagnostics* should be designed and built. Such diagnostics should permit investigation of phenomena with *microsecond temporal and nanometer spatial resolutions*. These findings will certainly lead to the novel synthetic routes that apply the CS paradigm.

REFERENCES

1. A. Varma, A.S. Mukasyan, A.S. Rogachev, K.V. Manukyan, Chem. Rev. 116 (2016) pp. 14493–14586.
2. E.A. Levashov, A.S. Mukasyan, A.S. Rogachev, D.V. Shtansky, Int. Mater. Rev. 62 (2017) pp. 203–239.
3. H.H. Nersisyan, J.H. Lee, J.R. Ding, K.S. Kim, K.V. Manukyan, A.S. Mukasyan, Prog. Energy Combust. Sci. 63 (2017) pp.79–118
4. A.S. Mukasyan, D.O. Moskovskikh, A.A. Nepapushev, J.M. Pauls, S.I. Roslyakov, J. Eur. Cer. Soc., 40 (2020) pp.2512–2526.
5. A.S. Mukasyan, A.S. Rogachev, J. Mat. Sci. 52, (2017) pp. 11826-11833.
6. A.S. Mukasyan, S. Roslyakov, J.M. Pauls, L.C. Gallington, T. Orlova, X. Liu, et al., Inorg. Chem. 58 (2019) pp. 5583–5592
7. M.T. Beason, J.M. Pauls, I.E. Gunduz, S. Rouvimov, K.V. Manukyan, K. Matouš, et al., Appl. Phys. Lett. 112 (2018) 171903.
8. W. W. Chapman, M. Örnek, J.M. Pauls, M. Zhukovskyi, S. F. Son, A.S. Mukasyan, Scripta Materialia, 189 (2020) pp. 58-62.
9. J.D.E. White, A.H. Simpson, A.S. Shteinberg, A.S. Mukasyan, J. Mater. Res. 23 (2008) pp. 160–169.
10. Y.-C. Lin, A.A. Nepapushev, P.J. McGinn, A.S. Rogachev, A.S. Mukasyan, Ceram. Int. 39 (2013) pp. 7499–7505.
11. Y.-C. Lin, P.J. McGinn, A.S. Mukasyan, J. Eur. Ceram. Soc. 32 (2012) pp. 3809–3818.

EXPLOSIVE CONSOLIDATION AND SYNTHESSES OF SUPERCONDUCTIVE COMPOSITES BASED ON MgB₂

A.Peikrishvili*¹, G.Tavadze¹, B.Godibadze², E.Chagelishvili², G.Mamniashvili², A.Shengelaya².

¹Ferdinand Tavadze Institute of Metallurgy and Materials Science, 8b E.Mindeli St. 0186 Tbilisi, Georgia,

²Iv., Javakhishvili Tbilisi State University, I. Chavchavadze Ave., 1, 0179 Tbilisi, Georgia 3G.Tsulukidze Mining Institute, 7 E.Mindeli St. 0186 Tbilisi, Georgia

*[apeikrishvili@yahoo.com](mailto:apecrshvili@yahoo.com)

INTRODUCTION

The superconductive properties of MgB₂ with C32 structure and critical transformation temperature of $T_c=39\text{K}$ was discovered in 2001 [1]. Since then, intensive investigation and development of different types of MgB₂ superconductive materials in various forms and efforts to increase their T_c above 39 K takes place worldwide [2-5]. The technology of development superconductive materials belongs to traditional powder metallurgy: preparing and densification Mg and B powder blends in static conditions with their further sintering processes [6,7]. Results described in [8], where Mg-2B blend powders were first compacted in cylindrical pellets and were after loaded in hot conditions at 2 GPa pressure, seem also interesting.

Existing data of the application of shock wave consolidation technology for fabrication of high dense MgB₂ billets with higher T_c temperature practically gave the same results and limit of $T_c=40\text{K}$ is still considered maximal. Additional sintering processes after the shock wave compression are highly recommended for providing full transformation of consolidating blend phases into the MgB₂ composites.

The purpose of the current investigation is to investigate superconductive MgB₂ based billets fabricated by hot shock wave consolidation technique without any further sintering processes

MATERIALS AND EXPERIMENTAL PROCEDURES

Superconductive Mg-2B and Magnetic nano-composite Mg-2B-1wt%Fe (coarse Mg and B (5-10 μ) and nano-Fe powder with a particle size of 25 nm) were consolidated above 900°C using two stage hot shock wave method described in [9,10-11].

RESULTS.

The experiments of hot shock wave consolidation/syntheses of Mg-2B based blend composites in steel container were performed below and above the melting point of Mg with intensity of loading around 5GPa. It was established that only loading by shock waves above the 900°C creates favorable conditions and allows to obtain cylindrical samples near to theoretical densities with high value of critical temperature under 40K.

The figure 1 represents the results of SEM investigation of nanostructured MgB₂-1%Fe composited consolidated/synthesized at 940°C temperature with intensity of shock wave loading around 5GPa.

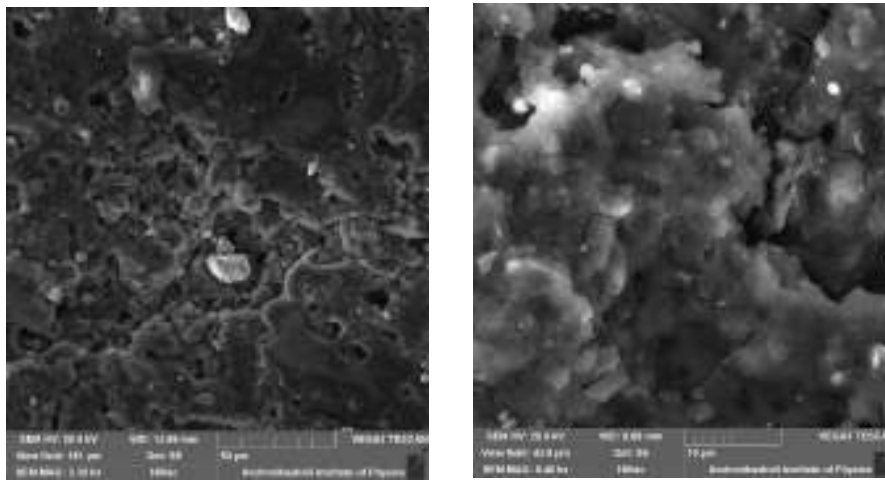


Fig. 1. The microstructures of MgB₂-1%Fe composites obtained after 2 stage hot shock wave loading at 940°C with intensity of loading around 5GPa. The structure have high density and shows good integrity between the consisting grains. The traces of melting-crystallization are observed too.

It was found earlier that doping of MgB₂ by C, Li, Be and other metals leads only to decrease of T_c. Positive effect was found only for the doping of MgB₂ with heavier alkali and alkali-earth metals which are capable of strong carrier donation to electron system and therefore essentially enhanced superconductivity properties of MgB₂ up to 45-58K [12].

In order to improve magnetic moment of fabricated superconductive compounds there was carried out comparative study of effects caused by added to Mg+2B mixture magnetic nanoparticles on the magnetic and electric properties of shock wave consolidated composites. These particles could introduce multiple pinning centers resulting in increased flux pinning and critical current density. The nanoscale Fe with a particle size of 25nm was added to Mg+2B

mixture precursors and were consolidated by 2 stage shock wave fabrication method described above [10,11]. The results of structural and magnetic investigations are presented on fig. 2.

The figure 2 represents the results of magnetic and electrical characteristics of nanostructured MgB₂-1%Fe composited consolidated/synthesized at 940°C temperature with intensity of shock wave loading around 5GPa.

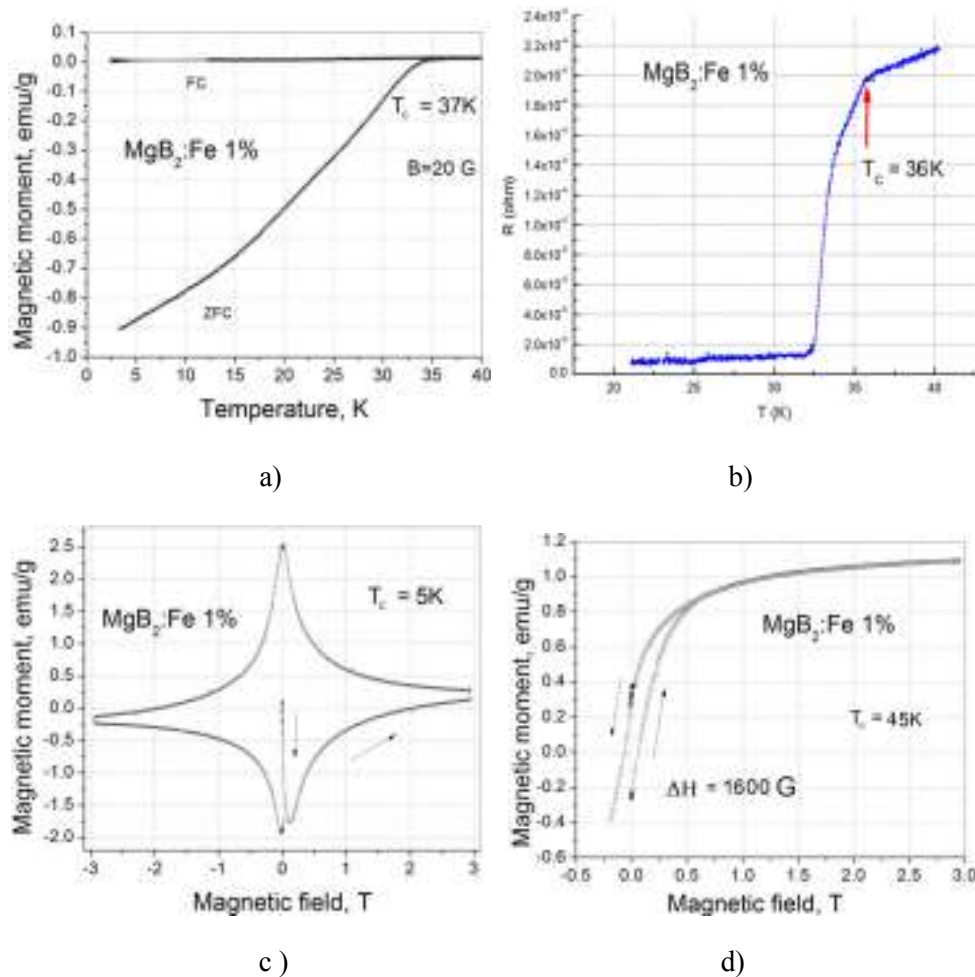


Fig. 2. The results of investigation Magnetic characteristics for MgB₂-1%Fe composites fabricated at 940°C temperature with intensity of shock wave loading around 5GPa: a) Temperature dependence of magnetization in ZFC and FC modes under a magnetic field of 20 G; b) Temperature dependence of resistance; c) Magnetization hysteresis loop at 5K; d) Magnetization hysteresis loop at 20K.

In order to evaluate the superconductive characteristics of obtained billets the magnetic moment temperature dependence in zero-field-cooled (ZFC) and field-cooled (FC) modes depending on experimental conditions and type of boron precursors were investigated. As reported in [9, 11, 12] the application of low temperatures up to 900°C and hot shock wave consolidation/syntheses of Mg-2B precursors in steel containers did not give results. In spite of

high density and uniform distribution of phases they did not obtain superconductive characteristics.

DISCUSSION

The hot shock wave consolidation-syntheses of Mg-2B composite powders were performed in steel containers below and above of Mg melting point. In order to determine the role of temperature, the consolidations were carried out at 500, 700 and 940°C. At 500°C and 700°C the consolidation gives no results and obtained compacts have no superconductive characteristics. The application of higher temperatures provides the formation of MgB₂ composition in the whole volume of fabricated billets with maximal value of $T_c=38.5$ K without any post sintering process. This confirms the important role of temperature in the formation of superconductive MgB₂ and corresponds with the literature data where only after sintering processes above 900°C the formation of MgB₂ phase with $T_c=40$ K takes place. The difference of T_c between the HEC and sintered MgB₂ composites may be explained due to unreacted Mg and B phases or due to the existence of oxides in the starting materials. This could be checked by increasing of consolidation-syntheses temperature or by the application of further sintering processes. The careful selection of initial Mg and B phases is important too and in case of consolidation Mg-2B precursors with corrections mentioned above the chance to increase critical temperature (T_c) of shock wave synthesized samples increases essentially. Next experimental stage is the fabrication of MgB₂ superconductive materials.

As it is seen from results of magnetic and electric measurements that MgB₂-1%Fe composites retains its superconducting properties and reveals a magnetic hysteresis in the normal state. The critical temperature is about 36K as compared with $T=38.5$ for Hot shock wave fabricated MgB₂ compounds.

CONCLUSION

The doping of Mg-2B precursors with 1% nanoscale Fe particles with dimensions 25nm and fabrication MgB₂-1%Fe samples shows that composites retains its superconducting properties and reveals a magnetic hysteresis in the normal state. The critical temperature is about 36K as compared with $T=38.5$ for Hot shock wave fabricated MgB₂ compounds.

REFERENCES

1. J. Nagamatsu, N. Nakagawa et al, J. Akimitsu, “Superconductivity at 39 K in magnesium diboride”, *Nature*, Vol. 410, No. 6824, pp. 63-64, 2001.
2. C. H. Jiang, T. Nakane et al, “Enhanced J_c property in nano-SiC doped thin MgB_2/Fe wires by a modified in situ PIT process”, *Physica C*, Vol. 422, No. 3-4, pp. 127-131, 2005.
3. V. I. Mali, V. A. Neronov, V. P. Perminov et al, “Explosive incited magnesium diboride synthesis”, *Chemistry for Sustainable Development*, Vol. 13, No. 3, pp. 449–451, 2005.
4. N. Orlinska, A. Zaleski, Z. Wokulski, G. Dercz, “Characterization of heat treatment MgB_2 rods obtained by PIT technique with explosive consolidation method”, *Archives of Metallurgy and Materials*, Vol. 33, No. 3, pp. 927-932, 2008.
5. M. J. Holcomb, “Supercurrents in magnesium diboride/metal composite wire”, [Physica C: Superconductivity and its Applications](#), Vol. 423, No. 3-4, pp. 103-108, 2005.
6. T. A. Priknha, W. Gawalek et al, “high gh-pressure synthesis of a bulk superconductive MgB_2 -based material”, *Physica C: Superconductivity*, Vol. 386, pp. 565-568, 2003.
7. A. G. Mamalis, I. N. Vottea, D. E. Manolakos. “Explosive compaction/cladding of metal sheathed/superconducting grooved plates: FE modeling and validation”, *Physica C: Superconductivity*, Vol. 410, pp. 881-883, 2004.
8. A. P. Shapovalov, “High pressure syntheses of nanostructured superconducting materials based on magnesium diboride”, *High Pressure Physics and Engineering*, Vol, 23, No. 4, pp. 35-45, 2013.
9. G. Mamniashvili, D. Daraselia, D. Japaridze, A. Peikrishvili, B. Godibadze, “Liquid-phase shock-assisted consolidation of superconducting MgB_2 composites”, *J. Supercond. Nov. Magn.* Vol. 28, No. 7, pp. 1926-1929, 2015.
10. T. Gegechkori, B. Godibadze, V. Peikrishvili, G. Mamniashvili, A. Peikrishvili, “One stage production of superconducting MgB_2 and hybrid power transmission lines by the hot shock wave consolidation technology, *International Journal of Applied Engineering Research (IJAER)*, 12, No. 14, pp. 4729-4734, 2017.
11. T. Gegechkori, G. Mamniashvili, A. Peikrishvili, B. Godibadze, V. Peikrishvili, “Using Fast Hot Shock Wave Consolidation Technology to Produce Superconducting MgB_2 ” *Engineering, Technology & Applied Science Research*, Vol. 8, No. 1, 2018, 2374-2378, PP 2374-2378
12. N.S.Sidorov A.V.Palnichenko et al, “Superconductivity of Mg/MgO interface formed by shock-wave pressure”, *Physica C: Superconductivity*, Vol. 488, pp. 18-24 (2013).

RADIATION-RESISTANT MATERIAL FOR THERMOELECTRIC PERFORMANCE

T.Qamushadze*, E.Khutsishvili, Z. Davitaja, N.Kobulashvili, Z.Chubinishvili, R. Razmadze

Ferdinand Tavadze Institute of Metallurgy and Materials Science, Tbilisi, Mindeli str.8b, 0186, Georgia

* t.qamushadze@g.mail.com

Among the sources of electrical energy such as photoelectric, thermoelectric, thermionic and magneto-hydrodynamic methods, which differ from existing ordinary ones by lack of intermediate complex huge aggregates, thermoelectric converters occupy a particular position. They are characterized by high reliability, full automation, simplicity of operation, functioning without service for a long time, the absence of short circuits and transmission lines, small sizes, etc. Thermoelements as autonomous independent energy sources are the most needed for inaccessible places and radiation conditions (space, nuclear reactors, terrestrial and interplanetary artificial satellites, radiation-contaminated territories. In some cases, thermocouples are independent sources of small and average energy. For example, for a spacecraft in the passive side thermoelements are much more convenient for power supply, than complex sources operating on chemical fuel derived from a rocket engine.

At the same time, it is very important that temperature drops of both low and high are characteristic for Space. In this case the use of thermocouples are most practical, optimal, advantageous and actually indispensable. The solution of this problem requires thermoelectric materials with high efficiency for different temperature ranges.

But that is not enough. The main trouble is that high-energy particles and electromagnetic radiation incapacitates devices in Space. At the same time, the thermoelements are needed operating in extreme conditions for many years with high reliability. There are still other extreme conditions when only nuclear energy sources can be used to obtain the energy for the hot part of the thermoelements. Therefore, for Space applications, as a heat source for thermocouples, atomic reactors (nuclear energy) or radioactive isotopes (for example radioactive generator (SNAP) are usually used. Many years of experience have shown that existing methods of radiation protection are not always sufficient. Solution of this problem demands to create radiation-resistant materials as an active element of generators, which defines a reliable guarantee of the operation of thermocouples.

Only radiation-resistant semiconductor materials, combining both high thermoelectric efficiency and radiation resistance, can satisfy the requirements of this technical problem. For this purpose re the best for producing radiation-resistant thermocouples.

It has been shown that polycrystalline InAs, easily prepared material, can be used for thermoelectric power conversion at efficiencies high enough to have practical interest [1]. Furthermore ternary III-V system of polycrystalline $\text{InP}_x\text{As}_{1-x}$ semiconductor alloys a may have peak figures of merit which are higher (about 20%) than that of the binary InAs.

In thermoelectrical studies the problem is to increase figures of merit $\eta = zT$, where z -thermoelectrical efficiency is defined as:

$$z = \alpha^2 \sigma / \chi$$

α – the Seebeck coefficient, σ – electrical conductivity, χ -thermal “*phononglass electron-crystals*”. This means that the materials must have low lattice thermal conductivity mechanism as in amorphous materials and high electrical conductivity in crystals. From the expression of thermoelectric efficiency z , it follows that an increase of z is possible by the increase in magnitude of σ/χ . This can be reached by alloying InAs by P up to 5at%. That is why ternary III-V system of polycrystalline $\text{InP}_x\text{As}_{1-x}$ semiconductor alloys improves thermoelectric properties of InAs. But alloying InAs with P not only improves InAs properties, it makes it radiation-resistant, despite the fact, that irradiation of InAs creates n -charged point defects that worsen the Seebeck coefficient and electrical conductivity, and leads to a deterioration of thermoelectric efficiency. The appearance of radiation-resistant properties is connected with that when phosphorus is added to InAs, irradiation creates disordered regions which are effective for scattering of short-wave phonons, but not of long-wave electrons. As a result, in InAs alloyed by P σ/χ increases and it exceeds a slight decrease in the Seebeck coefficient during irradiation. So thermoelectrical efficiency doesnot get worse. That means it is possible to create a radiation-resistant thermoelectric material for low temperatures application.

Choosing the appropriate concentration of P it is possible even to improve thermoelectrical efficiency. Fig. shows this improvement for InAs alloyed by P up to 3at%.

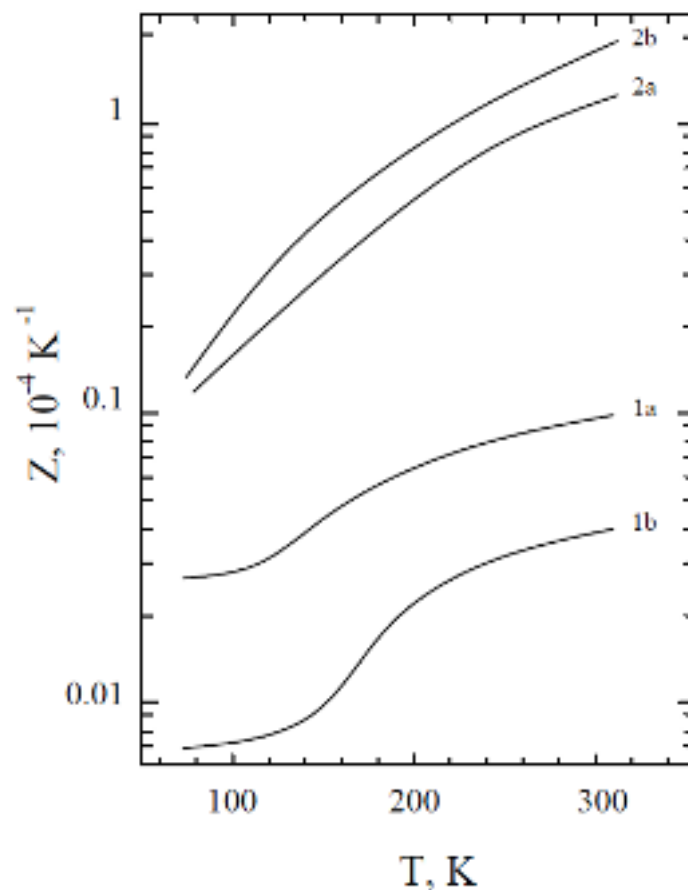


Fig. The dependence of thermoelectrical efficiency of InAs (curves 1a and 1b) and InAs alloyed by P with 3 at% (curves 2a and 2b); curves 1a and 2a refer to results before radiation, curves 1b and 2b refer to results after radiation by 7MeV energy electrons with fluences of $\Phi= 3,8 \cdot 10^{16}$ - $2,8 \cdot 10^{17}$ e/cm².

Obtained by us thermoelectrical material is one of the best low temperature thermoelectrical material, which can be used in a segmented arrangement of high temperature thermoelectrical materials to create a thermocouple in the entire operating range from low to high temperatures.

Thermally and electrically well compatible with Si-Ge alloys this helps [2-4]. Moreover this InAs is characterized by low effective mass and sufficiently high mobility. Indium-based alloys make it possible to create radiation-resistant material. In addition, InAs is technologically flexible, which makes it possible to create on its basis a new generation of highly effective thermoelements in a modern form, which are the layers of the quantum dimensions of homo and heterostructure.

REFERENCES

1. R. Bowers, J. E. Bauerle, and A. J. Cornish, *J.of Appl.Phys*, 30, 1959, pp. 1050-1054.
2. F.D.Rosi.*Solid-State Electronics*,11, 1968, pp. 833-868.
3. G. Slack, in *CRC Handbook of Thermoelectrics* (Ed: D.M. Rowe), CRC Press (1995), pp.407-440.
4. M.N. Tripathi, C.M. Bhandari,| *J.of physics*, 65, 2005, pp. 469-479.

CENTRIFUGAL METALLOTHERMIC SHS OF CAST CoCrFeNiMn BASED HIGH ENTROPY ALLOYS AND COATINGS OF THEM

V. Sanin^{1*}, D. Ikornikov¹, D. Andreev¹, S. Zherebtsov², V. Yuxhvid¹

¹ Merzhanov Institute of Structural Macrokinetics and Materials Science Russian Academy of Sciences, Academician Osipyan str., 8, Chernogolovka, Moscow Region, 142432, Russia.

² Belgorod State University, Pobeda 85, Belgorod, 308015, Russia

svn@ism.ac.ru

High entropy alloys (HEAs) have recently emerged as a new class of advanced metallic materials promising for various applications [1, 2]. Their main feature is high complexity of chemical composition; according to original definition, HEAs should be composed of at least 5 principal elements in close to equiatomic concentrations (5-35 at.%) [3].

One of the promising classes of the HEAs which attained particular attention is fcc-structured Co-Cr-Fe-Ni-Mn system alloys. The alloys have unique mechanical properties: very high ductility at room temperature becomes even higher when the temperature decreases into the cryogenic interval. Although composition-structure-properties relations of the Co-Cr-Fe-Ni-Mn system alloys are under extensive investigation at the moment, many aspects of behaviour of these alloys have not received significant attention yet.

Also, the problematic aspect is the production of HEAs with liquation free structure. Conventional casting processes for production of HEAs are the multistage vacuum-arc or induction remelting of extra-pure grade elements. To achieve the desired homogeneity, 4–6 remelts may be required, depending on the composition and content of the alloying components. Therefore, the conventional metallurgical technologies are rather expensive and energy-consuming. A promissory route to production of cast HEAs is using technique which was called the “SHS-technology of hightemperature melts” [4] or the “SHS-metallurgy” [5]. This is an energy-saving technique due to the use of internal energy released in high-caloric combustion reactions. Recently, the one firstly was demonstrate to prepare cast high-entropy transition metal alloys [6].

Powder mixtures of metal oxides—the components of the (Co₃O₄, Cr₂O₃, Fe₂O₃, NiO, MnO₂) alloy, along with the reducing agent (Al) and pure C and ScF₃ as a dopant, were used as the starting components to produce the cast Co-Cr-Fe-Ni-Mn alloy. The procedure of fabricating the SHS alloy and investigation have been thoroughly described in [6,7]. Fig. 1 illustrates phase composition and the microstructure of SHS produced as-cast CoCrFeNiMn alloy without additives.

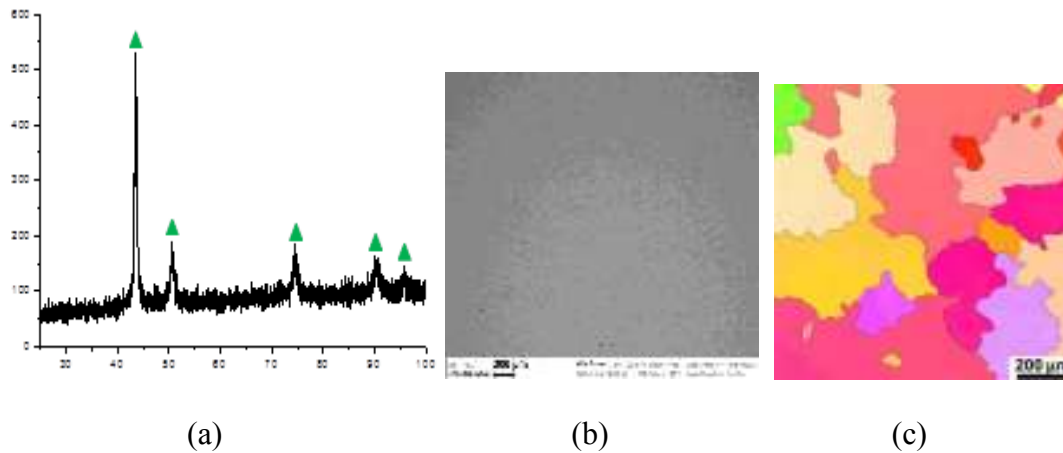


Fig. 1. Phase composition and microstructure the as-cast CoCrFeNiMn alloy:
 (a) – XRD pattern (FCC ($Im\bar{3}m$)), (b) – SEM , (c) – EBSD IPF map.

The XRD pattern and microstructure both demonstrate presence of single phase with fcc lattice. According to XRD, the fcc lattice parameter is $a = 3.588$ nm. In addition, both XRD and EBSD data show strong crystallographic texture, typical for the cast materials. The alloy has coarse structure with the grains size of 250-400 μm . The grain boundaries are often curved, and the shape of the grains is irregular. Additional investigations by SEM and TEM also have not revealed presence of any second phases.

To obtain the doped alloy compositions on the basis of the studied CoCrFeNiMn alloy in the starting mixture introduced alloying components which also took part in the formation of chemical composition directly in the combustion wave. The studies of doped components showed that the introduction of carbon to 0.2 Wt.% does not have a noticeable effect on the phase composition formation but significantly increases the hardness of the alloy. The introduction of Sc has a similar impact. The introduction of Al in the composition of the alloy markedly reduces the density of the alloy. The formation of intermetallic phase NiAl is observed at high concentrations of Al and it promote sharp decrease in plasticity.

Also in the work the possibility of forming the coating in-situ SHS (SHS-coating) for HEAs on a metal substrate (Ti alloy) was investigated for the first time. Figure 2 shows the transition zone structure of the deposited coating layer/ Ti substrate .

Analysis of the microstructure of the deposited layer revealed the presence of three zones (Fig. 2a) where the base material (Ti) gradient distributed over the height of the deposited layer. Fig. 2b shows that the hardness of the substrate and coating has a difference in hardness of more than 3 times.

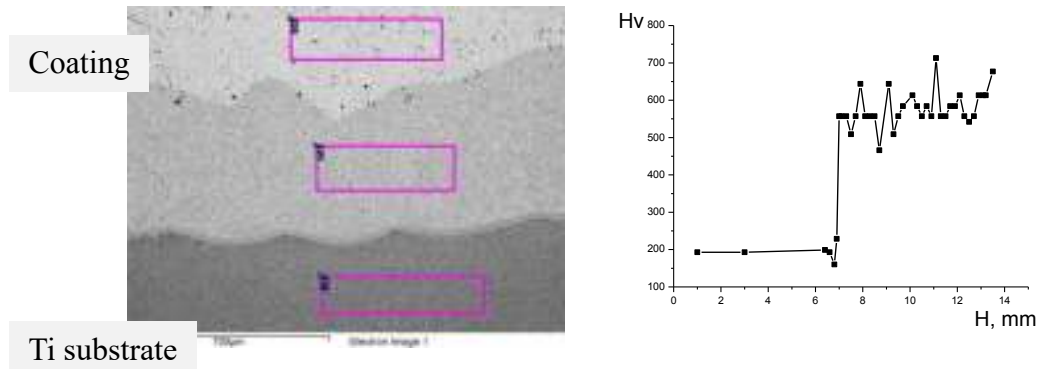


Fig. 2. The microstructure the SHS surfacing (a) and dependence of microhardness (b) on height of coating.

The analysis of the obtained data allows drawing a conclusion about the prospects of the materials under investigation and the method of their production for the formation of volumetric materials and coating of them. The production of metallic composite materials based on the new principle of formation of polymetallic alloys can significantly expand the basis for the creation of new materials and facilitate the creation of new technological models.

The research was supported by the Russian Foundation for Basic Research, (project no. 19-08-01108).

1. D.B.B. Miracle, O.N.N. Senkov, A critical review of high entropy alloys and related concepts, *Acta Mater.* 122 (2017) pp. 448–511. doi:10.1016/j.actamat.2016.08.081.
2. M.-H. Tsai, J.-W. Yeh, High-Entropy Alloys: A Critical Review, *Mater. Res. Lett.* 2 (2014) pp. 107–123. doi:10.1080/21663831.2014.912690.
3. D. Miracle, J. Miller, O. Senkov, C. Woodward, M. Uchic, J. Tiley, Exploration and Development of High Entropy Alloys for Structural Applications, *Entropy.* 16 (2014) 494–525. doi:10.3390/e16010494.
4. Merzhanov A.G. Combustion processes that synthesize materials. *J. Mater. Process. Technol.*, 1996, v.56, pp. 222-241. 10.4028/www.scientific.net/KEM.746.219
5. Sanin, V.N., Ikornikov, D.M., Andreev, D.E., and Yukhvid, V.I., Centrifugal SHS metallurgy of nickel aluminate based eutectic alloys, *Russ. J. Non-Ferr. Metall.*, 2014, vol. 55, no. 6, pp. 613–619. doi 10.3103/S1067821214060212
6. V.N. Sanin, V.I. Yukhvid, D.M. Ikornikov, D.E. Andreev, N. V. Sachkova, M.I. Alymov, SHS metallurgy of high-entropy transition metal alloys, *Dokl. Phys. Chem.* 470 (2016) 145–149. doi:10.1134/S001250161610002X.
7. Sanin V.N., Ikornikov D.M., Andreev D.E., Sachkova N.V., Yukhvid V.I. Synthesis of cast high entropy alloys with a low specific gravity by centrifugal metallothermic SHS-methods. *Advanced Materials and Technologies.* 2017. № 3. c. 24-33. DOI: 10.17277/amt.2017.03.pp.024-033

INTERACTION OF CARBON WITH A Ti-Al MELT DURING SELF-PROPAGATING HIGH-TEMPERATURE SYNTHESIS

A. Sytschev*, S. Vadchenko, A. Shchukin, O. Boyarchenko

Merzhanov Institute of Structural Macrokinetics and Materials Science Russian Academy of Sciences (ISMAN), Academician Osipyan str., 8, Chernogolovka, Moscow Region, 142432, Russia

* sytschev@ism.ac.ru

Ti-Al-based intermetallic are widely used as structural materials. An important material science task is to increase their properties, which is carried out by doping with various elements. The carbon (graphite, carbon black or carbon fibers) makes the alloying process more manageable and improves the final properties of the product. Wetting and possible interaction of carbon with metal melts is of great interest in the materials science of metallurgical processes [1,2]. Even small amounts of carbon affect the properties of the alloys. The mechanical activation treatment makes it possible to achieve a uniform distribution of carbon components into the volume of the matrix material [3-7]. Among the composite materials that can work in conditions of high temperatures and loads, Ti-Al alloys are very promising [8]. Various chemical states in the Al-Ti-C system are described, and the possibility of forming separate regions consisting of elementary metals, intermetallic compounds, and carbides is indicated in [9, 10]. One of the methods for producing intermetallic and coatings based on them, including in the Ti-Al system, is self-propagating high-temperature synthesis (SHS) [11, 12]. The features of structure formation in the Ti-Al system with a low graphite content (4 wt.%) in the SHS-process were studied in [13]. It was found that a thin layer of the TiC carbide phase (~500 nm) is formed on the surface of the graphite particles, followed by the growth of the Ti₂AlC MAX-phase, which has a laminate structure.

We used carbon fibers (Quorum Technologies Ltd.) [14] with a diameter of 10-15 microns. Reaction mixtures of the composition 60.8 wt. % Ti, 34.2 wt. % Al, and 5 wt. % C. The pressed samples with a diameter of 3 mm and a height of 1-2 mm were placed in a BN crucible and placed in a vacuum chamber on a graphite heating table with controlled heating to a temperature of 800 °C. The experiments were carried out in a vacuum. According to the results of the thermodynamic analysis according to the "Thermo" program [15], it can be concluded that as a result of the reaction in the system (Ti+Al+5 wt. % C) depending on the initial temperature. Combustion product consists of the TiAl, Ti, Al, and Ti phases. The

calculated adiabatic combustion temperature is about 1460-1510 °C, which is higher than the combustion temperature in the system (Ti+Al) and lower than in the system (Ti+C) [12, 16]. The calculated adiabatic combustion temperature is about 1460-1510 °C, which is higher than the combustion temperature in the system (Ti+Al) and lower than in the system (Ti+C) [12,16].

During the experiments, after heating in the furnace to a temperature of 690-700 °C, its self-ignition was observed. Combustion reaction proceeded in the thermal explosion mode. The synthesized sample has porosity of up to 45%. The results of X-ray phase analysis showed that the product mainly consists of the TiAl and Ti₃Al phases, and also has a low content of the Ti₃AlC₂ MAX-phase and TiC_x phase. Ti₃Al is formed during the ordering (α -Ti) in the temperature range of 850-1180 °C [17]. The presence of the Ti₃Al, TiAl, and Ti₃AlC₂ phases indicates a significant deviation from the initial stoichiometry of the TiAl intermetallic compound, which is explained by the evaporation of aluminum under high-temperature heating. All carbon fibers are coated with layers of the interaction product in the Ti-Al-C system (Fig. 1).

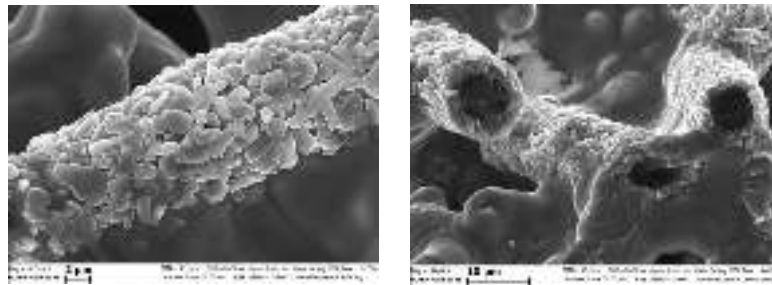


Fig. 1. SEM micrograph of carbon fibers.

As a result of interaction with the Ti-Al melt, a coating (layer) with a thickness of about 2 μ m was formed on the surface of carbon fibers. The coating has a developed relief and consists of disc-shaped plate grains with a size of 1-2 μ m. It is obvious that the formation of the layered structure is the result of wetting and chemical interaction of the Ti-Al melt and carbon fiber. As a result of interaction with the Ti-Al melt, a layer with a thickness of about 2-3 μ m was formed on the surface of carbon fibers. The layer has a developed relief and consists of disc-shaped plate grains with a size of 1-2 μ m. It is obvious that the formation of the layered structure is the result of wetting and chemical interaction of the Ti-Al melt and carbon fiber. The layer formed on the surface of carbon fibers consists of grains close in composition to the Ti₃AlC₂ MAX-phase [18]. Figure 2 shows a fracture surface of a carbon fiber with a layer of the reaction product “Ti-Al melt” – “carbon fiber”. It is clearly seen that a product layer

consisting of Ti_3AlC_2 grains with a multilayer nanolaminate structure has formed on the surface of the carbon fiber (Fig. 2b, c). The micrograph of the fracture in the secondary electrons on the surface of the unreacted graphite fiber shows a bright gray area that completely covers the surface of the graphite fibers and consists of globular grains up to 200 nm in size. This region is similar in composition to the TiC_x (Fig. 2b, c).

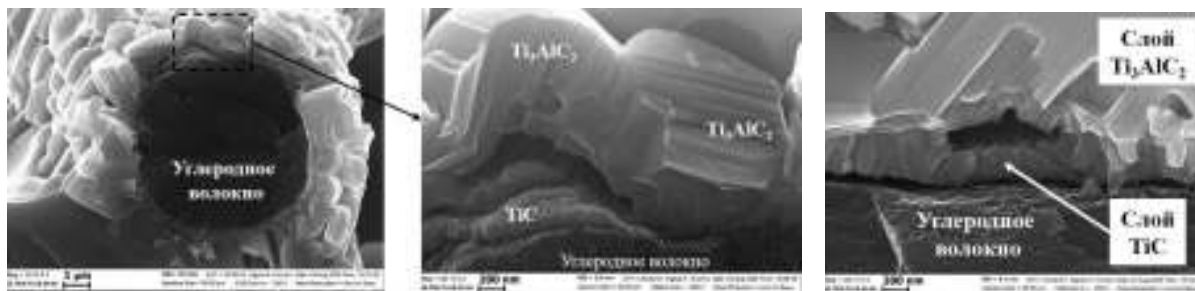


Fig. 2. Micrograph of (a) carbon fibers and (b, c) Ti_3AlC_2 -based coating fragment.

We can assume that ignition of the sample at a temperature of 690-700 °C leads to a sharp increase in temperature to a value not less than the melting point of the TiAl intermetallic compound (1460 °C). The Ti-Al melt intensively spreads over the carbon fibers, as evidenced by the above photos of the microstructure. The interaction of Ti-Al with carbon leads to the formation of TiC carbide and Ti_2AlC , Ti_3AlC , and Ti_3AlC_2 ternary phases, while the reactions begin to occur in the solid phase at a temperature of about 1420 °C [19]. The formation of Al_4C_3 carbide does not occur due to its metastability. Dissolution of carbon into the Ti-Al melt leads to the formation of TiC_x and laminate grains of the Ti_3AlC_2 phase, in the form of a coating on carbon fibers. The thickness of the Ti_3AlC_2 coating on carbon fibers is about 2 μm , which is due to the limited interaction time due to the rapid cooling of the sample.

The results of the study show that a thin layer of the carbide phase (~ 200 nm) is formed on the surface of carbon fibers, consisting of TiC_x globular grains, covered with a layer of nanolaminate grains of the Ti_3AlC_2 MAX-phase up to 2 μm in size. The of Ti_3AlC_2 -layer is formed as a result of the diffusion of carbon from TiC_x into the Ti-Al melt, which is formed as a result of the SHS-reaction between Ti and Al.

REFERENCES

1. Naidich Yu.V., in Progress in Surface and Membrane Science, Vol. 14, edited by Danielli J. F., London, Academic Press, 1981, P.353.
2. Найдич Ю.В., Колесниченко Г.А. Взаимодействие металлических расплавов с поверхностью алмаза и графита. Киев, Наукова думка, 1967, 89 С.
3. Suryanarayana C. Prog. Mater. Sci. 2001. V. 46. P.1-184.
4. Pérez-Bustamante R., González-Ibarra M.J., González-Cantú J., et al. J. Alloys Compd. 2012. V. 536. № S17-S20. P.17–20.
5. Poirier D., Gauvin R., Drew R.A.L. Composites Part A. 2009. V. 40. № 9. P.1482-1489.
6. Kallip K., Leparoux M., AlOgab Kh.A., et al. J. Alloys Compd. 2015. № 646. P.710-718.
7. Liu Z.Y., Xu S.J., Xiao B.L., et al. Composites Part A. 2012. V. 43. Issue 12. P.2161-2168.
8. Fleischer R.L. Dimiduk D.M., Lipsitt H.A. Annu. Rev. Mater. Sci. 1989. V. 19. P.231-263.
9. Seal S., Barr T., Sobczak N., Kerber S. J. Mater. Sci. 1998. № 33. P.4147-4158.
10. Witusiewicz V.T., Hallstedt B., Bondar A.A., et al. J. Alloys Compd. 2015. № 623. P.480-496.
11. Мержанов А.Г., Юхвид В.И., Боровинская И.П. ДАН СССР. 1980. Т.255. №1. С.120-124.
12. Итин В.И., Найбороденко Ю.С. Высокотемпературный синтез интерметаллических соединений. Томск. Изд. Томского Университета. 1989. 210 С.
13. Sychev A.E., Busurina M.L., Sachkova N.V., et al. Inorg. Mater. 2019. V.55. №8. P.780-784.
14. https://www.quorumtech.com/_assets_/ProductMultiCats/00013/Carbon.pdf
15. <http://www.ism.ac.ru/thermo/>
16. Merzhanov A.G. Self-propagating High-temperature Synthesis: Twenty Years of Search and Findings. In: Combustion and Plasma Synthesis of High-Temperature Materials. Eds. Munir Z.A., Holt J.B. N.Y., etc.: VCH Publ. 1990. P. 1-53.
17. Лякишев Н.П. Диаграммы состояния двойных металлических систем: Справочник в 3 т. // Москва. Машиностроение. 1996. Т. 1. 992 С.
18. Naguib M., Kurtoglu M., Presser V., et al. Adv. Mater. 2011. V. 23. Issue 37. P. 4248-4253.
19. Найдич Ю.В., Колесниченко Г.А., Лавриненко И.А., и др. Пайка и металлизация сверхтвердых инструментальных материалов. Киев. Наукова думка. 1977. 188 С.

THE IMPROVEMENT OF Ti/Al/Ni/Au OHMIC CONTACTS TO UNDOPPED AlGaN/GaN HEMT HETEROSTRUCTURES BY PULSE-PHOTON TREATMENT

T.Sakharova*¹, M.Heuken², Z.Jibuti¹, L.Sanikidze¹, M.Ksaverieva¹

¹ LEPL Institute of Micro- and Nanoelectronics, 13 Chavchavadze Ave., 0179, Tbilisi, Georgia

² AIXTRON SE, 52134 Herzogenrath, Germany

* tansakharova@gmail.com

The wide band gap semiconductors, such as gallium nitride (GaN), have attracted increasing attention of developers as a promising microelectronics material [1]. AlGaN/GaN high-electron mobility transistor (HEMT) is a challenging candidate for the power switching electronics, due to the high values of breakdown voltage, the ability to obtain high values of drain current and the high operating temperature. One of the critical points in HEMT fabrication technology is to obtain low-resistance ohmic contacts (OhC) with minimum spread of resistance values over the wafer. Furthermore, these contacts must have high thermal stability, smooth surface morphology for the unimpeded execution of subsequent technological processes, where precise alignment of layers is required as well as a sharp edge of ohmic metallization, especially in devices with a short channel.

To date, metallization based on the Ti/Al composition, such as Ti/Al/N/Au, Ti/Al/Mo/Au, is most widely used as ohmic contacts for AlGaN/GaN HEMT [2-5]. However, this metallization often demonstrates a very rough surface morphology as well as significant size deviation in the lateral plane of the contact. Spreading in the lateral plane can lead to a source-gate short circuit, especially in short-channel devices. A large number of studies are devoted to formation of optimal OhC for devices based on AlGaN/GaN. One of the areas of technology improvement is the correlation between the composition of the metallization layers and electrophysical parameters [2] of the contact, while other groups of researchers [5] focus on varying the annealing processes. Nevertheless, in the available literature there is very little information on the effect of changes in the metallization composition and the influence of high-temperature annealing on the quality of the surface morphology of OhC.

In this work, we consider a new method for optimizing OhC based on Ti/Al/Ni/Au for GaN/AlGaN HEMT. The method consists in low-temperature photon-stimulated treatment [6]. Contact resistance and surface morphology are studied depending on the annealing modes, and a comparison of the results with OhC obtained by standard high-temperature

annealing is also made. OhC were studied on the wide-band undoped AlGaN/GaN heterostructure. AlGaN/GaN was grown on Si substrates in the AIXTRON Planetary MOCVD Reactor® [7]. From top to bottom, the heterostructure consists of an 3nm GaN caplayer, 20nm Al_{0.22}Ga_{0.78}N barrier, 1nm AlN spacer, 3μm GaN active layer, 950nm AlGaN / AlN transition/nucleation layer, and 675μm thick p-Si (111) substrate. The contact resistance was investigated by the Transmission Line Method (TLM). The surface morphology was characterized using optical microscope and AlphaStep200 profilometer. Pulse-photon treatment was carried out on the genuine system PPI-1. The source of radiation in this setup is a set of halogen lamps KG 1000x220, providing uniform irradiation of the area of 100cm². The power density can be changed up to 190 W·cm⁻², and the pulse duration - from 0.1 to 1000 sec in increments of 0.1 sec. OhCs were formed by electron-beam deposition on the TEMESCAL-FC-1800 setup.

Two sets of samples were prepared to compare the physical characteristics and morphology of the formed OhC: with standard high-temperature annealing (annealing time of 30 sec) and with low-temperature photon-stimulated annealing (pulse duration 0.1 sec). The OhC composition, annealing regimes as well as the obtained characteristics are presented in table 1.

Table 1.

Ti/Al/Ni/Au metallization composition(Å)	High-temperature annealing mode (°C)	Photon-stimulated annealing regime		Contact resistance Ω·mm	Surface roughness (Å)
		Pulse number	Tmax, °C		
150/1500/400/700	830	-	-	0,75	10573
150/1500/400/700	870	-	-	0,45	1578
200/1500/720/400	830	-	-	0,35	965
200/1500/720/400	870	-	-	0,15	1255
150/1500/400/700	-	3	756	12	198
150/1500/400/700	-	5	768	10	205
150/1500/400/700	-	7	800	4	230
200/1500/720/400	-	3	756	10	180
200/1500/720/400	-	5	768	6	185
200/1500/720/400	-	7	800	1,2	204

Figure 1 shows the OhC images (magnification x1500). They clearly show that the surface of the optimized contact structure has a smoother relief with an even boundary of the contact edge compared to a structure with standard high-temperature annealing.

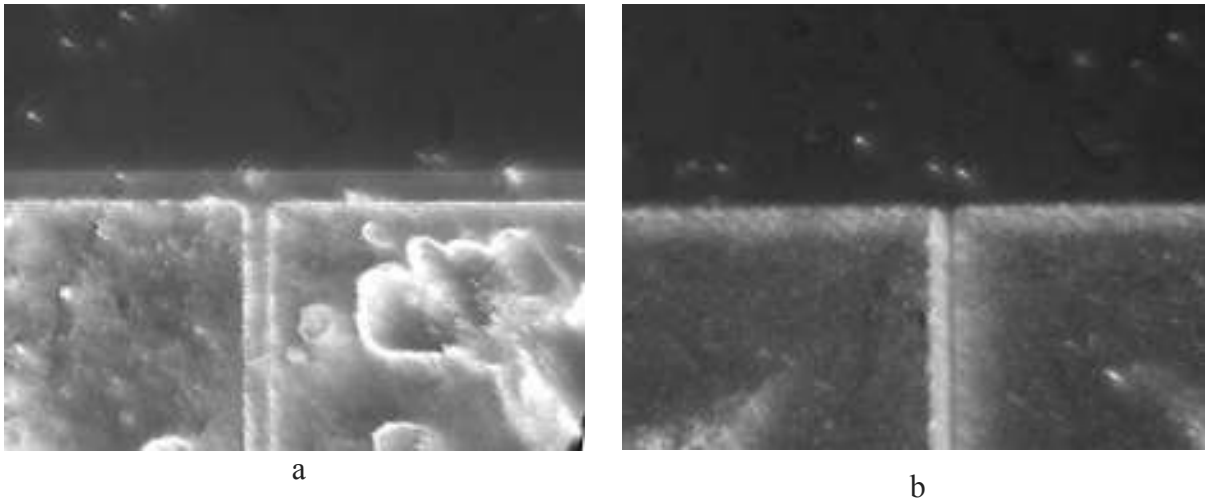


Fig.1. OhC surface microphotography: a – high-temperature annealing; b – pulse-photon treatment.

Fig. 2 shows the surface roughness profile of OhC obtained using an AlphaStep200 profilometer.

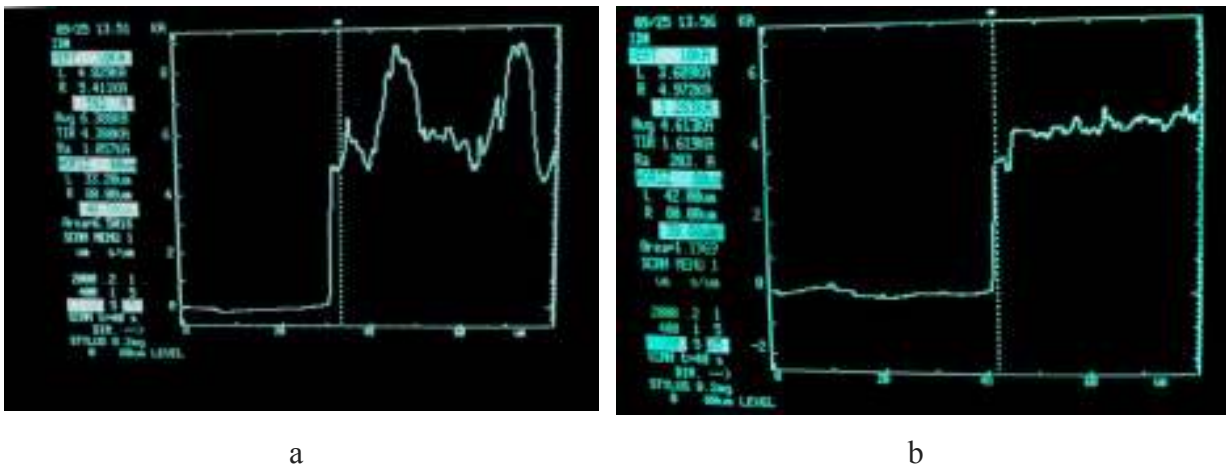


Fig.2. Surface roughness after: a – high temperature annealing; b – pulse-photon treatment.

It is quite obvious that the low-temperature photon-stimulated annealing leads to a significant reduction in roughness, but most importantly, there is no tendency to spreading of the OhC edges.

However, as can be seen from the table, the contact resistance obtained by photostimulated annealing exceeds at least several times that observed at standard high-temperature annealing. Nevertheless, the obtained values for contact resistance are quite acceptable for the fabrication technology of HEMT.

The mechanism of the formation of OhCs to wide band gap III-nitrides has not been fully studied. There are several models that explain the OhC formation by Ti/Al metallization. It is

known that at high-temperature annealing, TiN formation is necessary both at the boundary and in the depth of gallium nitride to form high-density donors. The Ti/Al alloy, also leads to the appearance of spikes that reach the layer with two-dimensional electron gas at the AlGaIn/GaN interface. However, at the short-time pulsed treatment, the spikes cannot reach the boundary of the AlGaIn/GaN heterojunction, which leads to an increase in the contact resistance. This problem requires further investigation.

Thus, the possibility of low-temperature photo-stimulated formation of OhCs to undoped AlGaIn/GaN heterostructures with a qualitatively improved contact surface morphology, with a clear metallization edge without spreading in the lateral region, and also with electrical parameters comparable to those obtained by standard high-temperature annealing is shown.

REFERENCES

1. Ahmed M. Nahhas, *American Journal of Nanomaterials*, Vol. 6, No. 1, 2018 , pp. 1-14
2. H.P.Xin, S.Poust, W.Sutton, D.Li, D.Lam, I.Smorchkova,R.Sandhu, B.Heying, J.Uyeda, M.Barsky, M.Wojtowicz,R.Lai, *Proceedings of CS MANTECH Conference*, May, 2010, Portland, Oregon, USA, pp.149-153
3. G.Hellings, J.John, A.Lorenz, P.Maliniwski, R.Mertens, *IEEE Transactions on Electron Devices*, vol.56,no.11, 2009, pp.2833-2839
4. A.Wiatrowski, B.Boratynski, *Opto-Electronics Review* 12(1), 2004, pp.165-168
5. Q.Feng, L.M.Li, Y.Hao, J.Y.Ni, J.C.Zhang, *Solid-State Electronics* 53,2009, pp.995-958
6. Dolidze N.D., Goderdzishvili G.I., Jibuti Z.V.and Eristavi G.L. , *Georgian Engineering News*, N1, 2000, pp. 35-37
7. L. Heuken, M. Alshahed, A. Ottaviani, M. Alomari, D. Fahle, M. Heuken, and J. N. Burghartz, *Japanese Journal of Applied Physics* 58, 2019, SCCD11

DESIGN OF VACUUM FURNACE WITH PRESSING CAPACITY FOR POLYMER COMPOSITE MATERIALS

R. Sakhvadze*^{1,2}, G. Abashidze¹, D. Tsverava¹, L. Kirtadze¹

¹ LEPL. G. Tsulukidze Mining institute, 7, E. Mindeli Str., Tbilisi 0186, Georgia

² Georgian Technical University, 77, Kostava Str., Tbilisi 0160, Georgia

* tmi@mining.org.ge.

Nowadays, fiber-reinforced polymer composites (FRC) and partially or large particle reinforced composites (PRC) have a growing potential for multifunctional applications. New materials can be designed with the variation of polymers and the reinforcing components to meet the requirements of working in hard conditions. An important factor in establishing a widespread use of new materials as a competitive product is the simplicity and cost of their production technology. Therefore, in parallel with the scientific research carried out on this class of materials, efforts are underway to develop industrial technologies and design the necessary equipment for their production. Currently, for the developing of polymer composites reinforced by inorganic fillers and fibers, devices with the possibility of thermal activation of the reaction mixtures followed by compaction on static pressing are used. The final product of the process is the hard polymer composite. The advantage of devices is the possibility to obtain a good index of density and strength under the influence of the compressive force. Despite the fact that this sort of devices and technology has wide application, there are still some disadvantages. In particular, one of those disadvantages is that during the heating process air bubbles are formed. If the process is carried out under atmospheric pressure and average load intensity, temperature and compressive force do not allow the liquid phases to release the air particles. Therefore, the obtained products have high porosity and reduced mechanical properties. To avoid air bubbles, it's highly recommended to perform above mentioned thermomechanical processes in a vacuum. There are numerous methods for removing gases from liquids. One of those methods are placing a solution under reduced atmospheric pressure. It makes the dissolved gas less soluble. This technique is often referred as vacuum degasification. Specialized vacuum chambers are used to degas materials through pressure reduction. Low-density particles are discharged to the surface of the liquid, in a vacuum environment, and are ejected from the mass because of the pressure gradient. High-temperature vacuum presses are used for this purpose. Modern high temperature, vacuum presses, which are widely used to create ceramic and metal-ceramic composite materials, are expensive

because they operate in high vacuum (10^{-1} - 10^{-7} Pa) and temperature modes (2500-3000 °C). Due to the technical characteristics of above-mentioned press-installations (the size of the vacuum chamber, as well as geometric dimensions) the sizes, as well as shape of obtained samples are very limited. Therefore, the use of this equipment to fabricate industrially applicable polymer composites is not beneficial in terms of both technical (size and shape) and economical (high price) aspects. Based on the above analysis, it is expedient to create an acceptable and semi-universal high temperature vacuum press for polymer composites. The purpose of this study is therefore to develop a methodology for designing of vacuum presses operating at medium temperatures and to determine the basic design parameters for its construction.

The basic technical requirements for the new equipment in this study, can be formulated as follow: Vacuum: (10^{-3} - 10^{-6})Pa; Working temperature range: (20-400) °C; Load intensity: 400kN. New device could be able: To produce particle reinforced polymeric composite with high physical and mechanical properties.

The machine will be required to provide the following steps of processing:

1. Melting the polymer through the temperature in the reservoir;
2. Removal of dissolved gases from molten substance, using a vacuum pump;
3. Management of the vacuum cycle for fiber injection molding;
4. Adjustment of the drying process in the chamber using temperature;
5. To apply force on the fused substance.

New device will be composite from: vacuum pump with capacity of 10^{-1} – 10^{-5} Pa; Tubes and valves for vacuum cycle management; Hydraulic press with capacity up to 40 tons; Heating elements (fig. 1).

For the processing of particular reaction mixtures in the new equipment, it is necessary to determine key parameters based on the published methodologies [1, 2, 3]: vacuum quality, temperature, and compressive force at the different stages of the technology, independently or in combination with each other.

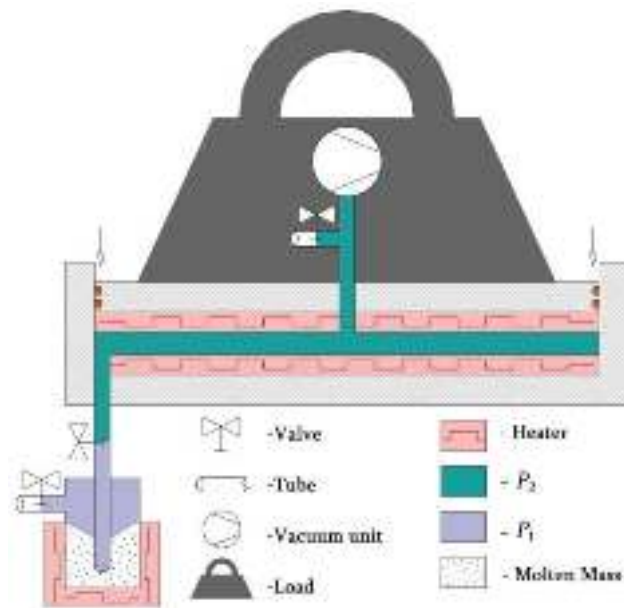


Fig. 1. Scheme of new design vacuum press equipment

Within the investigation is developed the new methodology for designing new equipment/machine, which enables to obtain sheet composited with the dimensions 500X500 mm and thickness between 4 to 30 mm. The machine is capable of processing both organic and inorganic polymer raw materials (Geopolymer). The realization and reaching the proper technical requirements, composite materials obtained by proposed methodology, can be used for the creation of composites of different function.

REFERENCES

1. Polymer physics, Michael Rubinstein, OUP Oxford, 2003;
2. Crystallization of Polymers Investigated by Temperature-Modulated DSC, Maria Cristina Righetti, MDPI AG, 2017;
3. Dynamics of Surface Crystallization and Melting in Polyethylene and Poly(ethylene oxide) Studied by Temperature-Modulated DSC and Heat Wave Spectroscopy, T. Albrecht S. Armbruster S. Keller G. Strobl, American Chemical Society, 2001.

INVESTIGATION OF TRIBOLOGICAL PROPERTIES OF WEAR-RESISTANT SURFACES WELDED BY POWDERY WIRE

J.Sharashenidze*¹, D.Gventsadze², S.Mebonia², G.Dadianidze¹, K.Papava¹

¹F.Tavadze Institute of metallurgy and materials, 0186, Mindeli, 8b, Tbilisi, Georgia

²R.Dvali Institute of Machine Mechanics, 0186, Mindeli,10, Tbilisi, Georgia

jemalsha@mail.ru

ABSTRACT. The most perspective method for hardening and recovery of the metallic surfaces is a process of welding (arc deposition), which ensures a solution to the very important task: optimal relation between the properties of surface and the bulk of a metallic material. In the presented work the hard and wear-resistant surfaces were obtained using a powdery wire and chrome carbide during the electric-arc welding. Tribological properties of these surfaces were studied in the conditions of 0.5 - 2,0MPa loading and 0.63 m/s speed during boundary friction using the 15W40 oil. It was established that under the same conditions the values of the sample's friction coefficients are smaller by the order of magnitude than those of non-welded 40X steel friction pairs. Wear of the welded samples is insignificant as well. In comparison to the one-layer surface, two-layer welded one has a less friction coefficient, and at biggest loading, wear was not detected at all.

KEY WORDS: wire with powdery core, welding, friction coefficient

INTRODUCTION

It is well known that during exploitation a lot of machines and their parts fail because of wear, impact loading, corrosion, etc. Modern technology gives a possibility of recovering and hardening the surfaces of critical parts. Practically, the failure process begins with damaging their surfaces. This requires the hardening of their surfaces and the recovery of their dimensions.

A most promising method for surface hardening and recovery is the welding process (method), which ensures the solution to a significant task - optimal relation between the metal's surface and bulk properties. In this case, it is not necessary to use the volume alloyed materials, and the cardinal task of machinery - increasing of reliability and durability of machines in their service conditions [1,2].

The aim of the presented work is to obtain wear resistant welds by the electric arc method using the wire with the powdery core and study the tribological properties of the produced surfaces.

THE MAIN PART

A wire with the powdery core, belted by 08KP type steel tape with sizes 12 x 0.5 mm filled with the chromium carbide Cr_3C_2 with the following content: 8.36 C; 1,0 Si; 0.3 Fe; 0.1 Mn; 0.01Cu; 0.005Mg. Preparation of the wire with the powdery core included the following operations: preparing of tape and smelter charge, formation of the profile and backfill of the smelter charge to it, wiredrawing and control of quality.

Surfacing of the above wire was realized with the use of wolfram- lanthanum alloy electrode with direct polarity by the installation of type TIG/MMA 320 and BDU-506 at 120-140 A. Welding was performed on the pipe-type samples with the dimensions: $\phi 28 \times \phi 20 \times 20$ mm.

Investigations of tribological properties were conducted on the laboratory friction machine of type IM-58 in the following regime:

1. The friction speed was constant (0.63 m/s, which corresponds to 500 turnover).
2. The friction was performed with the contact torsion surfaces (3 cm^2).
3. The loading of the samples 0,5: 0,7; 1,0; 1,5; 2,0 MPa. Duration of the test, 2 h.
4. The counterbody was a hardened steel.
5. For the aim of comparison the friction tests between two hardened steel of type 40X were conducted in the same conditions.
6. Based on the test results, temperature on the friction surfaces, friction coefficient and the sample weight were determined. The obtained results are presented in Table 1.

Table 1

#	Loading, MPa	0.5	0.7	1,0	1,5	2,0
The samples without surfacing						
1	Temperature	38	45	55	65	90
2	Friction coefficient	0.053	0.050	0.056	0.061	0.080
3	wear	5.0	4.0	3.0	4.0	6.0
One layer surfacing						
1	Temperature	28	35	36	35	80
2	Friction coefficient	0.0175	0.0047	0.008	0.0080	0.0610
3	wear	1.0	-	1.0	-	5.0
Two layer surfacing						
1	Temperature	28	28	18	32	48
2	Friction coefficient	0.0130	0.0170	0.0080	0.0062	0.0080
3	wear	5,0	4.0	-	-	-

In Table 1 one can see that the values of friction coefficients of the welded samples are by the order of magnitude smaller than those of the non welded 40X steel samples, measured in the same conditions. In addition, the wear rates of the surfaced samples are also very low. In comparison to the one-layer sample, two-layer one has a lower friction coefficient. At the end of loading, the wear is not detected at all, and the temperature of friction surfaces is no more than 48°C, while the loading temperature for the non-surfaced samples is about 90°C. The curves presented on Fig.1 show the advantage of the surfacing by carbide chromium samples in comparison with the samples without surfacing.

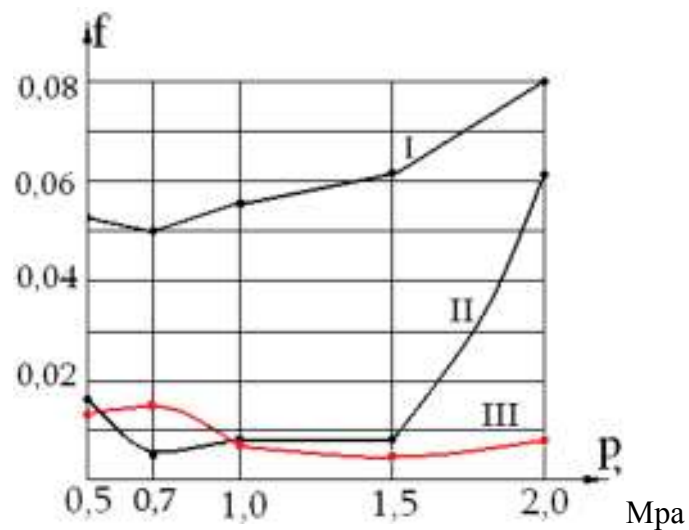


Fig.1. The dependence of friction coefficient on the loading for non-loading steel 40X (I), one layer surfacing (II) and two layer surfacing (III)

In our opinion, the advantages, which were manifested during the study of tribological properties of the surfaced materials (low friction coefficient, low wear), may be explained by the effect of different factors. First of them is that the microhardness of the surfaced samples is higher because of the formed carbide structures (for one-layer sample it corresponds to 12060 MPa, and for the two-layer - 13500 MPa). However, they do not differ one from another by usual hardness. The microstructure of the two-layer surface is more homogeneous and has a higher microhardness in comparison to the monolayer surfaces. These circumstances favor the creation of better-operating conditions for friction.

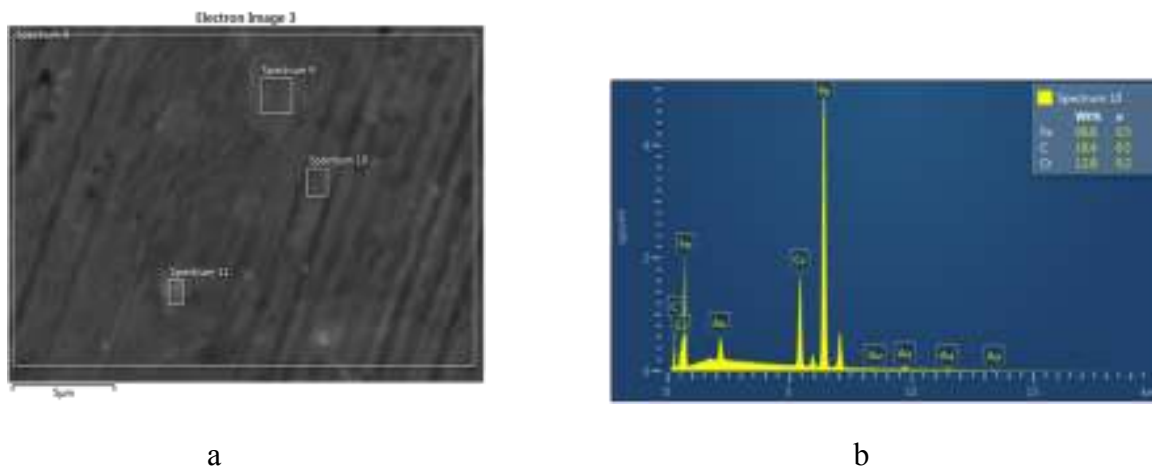


Fig.2. SEM image (a) and the respective EDX spectra (b) of a single-layer surfacing sample.

The spectral analysis shows, that the hardening phases of welding formed by wear are: chromium carbide Cr_3C_2 and iron carbide Fe_3C (Fig.2).

It may be concluded that one of the promising methods for hardening metal surfaces is the electric arc surfacing of wire with a powdery core and chromium carbide, which ultimately results in an increase in stiffness and a decrease of the coefficient of friction and wear resistance.

REFERENCES:

1. Khrushchov M.M., Babichev M.A., Berkovich E.S., Kozirev S.P., Kraposhina L.B., Pruzhanskii L.Yu. Wear resistance and structure of hard surfacing. Monograph. Mashinostroenie, 1971. -96 p.
2. V.E.Gromov, E.V.Kapralov, S.V.Raikov, Yu.F. Ivanov. Structure and properties of wear-resistant coatings deposited by flux-cored electric arc method on steel. Uspekhi Fiziki metallov, 2014, V.15, pp. 213-234.

PRODUCTION OF SUPER LARGE TUNGSTEN SINGLE CRYSTALS

V. Shapovalov*¹, O. Berdnikova¹, Yu. Nikitenko¹, V. Yakusha¹, O. Gnizdylo¹

¹ E. O. Paton Electric Welding Institute of the NAS of Ukraine, Kazimir Malevich Str., 03650, Kyiv, Ukraine

* shapovalov@paton.kiev.ua

Tungsten is characterized by extremely high and stable mechanical and physical properties over a wide range of temperatures. In the single crystal state, it exhibits anisotropy of properties that significantly increase the performance properties of tungsten products, taking into account the orientation of the structure in the individual elements.

Traditionally, tungsten single crystals are grown as rods with a diameter of 25-30 mm. Increasing the linear size of single crystals presents two problems: the retention of a large liquid volume metal and high thermo-mechanical stresses in the body of a single crystal. Temperature gradients create thermal stresses in the crystal that in critical cases can destroy the crystal [1]. High thermo-mechanical stresses contribute to the generation of an additional number of dislocations (the dislocation density can reach $10^7 - 10^8 \text{ cm}^{-2}$) and significant disorientation of the sub-grains, which significantly degrades the quality of the structure of single crystals.

The idea of simultaneous use of two different in nature and energy concentration of electric heating sources - plasma and induction was first proposed by specialists of the Institute of Electric Welding, EO Paton NAS of Ukraine (Fig. 1) [2].

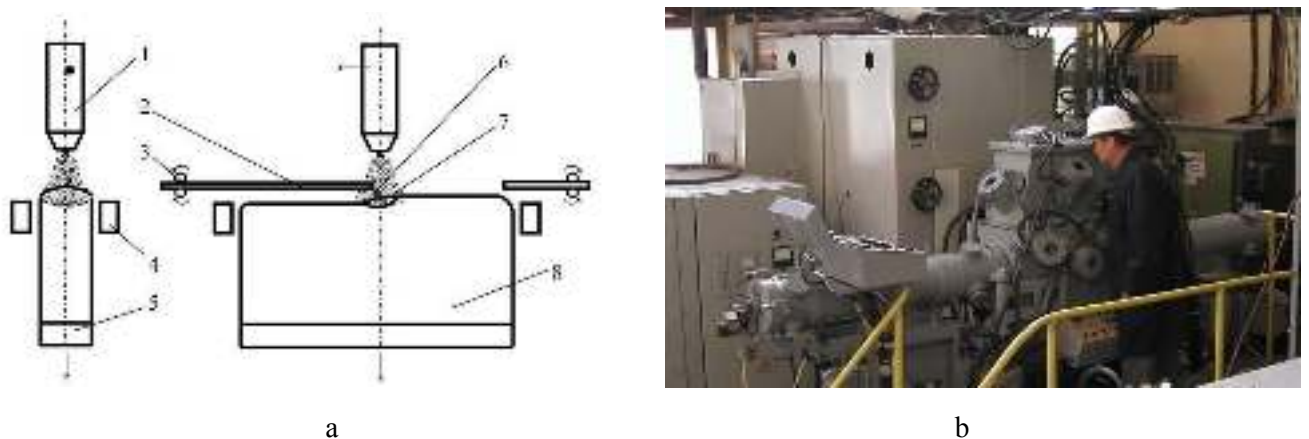


Fig. 1. Scheme of installation (a) and the equipment (b) for the additive growing of single crystals of refractory metals using the plasma-induction method: 1 - plasmatron; 2 - remelted rod; 3 - the mechanism of feeding rods; 4 - inductor; 5 - seed crystal; 6 - plasma arc; 7 - local bath melt ; 8 - single crystal

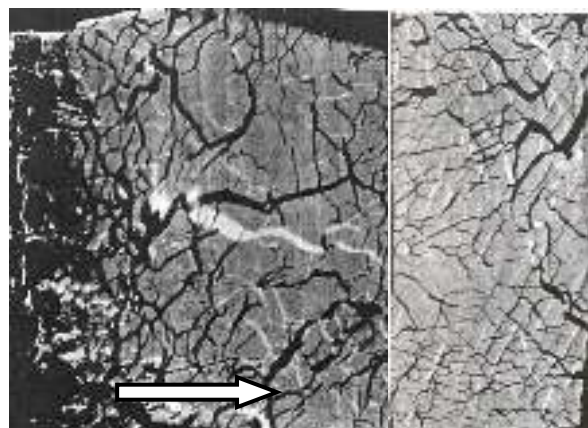
The additional heating of the crystal significantly reduces the radial and axial temperature gradients, which helps to reduce the density of dislocations and internal stresses and helps to form a more perfect structure.

The essence of the method is that the plasmatron, in the reciprocating motion, moves a metal bath, which, receiving the metal from the melting rods, forms a crystal layer by layer, reminiscent of the nature of the arc surfacing. After each passage of the plasmatron, the single crystal goes down to the height of the deposited layer, thus providing stable conditions for the growing process.

Using this method, equipment and technology for growing profiled single crystals in the form of plates were created (Fig. 2).



Fig. 2 Appearance of flat tungsten single crystals 170x160x20 mm



growth direction

a

b

Fig. 3. X-ray topograms by the Berg-Barrett method: longitudinal (a) and transverse (b)

The crystal is formed under conditions of heating by the high-frequency field of the inductor to the temperatures characteristic of the hot deformation range. It is known that at these temperatures the movement of dislocations occurs under the action of both external stresses and temperature. Dislocations are not rigidly tied to "their" slip plane and can move from one plane to another, choosing the easiest path. This is seen as an additional degree of freedom of dislocations. With such unregulated movement of dislocations, the probability of their meetings increases, and therefore, on the one hand, the number of cases of their annihilation increases (the density of dislocations decreases), and on the other - the tendency to form regular dislocation structures, characterized by the unification of dislocations within low-

angle boundaries. The conditions under which the formation of the single crystal occurs provide a higher quality of the single crystal structure than in the ways in which no additional heating (electron beam and plasma arc) is used.

Crystals grown using the above method have a less smooth lateral surface, but this does not prevent their use without additional machining as billets for widescreen rolling.

Interesting are the results of the study of the structure of crystals using optical and x-ray methods. In Fig. 3 shows the results of the X-ray study of single crystals.

Comparative studies have shown that the structure of such crystals is more perfect than plasma-arc, and there is practically no macromosaic.

The developed additive technology for the cultivation of large single crystals of refractory metals of technical purity is based on long-lasting thorough researches that allowed to establish and study:

- distribution of thermal fields of single crystals using mathematical models and experimental data [3];
- working ranges of changing technological parameters of the crystal growth process;



Fig. 4 The newest equipment with computer-controlled unit (a) for the production of single crystals of refractory metals of rotation bodies (b)

- structural characteristics and patterns of structure formation of grown single crystals [4].

Further study of the process allowed to create on the same basis the newest installation for growing super-large single crystals of tungsten in the form of bodies of rotation (Fig. 4), where the arrows indicate the rod movement direction into the melting zone of the plasma arc and the direction of rotation of the single crystal.

The equipment created is a qualitatively new generation of equipment, featuring a fully computerized control system for actuators, motion sensors and single crystal growth control. The design provides for the possibility of growing single crystals in the form of rotation bodies (cylinder or hollow cylinder) with an outer diameter of up to 100 mm (4 inches). Now a thermal module has been created and the technology of growing tungsten single crystals diameter 85 mm is being developed (Fig. 5).



Fig. 5 The appearance of a tungsten crystal with a diameter of 85 mm

Fundamentally the technology of growing cylindrical single crystals is based on the technology of growing flat single crystals, but in the new installation, the crystal is continuously rotated around the vertical axis. The crystal seed used is a cylindrical workpiece made of a flat single crystal of predetermined orientation.

Single crystals of refractory metals (tungsten, molybdenum) can find an alternative application, both in the form of wide-format rolled metal (sheets, thermal screens), and in the form of articles made of ingots. The most promising applications may be: X-ray technology (electrodes), electronics (sputtering targets, crucibles), electrical engineering (contacts), laser technology (mirrors for optical and X-ray lasers), nuclear power (thermionic power converters of space power plants, parts of structures reactors), aerospace engineering (nozzles).

REFERENCES

1. G. Marinelli, F. Martinaa, S. Gangulya, S. Williams. Development of Wire + Arc Additive Manufacturing for the production of large-scale unalloyed tungsten components // International Journal of Refractory Metals and Hard Materials, Volume 82, August 2019, Pages 329-335.
2. V.A. Shapovalov, V.V. Yakusha, A.N. Gnizdylo and Yu.A. Nikitenko. Application of additive technologies for growing large profiled single crystals of tungsten and molybdenum // The Paton Welding Journal № 5-6, 2016 p.134-136.
3. V.A. Shapovalov, V.V. Yakusha, Yu.A. Nikitenko, V.V. Dolinenko, A.N. Gnizdylo, V.V. Zholud. Studying the temperature field of profiled tungsten single-crystals produced by plasma-induction process // Advances in Electrometallurgy, Translated from Sovremennaya Elektrometallurgiya 2014, №3. pp. 31–35.
4. G.M. Grigorenko, L.I. Markashova, E.N. Berdnikova, V.A. Shapovalov, E.V. Polovetskii, V.V. Yakusha, Yu.A. Nikitenko and A.N. Gnizdylo. Structure and properties of profiled tungsten single-crystals produced by method of plasma-induction growing // 6-th International Samsonov conference “Materials science of refractory compounds”. May 22-24, 2018. Kyiv, Ukraine. P.34.

THE APPLICATION OF ADDITIVE TECHNOLOGIES TO CONTROL THE PROCESS OF SEGREGATION IN THE PRODUCTION OF INGOTS AND CASTING

V. Shapovalov*, С. Shapovalov, R. Kachan, T. Skuba, O. Berdnikova

E. O. Paton Electric Welding Institute of the NAS of Ukraine, Kazimir Malevich Str., 03650, Kyiv, Ukraine

* shapovalov@paton.kiev.ua

KEYWORDS: segregation, large ingot, local crystallization time, crystallization rate, local metal bath, processes of special electrometallurgy.

INTRODUCTION

In connection with the increase in the size of products for traditional and nuclear energy, heavy and petrochemical engineering, as well as the military-industrial complex, the demand for large and extra-large high-quality ingots and forging blanks is growing. The mass of ingots can reach several tens and hundreds of tons [1]. The quality of the ingots is determined by the number of shrinkage and segregation defects associated with a specific production method. With an increase in the size of ingots, the degree of alloying significantly deteriorates their quality. The axial porosity and volume of the shrinkage cavity shell increase. This significantly affects the homogeneity and uniform distribution of properties over the cross section of the ingot [2-3]. To ensure the corresponding properties and especially homogeneity structure over the entire cross section of the ingot, only part of the ingot is used, which reduces the yield. Therefore, increasing the chemical and physical homogeneity of ingots and castings is of priority importance.

The main reasons that must be overcome to improve the quality of cast metal are two: metal contamination by non-metallic inclusions and crystallization processes. The first reason metallurgists managed to overcome through the use of after-furnace treatment. They are still trying to overcome another reason related to crystallization phenomena. To do this, apply: vibration; ultrasound; electromagnetic effect, regulation of the temperature of the liquid metal, regulation of the thermal field on the surface of the bath, the introduction of refrigerators and the like. But significant achievements, especially in field the crystallization of large ingots, are not yet available. The main reason is the uncontrolled crystallization rate.

During crystallization of metals, a first-order phase transition occurs. It is inherent in such a phenomenon as segregation. segregation during crystallization of metals and alloys is

associated with different solubilities of elements in solid and liquid phases [4]. The ratio of element

concentrations in phases is determined by the distribution coefficient in the equilibrium stage [4]. Deviation from equilibrium leads to a change in the coefficient. In real conditions, it is necessary to talk about the effective coefficient of the distribution of elements in the solidification of metal [5], which can be calculated by the formula:

$$K = \frac{K_0}{K_0 + (1 - K_0)e^{-f\delta/D}}$$

where: f - is the crystallization rate, cm / s; δ - is the thickness of the diffusion layer adjacent to the crystallization front and enriched with impurities, cm; D - is the diffusion coefficient of the impurity, cm² / s.

PURPOSE OF THE STUDY

Development of a method for suppressing segregation, regardless of the size of ingots and cast products. To achieve the goal, we proposed to change the way the ingot is formed, replacing a large metal bath with a local one that moves at high speed. In this case, an additional outflow of heat from the end surface not covered by the bath appears, Fig. 1a. It becomes possible to set the crystallization rate, respectively suppress segregation and control the structure of the ingot.

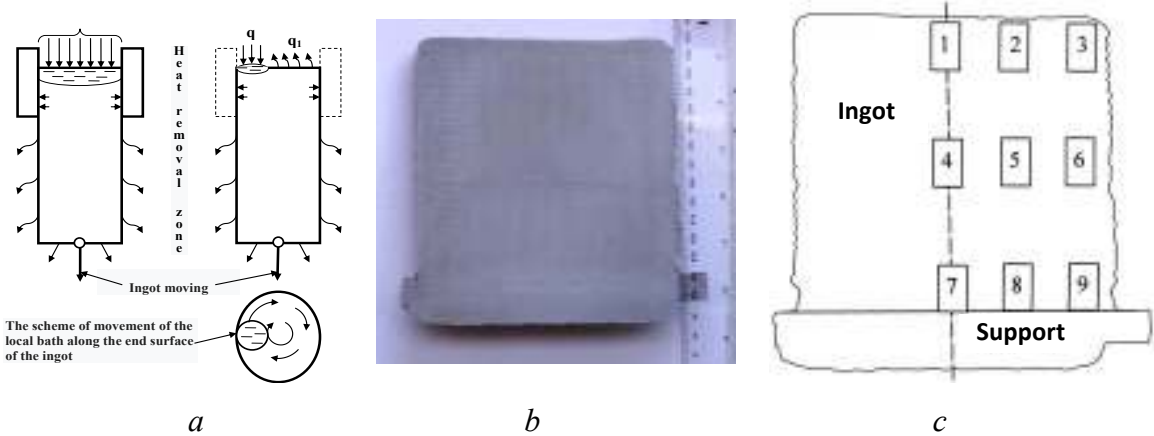


Fig. 1. Heat distribution when production ingots by different technologies (a), macro section of the ingot (b) and sampling scheme (c).

EXPERIMENT CONDITIONS

An ingot was smelted to verify the proposed approach under laboratory conditions. A local bath was formed using an arc heating source and moved at a speed of 3 mm/s. The arc current was 150 A, and the arc voltage was 19.4 V. Welding wire with a diameter of 1.2 mm 09G2S was used as a consumable.

THE DISCUSSION OF THE RESULTS

A macro section of the vertical section of the ingot and a metal selection map for research are presented in Fig. 1b, c. As follows from the figure, the macrostructure of the ingot is homogeneous and fine-grained. Further investigation of the microstructure of the samples taken at points 1–9 showed that grains in size correspond to 8–9 numbers, Fig. 2. The above results show that the creation of stable conditions for the formation of the ingot eliminates the scale factor and extends the results to almost any size ingots. The obtained large ingots can be used without removing the head and bottom parts. At the same time, the weight of especially large ingots can be reduced with the same loads on the products that will be made from these ingots, due to the equality to the unit coefficient, which takes into account the scale factor, and an increase in strength due to both the absence of zonal segregation and a decrease in the level of dendritic segregation. Other products, such as a bowl, were produced using a local bath. The main problem that was solved when forming the bowl was the formation of thin-walled products.

Measurements were made of the mechanical characteristics of the products. As measurements showed strength, toughness and other mechanical characteristics increased by 10-50% compared with the characteristics of the same grade of metal obtained by traditional technology, table 1.

This is especially important for products from highly alloyed alloys operating in extreme conditions. The proposed approach is a way to obtain large ingots with properties and structure that cannot be obtained using traditional technology. Further testing of products from such ingots in real conditions will confirm or refute the appropriateness of the proposed approach.

Table 1

Alloy 092S	Tensile strength, MPa	Yield strength, MPa	Relative extension, %	Impact strength, J / cm ²
Source metal	441,5	304,1	21	-
Ingot	497,7	359,5	37,5	227,9



Fig. 2. . Photos of microsections. Magnification 200. The arrangement of photographs corresponds to the scheme in Fig. 1c.

REFERENCES

1. Report on the world forum of manufacturers of large forgings (Santander, Spain, November 3-7, 2008), Santander, 2008, pp. 11-19.
2. Nekhenzi Yu.A. Steel casting, Moscow, 1948, 766 p.
3. Mitchell A., Belenstein A.S. Factors affecting the temperature and crystallization of ingots during ESR, In the book: Electroslag remelting, 1985, Issue 6, pp. 192-198.
4. Flemings M. Solidification processes [Russian translation], Mir, Moscow, 1977, 424 p.
5. Iglitsyn M.I. (Editor) Technology of semiconductor materials [Russian translation], Moscow, 1961, 314 p.

INTERMEDIATE RESULTS OF A STUDY OF THE SYNTHESIS OF GRAPHENE OXIDE

G.Tavadze, G.Zakharov, A.Khavadagiani, Z.Asalmazashvili, T.Batsikadze, A.Peikrishvili, G.Urushadze*

Ferdinand Tavadze Institute of Metallurgy and Materials Science. 8b .E.Mindeli str., Tbilisi 0186, Georgia, Tbilisi.

*guliko57@mail.ru

With the development of scientific and technological progress, the need for new functional materials with enhanced physical, mechanical and chemical properties increases. Obtaining 2D materials by graphene technology allowed us to create a new class of materials with unique properties. Research on improving the technology for obtaining such materials and studying their properties is an urgent task of modern materials science. Currently, graphene technology is divided into two separate areas - the production of graphene (G) and graphene oxide (GO).

Graphene-like materials are obtained by physical, electrochemical or chemical methods. Physical methods include micromechanical splitting and vapor deposition. This method allows to obtain 2D materials of a small area and with a minimum of defects. Chemical methods lead to the formation of 2D materials with a larger area and a large number of defects.

Graphene is a 2D carbon material in which the crystal lattice is a layer with a thickness of only one atom. Due to its unique properties, researchers all over the world are interested in graphene, which is called the material of the future [1]. Graphene is the most durable, lightest, heat and electrically conductive version of the carbon compound. Graphene oxide is a graphene-like material that can have many applications in a wide variety of fields. Graphene oxide is one of the most important graphene derivatives. For obtaining GO exists various technologies, for example, it is obtained by oxidation of graphite to form graphene oxide, and graphene is reduced from graphene oxide by chemical, electrochemical, high-frequency currents or photochemical methods [2].

The methods for obtaining of graphene-like materials are not perfect, energy-intensive and expensive. Due to the fact that the nomenclature of these materials and their production for many types are still limited, there are no technological regulations and technical conditions for their production, in accordance with which specific products must comply [3].

Scientific developments in modern materials science are aimed at reducing the mass and improving the physical, mechanical and chemical properties of new materials. Therefore, the synthesis of new compounds with enhanced physical and chemical characteristics that cannot be obtained using traditional chemical and physical methods is an urgent task. Therefore, the study of the mechanism of formation of graphene oxide and identification of areas of their application is undoubtedly of both scientific and practical interest. This work is related to the original scientific work, [4] previously published by a group of scientists, devoted to the synthesis of 2D

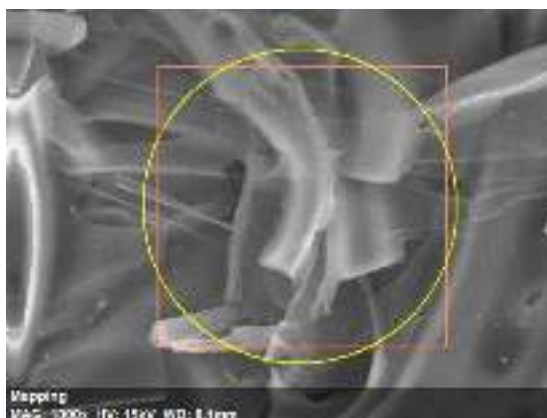
carbon structures by carbonization of natural biopolymers under conditions of self-propagating high-temperature synthesis (SHS-graphene).. Based on the researches of the authors of the above-mentioned article, we made the appropriate conclusions, reproduced experiments and introduced them new ideas. The interim results of the research are submitted for discussion. In addition to starch, other organic compounds from the C_x-Hy-O_z и C_x-Hy-N_z series were additionally used in the experiments. Synthesis was performed in various gaseous atmosphere using a specially developed reaction device. The container in which the reaction charge was placed was previously heated. The synthesis was performed at different initial temperatures. The device developed by us allows you to get two types of product:

- a highly porous black shapeless mass (photo 1), which, when magnified, is a volumetric-planar – "scaly" - particle (photo 2);
- an emulsion (photo 3 a), from which, after drying, an orange powder was obtained (photo 3c).

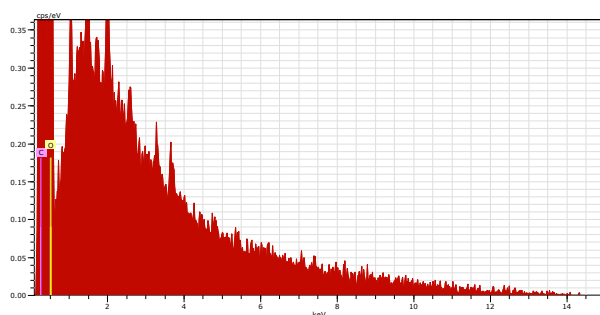
The density of the product shown in photo1 is in the range ($\rho = 0.015-0.025 \text{ g / cm}^3$). The experiments established that the density during the formation of the target product depends on the internal volume of the reaction zone.



.Fig. 1. Appearance of a highly porous product obtained in argon, in a new reaction device.



a



Spectrum: Point

Element AN Series norm. C Atom. C

[[wt.%]		[at.%]	
Carbon	6	K-series	80.53	84.64	
Oxygen	8	K-series	19.47	15.36	
Total:			100.00	100.00	

b

Fig. 2. Electron micrograph (obtained in an air atmosphere) of scaly particles of black mass (a) and distribution of elements (b)



a



b

Fig. 3. Appearance of the product in the form of an emulsion (a) and a powder after drying (b) obtained in argon atmosphere, on a new reaction device.

Electronic micrographs of the obtained products were examined using a HITACHI TM3030 Plus scanning electron microscope. The method of x-ray diffractometry was carried out on the diffractometer ДРОН 2 and ДРОН 4. Fig. 4a и 4b shows an x-ray diffractogram of a black mass and an orange powder obtained in an argon atmosphere, and in fig. 4c and 4d these same samples after microwave processing.

Raman spectroscopy was performed by passing a beam through the sample at a laser wavelength of 488 nm. The products obtained (under atmospheric conditions) were also subjected to heating under microwave radiation. Fig. 5a and 5b show Raman spectroscopy of scaly particles of black mass, before and after microwave processing, respectively.

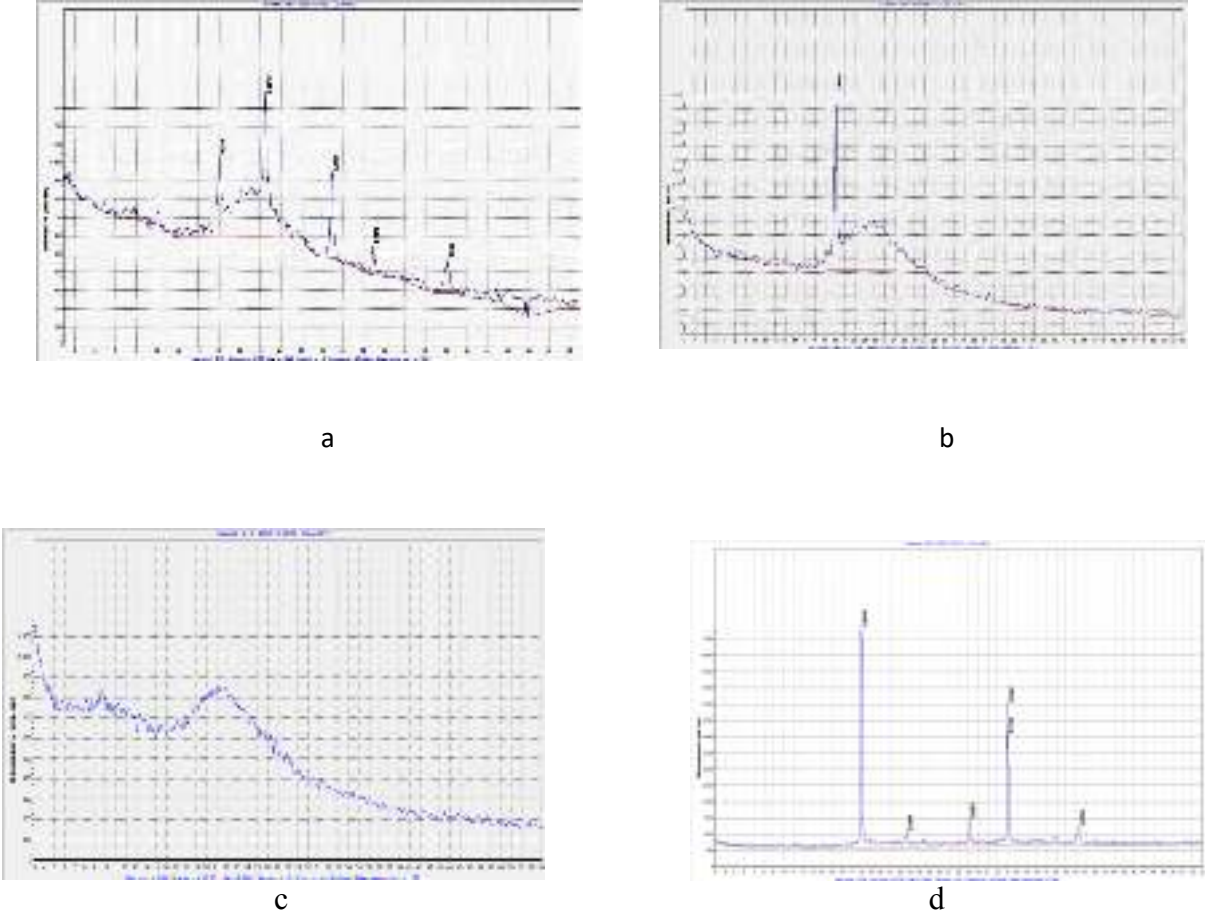


Fig. 4. X-ray diffraction patterns of the obtained material 4a of black mass and 4c of orange powder, and 4c, 4d these same samples after microwave processing.

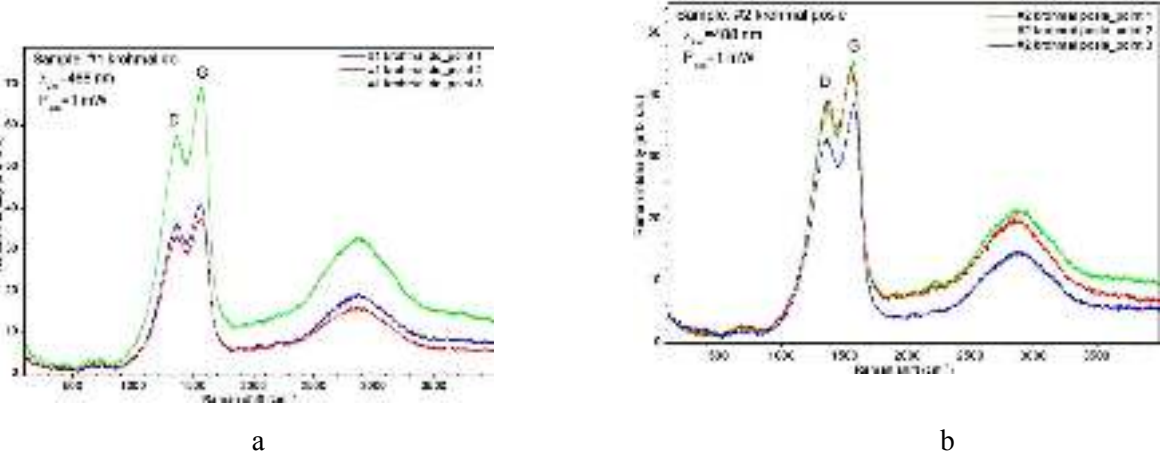


Fig. 5. Raman spectroscopy of scaly particles of black mass before (a) and after (b) Microwave processing.

At this intermediate stage of the experiments, it can be assumed that graphene oxide is obtained by carbonization of organo-inorganic materials in a gaseous medium using SHS technology. It can also be assumed that carbon atoms are replaced by oxygen-containing groups during the synthesis process. This will expand the potential scope of such materials.

REFERENCES

1. A. G. Alekseenko. Graphene. Derivative of an electronic edition based on print-
2. tion of the publication: M. : BINOM. Knowledge lab, 2014.-168 PP.
3. S. P. Gubin, S. V. Tkachev. Graphene and materials based on it. Radionics. nanosystems. Information technology.2010. Volume 2. Number 1-2. 99-137c.
4. Y.M. Shulga, S.A. Baskakov, V.A. Smirnov, N.Y. Shulga, K.G. Belay, G.L. Gutsev // Journal of Power Sources – 2014. – V. 245. – P. 33–36.
5. A. P. Wozniakowski, A. A. Poznyakovskiy, I. V. Shugaley. Available graphene synthesis as the first step in obtaining new-generation superhard materials. Rock-breaking and metal-working tools-equipment and technology of its production. Issue 20. 2017 316-323c.

OBTAINING AND STRUCTURAL ANALYSIS OF TiB_{0,6} METAL-CERAMIC TILES WITH SHS ELECTRIC-ROLLING PROCESS

G. Tavadze, G. Oniashvili, Z. Melashvili*, Z. Aslamazashvili, G. Zakharov

Ferdinand Tavadze Institute of Metallurgy and Materials Science. 8b.E.Mindeli str., Tbilisi 0186, Georgia, Tbilisi.

*metalurgi@mail.ru

Innovative SHS (self-propagating high-temperature synthesis) electric-rolling process developed at Ferdinand Tavadze Metallurgy and Materials Science Institute ensures SHS and hot deformation (rolling) continuity of specimens and obtaining any size of longitudinal measurement product.

The condition for continuity of SHS electric-rolling process is to ensure equality of the combustion front and billet movement velocities and to provide thermal energy to compensate for heat loss throughout the whole rolling process [1].

In order to determine optimum technological parameters of the SHS electric-rolling process, experiments were performed with variable shrinkage of TiB_{0,6} charge samples, both in a smooth barrel and in a box groove. Templet samples were cut from different points of the strip to determine the impact on the structure, hardness and density of the material obtained.

The billet obtained by SHS electric-rolling process is a porous material, from which, after further hot metal-forming (rolling), we can obtain product with intended thickness. In the deformation core, formed grains of the synthesized charge approach each other and at the exit cross section, hardened material is obtained, porous empties are significantly reduced, and at certain shrinkage, relative porosity decreases to 2-5%. As a result of billet shrinkage at the cross-section, compression takes place predominantly and the grains move in a vertical direction. Achieving some level of shrinkage, the charge begins to flow in a longitudinal direction. Thus, the process of SHS electric-rolling process progresses with intergranular and interparticle shear deformation. Increase in the material density along the deformation core depends on the compaction of the charge. On the basis of the experimental data, the image determining dependence of the relative deformation on the density has been obtained.

Synthetic charge-flowing studies in the deformation core reveal that movement speed of the billet is variable. In particular: at the entrance cross of the deformation core, billet velocity falls behind rolls' velocity in significant length ($\varepsilon = 0-53\%$). Intensive compaction takes

place, grains move predominantly in a vertical direction, shrinkage is minimal, and it's forestalling deformation core's exit-cross neighborhood ($\epsilon=54-58\%$).

At this time, compacting process is almost complete and shrinkage becomes of increasing type. When rolling TiB_{06} samples, it was found that during metal forming, which is followed by SHS process (lengthwise rolling in particular), in order to obtain high quality metal ceramic strips, it is essential to perform high shrinkage ($\epsilon \geq 54\%$) procedures in the deformation core in order to reduce porosity ($\Pi=2-3\%$). However, increase of deformation quality does not affect the macro hardness ($\epsilon=30-35\%$) [2]. As the deformation increases ($\epsilon = 54-55\%$), shrinkage of TiB_{06} grains and titanium phase is growing and therefore porosity decreases. Thus, we can conclude that in SHS electric-rolling regimen, rolling process should be carried out at $\epsilon > 54\%$ relative shrinkage conditions. Optimal mode for this process is $\epsilon = 54-58\%$, where the relative porosity is reduced to 2-3%. The maximum angle of bite is 25-27 degrees. Further deformation growth insignificantly affects material compaction, but it worsens the effectiveness of rolling mill (energy-force parameters are growing dramatically), biting conditions and hence stability of rolling process.

Experiments have shown that, compared to smooth barrel rolling, box groove rolling is preferred, since in the latter, free dilatation is limited and the degree of compaction increases.

Proposed SHS electric-rolling technology process produces gradient, corrosion-resistant, impact-resistant metal-ceramic billets.

The most important characteristics of metal-ceramic sintered-hard alloys are the strength limit on bending and hardness, and its characteristics for TiB_{06} material are present in Table1.

Table1. Limit of strength on bending and hardness of the material obtained by SHS electric-rolling method.

Material	Strength limit of bending, MPa	Hardness HRA
$TiB_{0,6}$	1300-1400	84-85

Typical images of structural analysis of X-ray images for the $TiB_{0,6}$ material are shown in Fig.1.

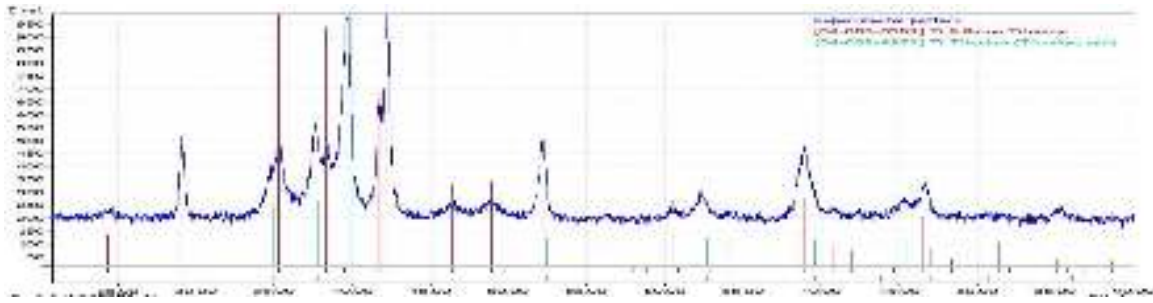


Fig.1. X-ray diagram of $TiB_{0.6}$ material

Presented x-Ray diagram shows that the material consists of orthorhombic titanium boride, TiB and hexagonal titanium. Figure 2. $TiB_{0.6}$ material microstructure is presented: A) X1000 and B) X 5000 enlargement

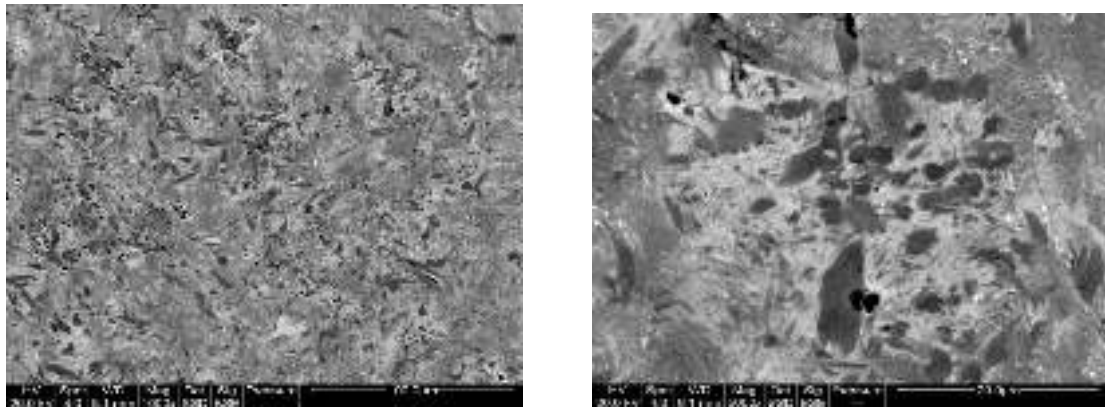


Fig.2. $TiB_{0.6}$ material microstructure: A) Enlargement X1000 B) Enlargement X 5000

As it can be seen from the microstructure, hexagonal titanium phase Ti is presented as chaotically oriented, very thin, tens of nm thick plates, suggesting that such a material structure, at high intensity dynamic impact loading, should provide impact energy accumulation and good material-resistance over dynamic loadings. Spectral analysis of the material was performed, in particular, Figure 3 presents the $TiB_{0.6}$ material microstructure of the corresponding (1-4) points with chemical constituents determined by spectral analysis, in both weight and atomic percentage (Table 2).

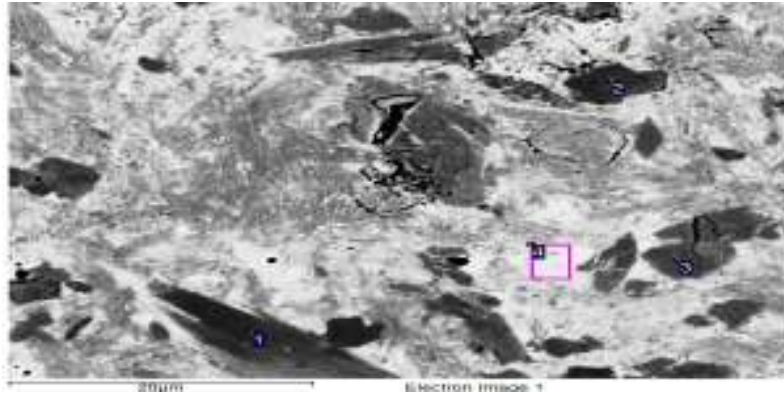


Fig.3. TiB_{0.6} material microstructure in corresponding (1-4) points.

Table2. Chemical constituents of TiB_{0.6} material points (1-4), shown in weight and atomic percentage.

Processing option: All elements analyzed (normalized)

All results in weight %

All results in atomic %

Spectrum	B	Ti	Spectrum	B	Ti	Total
1	50.1	49.9	1	18.5	81.5	100
2	51.0	49.0	2	19.0	81.0	100
3	47.7	52.3	3	17.1	82.9	100
Mean	49.6	50.4	Mean	18.2	81.8	100
Std. deviation	1.7	1.7	Std. deviation	1.0	1.0	
Spectrum	B	Ti	Spectrum	B	Ti	Total
4	1.3	98.7	4	0.3	99.7	100

CONCLUSION

The work presents the results of a structural study of the hot-compacted TiB_{0.6} charge in SHS electric-rolling process. X-ray structure and metallographic analysis of the rolled products in a box groove by SHS electric-rolling technology. Chemical composition in atomic and weight percentages is determined in the selected 4 points of rolled stock. Obtained product meets the requirements of the planned (highly physic-mechanical, dynamic impact-resistant, corrosion-resistant and scale-resistant) properties.

REFERENCES

1. T.Namicheishvili, A.Tutberidze, Z.Melashvili, G.Tavadze, Z.Asalmazashvili, G.Oniashvili, G.Zakharov. Method for obtaining inorganic product from powder exothermic chasm, Saqpatenti. Patent P 6541 . LEPL Ferdinand Tavadze Metallurgy and Materials Science Institute, 2016.
2. T.Namicheishvili, A.Tutberidze, Z.Melashvili, G.Tavadze, Z.Asalmazashvili, G.Zakharov. Innovative teqnology of receiving proteqtive plates from metal-ceramic composite. Inorganic materials science modern teqnologies and methods, Tbilisi, Georgia, 2018.

SECONDARY POROSITY OF MICROPOROUS ZEOLITES

V.Tsitsishvili*

Petre Melikishvili Institute of Physical and Organic Chemistry at Tbilisi State University, 31, A.Politkovskaia, str., 0186, Tbilisi, Georgia

* v.tsitsishvili@gmail.com

Crystalline polymeric aluminosilicates with general formula $M^{n+}_{x/n}[(SiO_2)_y(AlO_2)_x] \cdot wH_2O$ ($M = Na, K, Ca, Mg, \text{ etc.}$) are called zeolites. They have a three-dimensional framework that forms uniformly sized pores and channels of molecular dimensions on the base of alternating SiO_4 and AlO_4^- tetrahedrons linked to each other. Due to unique properties of uniform and precise nano-scale porosity, molecular shape selectivity, ion-exchange capacity, strong Brønsted acidity and high thermal and hydrothermal stability, zeolites find the greatest practical application. At present the zeolite group includes more than 40 naturally occurring species, and is the largest group of minerals among the silicates. To date, the Database of Zeolite Structures of the International Zeolite Association (<http://www.iza-structure.org/>) contains 237 types of synthetic zeolites, and this list is updated annually.

Synthetic zeolites, as a rule, are prepared in monocationic, usually Na-form, while natural zeolites can contain cations not only of elements of groups IA and IIA, but also of transition metals such as iron, copper, zinc, etc. However, the main difference between synthetic zeolites and natural ones is that the former have only pores with sizes defined by the type of crystal structure, while natural zeolites additionally can have highly developed systems of mesopores (2 – 500 nm) and macroscopic pores.

In some cases of zeolite application, the presence or absence of mesopores is of great importance. So, in our early works [1] it was shown that in contact with water contaminated with microorganisms, natural or modified zeolites exhibit bactericidal activity only when they have mesopores with sizes of 100-200 nm in their structure. It was found that natural clinoptilolite (IZA formula $[Ca_4(H_2O)_{24}][Al_8Si_{28}O_{72}]$) substantially reduces viability of *Escherichia coli* and, in particular, *Staphylococcus*, whereas the acid treated samples are inert. Native clinoptilolite is characterized by well developed (specific volume over $0.15 \text{ cm}^3/\text{g}$) system of mesopores with diameter in the range from 20-80 to 200 nm, the acid treatment of clinoptilolite leads to an alteration of mesopores and a decrease in their specific volume. For analcime and phillipsite the effect is the opposite: native zeolites are practically inert, acid-modified samples suppress viability of microorganisms, phillipsite impacts against both

bacteria, analcime – especially against *Staphylococcus*. Native zeolites have low specific volume of mesopores ($0.03 \text{ cm}^3/\text{g}$) with sizes the range from 4-8 to 60 nm, acid treatment results in formation of mesopores with diameter up to 200 nm and specific volume up to $0.1 \text{ cm}^3/\text{g}$. It should be noted that unlike clinoptilolite and other silica-rich zeolites, analcime cannot be dealuminated to a high degree ($\text{Si}/\text{Al} \rightarrow \infty$), analcime is acid leaching resistant and about 40% of aluminum does not come into contact with the aqueous acid phase.

All considered zeolites have macropores with a diameter of more than 500-800 nm, acid treatment does not significantly affect their size or specific volume. Thus, on the surface of these zeolites, both spherical *Staphylococcus* bacteria with a diameter of 500 to 1000 nm and a rod-shape *E. coli* bacteria with the width of about 500 nm and the length up to 5000 nm can be immobilized. At the same time, the bacteriostatic activity of the zeolite, apparently, is determined by mesopores, the sizes of which coincide with the sizes of such external structure elements of organisms as bacterial fibers and flagellum with thickness of about 200 nm. These results are very important for the use of zeolites as filter materials for drinking water.

Recently [2-4] it was found that when silver, copper or zinc is introduced into the zeolite structure, the bactericidal effect of the material is determined not only by the release of metals. Ag-, Cu-, and Zn-containing micro-mesoporous materials have been prepared on the basis of natural phillipsite using ion-exchange reactions between zeolite and a salt of a transition metal in the solid phase followed by washing. Synthesized adsorbent-ion-exchangers contain up to 230 mg/g of silver, or 66 mg/g of copper, or 86 mg/g of zinc and show bactericidal activity towards *Escherichia coli*. According to the changes in the relative number of viable cells of bacteria contacting with zeolites and the data on leaching of metals from modified zeolites compared to the minimal inhibitory concentration (MIC) values for corresponding ions toward *E. coli*, the Ag-containing zeolite exhibits a certain antibacterial activity even before the concentration of ions in the solution reaches the MIC value, and its bactericidal effect could be ascribed not only to released Ag^+ ions but also to Ag-phillipsite itself; the copper- and zinc-containing zeolites emit a small amount of ions (up to 0.5MIC) and their activity is entirely attributed to Cu-phillipsite and Zn-phillipsite themselves. Strong bacteriostatic activity of modified zeolites was established by the Kirby-Bauer test. SEM images show that the procedure of dry ion- exchange synthesis leads to an increase in the dispersion of the material, the study of the mesoporous system of modified samples continues. Another area where the mesopores plays an important role are catalytic processes. The effectiveness of the catalyst is determined by the specific surface area and the access of

reacting molecules to its active centers. The increase in the degree of dispersion of catalysts is limited, the use of nano-particles is associated with the difficulties of their separation. On the other hand, the presence of secondary porosity in the zeolite catalyst allows shorter diffusion paths and provides access of reagents to active sites on the surface of the catalyst. Modification of zeolite Beta by steaming and acid leaching results in the formation of secondary mesoporous structure, modified catalysts have been successfully used for the selective transformation of large molecules used in pharmacy and perfumery [5]. However, such processing is effective for high-silica zeolites like Beta ($\text{Si/Al} > 8$), for low-silica zeolites of the FAU type ($\text{Si/Al} = 2.31$), intensive leaching of aluminum atoms occurs, the properties of the final product strongly depend on temperature and other processing conditions, so it is rather difficult to achieve reproducible results.

An alternative to acid modification is the targeted recrystallization of natural zeolites. To obtain zeolites X (type FAU with $\text{Si/Al} < 3$) widely used in catalysis, natural phillipsite was used, which has a relatively low Si/Al ratio and suitable secondary building units in the crystal structure. It was found that phase-pure zeolite with the corresponding chemical composition can be prepared in the form of octahedral crystallites with uniform micrometric (2-7 μm) dimensions by hydrothermal crystallization (95°C) of aluminosilicate gel obtained from water suspension of natural phillipsite, treated with hydrochloric acid, mixed with sodium hydroxide, and aged (96 hr) at room temperature. The X-ray diffraction powder patterns of phillipsite recrystallization products show the strongest peak at $2\Theta = 6.1^\circ$, as well as all low intensity peaks listed in the IZA Database for hydrated Na-X zeolite. The mid infrared peak pattern in FT-IR spectra testifies formation of zeolite structure and reveals differences for samples of zeolite Na-X obtained under different conditions and having different Si/Al ratios.

It is found that at a high concentration of sodium in the reaction mixture, zeolite X with a high aluminum content ($\text{Si/Al} = 1.4$) is formed, while crystallization of a diluted gel with an average sodium content leads to the formation of zeolite X with a higher silicon content ($\text{Si/Al} = 2.5$).

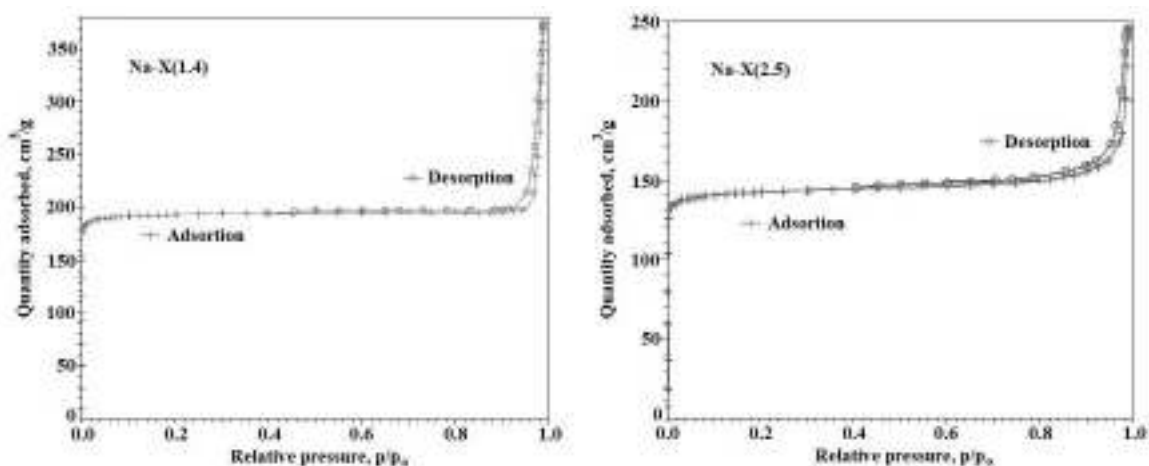


Fig. 1. N₂ adsorption-desorption isotherms of Na-X zeolites obtained from natural phillipsite

According to the nitrogen adsorption-desorption isotherms measured at 77 K (Figure 1), low-silicon sample Na-X(1.4) has high specific surface area (590 m²/g) of micropores (0.3 cm³/g) and cylindrical pore channels (0.28 cm³/g) with an average diameter of 55 nm, while high-silicon sample Na-X(2.5) has lower surface area (440 m²/g) of micropores (0.23 cm³/g) and irregular mesopores (0.15 cm³/g) with a diameter of 20-30 nm.

Obviously, modern methods of primary and secondary synthesis of zeolites with hierarchical porosity make it possible to obtain a variety of products used in various industries.

REFERENCES

1. G. Tsitsishvili, V. Tsitsishvili, N. Dolaberidze, M. Alelishvili, Chemistry of advance compounds and materials, ed. by N. Lekishvili, G.E. Zaikov, Nova Science Publishers, New York, 2008, pp. 115-121.
2. J. Milenkovic, J. Hrenovic, D. Matijasevic, M. Niksic, N. Rajic, Environmental Science and Pollution Research, 24, 2017, pp. 20273–20281
3. N.M. Dolaberidze, V.G. Tsitsishvili, B.T. Khutsishvili, N.A. Mirdzveli, M.O. Nijaradze, Z.S. Amiridze, New Materials, Compounds and Applications, 2(3), 2018, pp. 247-260.
4. V.G. Tsitsishvili, N.M. Dolaberidze, M.O. Nijaradze, N.A. Mirdzveli, Z.S. Amiridze, Chemistry, Physics and Technology of Surface, 10(4), 2019, pp. 327-339.
5. V. Tsitsishvili, Ts. Ramishvili, I. Ivanova, I. Dobryakova, T. Bukia, N. Kokiashvili, Bulletin of Georgian National Academy of Sciences, 12(3), 2018, pp. 62-68.

NATURAL ANALCIME AS A RAW MATERIAL FOR ION EXCHANGERS

V.Tsitsishvili*, N. Dolaberidze, M.Nijaradze, N.Mirdzveli, Z.Amiridze

Petre Melikishvili Institute of Physical and Organic Chemistry at Tbilisi State University, Tbilisi, 31

A.Politkovskaia str., 0186, Georgia

* v.tsitsishvili@gmail.com

Analcime is rather widespread among the zeolites known on the territory of Georgia [1]: an abundance of analcime connected with volcanic-sedimentary rocks is observable in the Middle-Eocene rock masses of the Achara-Trialeti folded system, beginning with Mtskheta district, including the Borjomi valley and westward in Bagdadi and Vani districts; analcime-containing stratified rocks are known in Western Georgia in the deposits of Jurassic carbonaceous and colored suites of Kutaisi area, as well as analcime from a basaltic geode (environs of Tbilisi), analcime crystallized in the chemical way (sedimentary rocks from Kutaisi environs), and analcime of diagenetic origin in volcanic-sedimentary rocks from the Akhaltsikhe deposit, along with other zeolites (phillipsite, laumontite, mordenite, etc.).

Analcime belongs to minerals of tectosilicate group with zeolitic structure (crystal chemical data $[\text{Na}_{16}(\text{H}_2\text{O})_{16}] [\text{Al}_{16}\text{Si}_{32}\text{O}_{96}]$ -ANA, cubic, $Ia3d$, $a=13.73 \text{ \AA}$ [2]) with high framework density of $18.5T/1000 \text{ \AA}^3$ ($T = \text{Si or Al}$). The analcime framework (Figure 1) consists of singly-connected 4-rings, irregular channels are formed by highly distorted eight-membered rings (8mR, Figure 2) and have small entrance windows of approx. 2.6 \AA , and regular channels are formed by six-membered rings (6mR) along the $[111]$ direction of the cubic lattice.

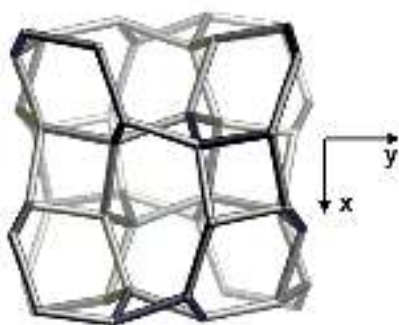


Fig. 1. Analcime framework viewed along $[001]$.

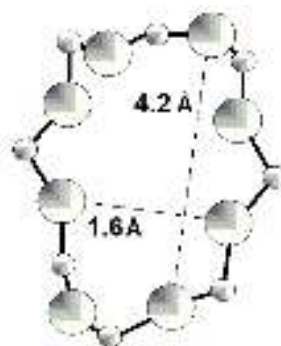


Fig. 2. Distorted 8mR viewed along $[110]$.

The compact structure of analcime also prevents the adsorption and diffusion of molecules in the cages and channels, therefore its use as an adsorbent or molecular sieve is limited. However, analcime has a scientific weight ion exchange capacity of 5.1 meq/g, and it was supposed to use natural analcime as an ion-exchanger for the nuclear wastewater treatment [3], but nothing is known about the practical implementation of this project.

The goal of our study was to demonstrate possibility to carry out synthesis of zeolite with high ion-exchange capacity by hydrothermal recrystallization of natural analcime and production of materials with different sizes of crystallites and suitable system of pores and channels.

Preparation of synthetic zeolite material was carried out using greenish-grey analcime-containing rock from the Chachubeti plot of the Tedzami deposit having high zeolite phase content (up to 95%) with chemical composition $(\text{Na}_{9.25}\text{K}_{2.25}\text{Ca}_{1.25}\text{Mg}_{0.95})\text{Me}_{0.30}[\text{Al}_{16.2}\text{Si}_{32.0}\text{O}_{96}] \cdot 18.4\text{H}_2\text{O}$ (Me – impurity metals such as Fe, Cu, etc.), characterized by the X-ray diffraction pattern, IR spectrum, thermal analysis data, and ion exchange properties [4].

Zeolite-containing rock powder (0.063-0.1 mm), washed in distilled water (solid : liquid =1:20, 3-5 times) and dried at 100-110°C was treated at room temperature by HCl water solution under stirring, washed by water before the complete disappearance of Cl^- ions, and dried at 100-105°C; water suspension of homogeneous amorphous (XRD tested) material was prepared with the solid to liquid ratio of 1 : 3; suspension was treated at room temperature by NaOH water solution, solid to liquid ratio of 1 : 6; homogenization of produced gel takes approx. 30 minutes, its aging at room temperature – several days. Crystallization of aged gel was carried out in the Teflon flasks using temperature-controlled water bath (OLS26 Aqua Pro); the temperature (up to 95°C) and duration (up to 120 hours) have been adjusted to prepare crystals with average diameter of 5 μm ; separation of produced crystalline material was carried out by filtration of mother solution, solid material was cleaned by distilled water until pH 8.0-8.5, and dried at 90-100°C.

The analysis of the XRD pattern (Fig. 3) allows us to attribute the obtained material to the Linde Type A synthetic zeolite ($[\text{Na}_{12}(\text{H}_2\text{O})_{27}]_8 [\text{Al}_{12}\text{Si}_{12}\text{O}_{48}]_8\text{-LTA}$). Experimental XRD pattern has the same peculiarities mentioned in [5,6] for the LTA zeolites produced from kaolin considered as an ideal raw material for the preparation of this type of zeolites. However, materials obtained from kaolin contain quartz (strong peak at $2\Theta = 26.63^\circ$) and the SOD type zeolite (characteristic peaks at $2\Theta = 14.14^\circ$ (0.53), 24.62° (1.00), 31.96° (0.98), and

35.1° (0.78)) as impurities, not observed in XRD patterns of samples obtained by recrystallization of analcime.

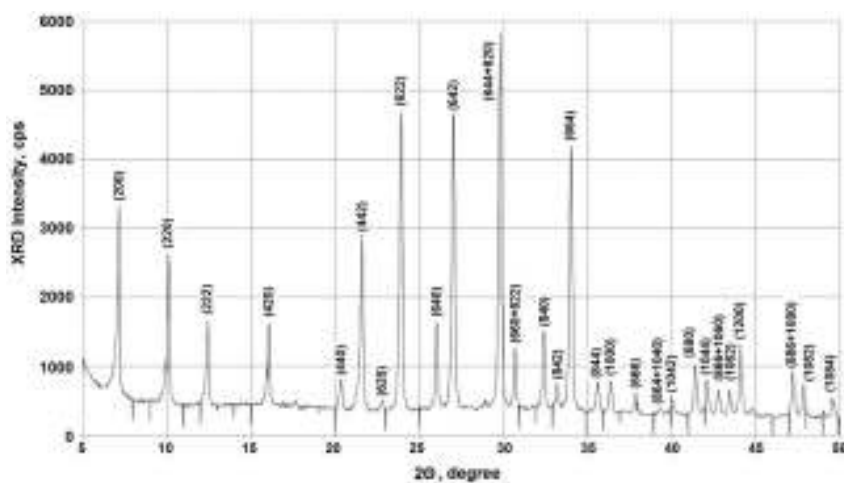


Fig. 3. Powder XRD pattern of the material obtained by the recrystallization of analcime; numbers in parentheses are Miller indices (hkl)

Zeolites have been produced from the $3.4\text{Na}_2\text{O}:\text{Al}_2\text{O}_3:1.1\text{SiO}_2$ reaction mixture, the chemical composition of prepared materials, $0.92\text{Na}_2\text{O}:\text{Al}_2\text{O}_3:2.04\text{SiO}_2:3.00\text{H}_2\text{O}$, is in a good accordance with corresponding crystal chemical data for LTA. Developed zeolitic crystal microporous structure in synthesized samples is confirmed by high value (>13 mmole/g) of water adsorption capacity under static conditions at the “plateau” pressure $p/p_s=0.40$ and room temperature. Share of impurity metals in compensation of the negative charge is 8%, but in some cases this value reaches 15%. In general, recrystallization of analcime retains a greater amount of impurity metals than recrystallization of clinoptilolite [7], but the preparation of LTA zeolite from clinoptilolite is possible only in two stages, with the intermediate production of sodalite.

The resulting material has a fairly high ion exchange capacity, 4.5 meq/g, and can be used as a builder in detergent powders and tablets for water softening.

Ratio of water molecules per compensating ion ($\text{H}_2\text{O}:\text{Na}$) in ideal LTA structure is 9:4, in synthetic samples it depends on conditions of crystallization: hydrated materials ($\text{H}_2\text{O}:\text{Na}=9:5.5$) are produced at low temperature, high temperature results in dehydration. Increasing basicity of reaction mixture results in creation of LTA structure with high aluminium content ($\text{Si}/\text{Al}\approx 1$), rapid crystallization gives nanoscale crystals and aggregates, while slow crystallization at comparatively low temperatures gives micrometric crystallites (Fig. 4).

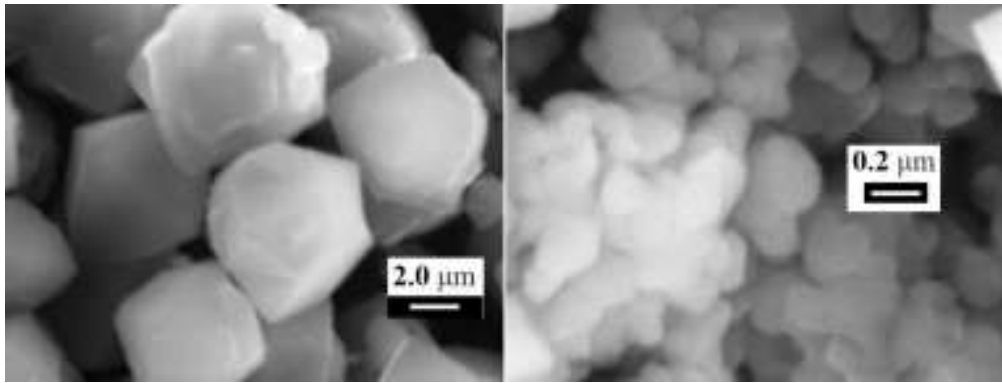


Fig. 4. SEM images of micrometric (left, x5,500) and nano (right, x55,000) crystals of LTA zeolites recrystallized from analcime

The proposed method for preparation of the LTA zeolites is based on the use of natural silica-alumina raw materials and inexpensive reagents (HCl, NaOH), it is characterized by the relative rapidity and low energy expenditures.

This work was supported by the Shota Rustaveli National Science Foundation of Georgia, project FR-18-2600.

REFERENCES

1. N. Skhirtladze. Genetic groups of Georgian zeolites, their main deposits and manifestations, Tbilisi State University, Tbilisi, 1997, p. 16.
2. Ch. Baerlocher, L.B. McCusker, D.H. Olson, Atlas of zeolite framework types, 6th revised edition, Elsevier, Amsterdam, 2007, p. 46.
3. M.H. Mallah, H. Soorchi, T.F. Jooybari, Annals of Nuclear Energy, 47, 2012, pp. 140-145.
4. V. Tsitsishvili, N. Dolaberidze, S. Urotadze, M. Alelishvili, N. Mirdzveli, M. Nijaradze, Chemistry Journal of Moldova, 12, 2017, pp. 95-101.
5. A. Shoumkova, V. Stoyanova. Journal of Porous Materials, 20, 2013, pp. 249-255.
6. M. Gougazeh, J.-Ch. Buhl, Journal of the Association of Arab Universities for Basic and Applied Sciences, 15, 2014, pp. 35-42.
7. V. Tsitsishvili, N. Dolaberidze, M. Alelishvili, M. Nijaradze, N. Mirdzveli, Proc. Georgian Nat. Acad. Sci., chem. ser., 42, 2016, pp. 133-137.
- 8.

DYNAMIC MODELLING OF METAL MELTING PROCESS

J. Khantadze, L. Chkhartishvili*, G.Mikaberidze

Ferdinand Tavadze Metallurgy and Materials Science Institute, 8b E Mindeli Str., Tbilisi, 0186, Georgia

chkharti2003@yahoo.com

ABSTRACT Process of melting in metals is modeled dynamically using specially designed device, in form of trihedral pyramid of closely packed identical hard balls, allowing one to change smoothly the pyramid base area. Thermodynamic limit, 6 – 8 %, of expansion of metals in the solid phase and the limit, ~ 4.8 %, of mechanical stability of the model structure are found to be in good agreement with each other.

The service characteristics of metal products gradually deteriorate with increasing temperature, and at the melting point their structural stability completely disappears. Why does the metal melt or what factors determine its stability? Obtaining answers to such questions remains one of the most urgent tasks of the solid state physics and, in particular, metal physics.

From the thermodynamic point of view, melting refers to first-order phase transitions. Various theories have been proposed to explain this process, which are ultimately based on the principles of Debye–Einstein atomic oscillator model of solids. Among them, the theories by Lindeman and Grüneisen are considered to be most successful (see, for example, [1]).

According to Lindeman, at melting temperature T_m relative change in the amplitude of atomic vibrations reaches a critical value at which the change in the unit cell parameter is so significant that the lattice loses stability and melts. According to Grüneisen, the arrangement of atoms near the fixed sites of the crystal lattice ceases to be stable, and the substance melts at certain critical expansion of the crystal in volume relative to that at absolute zero: $3\alpha T_m \approx 0.06 - 0.08$, where α denotes the relative linear expansion coefficient. It follows that the crystal cannot be overheated: its stability is limited by expansion in volume by 6 – 8 %.

What role does the metals structure play in the melting process? In general, the effect of structural characteristics on the metals stability in frames of irregular structures mechanical model [2] was posed in [3].

In the present work, an attempt is made to find out how the most densely packed face-centered cubic (fcc) lattice reacts to expansion, when and how the regular structure transforms into an irregular one and what geometric and topological factors determine such a transition.

In order to answer these questions, first it is necessary to study the mechanical stability of the structure itself as an abstract object.

To determine mechanical stability of the fcc structure, we have constructed a device described in detail in the recent work [4]. Using it, the stability limit of a trihedral pyramid built of the almost identical steel balls is determined experimentally. In such a structure, each ball is in contact with 6 similar ones in the horizontal plane and 3 and 3 balls in adjacent upper and lower layers, respectively. Thus, a fcc structure densely packed (with packing coefficient of ≈ 0.736) in the crystallographic plane (111) is obtained (**Figure 1a**).

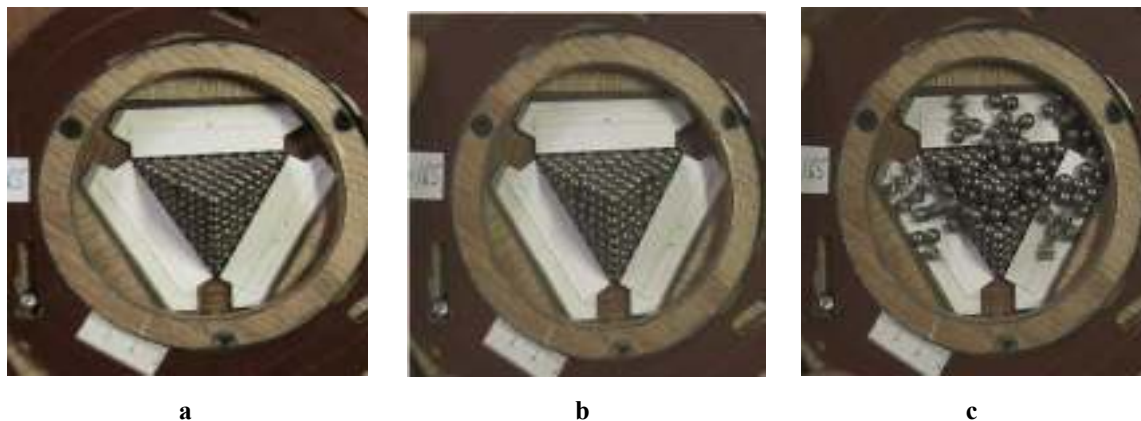


Fig. 1. Pyramidal cluster of $N = 165$ balls: initial ordered state (**a**), state of geometric disorder while maintaining original topology (**b**), and beginning of cluster destruction (**c**).

Numbers N of balls contained in such colonies – pyramidal clusters of balls – are the Pascal triangle’s tetrahedral numbers:

$$N = \frac{n(n+1)(n+2)}{6} = 1, 4, 10, 20, 35, 56, 84, \dots,$$

where $n = 1, 2, 3, \dots$ is the number of layers in the pyramid. Each layer contains $n(n + 1)/2$ balls. The pyramid stability in the gravity field is supported by the equilateral triangular barrier formed by the ends of three plates (shown in light color). The device allows one to change smoothly the barrier size, i.e. pyramid base area.

As the pyramid base area increases, the balls deviate from their sites in the regular lattice stochastically, and the system of balls becomes geometrically disordered, although at initial stage it retains the pyramidal shape, i.e. initial topology (**figure 1b**). After the sides of pyramid base are enlarged to a certain critical size, the structure loses its stability, collapses, and goes into a disordered state or undergoes a topological transformation (**figure 1c**).

Obviously, the structural stability limit for given N under the conditions of same balls and device surfaces treatment, i.e. at fixed friction coefficients, should not depend on the balls

diameter d . When $d = 1$, pyramid degenerates into a single ball. The smallest pyramidal structure in form of tetrahedron of $N = 4$ balls loses stability and collapses when three balls located on its base are displaced from each other by $\sqrt{3}d$ and the fourth of them is placed in the cavity formed. As a result, the 3D structure turns into 2D one. At $d > 4$, in contrast to this trivial case, the determining stability limit for pyramidal structures is devoid of such clarity. However, problem itself lends to experimental study using above mechanical model. Our goal is to establish the stability of the fcc structure by extrapolating to the stability limit of the pyramidal colonies consisting of a finite number of balls to the case of infinite number of balls in the pyramid: $N \rightarrow \infty$.

Experiments using above device consist in measuring the coefficient of linear expansion of sides of the base of a pyramid constructed of balls, $\alpha = (l - l_0)/l_0$, where l_0 is the initial length of the pyramid base sides and l is their length at the moment of losing stability. However, the relative volume expansion coefficient $\beta = (V - V_0)/V_0 = \Delta V/V$ is of final interest. Here V_0 is the initial volume of the pyramid, V is the volume at the moment of losing the stability, and ΔV is the corresponding change in crystal volume. It can be shown (for details of geometric considerations see [4]) that at small expansions, $\alpha \ll 1$, these two parameters are related to each other as follows: $\beta \approx 3\alpha/2$.

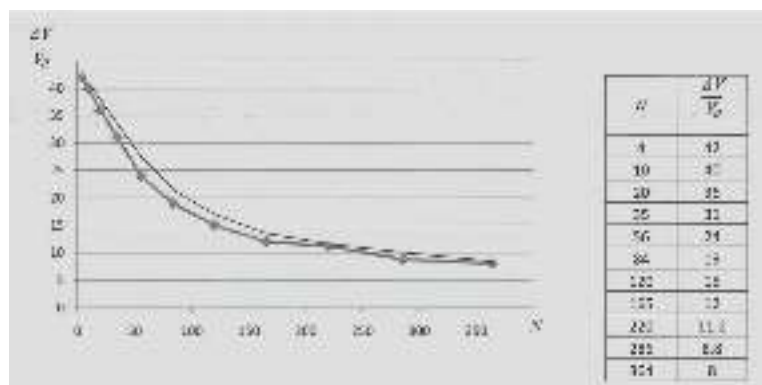


Fig. 2. Relative change in pyramid volume at destruction in dependence on balls number.

Experimental results obtained using designed device and taking into account this relation are shown in Fig. 2. From this figure it follows that with increasing N the structure stability decreases monotonically. Obviously, at the losing pyramid stability the ratio $\Delta V/V_0$ asymptotically tends to a certain limit, the exact estimation of which due to far extrapolation is associated with significant errors.

Therefore, it is advisable to draw the dependence of relative change in the pyramid volume at destruction on the inverse number of balls – see **figure 3**.

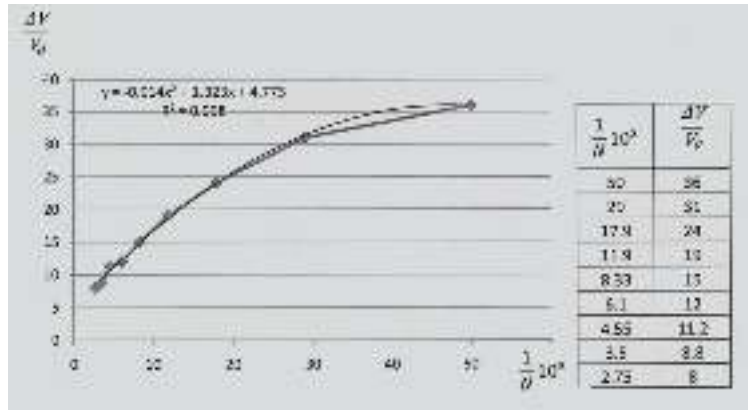


Fig. 3. Relative change in pyramid volume at destruction in dependence on inverse number of balls.

If we exclude from the consideration smallest colonies of balls ($N = 1$, $N = 4$, and $N = 10$), then by approximating the experimental data we obtain the following equation for the $\Delta V/V_0 - 1/N$ curve:

$$\frac{\Delta V}{V_0} \approx -0.014 \left(\frac{10^2}{N} \right)^2 + 1.323 \left(\frac{10^2}{N} \right) + 4.770 .$$

Its extrapolation to the infinite number of particles determines limiting value of the coefficient of volume expansion as $\approx 4.8\%$, which is close to above thermodynamic estimates.

Based on the conducted study, we can conclude that the limit of expansion of metals in the solid phase and the limit of mechanical stability of the model structure of hard balls are of the same order of magnitude, although the reasons for their stability are of completely different physical nature: in the first case, stability is due to interatomic interactions and in the second, mechanical equilibrium of systems of absolutely hard balls in uniform external (gravity) field under the presence of friction between balls and fixed system size in base plane perpendicular to the field.

REFERENCES

1. A. R. Ubbelohde. The molten state of matter: Melting and crystal structure. 1978, Chichester, John Wiley & Sons.
2. J. Khantadze. Structural models and properties of metallic melts. 2009, Tbilisi, Forma.
3. J. Khantadze. Spatial and structural characteristics and stability of metal phases. In: Proc. 2nd Int. Conf. Mod. Technol. & Meth. Inorg. Mater. Sci. 2011, Tbilisi, Sachino, 15-23.
4. J. Khantadze, L. Chkhartishvili. Dynamic model of melting – Investigation of stability for nanopyramid of spherical atoms. Int. J. Eng. Sci. Inv., Ser. II, 2019, 8, 8, 79-94.

CHARACTERISTICS OF INFRARED P-I-N PHOTODIODES BASED ON VARIOUS $\text{In}_{0.53}\text{Ga}_{0.47}\text{As}/\text{InP}$ HETEROSTRUCTURES

N.Khuchua*¹, R.Melkadze¹, A.Tutunjyan², N.Dolidze², T.Sakharova², L.Sanikidze², M.Ksaverieva², R.Gulyaev²

¹* Institute of Applied Semiconductor Technology, TSU, 13 Chavchavadze Ave. 0179, Tbilisi, Georgia

² LEPL Institute of Micro and Nanoelectronics, 13 Chavchavadze Ave. 0179, Tbilisi, Georgia

[*ninakhuchua@mail.ru](mailto:ninakhuchua@mail.ru)

Over the past two decades, there has been a steadily growing interest in $\text{In}_x\text{Ga}_{1-x}\text{As}$ compounds where the photosensitivity range depends on the molar fraction of x . The composition with $x = 53$ is lattice-matched with InP, has a band gap of 0.74 eV, and covers a sensitivity range from 0.9 to 1.7 μm . Such a composition is called "standard" and the value of x is not indicated.

The basis of instrument engineering on these materials, are, as a rule, p-i-n diodes. The scope of such products is rather wide - from diagnosis of semiconductor devices to fiber-optic communication systems and night-vision cameras [1].

The architecture of InGaAs heterostructures, (sequence, thickness, and doping of layers) on a n^+ - or p^+ -type InP substrate is very diverse. Here, particular attention is paid to the thickness (from 1 to 5 μm) and impurity concentration (from 1×10^{14} to $5 \times 10^{17} \text{cm}^{-3}$) of the i-InGaAs adsorber [2]. The p-i-n photodiode technology requires special approaches to the formation of ohmic contacts to p^+ -InP, [3].

The aim of this work is to develop a p-i-n photodiode technology based on InGaAs/InP heterostructures that differ in architecture, and to compare their electrical and optical characteristics.

Figure 1 schematically shows p-i-n photodiodes made on the basis of the material grown by MOSVD technology at PAM-XIAMEN (China).

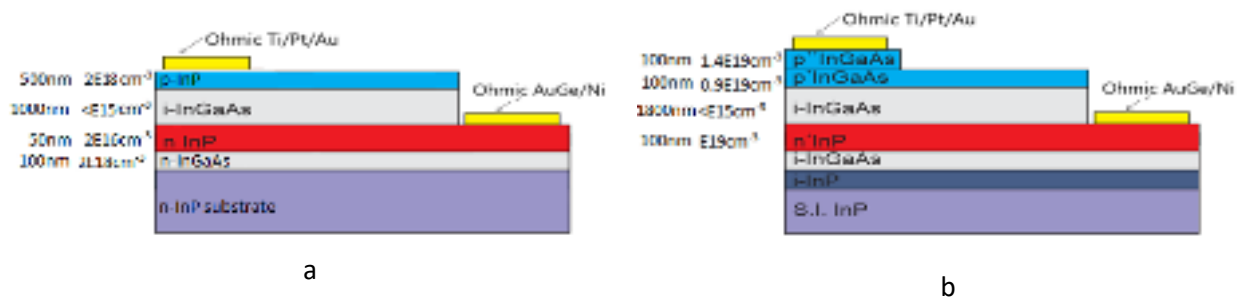


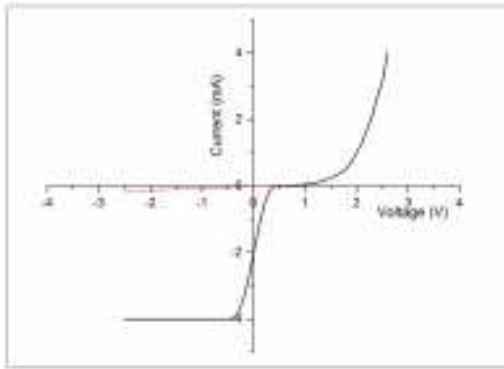
Fig.1. Schematic representation of the cross section of p-i-n photodiodes based on: a) p^+ -InP/InGaAs/ n^+ -InP (type I); b) p^{++} -InGaAs/ p^+ -InGaAs/InGaAs/ n^+ -InP on a semi-insulating substrate (type II).

The quality of the crystal lattice of the structures was studied by X-ray diffractometry on a Drone 3 setup. It was shown that the main diffraction peaks have a narrow width of several hundredths of a degree, which indicates the structural perfection of the grown layers. However, the x value is slightly different from the required one (+ 0.4% and - 1.3%). This indicates a certain mismatch in the lattice parameters, which, however, cannot affect the band structure of the material.

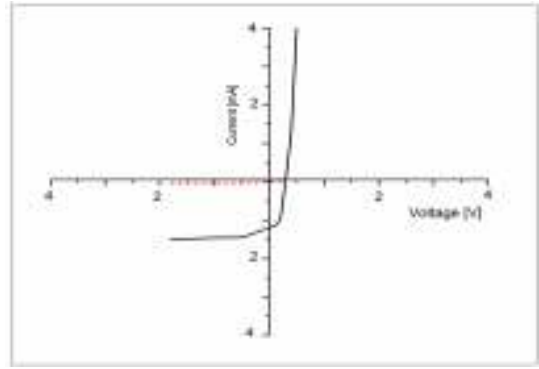
P-i-n diodes had a circular configuration with different diameters of the sensitive area (0.5, 1.0, and 1.5 mm).

The method of lift-off photolithography was used. For the formation of ohmic contacts to n^+ -layers, the composition of metals Ge/Au/Ni /Au (13/27/10/200 nm), and to the p^+ - layers - Ti/Pt/Au (20/30/150 nm) was chosen. To simplify the technology, a fast annealing regime was developed that made it possible to form contacts of both types in a single process. At the same time, a smooth morphology of the metal surface was preserved. Mesa etching was carried out by liquid selective etching in different etchants for InGaAs and InP.

Fig. 2 shows I-V characteristics of p-i-n diodes. A comparison of Fig. 2 a) and b) shows that the contacts to the p^+ -region for type I samples are rectifying, and for type II samples, as expected, a well pronounced ohmic character is observed. The latter is due to approximately 2 orders of magnitude higher concentration of the Zn impurity in the p^{++} -layer. However, the leakage currents in the second case (Fig. 2, b) are almost 20 times higher than those in type I samples.



a



b

Fig.2 I-V characteristics of p-i-n diodes for the type I (a) and type II (b) structures.

Figures 3 and 4 illustrate the photosensitivity spectra of p-i-n diodes of both types measured on MDR-2 monochromator using TKS-5 (850 - 3000 nm) optical filters. For these samples, measurements were performed at 300K and 77K, and for type II, also under the conditions of front-side and back-side illumination.

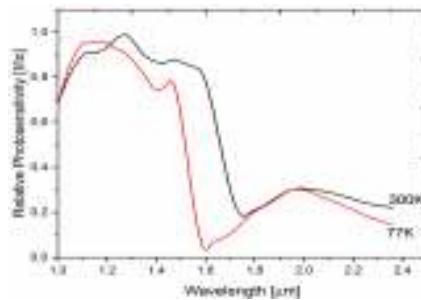
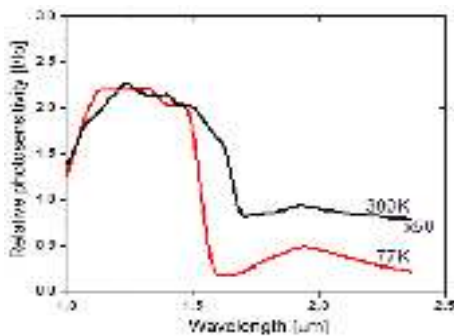
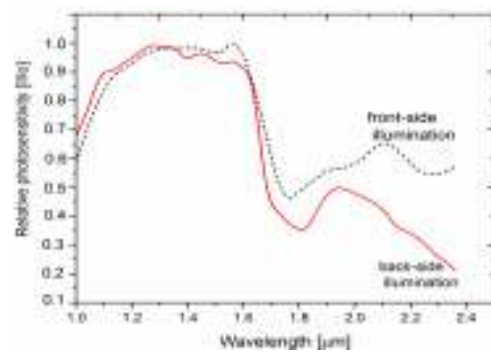


Fig.3. The photosensitivity spectrum (relative units) of the type I p-i-n diode at 300K and 77K.



a



b

Fig.4. The photosensitivity spectra (relative units) of the type II p-i-n diodes: a) at different temperatures; b) under different illumination conditions.

Common to Figs. 3 and 4 is that, according to the known data, the main photoresponse for both types of diodes lies in the range of 1.0-1.7 μm , as well as the fact that the upper boundary of the spectrum is shifted at low temperatures. In this case, the spectral shape of type II samples more fully corresponds to the known published data for InGaAs/InP heterostructures [2].

The position of the low blurred maximum that we found in the range of 1.8–2.2 μm (Fig. 3.4) does not change with temperature (Fig. 4, a), but depends on the illumination conditions (Fig. 4, b). To explain this maximum, which is undoubtedly associated with the features of the heterostructures, the following physical mechanisms can be used. This effect may be due to the transition from the surface state of the acceptor Zn located near the interface [4] and also due to the formation of InAs clusters in the MOSVD growth process [5].

Thus, the studies made it possible: to develop a genuine technology for p-i-n photodiodes based on InGaAs/InP heterostructures, to obtain comparative characteristics of diodes for the two types structures and new data on the characteristics of photosensitivity spectra, as well as to offer the third, further improved, version of the heterostructure architecture, where the contact layer consists of p^{++} -InGaAs and p^{+} -InP. In the future - the development of methods for reducing leakage currents, and application oriented technologies.

REFERENCES

1. I.D. Burlakov, L.I.Grinchenco, A.I.Dirochka, N.B.Zaletaev, *Uspechi prikladnoi Fiziki* 2(6), 2014,pp.131-162.
2. A.Rogalski, *Infrared Physics&Technology*, 43, 2002, pp.178-210.
3. T.Clausen, A.Pedersen and O.Leistiko. *Microelectronic Engineering*, 15, 1991, pp.157-160.
4. K.Moiseev, E.Ivanov et.al.. *Physics Procedia*, 3, 2010, pp.1189-1193.
5. D.A.Vinokurov, V.A.Kapitonov et al. *Physika and Tekhnika Poluprovodnikov*, 33, 7, 1999, pp. 858-862.

SHS-METALLURGY OF MOLIBDENUM-BASED COMPOSITE MATERIALS

V.Yukhvid*, D.Andreev, Yu.Vdovin

¹Merzhanov Institute of Structural Macrokinetics and Materials Science Russian Academy of Sciences (ISMAN)

*yukh@ism.ac.ru

Composite materials (CM) based on Mo–Si–B and Mo–Nb–Si–B [1,2] have great potential for implementation in the aircraft engine industry. These materials may have a higher operation temperature than industrial heat-resistant materials. Nowadays powder metallurgy methods are widely used for obtaining heat-resistant materials. SHS-metallurgy is very promising in this field too [3, 4]. The paper demonstrates the possibility of synthesizing cast composite materials (CCM) based on Mo alloyed with niobium, silicon and boron by centrifugal SHS-metallurgy and the results obtained in governing the process and CM composition and structure.

THERMODYNAMIC CALCULATIONS

The calculations showed that when a stoichiometric MoO₃/2Al mixture is burned, a high temperature (up to 3800 K) was achieved and the condensed combustion products, Mo and Al₂O₃, were in a liquid-phase state. The high combustion temperature makes it possible to introduce various alloying and technological additives into the MoO₃/Al mixture and to obtain cast alloys based on molybdenum. The calculated composition of the combustion products contains a significant amount of gases (metal vapors and suboxides).

EXPERIMENTAL METHODS

Combustion of thermite mixtures with a high level of gas formation is accompanied by intense scattering of the mixture, therefore, in order to suppress this process, the experiments were carried out in centrifugal installations under the influence of overloading, and combinations of high exothermic thermite mixtures (1) or (3) and low exothermic elemental mixtures (2) or (4), Table 1, were used. The experiments were carried out at overloading of $a = 1 - 400$ g. Mixtures of 20 g in weight were burnt in quartz glasses of 25 mm in diameter and 70 mm in height. The linear combustion rate (u), the relative mass loss during the combustion (η_1), and the completeness of the target element yield into the ingot (η_2) were determined. The characteristics were calculated by the formulas: $u = h/t_c$, $\eta_1 = [(m_1 - m_2)/m_1] \cdot 100\%$, $\eta_2 = (m/m_c) \cdot 100\%$, where h is the height of the initial mixture layer, t_c is the

layer combustion time, m_1 and m_2 are the masses of the initial mixture and combustion products, m and m_c are experimental and calculated masses of the ingot.

Table 1. Mixture compositions (1-4)

Initial composition, No.	MoO ₃	Nb ₂ O ₅	Al	Mo	Nb	Si	B
1	71.6	–	26.5	–	–	1.4	0.5
2	–	–	–	96.2	–	2.8	1.0
3	68.9	2.4	26.7	–	–	1.4	0.5
4	–	–	–	92.5	3.4	2.8	1.0

Carl Zeiss Ultra plus auto-emission scanning electron microscope based on Ultra 55 was used to determine the chemical composition and structure of the synthesis products. The phase composition of the combustion products was determined using the X-ray diffractometer DRON-3M. The X-ray tube of the BSV-27 type with a copper anode ($\lambda = 1.54178 \text{ \AA}$) was used as the radiation source. The content of light elements, C and B, was determined by the methods of analytical chemistry.

EXPERIMENTAL RESULTS

Thermite mixtures (1) and (3) are shown to burn with a complete scattering of the mixture at the atmospheric pressure without overloading. The effect of overloading and dilution of the thermite mixtures with elemental compositions (2) and (4) suppress the mixture scattering. At $a > 40 \text{ g}$ after the ignition of mixtures (1) – MoO₃/Al/Si/B+ α (Mo/Si/B) and (2) – MoO₃/Nb₂O₅/Al/Si/B+ α (Mo/Nb/Si/B) the following sequence of processes is observed: the combustion front is formed and propagates along the mixture; the chemical transformation of the initial mixture into final products takes place in the combustion front; the initial reagents and the combustion products melt due to the high temperature; the melts of metal and oxide phases of the combustion products are separated due to gravity; the two-phase melt is cooled, and the phase composition and structure of the CCM and the slag layer are formed. It was shown that with an increase in overloading (a) from 1 to 400 g – u and η_2 grow, and the scattering (η_1) decreases remarkably. The optimal intervals for obtaining cast Mo–Si–B and Mo–Nb–Si–B are $\alpha = 30 - 60 \text{ wt \%}$ and $a > 100 \text{ g}$. The combustion products obtained at these terms consist of an ingot, clearly divided into 2 layers: the upper slag (Al₂O₃) one and the lower target product (CCM).

Due to the obtained microstructure analysis and X-ray phase analysis, Fig. 1-a and 1-b, we can see that the introduction of Si and B additives into the initial mixture results in the formation of CCM with its base (the light phase) being formed by a solid solution based on Mo, and Mo_3Si and Mo_5SiB_2 phases (the gray and dark phases) are distributed along the boundaries. When Nb, Si, and B were introduced into the CCM, the X-ray phase analysis did not reveal any phases with Nb. Spectral electron microscopy detected the localization of dissolved Nb in Mo_3Si and Mo_5SiB_2 lattice, Fig. 2-a and 2-b.

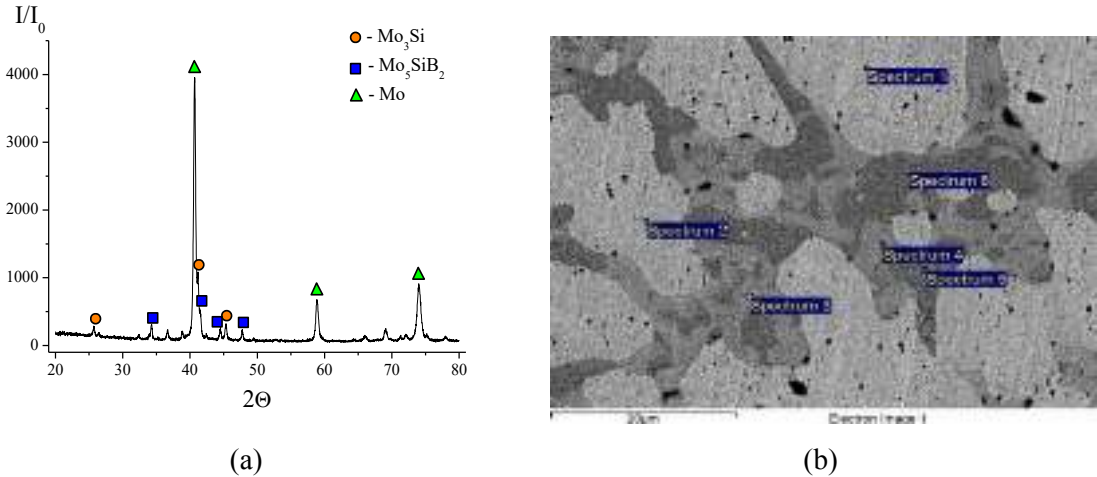


Fig.1. X-ray pattern (a) and microstructure (b) of CCM (Mo-Si-B); $\alpha = 20\%$, a = 400 g.

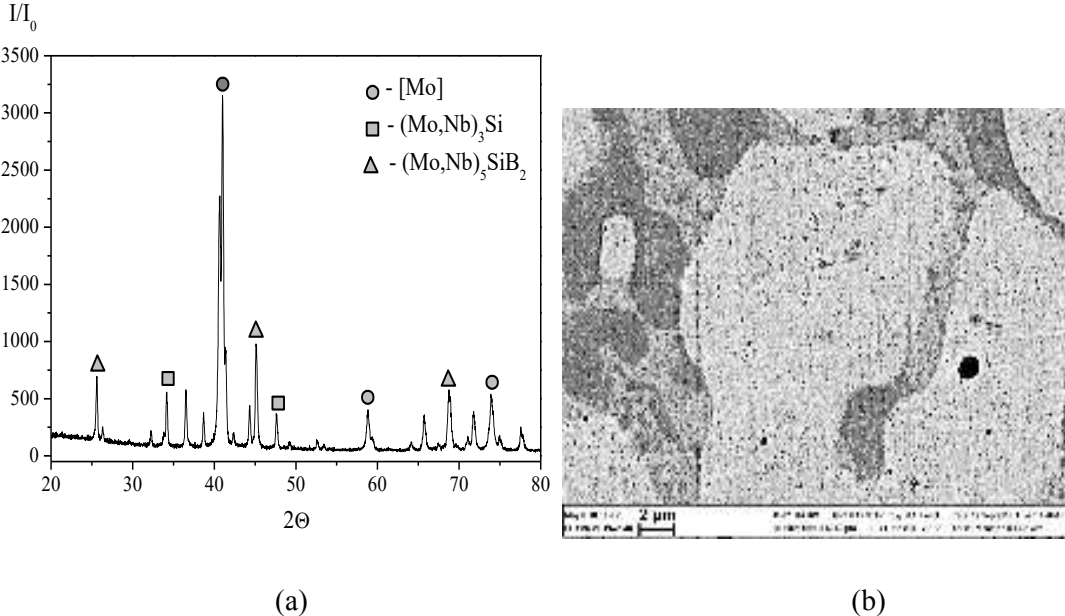


Fig.2. X-ray pattern (a) and microstructure (b) of CCM (Mo-Nb-Si-B); $\alpha = 20\%$, a = 400 g.

CONCLUSION

It is shown that the use of integral mixtures that include high-exothermic ($\text{MoO}_3/\text{Al}/\text{Si}/\text{B}$) or ($\text{MoO}_3/\text{Nb}_2\text{O}_5/\text{Al}/\text{Si}/\text{B}$) and low-exothermic ($\text{Mo}/\text{Si}/\text{B}$) or ($\text{Mo}/\text{Nb}/\text{Si}/\text{B}$) compositions and the effect of overloading makes it possible to obtain composite materials based on Mo alloyed with Nb, Si and B, similar in their composition to those obtained by the powder metallurgy methods; the materials are characterized by high thermal stability and heat resistance.

The work was carried out with the financial support of the Russian Foundation of Fundamental Investigations (Project 18-08-00228).

REFERENCES

1. J.C. Zhao and J.H. Westbrook - Ultrahigh-Temperature Materials for Jet Engines. MRS Bull. 28(9), 622-627, 2003.
2. S. Drawin, J.F. Justin. Advanced Lightweight Silicide and Nitride Based Materials for Turbo-Engine Applications. AerospaceLab, 2011, p. 1-13.
3. V.I. Yukhvid, M.I. Alymov, V.N. Sanin, D.E. Andreev, N.V. Sachkova. Synthesis of composite materials based on niobium silicides By SHS metallurgy methods. Neorganicheskiye materialy, 2015, vol.51, No.12, p.1347-1354.
4. V.I. Yukhvid, D.E. Andreev, V.N. Sanin, V.A. Gorshkov, and M.I. Alymov. Synthesis of Cast Composite Materials by SHS Metallurgy Methods. KEM, 2017, Vol.746, pp.219-232.

OBTAINING OF LOW CARBON LIGATURE IN THE Fe-B SYSTEM FROM STEEL ROLLING WASTE BY THE TECHNOLOGY SHS METALLURGY

G.Zakharov*, Z. Aslamazashvili, D.Kvashvadze, G.Tavadze, G.Oniashvili, G.Mikaberidze,
G.Urushadze

Ferdinand Tavadze Institute of Metallurgy and Materials Science. 8b.E.Mindeli str., 0186, Georgia, Tbilisi
algar12@mail.ru

The uniqueness of Boron is that its low content can affect the properties of steel, which can only be found in a significant number of other alloying components. The traditional material for alloying steel is ferroboron. In boron-containing steels, the boron content ranges from 0.0008 ... to 0.0030mas %[1].

In industry, ligatures, in the system Fe-B, are produced by the method of carbothermic [2] and metallothermic (both in the furnace and without the furnace) [3].

Considering the high requirements for boron alloys, at casting of special steels and alloys, it is very important to find ways to obtain the target product with high yield, extract and minimal boron losses.

For micro-alloying of steels, the most cost-effective ways to produce boron-containing ligature is the method of self-propagating high-temperature synthesis (SHS). (Discovered in the seventies of the twentieth century) [4]. SHS - metallurgy is a new scientific field based upon the technologies of aluminothermy, magnesium thermal and advanced SHS technology. Research in this area shows that the processes of phase separation and scattering reactions, the formation of phase and chemical constituents,, microstructures, the composition and density of the mixture, the dispersion of components, the magnitude of the centrifugal force affect on obtaining new materials and products from them [5-7].

In this study is presented modern methods and researches of obtaining ligatures for development and production of low-carbon boron-containing ligature in the Fe-B system.

The thermodynamic calculation of systems with a temperature dependence of the process of self-propagating high-temperature synthesis in a wide range of component ratios is studied. In order to achieve the set task there were used:

-Drilling waste and waste from the Rustavi Metallurgical Plant, which also mainly contain magnetite;

- Used as boron-containing materials: KBF_4 , H_3BO_3 and B_2O_3 ;

- Metal - reducing agents Al and Mg were used;

- In the form of energy additives NaNO_3 , CaO_2

Experiments were carried out under the influence of a centrifugal force at rotation 500-2500rpm / min (Fig.1) in an inert gas atmosphere at a pressure of 30-50 atm (Fig.2).

Experiments have shown that it is impossible to obtain the target product in a high-pressure reactor due to its low yield. However, it should be noted that this is due to the low weight of the sample (0.1 kg). It is expected that with an increase in the weight of the sample to 1 kg, the energy state of the system will improve, as well as the pressure in the reactor, which, in turn, will significantly increase the productivity of the target product. In the future, it is planned to continue work in this direction.

Samples were subjected to x-ray analysis using ДРОН 2 and ДРОН 4, chemical analysis with MAGELLAN and microanalysis using a HITACHI TM3030 Plus scanning electron microscope.

Results of the Fe-b system experiments performed under the action of centrifugal forces.

In order to reduce the cost of the final product and improve the environmental situation in the country, iron oxide containing waste were used for obtaining of Fe-B. The composition of the exothermic mixture to obtain the target product from drill production (a) waste in form of magnetite is: **a**: B_2O_3 :Al: NaNO_3 : CaF_2 = 47,4:23,0: 36,8:5,1:4,0. Samples obtained from this charge in a centrifugal field at a rotation speed of 2000 rpm contain ~80% FeB, 20% Fe_2B (Fig. 3) and impurities, mainly Si-3.23% and Al-4.03%. It should be noted that the yield of ferroboration is >91%. Because of the chemical analysis of MAGELLAN in the ligature shows the presence of elements not included in the HITACHI scanning electron microscope, extraction of boron is ~ 83%, and carbon is 0.14%.

The composition of the exothermic mixture to obtain the target product from Rustavi rolling plant waste (b) is: **b**: B_2O_3 :Al: CaO_2 = 46,8:22,0: 35,2:10,0. Samples obtained from this charge in a centrifugal field at a rotation speed of 2000 rpm contain ~ 80% FeB, 20% Fe_2B , and impurities, mostly Al-3.9%.

The composition of the exothermic mixture to obtain the target product from Rustavi rolling plant waste is: **b** : B_2O_3 :Al: CaO_2 = 46,8:22,0: 31,2:10,0. Samples obtained from this charge in

a centrifugal field at a rotation speed of 2000 rpm contain ~17% FeB, 83% Fe₂B and impurities, mainly Si-0.19% and Al-2.36%. It should be noted that the yield of ferroboron is >93%. Because of the chemical analysis of MAGELLAN in the ligature shows the presence of elements not included in the HITACHI scanning electron microscope, extraction of boron is ~ 83%, and carbon is 0.13%.

It should also be noted that in industrial of Aluminothermic production, the maximum yield of boron in ferroborum is 75%.

As a result of studies, it was found that:

- In the resulting ligatures, Si and Al are not harmful impurities when alloying steel;
- Thanks to the technology SHS metallurgy under of centrifugal force, Boron extraction increased by at least 8%, and the yield was 91-93%.
- It should be noted that it is more convenient to use ligature on Fe₂B bases with a boron content of ~8% by weight due to a lower melting point (1400°C) than on FeB bases with a boron content of ~18 - 20% by weight, which has a relatively higher melting point (1590°C).



Fig.3. Laboratory centrifugal SHS - installation



Fig. 2. High pressure reactors



Fig. 3 Ligatures obtained in the Fe-B system

REFERENCES

1. N. Kachanov. Hardenability of steel. 1978.
2. M. Gasik, A. Porada, O. Kiselgof, and others. / Development and industrial development of high-percentage ferroboration smelting technology by carbothermic method // *Stal*, 1995. - No. 3 . - Pp. 31-34.
3. M. Riss. Production of ferroalloys-Moscow: metallurgy, 1985. — 344 c.
4. A.Merzhanov, I. Borovinskaya, V. Shkiro. The phenomenon of wave localization of auto-braking solid-phase reactions. State register of discoveries No. 287, 1984.
5. V.Yukhvid, A.Kachin and G.Zakharov. Centrifugal SHS Surfacing of the Refractory Inorganic Materials. *International Journal of Self-Propagating High-Temperature Synthesis* Volume 3, Number 4, 1994.
6. G.Oniashvili, G.Tavadze, G.Zakharov, Z. Aslamazashvili. Self-propagating High-temperature Synthesis of Ferroalloys. LAP Lambert Academic Publishing. 2018.
7. G. oniashvili, V. Yukhvid and G. Zakharov. Centrifugal SHS-surfacing on steel. *Foundry magazine* No. 7, 2001.

THE IDEAL REACTION AREA AND THE THRESHOLD OF SHS

G. Mikaberidze^{1,2}, K. Ukleba*¹, J. Khantadze¹

1. Ferdinand Tavadze Institute of Metallurgy and Materials Science, 8b.E.Mindeli str., 0186, Georgia, Tbilisi
2. Department of mathematics, University of California, Davis, CA 95616, U.S.A.

* ketino.ukleba@gmail.com

The charge of Self-propagating high-temperature synthesis (SHS) is a mixture of metallic and nonmetallic powders. The chemical reaction can be initiated at the contact points between dissimilar particles. The regions containing such points are called reaction areas and are highlighted in gray in Fig. 1. On the other hand, the regions with an abundance of a single type of particles (shown in white in Fig. 1) do not contain heterogeneous contact points and can be regarded as ballast in this sense.

It is clear that the number of heterogeneous contact points between metallic and nonmetallic particles influences the success of the synthesis. A higher number of dissimilar contacts should result in a more effective chemical reaction.

A structural model for two-type particulate mixtures has been proposed in [1]. According to this model, depending on the chemical composition of the reagents and the size ratio of the corresponding particles (i.e., dimensional factor), it is possible to form a structure with ideal reaction areas (IRA). Such a structure achieves the maximal possible number of dissimilar contacts, thus creating the most favorable condition for an effective SHS process.

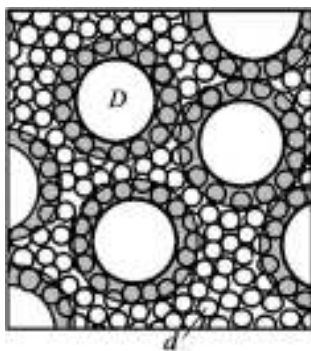


Fig. 1. Model structure of a biparticulate powder mixture with particle sizes $D > d$.

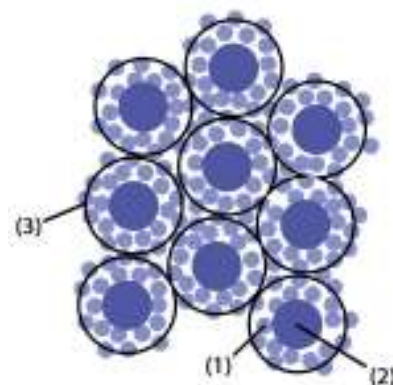


Fig. 2. IRA structure according to [2]: In the vicinity of reaction areas (3), the ratio of coarse (2) and fine (1) particles is approximately consistent ($N/n = \text{const.}$).

For a given chemical composition, i.e., for a specific mass ratio of the reagents (m_1/m_2), one can vary the dimensional factor D/d for the initial charge in a wide range. This can be achieved by changing the number of coarse (N) and fine (n) particles while keeping $(n \cdot d^3)/(N \cdot D^3) = \text{const}$. From all the resulting structural configurations, for each chemical composition (m_1/m_2), only one value of the dimensional factor $(D/d)_m$ will allow for the IRA to form. That is, the unique value $(D/d)_m$ will maximize the number of heterogeneous contacts for the coarse particles and minimize the volume of the regions with an excess of single type particles, i.e., the “ballast” (see Fig. 2). Therefore, any deviation from $(D/d)_m$ will reduce the number of reagent contacts, weaken the synthesis process, and in the extreme case with $D \gg d$, it will cause the process to terminate. For example, if we place large chunks of titanium in an arbitrarily fine powder of boron, the SHS process will not carry out. This is an extreme case, and therefore there must be some threshold of grinding the reagent powders below which the SHS will proceed in the form of burning wave front without quenching.

This paper is devoted to the study of this thesis. The propagation speed of the SHS burning front is investigated for powder mixtures of titanium and boron. The starting materials are: Powder of amorphous boron of Chinese production, 99% pure, with a particle size of 1 μm ; And powder of crystalline titanium, 99.5% pure or higher, three fractions with different particle sizes were obtained by sifting: 25, 40, 50 μm .

Synthesis was conducted in open, the powders were burnt in the standard porcelain combustion boats, 70 mm long, 8 mm deep, holding approximately 17 g of hand-tamped mixture. The thermal impulse was provided by heating a tungsten wire with diameter 0.4 mm.

As a result, three different compounds were observed during the SHS process. Each compound was designed to have the IRA structure with distinct dimensional factors (see Table 1). For greater clarity, below is a fragment of the table and the formula used to describe the IRA structure [1].

$$n \left(\frac{d}{D} \right)^3 = \frac{m_1}{m_2} \frac{\gamma_2}{\gamma_1}.$$

For each given dimensional factor (d/D) , we find the quantity $n(d/D)^3$ using Table 2. Then, taking into account the densities of boron ($\gamma_1 = 2,54 \text{ g/cm}^3$) and titanium ($\gamma_2 = 4,51 \text{ g/cm}^3$), we use the above equation and determine the chemical composition m_1/m_2 of the mixture. For these parameters, the IRA structure contains n fine particles for each coarse particle.

Apparently, the role of dimensional factor is distorted by the reactions of the charge reagents with oxygen and nitrogen in the air. Yet, the data given in Table 1 demonstrates that when the dimensional factor increases, the speed of synthesis decreases, which indicates the presence of the SHS threshold.

In particular, by extrapolating the table 1 data to zero speed, it can be assumed that at $d/D < 150$ SHS it is impossible to implement.

Table 1. Experimental results

№ Charge	Particle size, μm		Dimension factor, d_B/D_{Ti}	$n \left(\frac{d}{D}\right)^3$	Mass ratio of components, m_B/m_{Ti}	Front movement speed, m/s	n
	Boron	Titanium					
1	1	25	0,04	0,151	0,0850	0,0060 0,0060	2400
2	1	40	0,025	0,915	0,0515	0,0049 0,0050 0,0050	5900
3	1	50	0,02	0,073	0,0411	0,0040 0,0047	9100

Table 2. Disperse characteristics of the initial furnace charge of reactants, ensuring the formation of an IRA (Ideal Reaction Area) structure with a maximum of heterogeneous contacts.

$n(d/D)^3$	d/D	$n = 3,5 \left(1 + \frac{D}{d}\right)^2$
1	2	3
1,0	0,199	127
0,95	0,192	134
0,90	0,184	144
0,85	0,176	156
0,80	0,168	169
0,75	0,159	186
0,70	0,151	203
0,65	0,142	227
0,625	0,138	238

$n(d/D)^3$	d/D	$n = 3,5 \left(1 + \frac{D}{d}\right)^2$
1	2	3
0,250	0,063	1000
0,225	0,058	1155
0,200	0,052	1430
0,193	0,050	1544
0,184	0,048	1663
0,176	0,046	1800
0,168	0,044	1971
0,160	0,042	2154
0,151	0,040	2365

0,600	0,133	255
0,575	0,129	267
0,550	0,125	282
0,525	0,120	303
0,500	0,115	329
0,475	0,110	357
0,450	0,105	388
0,425	0,100	425
0,400	0,095	469
0,375	0,090	514
0,350	0,085	570
0,325	0,080	635
0,300	0,075	711
0,275	0,069	836

0,143	0,038	2612
0,135	0,036	2903
0,127	0,034	3237
0,119	0,032	3640
0,011	0,030	4118
0,104	0,028	4717
0,095	0,026	5450
0,088	0,024	6373
0,080	0,022	7552
0,073	0,020	9104
0,065	0,018	11212
0,058	0,016	14113
0,050	0,014	18361
0,043	0,012	24890

REFERENCES

1. Khantadze D.V., Tavadze G.F., and Mukasian A.S. "Structural Model of Two-Component Particulate Mixtures with Maximum Heterogeneous Contacts." *Powder Metallurgy and Metal Ceramics* 59, no. 3 (2020): 121-126.
2. Rogachev A.S., and Mukasian A.S.. "Combustion for the Synthesis of Materials: Introduction to Structural Macrokinetics [in Russian], Izd." *Fiz. Mat. Tekh. Lit., Moscow* (2012): 398.



შპს „დომბა“
თბილისი - 2021
წერეთლის გამზირი 140

LTD “DOMBA”
Tbilisi – 2021
140, Tsereteli Ave.